Uniaxial Orientation of Polyethylene Films for Recyclable Flexible Packaging

Dixit Guleria

Uniaxial Orientation of Polyethylene Films for Recyclable Flexible Packaging

PROEFSCHRIFT

ter verkrijging van de graad van doctor in de scheikundige technologie en scheikunde aan de Technische Universiteit Eindhoven, op gezag van de rector magnificus prof. dr. S.K. Lenaerts,

en de graad van doctor in de industriële wetenschappen: chemie en in de bio-ingenieurswetenschappen aan de Universiteit Gent, op gezag van de rector magnificus prof. dr. R. Van de Walle,

voor een commissie aangewezen door het College voor Promoties, in het openbaar te verdedigen op woensdag 21 mei 2025 om 13:30 uur

door

Dixit Guleria

geboren te Hamirpur, Himachal Pradesh, India

Dit proefschrift is goedgekeurd door de promotoren en de samenstelling van de promotiecommissie is als volgt:

voorzitter: prof. dr. ir. R. Tuinier

co-voorzitter: prof. dr. ir. J. Degroote (Universiteit Gent)

promotoren: prof. dr. ir. C.F.J den Doelder PDEng

prof. dr. L. Cardon (Universiteit Gent)

co-promotor: prof dr. ir. P. Ragaert (Universiteit Gent)

leden: prof. dr. ir. F. Desplentere (KU Leuven)

prof. dr. ing. I. Sampers (Universiteit Gent)

prof. dr. A. Lyulin

prof. dr. M. Edeleva (Universiteit Gent)

prof. dr. A.P.H.J Schenning

Het onderzoek of ontwerp dat in dit proefschrift wordt beschreven is uitgevoerd in overeenstemming met de TU/e Gedragscode Wetenschapsbeoefening.

“To my family and friends”

Uniaxial Orientation of Polyethylene Films for Recyclable Flexible Packaging

Dixit Guleria

The doctoral research reported in this dissertation was jointly supervised and conducted under a Double Doctoral Degree Agreement between Eindhoven University of Technology (TU/e) and Ghent University (UGent).

A catalogue record is available from Eindhoven University of Technology Library

ISBN: 978-90-386-6368-5

Copyright © Dixit Guleria

Cover Design: Dixit Guleria
Layout: Dixit Guleria
Printing: ProefschrijftMaken – proefschrijftmaken.nl

C-PlaNeT
CIRCULAR PLASTICS NETWORK FOR TRAINING

This work has been performed in the framework of the C-PlaNet project which has received funding from the European Union's Horizon 2020 research and innovation programme under the Marie Sklodowska-Curie grant No. 859885.

SUMMARY

“Uniaxial Orientation of Polyethylene Films for Recyclable Flexible Packaging”

Multi-material multi-layer flexible packaging is extensively employed in the food and pharmaceutical industries due to its outstanding mechanical and barrier properties, as well as user-friendly characteristics such as lightweight design and enhanced portability. However, recycling this type of packaging presents significant challenges as they are composed of multiple layers of different plastics (e.g., polyethylene (PE), polypropylene (PP), polyethylene terephthalate (PET), polyamide (PA)) and non-polymeric materials (e.g., aluminium foil, metallized films), which are laminated together. The limitations in recycling mixed-material structures, results in most of these packages being disposed of through landfilling or incineration. This practice impedes recycling efforts and undermines the principles of circular economy.

Mono-material multi-layer flexible packaging systems are emerging as a promising alternative to improve recycling rates. While multiple variations are often needed to maintain functionality, using a single chemical composition allows for better recycling outcomes. PE with its different types (low-density, linear low-density and high-density) is widely used in several applications due to its versatility in structural and functional properties. Combining these PE types in packaging can offer both functionality and recyclability. Traditionally, the outer layers of flexible packaging use non-PE polymers (e.g, PET, PA) for stiffness, and barrier properties. However, advancements in polyethylene film orientation techniques, specifically uniaxial orientation or machine direction orientation (MDO) process have demonstrated significant potential for enhancing the mechanical and barrier performance of PE films. This advancement offers the opportunity to replace non-PE materials in outer layers with machine direction oriented polyethylene (MDO-PE) films, thereby supporting the development of recyclable mono-material PE-based flexible packaging.

During the MDO process, the precursor polymer film is stretched in the machine direction at a certain rate, and at a certain orientation temperature which depends on the polymer’s chemical nature and is typically close to the melting point of the polymer. As a result, significant improvements are observed in the film's physical properties, including modulus, stiffness, tensile strength, as well as barrier properties.

This thesis investigates the influence of key PE resin characteristics (e.g., density, average molecular weight, branching, branching distribution, molecular weight distribution) and MDO process parameters (e.g., draw ratio) on the targeted mechanical, barrier and optical properties of MDO-PE films. A comprehensive understanding of structure-property relationships is developed through extensive microstructural characterizations and morphological analysis. Additionally, the mechanical recyclability of virgin PE films and the

incorporation of post-consumer recyclate (PCR) material with virgin materials for subsequent MDO operation is investigated for high performance applications.

The design challenges associated with achieving efficient mechanical recycling of conventional flexible packaging are outlined in Chapter 1, with an examination of current strategies and technological adaptations aimed at addressing these challenges to support the circular economy for such systems. PE-based mono-material flexible packaging is highlighted as a promising solution to these challenges. Furthermore, the potential of the MDO or uniaxial orientation process in enhancing the performance of PE films for the PE-based mono-material flexible packaging is explored.

As mentioned earlier, conventional multilayer flexible packages typically use some non-PE material (e.g. PET or PA) to impart stiffness and gas barrier properties against gases like oxygen. PE can reach a certain modulus by increasing resin density, but this is typically not sufficient. Stiffness of a material is a function of its modulus and therefore, enhancement in modulus of PE film enhances stiffness. Sufficient polymer film stiffness is required for various packaging operations such as printing and lamination, and for the efficient running of packaging machine lines. Low-stiffness films might sag while running on packaging lines. Existing research recognizes the critical role played by MDO process parameters such as orientation temperature, draw ratio, stretch rate, and annealing time on final mechanical properties attained by MDO films. However, only a few studies have systematically investigated the role of resin parameters such as density, branching, branching distribution (BD), average molecular weight, and polydispersity on final mechanical properties attained by the MDO-PE films.

The role of principal resin parameters of PE, i.e., dominantly resin density and short-chain branching (SCB) distribution coupled with molecular weight, in lab-scale MDO film stretching at the fixed MDO process parameters of orientation temperature, stretch rate, annealing time, and process draw ratio was investigated in Chapter 2. Five distinct PE resins and blends were processed in a lab-scale setup to produce compression molded base sheets and further MDO-PE films. Uniaxial stretching or MDO operation notably enhanced the tensile modulus of MDO-PE films along the machine direction, particularly in higher density blends to as much as about 350%, comparable to conventionally used polymers. Challenges related in stretching extremely high-density base sheet led to breakage. Certain resin compositions exhibited unique molecular architecture, facilitating enhanced tensile modulus and axial stiffness. The study further addressed the structural evolutions and changes in surface morphology of the PE base sheets after going through MDO operation and how they relate to the final overall tensile properties of the MDO films. MDO-PE films consistently demonstrated fibrillated and oriented microstructure aligned parallel to the stretch direction.

In Chapter 2, compression molded base sheets which are usually mechanically isotropic in nature were used as a starting material to produce lab-scale MDO-PE films. The study in Chapter 2 presented critical insights of structural evolutions in MDO process through a lab-scale setup. However, at industrial scale, MDO process is performed on precursor cast or

blown films, which are in general mechanically anisotropic. Blown film extrusion ranks among the foremost polymer processing methodologies, with an annual processing capacity of billions of kilograms of polymer, predominantly polyethylene. Integrating the MDO process sequentially with film blowing presents the potential to enhance the packaging materials characteristics and streamline the shift towards mono-material packaging, thereby positively impacting recyclability and polymer circularity. Therefore, for subsequent studies, lab-scale setup was scaled up to pilot-scale setup to produce MDO-PE films. In this setup, blown films produce by pilot-scale blown film extrusion line were used as a precursor starting materials to perform MDO operation on a pilot-scale MDO setup.

The influence of MDO on the blown film with pre-existing random orientation has not been yet explored extensively. After gaining insights on impact of resin density and SCB distribution in Chapter 2, focus was to investigate the impact of other key resin molecular properties and MDO process parameter of draw ratio. Hence, the influence of PE molecular properties such as number-average molecular weight (M_n), weight-average molecular weight (M_w), polydispersity and comonomer content, as well as the effects of the key MDO process parameter of draw ratio, on the structural evolution, morphology and mechanical properties of MDO-PE films intended for use as outer layers in mono-material flexible packaging design was investigated in Chapter 3. Five PE grades and their blends were processed into blown films, and selected films were subjected to pilot-scale MDO at varying draw ratios. The findings reveal that higher fraction of low-molecular-weight chains results in a higher natural draw ratio, leading to the higher modulus in the MDO films. Furthermore, extremely higher MDO draw ratios lead to increased fibrillation, microstructural orientation and enhanced crystallinity, which further significantly enhances the modulus of MDO films (up to 13 times of the starting blown film), comparable to those of conventionally used polymers in the outer layers of conventional multilayer flexible packaging.

One of the important aspects of the work performed in this thesis was to experimentally validate the mechanical recyclability of mono-materials fractions. Re-extrusion is a widely used method for recycling mono-material fractions. Re-extrusion involves shredding the material (blown films in this study) into small flakes after sorting and cleaning which is then used as an input material in an extruder to re-pelletize the material. The re-pelletized resins can be further used to make new materials (blown films and subsequent MDO films in this study). Blending recycled and virgin polyethylene stands as a recognized method for modifying the properties of recycled material. While numerous studies have investigated the recycling and degradation of polyethylene during processing, particularly those used in packaging applications, research on blown films containing recycled polyethylene is limited. Thus, the mechanical recyclability of virgin PE blown films and the incorporation of post-consumer recyclate (PCR) for in-line MDO-PE film applications, with a focus on targeted mechanical properties of modulus and stiffness for the outer layer of mono-material PE-based flexible packaging design was investigated in Chapter 4. Experiments reveal that MDO-PE films from reprocessed material (after 5 reprocessing cycles) retained 77% of their virgin MDO film tensile modulus, despite exhibiting onset of slight molecular degradation.

Moreover, incorporating 5% PCR into PE blends yielded tensile properties comparable to those of virgin MDO films, demonstrating the feasibility of these blends for high-performance MDO-PE films in mono-material PE-based flexible packaging applications.

After investigating key mechanical properties, the focus was to investigate vital barrier properties (oxygen barrier, functional barrier) and optical properties of MDO-PE films, intended to be used as outer layers in mono-material PE based flexible packaging. A good barrier against oxygen is required to prevent the spoilage of food products inside the package, and for prolonging the shelf life of the food product. A major issue with PE is its high oxygen permeability. However, it has been demonstrated in the previous studies that oxygen as well as moisture barrier of PE films can be enhanced by MDO operation. The optical properties of polymers, including gloss, transparency, clarity, haze, color, surface appearance, and refractive index, are closely associated with the quality and visual performance of plastic products. MDO operation significantly impacts the optical properties of films due to evolutions in microstructure and surface morphology. Thus, the effects of MDO on the barrier and optical properties of PE films for applications in PE-based mono-material flexible packaging was investigated in Chapter 5. The MDO process in general enhanced oxygen and functional barrier properties by increasing crystallinity and microstructural orientation under specific parameters, with results varying based on resin density and processing conditions. Despite these improvements, the oxygen barrier performance of MDO-PE films remained inferior to conventional high oxygen barrier performance polymers like PET and PA, highlighting the need for additional barrier layers for advanced applications which must be further compatible with mechanical recycling. MDO also influenced optical properties, increasing haze due to changes in crystalline microstructure and surface morphology, while gloss initially decreased and subsequently increased at higher draw ratios.

The key learnings and conclusions from experimental work in Chapters 2,3,4 and 5 of this thesis are summarised in Chapter 6. Further, the future research directions to advance the design of PE-based mono-material flexible packaging are outlined. Possible key challenges in large-scale adaptation of MDO-PE films to sustain the circular economy of flexible packaging systems are explored. Lastly, concluding thoughts for the performed investigations in entire thesis are presented.

SAMENVATTING

"Uniaxiale oriëntatie van polyethyleenfolies voor recycleerbare flexibele verpakking"

Meerlaagse flexibele verpakkingen van meerdere materialen worden veel gebruikt in de voedingsmiddelen- en farmaceutische industrie vanwege hun uitstekende mechanische en barrière-eigenschappen en gebruiksvriendelijke eigenschappen zoals een lichtgewicht ontwerp en verbeterde draagbaarheid. Het recyclen van dit soort verpakkingen brengt echter aanzienlijke uitdagingen met zich mee, omdat ze zijn samengesteld uit meerdere lagen van verschillende kunststoffen (bijv. polyethyleen (PE), polypropyleen (PP), polyethyleentereftalaat (PET), polyamide (PA)) en niet-polymere materialen (bijv. aluminiumfolie, gemetalliseerde folies) die aan elkaar zijn gelamineerd. Door de beperkingen in het recyclen van gemengde materiaalstructuren worden de meeste van deze verpakkingen gestort of verbrand. Deze praktijk staat recycling in de weg en ondermijnt de principes van de circulaire economie.

Meerlaagse flexibele verpakkingssystemen op basis van één materiaal zijn in opkomst als veelbelovend alternatief om het recyclingpercentage te verhogen. Hoewel er vaak meerdere variaties nodig zijn om de functionaliteit te behouden, zorgt het gebruik van één chemische samenstelling voor betere recyclingresultaten. PE met zijn verschillende soorten (lage dichtheid, lineaire lage dichtheid en hoge dichtheid) wordt veel gebruikt in verschillende toepassingen vanwege zijn veelzijdigheid in structurele en functionele eigenschappen. Het combineren van deze PE-types in verpakkingen kan zowel functionaliteit als recycleerbaarheid bieden. Traditioneel worden voor de buitenste lagen van flexibele verpakkingen niet-PE-polymeren gebruikt (zoals PET en PA) voor stijfheid en barrière-eigenschappen. Vooruitgang op het gebied van polyethyleen folieoriëntatietechnieken, met name uniaxiale oriëntatie of machinerichtingsoriëntatie (MDO), heeft echter aangetoond dat de mechanische en barrière-eigenschappen van PE-folies aanzienlijk kunnen worden verbeterd. Deze vooruitgang biedt de mogelijkheid om niet-PE-materialen in buitenlagen te vervangen door MDO-PE-folies, waardoor de ontwikkeling van recycleerbare monomateriaal PE-gebaseerde flexibele verpakkingen wordt ondersteund.

Tijdens het MDO-proces wordt de polymeerfolie in de machinerichting uitgerokken een bepaalde snelheid en bij een bepaalde oriëntatietemperatuur die afhangt van de chemische aard van het polymeer en die meestal dicht bij het smeltpunt van het polymeer ligt. Hierdoor worden aanzienlijke verbeteringen waargenomen in de fysische eigenschappen van de folie, zoals modulus, stijfheid, treksterkte en barrière-eigenschappen.

In dit proefschrift wordt de invloed onderzocht van belangrijke eigenschappen van PE-polymeren (bijv. dichtheid, gemiddeld moleculair gewicht, vertakking, vertakkingsverdeling, molecuulgewichtverdeling) en MDO-procesparameters (bijv. trekverhouding) op de beoogde mechanische, barrière- en optische eigenschappen van MDO-PE-folies. Een

uitgebreid begrip van structuur-eigenschap relaties wordt ontwikkeld door middel van uitgebreide microstructurele karakteriseringen en morfologische analyse. Daarnaast wordt de mechanische recycleerbaarheid van nieuwe PE-folies en de integratie van post-consumer recyclaat (PCR) met nieuwe materialen voor MDO onderzocht voor hoogwaardige toepassingen.

De ontwerpuitdagingen die samenhangen met het bereiken van efficiënte mechanische recycling van conventionele flexibele verpakkingen worden geschetst in hoofdstuk 1, met een onderzoek naar huidige strategieën en technologische aanpassingen gericht op het aanpakken van deze uitdagingen om de circulaire economie voor dergelijke systemen te ondersteunen. PE-gebaseerde monomateriaal flexibele verpakkingen worden belicht als een veelbelovende oplossing voor deze uitdagingen. Verder wordt het potentieel onderzocht van het MDO- of uniaxiale oriëntatieproces voor het verbeteren van de prestaties van PE-folies voor flexibele monomateriaalverpakkingen op basis van PE.

Zoals eerder vermeld, gebruiken conventionele meerlaagse flexibele verpakkingen meestal een ander materiaal dan PE (bijv. PET of PA) om stijfheid en gasbarrière-eigenschappen tegen gassen zoals zuurstof te geven. PE kan een bepaalde modulus bereiken door de dichtheid te verhogen, maar dit is meestal niet voldoende. De stijfheid van een materiaal is een functie van de modulus en daarom verbetert een verhoging van de modulus van PE-folie de stijfheid. Voldoende stijfheid van polymeerfolie is nodig voor verschillende verpakkingsbewerkingen, zoals bedrukken en lamineren, en voor een efficiënte werking van verpakkingslijnen. Folies met een lage stijfheid kunnen doorzakken tijdens het draaien op verpakkingslijnen. Bestaand onderzoek erkent de kritieke rol van MDO procesparameters zoals oriëntatietemperatuur, trekverhouding, reksnelheid en gloeitijd op de uiteindelijke mechanische eigenschappen van MDO folies. Er zijn echter maar een paar studies die systematisch de rol van polymeerparameters zoals dichtheid, vertakking, vertakkingsdistributie (BD), gemiddeld moleculair gewicht en polydispersiteit op de uiteindelijke mechanische eigenschappen van MDO-PE-folies hebben onderzocht.

De rol van de belangrijkste polymeerparameters van PE, d.w.z. voornamelijk dichtheid en korte-ketenvertakking (SCB) distributie gekoppeld aan moleculair gewicht, in het verstrekken van MDO-folies op labschaal bij de vaste MDO-procesparameters oriëntatietemperatuur, reksnelheid, gloeitijd en trekverhouding is onderzocht in hoofdstuk 2. Vijf verschillende PE-polymeren en -mengsels werden verwerkt in een laboratoriumopstelling om onder druk gevormde basisplaten en verdere MDO-PE-folies te produceren. Uniaxiaal verstrekken of MDO-bewerking verbeterde de trekmodulus van MDO-PE folies in de lengterichting van de machine, vooral bij mengsels met een hogere dichtheid tot ongeveer 350%, vergelijkbaar met conventioneel gebruikte polymeren. Uitdagingen bij het verstrekken van basisfolies met een extreem hoge dichtheid leidden tot plaatselijke rek en breuk. Bepaalde polymeersamenstellingen vertoonden een unieke moleculaire architectuur, wat verbeterde trekmodulus en axiale stijfheid mogelijk maakte. Het onderzoek richtte zich verder op de structurele ontwikkelingen en veranderingen in de oppervlaktemorfologie van de PE-basisfolies nadat ze MDO hadden ondergaan en hoe deze samenhingen met de uiteindelijke algemene trekeigenschappen van de MDO-folies. MDO-

PE folies vertoonden consistent een gefibrilleerde en georiënteerde microstructuur parallel aan de rekrichting.

In hoofdstuk 2 werden persgevormde basisplaten, die meestal mechanisch isotroop van aard zijn, gebruikt als uitgangsmateriaal om MDO-PE folies op laboratoriumschaal te produceren. Het onderzoek in hoofdstuk 2 gaf een kritisch inzicht in de structurele ontwikkelingen in het MDO-proces door middel van een laboratoriumopstelling. Op industriële schaal wordt het MDO-proces echter uitgevoerd op gegoten of geblazen folie, die over het algemeen mechanisch anisotroop is. Extrusie van geblazen folie behoort tot de belangrijkste polymeerverwerkingsmethoden, met een jaarlijkse verwerkingscapaciteit van miljarden kilo's polymeer, voornamelijk polyethyleen. Door het MDO-proces opeenvolgend te integreren met het blazen van folie kunnen de eigenschappen van het verpakkingsmateriaal worden verbeterd en kan de verschuiving naar monomateriaalverpakkingen worden gestroomlijnd, wat een positieve invloed heeft op de recycleerbaarheid en circulariteit van polymeren. Daarom werd de laboratoriumopstelling voor vervolgonderzoek opgeschaald naar een proefopstelling voor de productie van MDO-PE-folies. In deze opstelling werden geblazen folies, geproduceerd door een extrusielijn voor geblazen folie op pilotschaal, gebruikt als uitgangsmateriaal om MDO uit te voeren in een MDO-installatie op pilotschaal.

De invloed van MDO op de geblazen folie met reeds bestaande willekeurige oriëntatie is nog niet uitgebreid onderzocht. Na het verkrijgen van inzicht in de invloed van dichtheid en SCB-verdeling in hoofdstuk 2, lag de focus op het onderzoeken van de invloed van andere belangrijke moleculaire eigenschappen van polymeer en MDO-procesparameter van trekverhouding. Daarom werd in hoofdstuk 3 de invloed van de moleculaire eigenschappen van PE onderzocht, zoals het aantalgemiddelde molecuulgewicht (M_n), het gewichtgemiddelde molecuulgewicht (M_w), de polydispersiteit en het comonomeergehalte, evenals de effecten van de belangrijkste MDO-procesparameter, de trekverhouding, op de structurele evolutie, morfologie en mechanische eigenschappen van MDO-PE folies die bedoeld zijn om te worden gebruikt als buitenste lagen in monomateriaal flexibele verpakkingen. Vijf PE-materialen en hun mengsels werden verwerkt tot geblazen folies en de geselecteerde folies werden onderworpen aan MDO op proefschaal bij verschillende trekverhoudingen. De bevindingen laten zien dat een hogere fractie laagmoleculaire ketens resulteert in een hogere natuurlijke trekverhouding, wat leidt tot een hogere modulus in de MDO-folies. Bovendien leiden extreem hogere MDO trekverhoudingen tot meer fibrillatie, microstructurele oriëntatie en verbeterde kristalliniteit, waardoor de modulus van MDO-folies nog verder toeneemt (tot 13 keer die van de geblazen beginfolie), vergelijkbaar met die van conventioneel gebruikte polymeren in de buitenlagen van conventionele meerlaagse flexibele verpakkingen.

Een van de belangrijke aspecten van het werk in dit proefschrift was het experimenteel valideren van de mechanische recycleerbaarheid van monomateriaalfracties. Re-extrusie is een veelgebruikte methode voor het recyclen van monomateriaalfracties. Bij re-extrusie wordt het materiaal (in dit onderzoek geblazen folie) na sortering en reiniging versnipperd

tot kleine vlokken die vervolgens worden gebruikt als invoermateriaal in een extruder om het materiaal opnieuw te pelletiseren. De opnieuw gepelletiseerde polymeren kunnen verder worden gebruikt om nieuwe materialen te maken (geblazen folies en daaropvolgende MDO-folies in dit onderzoek). Het mengen van gerecycleerd en nieuw polyethyleen is een erkende methode om de eigenschappen van gerecycleerd materiaal te wijzigen. Hoewel veel studies de recycling en degradatie van polyethyleen tijdens de verwerking hebben onderzocht, met name die welke worden gebruikt in verpakkingstoepassingen, is het onderzoek naar geblazen folies die gerecycleerd polyethyleen bevatten beperkt. Daarom werd in hoofdstuk 4 de mechanische recycleerbaarheid van nieuw PE geblazen folies en de integratie van PCR voor in-line MDO-PE folietoepassingen onderzocht, met de nadruk op gerichte mechanische eigenschappen van modulus en stijfheid voor de buitenlaag van monomateriaal PE-gebaseerd flexibel verpakkingsontwerp. Experimenten tonen aan dat MDO-PE-folies van opgewerkt materiaal (na 5 opwerkingscycli) 77% van hun nieuwe MDO-trekmodulus behielden, ondanks een begin van lichte moleculaire degradatie. Bovendien leverde het opnemen van 5% PCR in PE-mengsels trekeigenschappen op die vergelijkbaar zijn met die van nieuwe MDO-folies, wat de haalbaarheid aantoont van deze mengsels voor hoogwaardige MDO-PE-folies in monomateriaal PE-gebaseerde flexibele verpakkingstoepassingen.

Na het onderzoeken van de belangrijkste mechanische eigenschappen, lag de focus op het onderzoeken van essentiële barrière-eigenschappen (zuurstofbarrière, functionele barrière) en optische eigenschappen van MDO-PE folies, bedoeld om te worden gebruikt als buitenste lagen in mono-materiaal PE gebaseerde flexibele verpakkingen. Een goede barrière tegen zuurstof is nodig om te voorkomen dat voedingsmiddelen in de verpakking bederven en om de houdbaarheid van het voedingsmiddel te verlengen. Een groot probleem met PE is de hoge zuurstofdoorlaatbaarheid. In eerdere onderzoeken is echter aangetoond dat de zuurstof- en vochtbarrière van PE-folies kan worden verbeterd door MDO toe te passen. De optische eigenschappen van polymeren, zoals glans, transparantie, helderheid, waas, kleur, uiterlijk van het oppervlak en brekingsindex, zijn nauw verbonden met de kwaliteit en visuele prestaties van kunststof producten. MDO heeft een significante invloed op de optische eigenschappen van folies door evoluties in microstructuur en oppervlaktemorfologie. Daarom werden in hoofdstuk 5 de effecten van MDO op de barrière- en optische eigenschappen van PE-folies voor toepassingen in monomateriaal flexibele verpakkingen op basis van PE onderzocht. Het MDO-proces verbeterde in het algemeen de zuurstof- en functionele barrière-eigenschappen door de kristalliniteit en microstructuuroriëntatie te vergroten onder specifieke parameters, waarbij de resultaten varieerden op basis van dichtheid en verwerkingsomstandigheden. Ondanks deze verbeteringen bleven de zuurstofbarrièreprestaties van MDO-PE folies inferieur aan conventionele polymeren met een hoge zuurstofbarrièreprestatie zoals PET en PA, wat de noodzaak benadrukt van extra barrièrelagen voor geavanceerde toepassingen die verder compatibel moeten zijn met mechanische recycling. MDO beïnvloedde ook de optische eigenschappen: de waas nam toe door veranderingen in de kristallijne microstructuur en

oppervlaktemorfologie, terwijl de glans aanvankelijk afnam en vervolgens toenam bij hogere trekverhoudingen.

De belangrijkste lessen en conclusies van het experimentele werk in hoofdstuk 2, 3, 4 en 5 van dit proefschrift worden samengevat in hoofdstuk 6. Verder worden de toekomstige onderzoeksrichtingen geschetst om het ontwerp van op PE gebaseerde monomateriaal flexibele verpakkingen te bevorderen. Mogelijke belangrijke uitdagingen bij grootschalige aanpassing van MDO-PE-folies om de circulaire economie van flexibele verpakkingssystemen te ondersteunen, worden verkend. Tot slot worden afsluitende gedachten voor het uitgevoerde onderzoek in het gehele proefschrift gepresenteerd.

Contents

Chapter 1 Introduction 1

1.1 Motivation 2

1.2 Introduction to flexible packaging 3

1.3 Transition from multi-materials to PE based mono-materials 5

1.4 Introduction to MDO process 6

1.5 Introduction to amorphous and semi-crystalline polymers 8

1.6 Introduction to polyethylene and its different types 10

1.7 Insights into PE microstructure 11

1.8 Methods used to fabricate PE films during investigations 13

1.9 Impact of MDO on PE microstructure 16

1.10 Scope and outline of this thesis 19

1.11 Bibliography 25

Chapter 2 Impact of resin density and short-chain branching distribution on structural evolution and enhancement of tensile modulus of MDO-PE films 37

2.1 Introduction 38

2.2 Materials and methods 40

2.2.1 Materials 40

2.2.2 Characterization of base materials 41

2.2.3 Base sheets, lab scale MDO stretching and cast films 42

2.2.4 Characterization of base sheets and their MDO films 43

2.3 Results and discussion 46

2.3.1 Base resins characterizations 46

2.3.2 Compression molded base sheets, cast films and MDO films characterization 50

2.3.3 Investigation of tensile properties 59

2.4 Concluding remarks 68

2.5 Bibliography 69

2.6 Appendix 2 74

Chapter 3 Impact of molecular architecture and draw ratio on enhancement of targeted mechanical properties of MDO-PE films produced after blown film extrusion 77

3.1 Introduction 78

3.2 Materials and methods 82

3.3 Results and discussion 87

3.3.1 Molecular properties 87

3.3.2 Thermal properties of the blown films from blends 94

3.3.3 Material properties 94

3.3.3.1 Tensile properties of blown films of all five base resins 94

3.3.3.2 Molecular architecture effects on MDO-PE film tensile modulus 96

3.3.3.3 Process draw ratio effects on MDO-PE film tensile modulus 99

3.4 Concluding remarks 103

3.5 Bibliography 105

3.6 Appendix 3 111

Chapter 4 Assessing mechanical recyclability of blown films and integration of PCR for high modulus MDO-PE film application 113

4.1 Introduction 114

4.2 Materials and methods 117

4.3 Results and discussion 122

4.3.1 Molecular properties 122

4.3.2 Analysis of mechanical properties 130

4.3.3 Morphological analysis by SEM and AFM 133

4.4 Concluding remarks 136

4.5 Bibliography 138

4.6 Appendix 4 145

Chapter 5 Influence of uniaxial orientation on gas barrier, functional barrier, and optical properties of polyethylene films 147

5.1 Introduction 148

5.2 Materials and Methods 151
5.3 Results and Discussions 164
5.3.1 Oxygen barrier analysis 164
5.3.1.1 WAXS analysis of microstructural evolution during lab-scale MDO stretching 166
5.3.1.2 Analysis of the crystal orientations from WAXS 167
5.3.2 Functional barrier analysis 172
5.3.3 Optical properties analysis 176
5.4 Concluding remarks 178
5.5 Bibliography 180
5.6 Appendix 5 187

Chapter 6 Epilogue 189
6.1 General conclusions 190
6.2 Outlook for future research 191
6.3 Key challenges moving forward 193
6.4 Concluding thoughts 194
Curriculum Vitae 195
List of publications 197
Acknowledgements 199

List of abbreviations

AlOx	aluminium oxide
AFM	atomic force microscopy
BD	branching distribution
BOPE	biaxially oriented polyethylene
BUR	blow up ratio
CEFLEX	the circular economy of flexible packaging
DDR	draw down ratio
DIPN	2,6-diisopropyl naphthalene
DMS	dynamic mechanical spectroscopy
DPP	di-n-propyl phthalate
DR	draw ratio
DSC	differential scanning calorimetry
EPR	extended producer responsibility
EtOH	ethanol
EVA	ethylene vinyl acetate
EVOH	ethylene vinyl alcohol
FID	flame-ionization detector
FMCG	fast moving consumer goods
GPC	gel permeation chromatography
HDPE	high-density polyethylene
HMW	high molecular weight
IPA	isopropyl alcohol
iCCD	improved chemical composition distribution
LCB	long-chain branching
LDPE	low-density polyethylene
LLDPE	linear low-density polyethylene
MD	machine direction
MDO	machine direction oriented
MeOH	methanol
MFI	melt flow index
MWD	molecular weight distribution
MOAH	mineral oil aromatic hydrocarbon
MOSH	mineral oil saturated hydrocarbon
MPO	mixed polyolefin
MTBE	methyl-t-butyl ether

PA	polyamide
PCR	post-consumer recyclate
PE	polyethylene
PET	polyethylene terephthalate
PO	polyolefins
PP	polypropylene
PS	polystyrene
PVC	polyvinyl chloride
PVDC	polyvinylidene chloride
SAXS	small-angle x-ray scattering
SEM	scanning electron microscopy
SiOx	silicon oxide
SCB	short-chain branching
TBA	t-butyl anthracene
TCB	1,2,4-trichlorobenzene
TD	transverse direction
TD-GPC	triple detector gel permeation chromatography
TEM	transmission electron microscopy
TTBB	1,3,5-tri-t-butylbenzene
WAXS	wide angle x-ray scattering
XRD	x-ray diffraction

Chapter – 1

Introduction

1.1 Motivation

Plastic, an extensively used material in modern society, has witnessed a steady increase in production due to its cost-effectiveness, adaptability, and durability in various useful applications. However, the surge in plastic production has led to concerns regarding waste management and environmental sustainability. Should the current trajectory of plastics demand persist, projections indicate that global volumes of plastic waste could escalate to about 460 million tons annually by the year 2030 [1]. In 2020, within the EU27+3 countries, out of about 30 million tonnes of post-consumer plastic waste collected, merely 35% underwent recycling, while 42% was incinerated for energy recovery, and the remaining 23% was disposed of in landfills [2].

Nearly 44% of the overall plastics produced in the world are used in the packaging industry [3]. Flexible packaging accounts for about 45% of the overall plastic packaging in the EU [4]. The food and beverages segment was the most prominent sector for flexible packaging in 2023, commanding a substantial market share of about 55% globally [5]. Food packaging requires polymer films with specific properties, essential for preserving the quality and safety of food products. Typical application requirements are good barrier against permeation of oxygen and moisture for prolonging the food product shelf-life and good optical properties such as high clarity and low haze, for example, in the case of see-through packaging. In addition, the right balance of mechanical properties like modulus, stiffness, and tensile strength is also very critical to ensure integrity of the package and to allow easy handling. Further, appropriate sealing properties are required in the sealant layers to properly seal the package and safeguard the product from external environment. To combine all these properties, many flexible packages nowadays are composed of different layers made of different plastics [6].

Two major approaches utilized for plastic waste recycling are mechanical and chemical recycling with the former being the predominant approach. This method generally involves the collection, sorting, washing, grinding, extrusion and quenching of the material for re-pelletization without significantly changing the chemical structure [7], [8], [9]. A significant challenge in the mechanical recycling of flexible packaging plastic waste stems from its multi-layered structure, which often consists of diverse thin plastic film layers, such as polyethylene (PE), polypropylene (PP), polyamide (PA), polyethylene terephthalate (PET), and polyvinyl chloride (PVC), along with non-ferrous metals like aluminium. Mechanical recycling becomes ineffective for such multi-material, multi-layered configurations due to inherent chemical incompatibilities between the constituent layers [10], [11]. Thus, embedded heterogeneity of these flexible packaging systems poses significant challenges to current recycling systems, as conventional waste management infrastructure lacks the capability to effectively identify, sort, and recycle these complex materials, thereby undermining the principles of a circular economy [12], [13], [14], [15], [16].

In 2020, approximately 30 million tonnes of post-consumer plastic waste were collected across the EU27+3. Recycling rates for plastics were 13 times higher when waste was collected separately compared to mixed collection systems [2]. These significant statistics highlight the critical need to adopt mono-material flexible packaging designs, enabling post-

consumer flexible packaging waste to be collected through a single waste stream and subsequently recycled with greater efficiency.

Polyolefin-based mono-material flexible films are receiving attention as promising candidates for meeting the circular economy's demands due to their facile mechanical recyclability, as documented by several studies [17], [18], [19], [20].

Polyethylene (PE) is one of the most used polymers in flexible packaging applications as it can provide various useful structural and functional properties because of its distinct available types like low-density polyethylene (LDPE), linear low-density polyethylene (LLDPE), and high-density polyethylene (HDPE). There is promise in achieving both package functionality and recyclability when combining different types of PE into a single package. Traditionally, the outer layers of flexible packaging incorporate non-PE materials to achieve the required stiffness and barrier properties. However, recent advancements in PE film orientation techniques present opportunities to significantly enhance the mechanical and barrier properties. This advancement motivated the investigation of uniaxial orientation or machine direction orientation (MDO) of PE films to gain a deeper understanding of the structure-property relationships, facilitating the development of recyclable mono-material PE-based flexible packaging and supporting circular economy of flexible packaging systems.

1.2 Introduction to flexible packaging

Historically, the predominant materials utilized for food packaging have included glass, metals (such as aluminium foil, tin-free steel, and tin-plated steel), and various types of chemically composed paper [21], [22]. Metal packaging ensures a long shelf life by blocking light, moisture and oxygen, while glass offers inert protection with excellent barrier properties; however, both are increasingly being replaced by plastics based flexible packaging due to flexibility, tailored functionality, versatility, lightweight and less energy demanding nature because of utilization of much less materials, which further brings portability and user convenience [23].

Multi-material multi-layer flexible packaging, commonly used in fast-moving consumer goods (FMCG), integrates functionalities from various materials. These structures improve resource-use efficiency and barrier performance, resulting in extended shelf life. They are extensively utilized in food packaging due to their exceptional performance, including mechanical strength, thermal characteristics, and effective barriers against moisture, gases, and light. Typical examples of food products packaged in flexible packaging are presented in Figure 1.1.

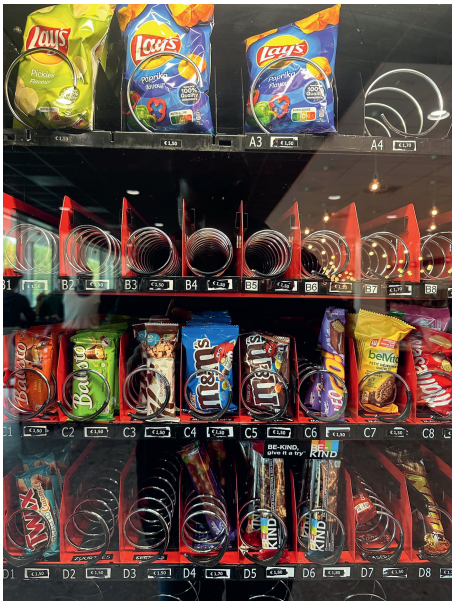

Figure 1.1 A vending machine containing some food products packaged in multilayer flexible packaging.

These configurations typically consist of multiple layers, sometimes as many as 11, providing optimal protection to the product, as well as required mechanical properties, sealing properties and printability [24]. A typical multilayer flexible packaging configuration with co-extruded or laminated outer, intermediate and inner layers is presented in Figure 1.2.

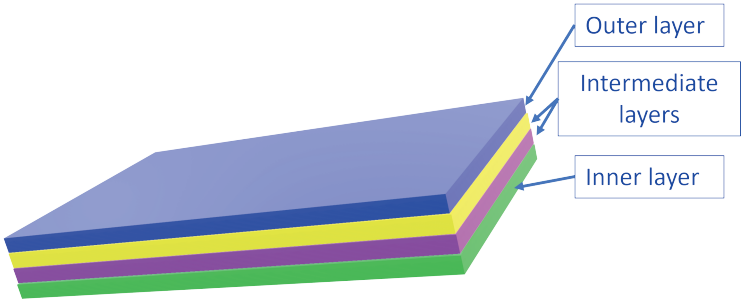

Figure 1.2 Typical multilayer flexible packaging configuration with outer, intermediate and inner layers.

These different layers contain mostly plastics-based material to provide tailored functionality to the whole package, which is briefly presented in Table 1.1.

Table 1.1 Commonly used material and functionalities provided by them in the outer, intermediate and inner layers of multilayer flexible packaging [25], [26].

	Outer layer	Intermediate layers	Inner layer
Functionalities Provided	Abuse resistance, heat resistance, stiffness, structural integrity, thermoforming, surface for printing, barrier properties (oxygen, moisture etc).	Adhesion, barrier properties (moisture, oxygen, light etc), recycled materials, printing, puncture resistance etc.	Sealing, Easy opening, barrier (oils,chemicals, oxygen, moisture)
Materials commonly used	HDPE, PET, PA, PP, PS (polystyrene), Paper etc.	PVDC (polyvinylidiene chloride), EVOH (Ethylene vinyl alcohol), metallized-PET, HDPE, Aluminium foil, PA, PU based adhesives etc.	LDPE, LLDPE, ionomers, mPE, EVA (Ethylene-vinyl acetate), VLDPE, etc.

Despite providing excellent tailored functionalities, multi-material multilayer flexible packaging embedded heterogeneity poses limitations on its mechanical recycling. Hence, the mono-material multi-layer structure is being explored.

1.3 Transition from multi-materials to PE based mono-materials

Mono-material multi-layer flexible packaging systems are emerging as a promising alternative to improve recycling rates. While multiple variations are often needed to maintain functionality, using a single chemical composition allows for better recycling outcomes. PE with its different grades (low-density, linear low-density and high-density) is widely used in several applications due to its versatility in structural and functional properties. Combining these PE grades in packaging can offer both functionality and recyclability. Traditionally, outer layers of flexible packaging use non-PE materials for stiffness and barrier properties, but advancements in PE film orientation techniques e.g. MDO operation have the potential to enhance the mechanical and barrier properties, supporting the development of recyclable mono-material PE based flexible packaging.

A typical example of mono-material PE based structural design, replacing the outer layer of conventional multilayer flexible packaging containing plastics like PET, PP, PA with MDO-PE film is represented in the Figure 1.3.

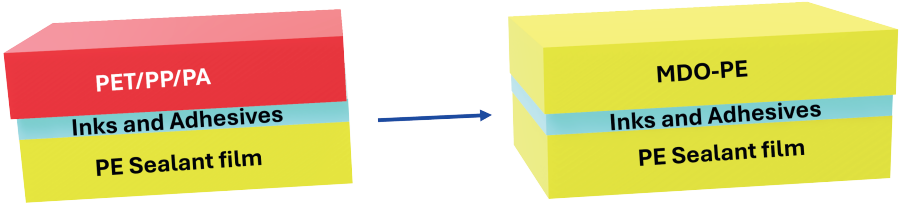

Figure 1.3 Structural design representation of substituting outer layer of conventional multilayer flexible packaging with MDO-PE film for recyclable PE based mono-material flexible packaging. (Note: The design presented in the figure is simplified for easier comprehension. In reality, each polymer film layer shown in the design can consist of multiple co-extruded or laminated layers, with thicknesses ranging from as thin as about 5 microns to a few hundred microns). Further details regarding MDO operation are introduced in the next section.

1.4 Introduction to MDO process

The MDO process (Figure 1.4) is a commercial process used in the flexible packaging industry in which the plastic film is stretched in the machine direction to a certain extent and at a certain rate and temperature which depend on the polymer's chemical nature [27]. Consequently, numerous enhancements are observed in the physical and barrier properties of the films for food packaging applications, including stiffness, tensile strength, gloss, oxygen barrier, and moisture barrier [28], [29], [30].

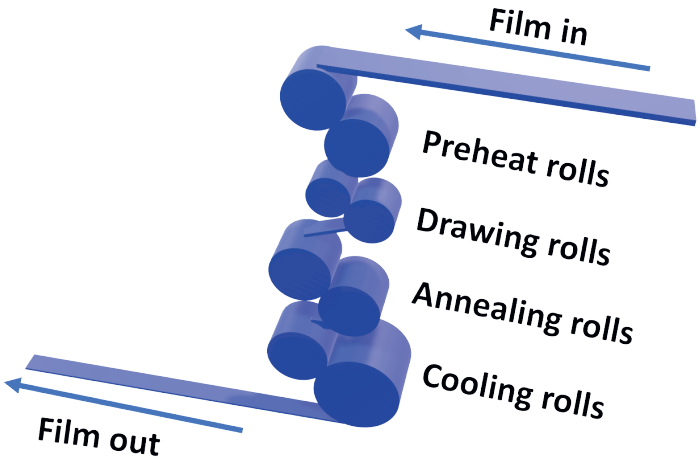

Figure 1.4 MDO process.

The precursor film utilized for MDO process is typically a co-extruded, multilayered blown or cast film. A standard coextrusion process entails subjecting two or more polymeric materials, typically in the form of granules or pellets to heat treatment, resulting in their melting [25], [31]. The molten polymer streams are subsequently merged and extruded as a unified structure comprising multiple layers [32].

The various rolls employed in different sections [27] of the MDO process, as depicted in Figure 1.4, through which the film web traverses during uniaxial orientation, are described along with their respective functionalities as follows:

Preheating: The preheat rolls serve to uniformly elevate the film temperature to the target orientation temperature necessary for stretching the film in the machine direction. This section also includes a nip roll to regulate the tension of the incoming web.

Drawing: The draw rolls positioned between the preheating and annealing rolls facilitate film stretching. It is done by setting different desired speeds to each of the two draw rolls, once the desired orienting temperature is achieved. The difference in speed of the two draw rolls provides uniaxial tensile forces required for stretching. These rolls have a smaller diameter compared to the preheat rolls, reducing the distance between the tangent points of adjacent rolls. The gap between the draw rolls is adjustable to achieve the desired film gauge, properties, and appearance. In this section, the film can be stretched multiple times. Additionally, nip rolls on the slower and faster rolls are employed for precise tension control.

Annealing: The annealing rolls heat-set the film by maintaining or increasing the process temperature for some period of time, stabilizing the property changes imparted during orientation and locking them into the film. The film stretching process results in polymer chains that are significantly displaced from their equilibrium state. These chains exhibit an inherent tendency to revert to their equilibrium configuration, a process that is associated with notable dimensional changes or shrinkage in the film. To mitigate this effect, annealing step is employed to "freeze" the orientation imparted during the stretching phase. This stabilization ensures that the film can subsequently withstand exposure to progressively higher temperatures without experiencing a loss of orientation or the associated decline in its mechanical properties [33]. This process also determines the extent of film shrinkage when subsequently exposed to heat. Nip rolls are used to maintain tension control.

Cooling: The cooling section consisting of cooling rolls uniformly lower the temperature of the oriented film to near ambient levels while preventing the formation of wrinkles or damage to the film surface. The cooling section typically consists of either a few large-diameter rolls or multiple small-diameter rolls, depending on the specific system configuration.

The ultimate film properties after MDO are not only dependent on plastic's structural and molecular parameters but also on key MDO process parameters like orientation temperature, stretch rate, draw ratio, annealing temperature and time. Therefore, process optimization is required to achieve desired targeted properties in MDO films. The key process parameters and their importance in MDO process is explained as follows:

Orientation temperature: Orientation temperature is the temperature at which the film is stretched and oriented. Typically, temperatures above the glass transition temperature and below the peak melting point temperature, at which macroscopic flow of the polymer is observed, are used. Usually with increasing orientation temperature, the stretch ratios which can be obtained without film breakage increase [33]. It should be noted that optimum stretching or orientation temperature is dependent on micro-structural aspects of the polymer, and it can be different for different applications to produce desired results.

Draw ratio or stretch ratio: The stretch ratio, also referred to as the draw ratio, is a fundamental process parameter in MDO. It serves as a measure of the total elongation experienced by a film or sheet during processing. Fundamentally, the stretch ratio is defined as the ratio of the final length of the material to its original length. In practical terms, it is typically expressed as the ratio of the output speed to the input speed within the draw section of the MDO process [34].

Stretch rate: The stretch rate, or strain rate, describes how quickly the length of a material increases during the stretching process. For example, in a universal tensile testing machine, it corresponds to the speed at which the moving gripper pulls the fixed sample, expressed as the change in length per unit of time relative to the original length of the sample. However, in a machine direction orientation (MDO) process, this concept is more complex because the "sample" is not stationary. Instead, the material continuously moves through the machine, and the stretching occurs over a defined distance within the system [34].

Annealing temperature and time: Annealing step freezes the orientation provided in the stretching step and stabilizes the film from further dimensional changes. The annealing temperature and time also influence properties of the final MDO film, and it can be different for different desired final properties [24]. Few academic and industrial studies on MDO and bi-axial orientation process technologies explicitly discuss the annealing temperature. Those that do comment on it either suggest same annealing temperature [29] as it is stretched or slightly higher [33], [35], [36]. Annealing semi-crystalline polymers at temperatures above their glass transition temperature (T_g) for appropriate time durations promotes crystal growth and additional crystallization [37]. Previous researchers have reported that the crystallinity of MDO-PE films increases with increasing annealing temperature, which further improved properties like modulus which are dependent on overall crystallinity [38]. This is possibly because above the glass transition temperature, where the amorphous region has molecular motion, additional crystallization occurs until the polymer reaches its equilibrium crystal content [37].

1.5 Introduction to amorphous and semi-crystalline polymers

Polymers are classified as either amorphous or semi-crystalline based on the arrangement of their molecular chains and the degree of order in their structure. These classifications significantly influence the physical, thermal, and mechanical properties of the material.

Amorphous polymers are characterized by a completely random arrangement of polymer chains, with no order or association within or between adjacent chains. The chains are distributed randomly throughout the polymer matrix [37], [39]. These polymers lack a distinct melting point, instead transitioning from a brittle, glassy state to a rubbery state as

heat is applied. Above the glass transition temperature, the material softens and behaves like an elastomeric or rubbery substance, while below T_g, it remains rigid and brittle. Common types of amorphous polymers include polyvinyl chloride (PVC), polystyrene (PS), acrylonitrile butadiene styrene (ABS), polycarbonate (PC), and polymethyl methacrylate (PMMA).

Many polymers contain some crystalline structure upon solidification of polymer melt [40]. These polymers are known as semi-crystalline polymers. Semicrystalline polymers contain both amorphous and crystalline regions within the same polymer matrix. In crystalline regions, polymer chains are arranged in a precise ordered pattern, formed by folding and stacking of the polymer chains that align in a consistent spatial arrangement, either within the same chain (fold back) or between adjacent chains [37], [39]. Semi-crystalline polymers exhibit both a distinct melting temperature (T_m) associated with the crystalline regions and a glass transition temperature associated with the amorphous regions. Polymers like PE, PP and nylon are common examples of semi-crystalline polymers. The density of semi-crystalline polymers increases with a higher degree of crystallinity due to the tighter packing of polymer chains in the crystalline regions.

The crystalline and amorphous regions in a semi-crystalline polymer are represented in Figure 1.5

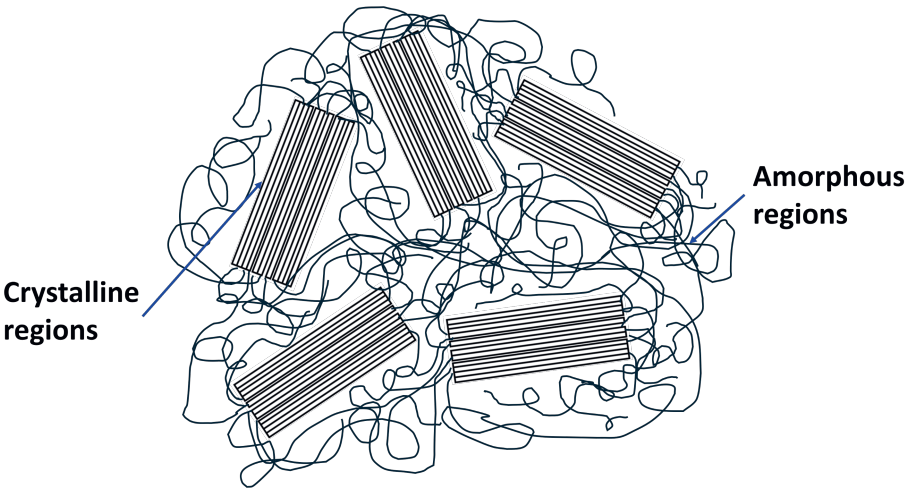

Figure 1.5 Representation of crystalline and amorphous region in a semi-crystalline polymer.

Regarding mechanical properties, the crystalline regions in semi-crystalline polymers contribute to increased stiffness and strength, whereas amorphous polymers exhibit high impact resistance [41], [42], [43].

1.6 Introduction to polyethylene and its different types

Polyethylene is a common plastic mostly used for packaging. It is a thermoplastic polymer produced by polymerization of ethylene (C2H4) gas. The generic chemical formula for polyethylene is –(C2H4)n–, where n is the degree of polymerization [44], [45]. The chemical structures of ethylene (monomer) and polyethylene (polymer) are represented in **Figure 1.6.**

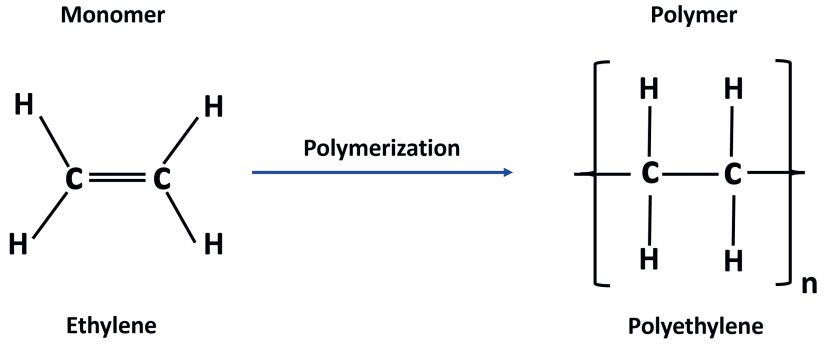

Figure 1.6 Polymerization of ethylene to polyethylene.

Polyethylene resins are broadly categorized into three main types [45], [46], [47], [48] : low-density polyethylene (LDPE), linear low-density polyethylene (LLDPE), and high-density polyethylene (HDPE). This classification is traditionally based on their density ranges, which are typically 0.915–0.940 g/cm³ for LDPE, 0.915–0.940 g/cm³ for LLDPE, and 0.940–0.970 g/cm³ for HDPE, although these limits may vary slightly depending on the source. Polyethylene resins with densities below 0.915 g/cm³ are often referred to as ultra-low-density polyethylene (ULDPE) or very-low-density polyethylene (VLDPE). Additionally, HDPE with molecular weight averages in the range of several million is classified as ultrahigh molecular weight polyethylene (UHMWPE).

The synthesis methods and structural characteristics of polyethylene types differ significantly. HDPE and LLDPE are synthesized using coordination catalysts, whereas LDPE is produced via free radical initiators under high-pressure conditions. LDPE is characterized by the presence of both short-chain branching (SCB) and long-chain branching (LCB), with LCB formed through transfer-to-polymer reactions and SCB resulting from backbiting reactions. In contrast, HDPE is essentially a linear molecule with minimal SCB and no LCB. LLDPE, also a linear molecule without LCB, exhibits a higher degree of SCB than HDPE. Short-chain branching in HDPE and LLDPE is generated through the copolymerization of α-olefins, which are introduced into the reactor as comonomers. The general representation of LDPE, LLDPE, and HDPE with different branching structures are presented in **Figure 1.7.**

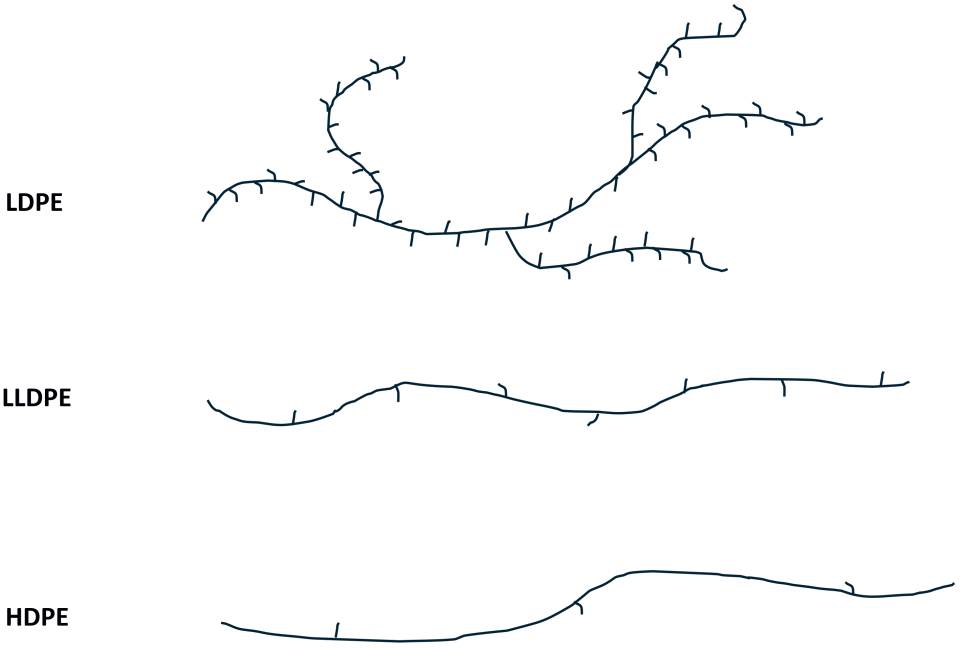

Figure 1.7 Classification of polyethylene types (LDPE, LLDPE and HDPE) according to branching structure.

The physical properties of the PE depend significantly on resin parameters such as the extent and type of branching, crystal structure and average molecular weight.

1.7 Insights into PE microstructure

PE typically demonstrates a semicrystalline microstructure. The degree of crystallinity is influenced by specific molecular characteristics, such as the degree of branching and the length of the branches [49]. The most prevalent higher-order structure observed in crystalline polymers is referred to as a spherulite [50].

When a polymer melt solidifies without simultaneous deformation, a spherulitic aggregate containing the crystalline matter is formed, which is mechanically isotropic [49], [51]. Each spherulite consists of a radial assembly of thin crystalline lamellae which are separated by amorphous layers. A transmission electron microscopy (TEM) image of PE microstructure with spherulites is represented in Figure 1.8.

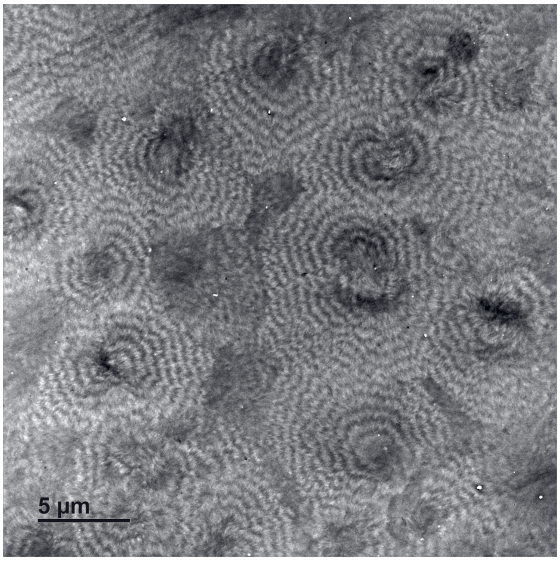

Figure 1.8 A transmission electron microscopy (TEM) image PE microstructure with spherulites. (Note: Image taken from a self-produced sample used for the investigations in this thesis)

The application of external flow during the solidification of semi-crystalline polymer melts is a well-established method for modifying the crystallization behavior and resulting structure of polymers. This process can induce a significant transformation in crystalline morphology, shifting from isotropic spherulites to highly oriented shish-kebab structures [52], [53], [54], [55], [56]. Shish-kebab morphology (Figure 1.9) consists of a central, thread-like core (shish) surrounded by parallel-aligned, disk-like lamellae (kebab).

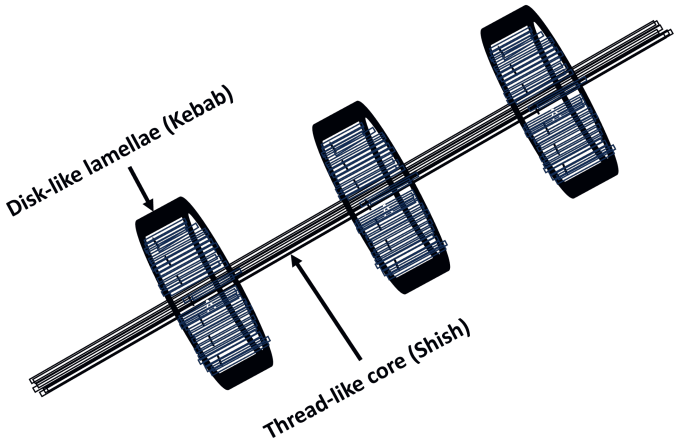

Figure 1.9 A representative figure of shish-kebab morphology.

This structure has garnered significant attention due to reinforcement on material stiffness and strength towards fibre axis [52], [57], [58].

1.8 Methods used to fabricate PE films during investigations

For initial lab-scale investigations in this thesis, PE resins were processed in a compression molding machine to produce compression molded base sheets, which were further used as precursor material for lab-scale MDO process.

Compression molding is a widely utilized polymer processing technique that involves shaping thermoplastic or thermosetting resins into desired structures. These resins can be introduced in either free-flowing granular forms, such as pellets, or as viscous materials. The process begins by placing the polymer material between two plates, where it is subjected to high temperatures and pressure using a hydraulic press [59]. This combination of heat and pressure melts the material and molds it into the desired shape. Subsequently, the mold is cooled by circulating cooling fluids, such as water, at a controlled cooling rate to achieve the desired morphology. Compression molding is a cost-effective method, particularly suitable for small-scale batch wise production. Notably, polymer sheets produced through this process are generally mechanically isotropic due to the absence of significant melt flow during molding. The pictorial representation of compression molding is presented in Figure 1.10.

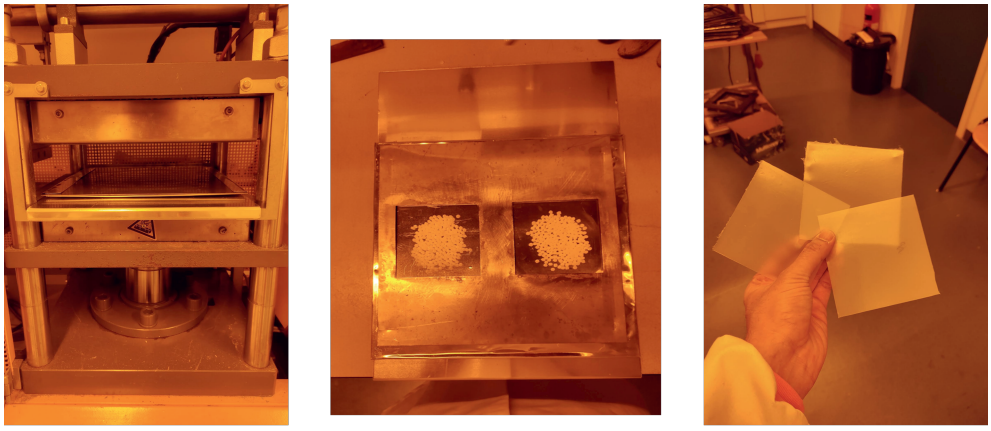

Figure 1.10 Compression molding process. **a)** hydraulic press, **b)** charge kept inside the molds, **c)** fabricated PE compression molded sheets.

To transition from a lab-scale to a pilot-scale setup, two widely employed industrial film production techniques, cast film and blown film extrusion processes, were utilized to fabricate monolayered PE films. These processes were chosen for their ability to produce films with distinct molecular orientations resulting from variations in melt flow dynamics and solidification mechanisms. The resulting films were subsequently analysed to evaluate

their physical properties. Additionally, blown films served as precursor materials for the pilot-scale MDO process.

An extruder is a machine used in the production of plastic products by melting raw plastic materials, typically in the form of pellets, granules, or powder, and shaping them into a continuous profile [60], [61]. The process begins with plastic resins being loaded into a feed hopper, which feeds the material into a heated barrel containing a screw. As the screw rotates, it moves the material along the barrel, which is heated to a temperature above the polymer's melting point, causing the plastic to melt. A temperature profile is usually established along the barrel, with the temperature gradually increasing from the rear, where the material enters, to the front. This controlled temperature increase ensures that the plastic melts progressively, reducing the risk of overheating and preventing thermal degradation. Once the plastic is fully molten, it flows into the die located at the front of the barrel. The die shapes the molten plastic into the desired profile by evenly distributing the material as it transitions from a cylindrical form to the specific shape of the final product.

In the cast film extrusion process, molten polymer is extruded and rapidly quenched on rotating, chilled, and highly polished rolls to form a polymer film [62]. This continuous process operates at high output rates, enabling large-scale production. The draw-down ratio and film thickness are determined by the speed of the casting roll. Following quenching, the film is transferred to a stripping roll, which rotates in the opposite direction to the casting roll. The film then passes through a series of rolls before being wound onto a roller. This process typically induces slight uniaxial molecular orientations within the film. The pictorial representation of a pilot scale cast film line is presented in Figure 1.11.

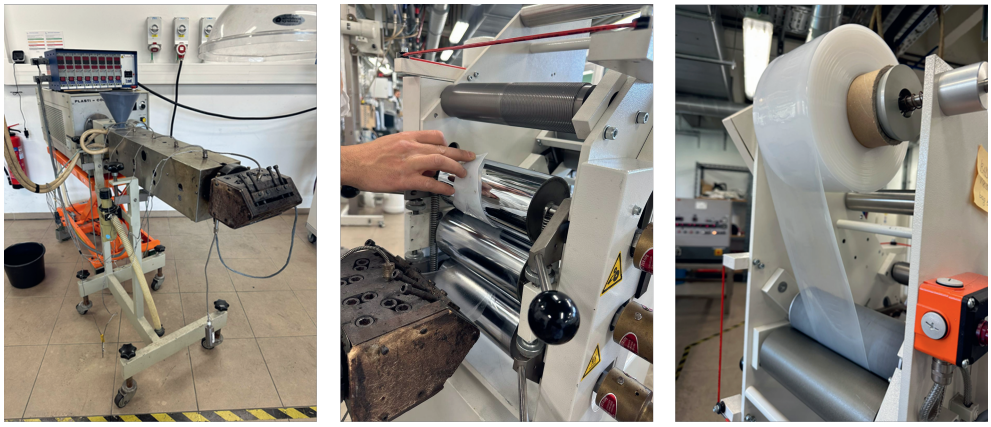

a) **b)** **c)**

Figure 1.11 Pilot-scale cast film process. **a)** extruder, **b)** molten extrudate being quenched on chilled polished rolls, and **c)** film wind-up station**.**

Blown film extrusion [63], [64], [65] is a widely used polymer processing method, with several billion kilograms of polymer, primarily polyethylene, being processed annually using

this technique. In this process, the molten resin is forced through a circular die head, shaping the resin into a tubular form. Air is introduced through a hole in the centre of the die, inflating the tube like a balloon and causing it to expand while maintaining its cylindrical shape. This stage is referred to as bubble or tube formation. Cooling of the hot film is achieved using a high-speed air ring mounted above the die, which blows air onto the expanding film.

The final thickness of the film is influenced by the size of the die, speed of the nip rollers and the extrusion speed. As the tube expands, it is pulled upward and cooled simultaneously by the air, which solidifies the molten resin to form a stable film structure. The speed at which the film is drawn from the die determines its orientation and mechanical properties. Stretching the film during this stage improves its strength, clarity, and barrier properties. Once the film has been cooled and solidified, it is drawn away from the die using nip rollers or collapsing frames, which regulate the tension and speed of the process. Finally, the film is wound onto a roll.

Blow-up ratio (BUR) and draw-down ratio (DDR) are critical parameters in the film-blowing process, influencing the final properties of the produced film. BUR is defined as the ratio of the maximum tube diameter to the diameter of the circular die head, reflecting the extent to which the extruded tube expands. DDR, on the other hand, quantifies the reduction in film thickness during processing and is expressed as the ratio of the annular die gap width, from which the melt exits, to the final film thickness times BUR. A BUR greater than 1 indicates that the extruded bubble or tube has expanded beyond the diameter of the die orifice, resulting in film thinning and imparting molecular orientation in the transverse direction (TD). Similarly, a DDR greater than 1 signifies that the melt is drawn away from the die at a higher rate than its extrusion, leading to film thinning and molecular orientation in the machine direction (MD). Thus, blown film extrusion can generally introduce biaxial or random molecular orientations in the prepared blown films according to the used BUR and DDR. The pictorial representation of a pilot scale blown film line is presented in Figure 1.12.

Figure 1.12 Pilot- scale blown film process. **a)** formation of tube or bubble, and **b)** film wind-up.

The MDO process was performed on prepared precursor PE films using both lab-scale and pilot-scale MDO setups. Detailed descriptions of these setups are provided in subsequent Chapters. The lab-scale setup utilized compression-molded base sheets as the precursor material, while the pilot-scale MDO setup was capable of processing blown films as precursor material. This approach facilitated a comprehensive understanding of the orientations induced by the MDO process in various types of differently oriented precursor materials.

1.9 Impact of MDO on PE microstructure

The MDO process involves applying uniaxial tensile forces to stretch the preheated polymer web between the drawing rolls through precise speed adjustment. This operation is conducted at elevated temperatures, typically within a range above the plastic glass transition temperature and below its peak melting temperature. Generally, as the orientation temperature increases, higher stretch or draw ratios can be achieved without film breakage [33].

An important distinction to note is that, unlike the polymer melt flow-induced orientation described in the previous section, the stretching and orientation in the MDO process occur in a semi-solid state at temperatures below the polymer's peak melting temperature, rather than in the fully molten state. The work performed in this thesis examines and compares the orientation induced in polyethylene, both in the molten state by melt flow (cast film or blown film) and in the semi-solid state by MDO, providing a comprehensive discussion of the results.

The structural evolution during the MDO process is generally characterized by a transition from a lamellar to a fibrillar morphology (**Figure 1.15**), followed by further refinement of the fibrillar structure at high draw ratios. Initially, the amorphous regions undergo elastic deformation, after which orientation occurs through a complex plastic deformation mechanism. During tensile drawing, stresses are often distributed non-homogeneously across the semi-crystalline regions [66].

During the initial stages of deformation, plastic deformation in crystalline regions of semi-crystalline polymers is primarily governed by fine slip mechanisms [67], [68]. In the fine slip mechanism, a small magnitude of deformation is uniformly distributed across a large number of slip planes. At higher strain levels, fine slip is accompanied by coarse slip (Figure 1.13), characterized by large deformations localized on few slip planes, leading to the fragmentation of crystalline lamellae [69], [70].

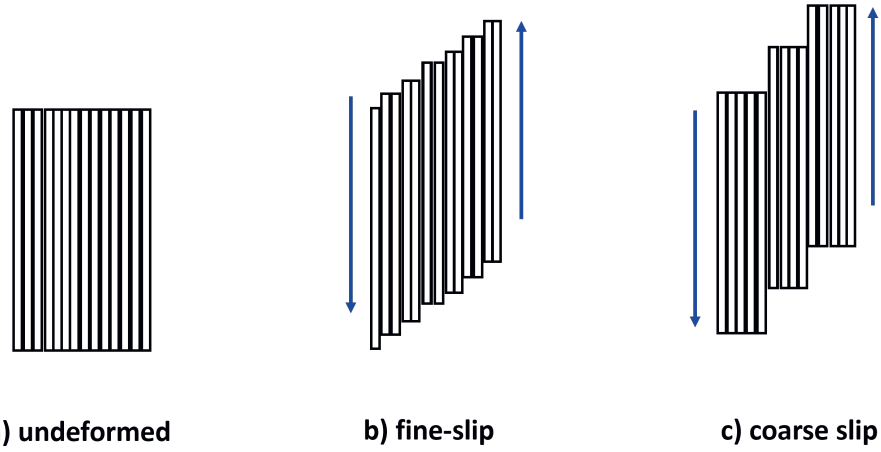

Figure 1.13 Plastic deformation due to crystallographic slip, a) undeformed, b) fine slip at low strains, c) coarse slip at higher strains.

At high draw ratios, crystalline segments undergo further fragmentation and ultimately separate into a fibrillar structure (Figure 1.14). The entangled polymer chains in the amorphous regions resist this process, resulting in strain-induced orientation and crystallization, which results in a strain-hardening effect.

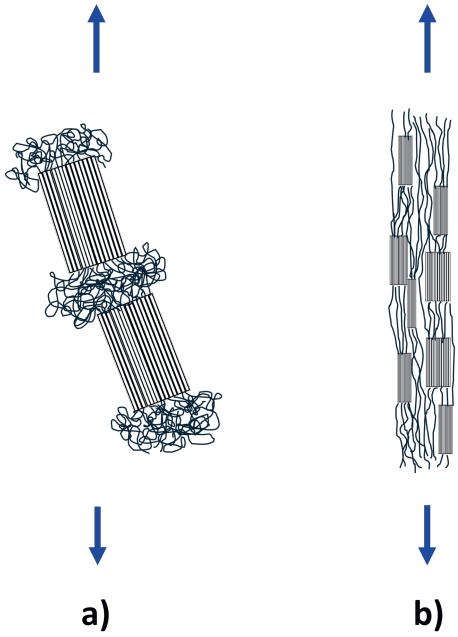

Figure 1.14 Morphology change in semi-crystalline polymer microstructure from **a)** undeformed (at the start of tensile loading) to **b)** formation of fibrillar structure at high draw ratios with oriented amorphous phase. (Note: Blue arrows indicating the tensile load)

The impact of MDO operation on a randomly oriented semi-crystalline PE precursor blown film morphology is demonstrated by scanning electron microscopy (SEM) images from low to moderate to high draw ratios in Figure 1.15. The SEM images with increasing draw ratio shows the destruction of randomly oriented microstructure in precursor blown film (Figure 1.15 a) to fibril development oriented towards the stretch direction in high draw ratio MDO film (Figure 1.15 d).

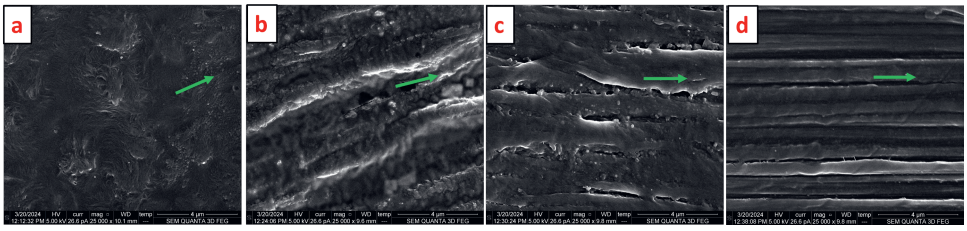

Figure 1.15 Representative SEM images demonstrating morphology change by MDO operation in PE film from **a)** randomly oriented precursor blown PE film **b)** MDO-PE film at low draw ratio **c)** at moderate draw ratio and **d)** at high draw ratio. (Note 1: green arrow is representing the stretch direction. Note 2: Images taken from self-produced samples used for the investigations in this thesis)

MDO operation on semi-crystalline PE has shown enhancement in overall crystallinity due to disintegration and fibrillation of the initial crystalline microstructure with strain induced crystallization in amorphous phase during stretching along with highly oriented crystalline and amorphous microstructure towards the stretch direction [71], [72]. This enhanced crystallinity and high molecular orientation towards the stretch direction shows potential for enhancement of targeted properties in MDO-PE films to be integrated as outer layers in PE-based mono-material flexible packaging systems.

Nonetheless, questions remain regarding whether MDO-PE films can achieve comparable performance in terms of critical mechanical properties, such as modulus and stiffness, as well as barrier properties, specifically oxygen permeability, when compared to conventionally used plastics like PET and polyamide (PA) for outer layers in flexible packaging. This thesis addresses these challenges by providing a comprehensive investigation of the structure-property relationships in MDO-PE films.

1.10 Scope and outline of this thesis

The experimental work in this thesis investigates the influence of key PE resin characteristics (e.g., density, average molecular weight, branching, branching distribution, comonomer content, molecular weight distribution) and MDO process parameters (e.g., draw ratio) on the targeted mechanical, barrier and optical properties of MDO-PE films. A comprehensive understanding of structure-property relationships is developed through extensive microstructural characterizations and morphological analysis. Additionally, the mechanical recyclability of virgin PE films and the incorporation of post-consumer recyclate (PCR) material with virgin materials for subsequent MDO operation is analysed and investigated for high performance applications.

As previously discussed, conventional multilayer flexible packaging often utilizes non-PE materials, such as PET or PA, to achieve the required stiffness and gas barrier properties against permeants like oxygen. While PE can achieve a certain level of modulus by increasing resin density, this improvement is typically insufficient to meet the desired stiffness levels. Stiffness is directly related to the modulus of the material, and an enhancement in the modulus of PE films results in improved stiffness. Modulus and stiffness are related but distinct concepts that characterize how materials and structures respond to deformation. Modulus, such as Young's modulus, is an intrinsic material property that quantifies the relationship between stress and strain during elastic deformation, providing a measure of a material's elasticity. In contrast, stiffness refers to a structure's ability to resist deformation under an applied force and depends not only on the material's modulus but also on the geometry of the structure. Adequate stiffness in polymer films is crucial for various packaging operations, including printing, lamination, and the efficient operation of packaging machinery. Insufficient stiffness can lead to issues such as film sagging during processing and handling on packaging lines.

Various previous researchers have studied semi-solid state stretching of PE to produce ultra-drawn high modulus fibres and films [73], [74], [75], [76], [77]. Existing research

recognizes the critical role played by MDO process parameters such as orientation temperature, draw ratio, stretch rate, and annealing time on final mechanical properties attained by MDO films. Tabatabaei *et al*. [78] studied the effect of machine direction orientation process conditions on the mechanical properties of HDPE films and found that modulus decreased around the relatively low draw ratio of 6.5 and then started to increase beyond that. The modulus of the films also increased with rising annealing temperature and decreased slightly with increase in stretching orientation temperature near the melting point. Chen *et al*. [79] also reported about 2 times increment in tensile modulus and about 4.5 times in tensile strength in sequential biaxial orientation (first machine direction and then transverse direction) of polyethylene films with an increase in draw ratio. However, only a few studies have systematically investigated the role of resin parameters such as density, short chain branching (SCB), branching distribution (BD), average molecular weight, and polydispersity on final mechanical properties attained by the MDO-PE films.

Thus, the influence of key PE resin parameters, specifically resin density, SCB distribution coupled with molecular weight, on lab-scale MDO film stretching under fixed MDO process conditions of orientation temperature, stretch rate, annealing time, and draw ratio was investigated in Chapter 2. Five distinct PE resins and their blends were utilized to produce compression-molded base sheets, which were subsequently stretched into MDO-PE films using a lab-scale setup. Blends were prepared to achieve intermediate densities and crystallinities to facilitate the study. Comprehensive characterization of the resins and blends was conducted using shear rheology, GPC (gel permeation chromatography), DSC (differential scanning calorimetry), and iCCD (improved chemical composition distribution) analyses. Tensile tests were performed on the films both before and after machine direction stretching to evaluate tensile modulus. Structural analysis of the shape, size, and orientation of crystals was carried out using SAXS (small-angle X-ray scattering) and WAXS (wide-angle X-ray scattering). Surface morphology was examined through AFM (atomic force microscopy).

In Chapter 2, compression-molded base sheets, which are typically mechanically isotropic, were used as the starting material to produce lab-scale MDO-PE films. This Chapter provided critical insights into the structural evolutions occurring during the MDO process using a lab-scale setup. However, at an industrial scale, the MDO process is performed on precursor cast or blown films, which are generally mechanically anisotropic. Among polymer processing methods, blown film extrusion is one of the most widely utilized, with an annual processing capacity of billions of pounds of polymer, predominantly polyethylene. Integrating the MDO process with blown film extrusion offers the potential to enhance the properties of packaging materials while facilitating the transition to mono-material packaging, thereby improving recyclability and advancing polymer circularity. Consequently, subsequent MDO studies were scaled up from a lab-scale setup to a pilot-scale setup to produce MDO-PE films. In this pilot-scale setup, blown films produced using a pilot-scale blown film extrusion line were used as precursor materials to produce MDO-PE films on a pilot-scale MDO setup.

Molecular properties of polymers play a significant role in the MDO process and mostly determine the improved tensile properties after drawing. A few studies have discussed how the molecular weight and process draw ratio affects the oriented PE drawing behaviour and tensile properties. Jarecki *et al.* studied ultra-high modulus polyethylene and found that the high-molecular-weight fraction in ultra-high modulus polyethylene imparts the high modulus, while the low-molecular-weight fraction facilitates chain alignment and suppresses internal voiding during drawing at elevated temperatures [80], [81]. Andrews and Ward [82] studied cold drawing HDPE and reported the natural draw ratio increased as molecular weight decreased. They defined natural draw ratio as the ratio of the cross-sectional areas before and after drawing. Séguéla [83] in his review also mentioned the draw ratio in the stable neck region of semi-crystalline polymers as natural draw ratio. High natural draw ratios result in higher microstructure fibrillation resulting in higher overall crystallinity and highly oriented microstructure towards the stretch direction which further increases the tensile modulus. Sherman *et al.* [84] studied the microstructure of high modulus solid state extruded polyethylene and reported that axial tensile modulus increased almost linearly with an increase in draw ratio.

These prior studies gave insights regarding how molecular weight averages and polydispersity influence PE drawing, orientation and mechanical properties. However, in most of these studies, PE with isotropic structure before drawing in the form of compression molded sheets were used as the starting material, which is not always relevant for packaging materials. The influence of MDO on the blown film with pre-existing random orientation has not been yet explored extensively. After gaining insights on impact of resin density and SCB distribution in Chapter 2, focus was to investigate the impact of other key resin molecular properties and MDO process parameter of draw ratio. Hence, the influence of PE molecular properties such as number-average molecular weight (M_n), weight-average molecular weight (M_w), polydispersity, comonomer content, as well as the effects of the key MDO process parameter of draw ratio, on the structural evolution, morphology and mechanical properties of MDO-PE films intended for use as outer layers in mono-material flexible packaging design was investigated in Chapter 3. Further, techniques such as GPC, iCCD, DSC, FTIR, SEM and AFM were leveraged for detailed molecular characterizations and morphological analysis.

One of the important aspects of the work performed in this thesis was to experimentally validate the mechanical recyclability of mono-materials fractions. Polyolefins tend to undergo thermo-mechanical degradation during compounding and conversion into final products, leading to alterations of the molecular properties like molar mass, branching degree and molar mass distribution [85]. Thermo-mechanical and thermo-oxidative degradation processes during processing expose polymeric materials to chain scission, branching, and crosslinking reactions [86]. Linear PE grades such as LLDPE and HDPE mainly experience degradation through chain scission [87], [88], [89], [90], [91]. Blending recycled and virgin polyethylene stands as a recognized method for modifying the properties of recycled material [92].

Re-extrusion is a widely used method for recycling mono-material fractions. Re-extrusion involves shredding the material into small flakes after sorting and cleaning which is then used as an input material in an extruder to re-pelletize the material. The re-pelletized resins can be further used to make new materials. Blending recycled and virgin polyethylene stands as a recognized method for modifying the properties of recycled material. While numerous studies have investigated the recycling and degradation of polyethylene during processing, particularly those used in packaging applications [92], [93], [94], [95], [96], research on blown films containing recycled polyethylene [97] remains limited [86]. Thus, the mechanical recyclability of virgin PE blown films and the incorporation of post-consumer recyclate (PCR) for in-line MDO-PE film applications, with a focus on targeted mechanical properties of modulus and stiffness for the outer layer of mono-material PE-based flexible packaging design was investigated in Chapter 4.

In the first set of experiments in Chapter 4, the analysis of mechanical re-processability of virgin blown films was investigated. Blown films were produced using equal fractions of two virgin PE resins. These films were shredded, re-pelletized, and reprocessed to create new blown films. The process was repeated twice, resulting in three sets: virgin (V), reprocessed once (R1), and reprocessed twice (R2). MDO films were then made from each set, and their mechanical properties were assessed. In the second set of experiments, PCR material was blended with virgin materials at two different weight percentages to study its effect on the mechanical properties of blown and MDO films. It was expected that PCR integration could impact modulus and stiffness due to its composition and potential contamination or degradation from previous lifecycle. Extensive characterizations for the analysis was performed using techniques like GPC, FTIR, DSC, SEM, AFM and tensile testing.

The primary purpose of food packaging is to preserve food quality from production to consumer use [98]. Effective barrier properties are essential for plastic films in food packaging to preserve nutritional and organoleptic qualities as well as safety of the product [99]. Thus, after investigating key mechanical properties, the focus was to investigate vital barrier properties (oxygen barrier, functional barrier (barrier against migration of harmful substances like MOSH (mineral oil saturated hydrocarbon) and MOAH (mineral oil aromatic hydrocarbons) from recycled material)) and optical properties of MDO-PE films, intended to be used as outer layers in mono-material PE based flexible packaging.

A good barrier against oxygen is required to prevent the spoilage of food products inside the package, and for prolonging the shelf life of the food product. A major issue with PE is its high oxygen permeability. However, it has been demonstrated in the previous studies that oxygen as well as moisture barrier of PE films can be enhanced by MDO operation [28], [29], [30]. Multiple factors have been suggested to account for the enhanced barrier properties observed in oriented polymers. These include reduced free volume in amorphous regions, increased diffusion path tortuosity due to crystal alignment, and higher overall crystallinity, along with denser packing and microfibrillar crystal formation [30], [100], [101], [102], [103]. Chatterjee *et al.* [30] investigated water vapor barrier of HDPE MDO films and reported that

initially the oriented films demonstrated an increase in the water vapor transport rate with increasing draw ratio and beyond a critical draw ratio it gradually decreased. Breese *et al.* [103] investigated effect of MDO on the moisture and oxygen barrier properties of high molecular weight polyethylene (HMW-PE) films and reported that a significant decrease in both moisture and oxygen transmission rates is observed with the machine direction orientation of homopolymer HMW-PE films. They further reported that intermediate and lower density films do not show such a significant decrease and actually present a maximum at moderate draw ratios where the transmission rate is greater after orientation than that of the undrawn sample.

Most of the studies in literature to investigate the barrier properties are based on MDO process parameters like draw ratio but only few studies focus on the role of structural parameters of the resins like resin density and correlate it with changes in structural morphology during stretching. Thus, the effects of MDO on the barrier and optical properties of PE films for applications in PE-based mono-material flexible packaging was investigated in Chapter 5. In the first and second set of experiments of this Chapter, oxygen and functional barrier of the MDO films was evaluated and further correlated with resin density and film morphology while keeping the other MDO process parameters constant like draw ratio, orientation temperature and stretch rate. Characterization techniques such as oxygen permeability, GC-FID (gas chromatography), DSC and WAXS were leveraged for the analysis.

The optical properties of polymers, including gloss, transparency, clarity, haze, color, surface appearance, and refractive index, are closely associated with the quality and visual performance of plastic products [104]. The internal and surface microstructure of the film collectively plays a crucial role in determining its overall optical properties [105]. Consumers frequently base their purchasing decisions primarily on the visual appearance of a product. Packaging with high gloss enhances the appeal of the package and increases the likelihood of consumer purchase [106]. Optical transparency enables consumers to assess food freshness and appearance through visual inspection before purchasing[22], [107]. Additionally, transparency is crucial for integrating optical sensing systems into the development of intelligent food packaging materials [22], [108]. Hatfield *et al.* [29], [109] studied properties of medium molecular weight MDO HDPE films and reported gloss increased by over 70 percent at a draw ratio of 6:1. Chatterjee *et al.* [30] studied barrier and optical properties of MDO HDPE films and reported that MD orientation significantly reduced the total haze of the stretched films compared to blown films at similar thickness. Thus lastly, in the third set of experiments of Chapter 5, impact of orientation was evaluated on optical properties like clarity, haze and gloss to assess optical performance of MDO-PE films. Characterization techniques such as UV-VIS spectroscopy, DSC, SEM and AFM were utilized for the comprehensive structure-property analysis.

The schematic overview of the thesis is presented as follows:

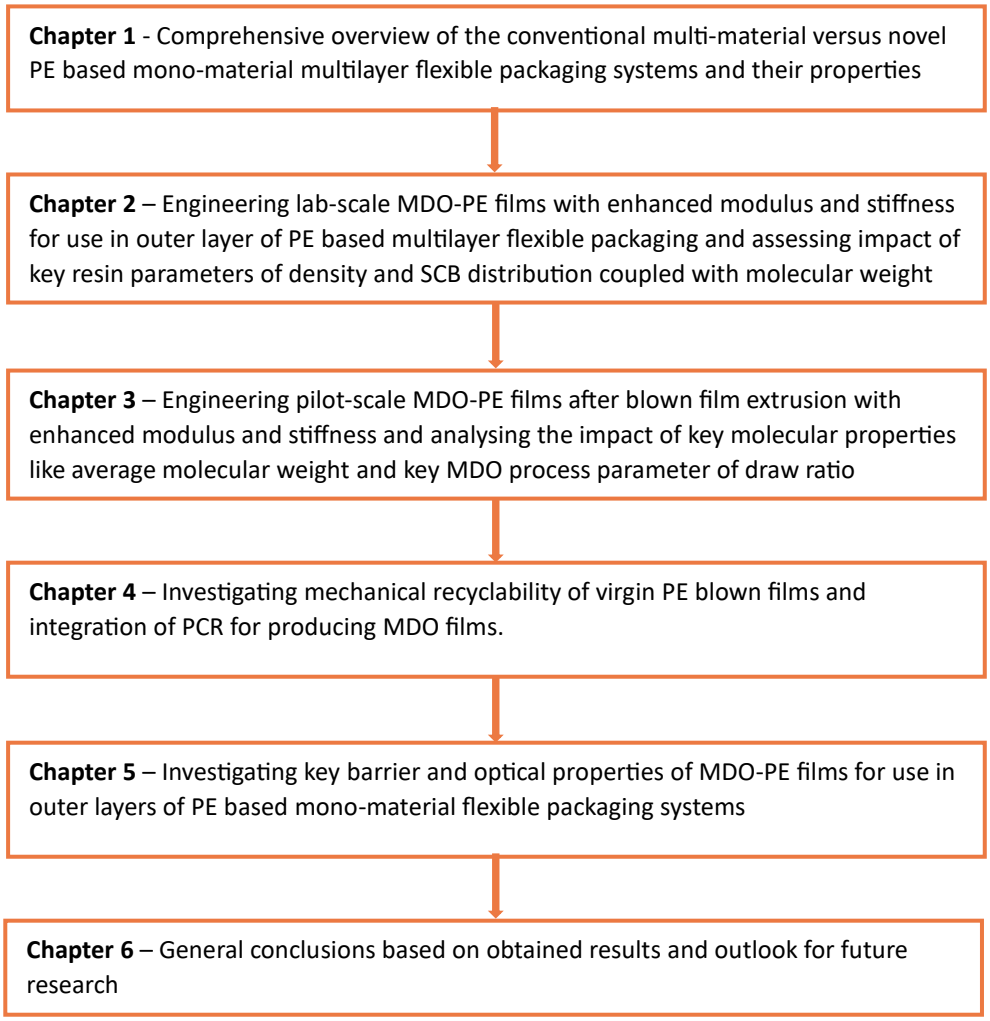

1.11 Bibliography

[1] "Recycling and the future of the plastics industry | McKinsey." Accessed: Sep. 23, 2024. [Online]. Available: https://www.mckinsey.com/industries/chemicals/our-insights/how-plastics-waste-recycling-could-transform-the-chemical-industry

[2] "Plastics - the Facts 2022 • Plastics Europe." Accessed: Sep. 23, 2024. [Online]. Available: https://plasticseurope.org/knowledge-hub/plastics-the-facts-2022/

[3] "Plastics-the Facts 2022 OCTOBER 2022, Plastics Europe." Accessed: Feb. 01, 2024. [Online]. Available: https://plasticseurope.org/knowledge-hub/plastics-the-facts-2022/

[4] "ETC/CE Report 4/2022 Flexible plastics in Europe's circular economy — Eionet Portal." Accessed: Apr. 08, 2024. [Online]. Available: https://www.eionet.europa.eu/etcs/etc-ce/products/etc-ce-products/etc-ce-report-4-2022-flexible-plastics-in-europe2019s-circular-economy

[5] "Flexible Packaging Market Size and Share Report, 2030." Accessed: Feb. 01, 2024. [Online]. Available: https://www.grandviewresearch.com/industry-analysis/global-flexible-packaging-market

[6] V. Ratta, G. L. Wilkes, and T. K. Su, "Structure–property-processing investigations of the tenter-frame process for making biaxially oriented HDPE film. I. Base sheet and draw along the MD," *Polymer (Guildf)*, vol. 42, no. 21, pp. 9059–9071, Oct. 2001, doi: 10.1016/S0032-3861(01)00387-1.

[7] D. Jubinville, E. Esmizadeh, S. Saikrishnan, C. Tzoganakis, and T. H. Mekonnen, "A comprehensive review of global production and recycling methods of polyolefin (PO) based products and their post-recycling applications," *Sustainable Materials and Technologies*, vol. 25, 2020, [Online]. Available: https://api.semanticscholar.org/CorpusID:225221815

[8] S. M. Al-Salem, P. Lettieri, and J. Baeyens, "Recycling and recovery routes of plastic solid waste (PSW): A review," *Waste Management*, vol. 29, no. 10, pp. 2625–2643, 2009, doi: https://doi.org/10.1016/j.wasman.2009.06.004.

[9] K. Ragaert, L. Delva, and K. Van Geem, "Mechanical and chemical recycling of solid plastic waste," *Waste Management*, vol. 69, pp. 24–58, 2017, doi: https://doi.org/10.1016/j.wasman.2017.07.044.

[10] Y. Ma, "Changing Tetra Pak: From waste to resource," *Sci Prog*, vol. 101, no. 2, pp. 161–170, Jun. 2018, doi: 10.3184/003685018x15215434299329.

[11] C. Y. Barlow and D. C. Morgan, "Polymer film packaging for food: An environmental assessment," 2013. doi: 10.1016/j.resconrec.2013.07.003.

[12] C. T. de M. Soares, M. Ek, E. Östmark, M. Gällstedt, and S. Karlsson, "Recycling of multi-material multilayer plastic packaging: Current trends and future scenarios," *Resour Conserv Recycl*, vol. 176, Jan. 2022, doi: 10.1016/j.resconrec.2021.105905.

[13] T. W. Walker *et al.*, "Recycling of multilayer plastic packaging materials by solvent-targeted recovery and precipitation," 2020. [Online]. Available: https://www.science.org

[14] K. Kaiser, M. Schmid, and M. Schlummer, "Recycling of polymer-based multilayer packaging: A review," 2018, *MDPI AG*. doi: 10.3390/recycling3010001.

[15] L. S. Dilkes-Hoffman, J. L. Lane, T. Grant, S. Pratt, P. A. Lant, and B. Laycock, "Environmental impact of biodegradable food packaging when considering food waste," *J Clean Prod*, vol. 180, pp. 325–334, Apr. 2018, doi: 10.1016/j.jclepro.2018.01.169.

[16] G. Faraca and T. Astrup, "Plastic waste from recycling centres: Characterisation and evaluation of plastic recyclability," *Waste Management*, vol. 95, pp. 388–398, Jul. 2019, doi: 10.1016/j.wasman.2019.06.038.

[17] K. Ragaert *et al.*, "Design from recycling: A complex mixed plastic waste case study," *Resour Conserv Recycl*, vol. 155, Apr. 2020, doi: 10.1016/j.resconrec.2019.104646.

[18] V. Srebrenkoska, G. B. Gaceva, M. Avella, M. E. Ericco, and G. Gentile, "Utilization of recycled polypropylene for production of Eco-composites," *Polymer - Plastics Technology and Engineering*, vol. 48, no. 11, pp. 1113–1120, 2009, doi: 10.1080/03602550903147247.

[19] M. Guerritore *et al.*, "Recyclable-by-design mono-material flexible packaging with high barrier properties realized through graphene hybrid coatings," *Resour Conserv Recycl*, vol. 179, Apr. 2022, doi: 10.1016/j.resconrec.2021.106126.

[20] C. Y. Barlow and D. C. Morgan, "Polymer film packaging for food: An environmental assessment," *Resour Conserv Recycl*, vol. 78, pp. 74–80, 2013, doi: https://doi.org/10.1016/j.resconrec.2013.07.003.

[21] S. J. Risch, "Food Packaging History and Innovations," *J Agric Food Chem*, vol. 57, no. 18, pp. 8089–8092, Sep. 2009, doi: 10.1021/jf900040r.

[22] S. Guzman-Puyol, J. J. Benítez, and J. A. Heredia-Guerrero, "Transparency of polymeric food packaging materials," *Food Research International*, vol. 161, p. 111792, 2022, doi: https://doi.org/10.1016/j.foodres.2022.111792.

[23] "Why barrier properties are critical to food product quality." Accessed: Aug. 12, 2024. [Online]. Available: https://terinexflexibles.com/wp-content/uploads/2023/10/TER012-White-Paper-Barrier-properties_v1.2_Pages-Web.pdf

[24] D. Carullo *et al.*, “Testing a coated PE-based mono-material for food packaging applications: an in-depth performance comparison with conventional multi-layer configurations,” *Food Packag Shelf Life*, vol. 39, Nov. 2023, doi: 10.1016/j.fpsl.2023.101143.

[25] T. Anukiruthika, P. Sethupathy, A. Wilson, K. Kashampur, J. A. Moses, and C. Anandharamakrishnan, “Multilayer packaging: Advances in preparation techniques and emerging food applications,” *Compr Rev Food Sci Food Saf*, vol. 19, no. 3, pp. 1156–1186, May 2020, doi: 10.1111/1541-4337.12556.

[26] T. I. Butler and B. A. Morris, “17 - PE-Based Multilayer Film Structures,” in *Multilayer Flexible Packaging (Second Edition)*, J. R. Wagner, Ed., William Andrew Publishing, 2016, pp. 281–310. doi: https://doi.org/10.1016/B978-0-323-37100-1.00017-X.

[27] E. Hatfield, “Machine direction oriented film technology,” in *Multilayer Flexible Packaging: Technology and Applications for the Food, Personal Care, and Over-the-Counter Pharmaceutical Industries*, Elsevier, 2009, pp. 113–118. doi: 10.1016/B978-0-8155-2021-4.10010-3.

[28] D. Carullo *et al.*, “Testing a coated PE-based mono-material for food packaging applications: an in-depth performance comparison with conventional multi-layer configurations,” *Food Packag Shelf Life*, vol. 39, Nov. 2023, doi: 10.1016/j.fpsl.2023.101143.

[29] E. Hatfield, R. Tate, K. Williams, and W. Todd, “NEW MDO MEDIUM MOLECULAR WEIGHT HIGH DENSITY POLYETHYLENE FILMS*,” *JOURNAL OF PLASTIC FILM & SHEETING*, vol. 18, 2002, doi: 10.1177/875608702032871.

[30] T. Chatterjee *et al.*, “Machine direction orientation of high density polyethylene (HDPE): Barrier and optical properties,” *Polymer (Guildf)*, vol. 55, no. 16, pp. 4102–4115, 2014, doi: https://doi.org/10.1016/j.polymer.2014.06.029.

[31] A. R. Ajitha, M. K. Aswathi, H. J. Maria, J. Izdebska, and S. Thomas, “Multilayer Polymer Films,” in *Multicomponent Polymeric Materials*, J. K. Kim, S. Thomas, and P. Saha, Eds., Dordrecht: Springer Netherlands, 2016, pp. 229–258. doi: 10.1007/978-94-017-7324-9_8.

[32] T. Messin *et al.*, “Confinement effect in PC/MXD6 multilayer films: Impact of the microlayered structure on water and gas barrier properties,” *J Memb Sci*, vol. 525, pp. 135–145, 2017, doi: https://doi.org/10.1016/j.memsci.2016.10.039.

[33] M. T. DeMeuse, “Equipment design and requirements of biaxially stretched films,” in *Biaxial Stretching of Film*, Elsevier, 2011, pp. 14–26. doi: 10.1533/9780857092953.1.14.

[34] "The Key Aspects of a Machine Direction Orienter - Part 2 Process Conditions." Accessed: Jan. 19, 2025. [Online]. Available: https://parkinsontechnologies.com/index.php/blog/the-key-aspects-of-a-machine-direction-orienter-part-2-process-conditions

[35] "The Key Aspects of a Machine Direction Orienter - Part 1 Heating Methods." Accessed: Apr. 18, 2024. [Online]. Available: https://parkinsontechnologies.com/index.php/blog/the-key-aspects-of-a-machine-direction-orienter-part-1-heating-methods

[36] J. G. Drobny, "Processing Methods Applicable to Thermoplastic Elastomers, Pg. 141," in *Handbook of Thermoplastic Elastomers*, Elsevier, 2014, pp. 33–173. doi: 10.1016/b978-0-323-22136-8.00004-1.

[37] J. R. Wagner, E. M. Mount, and H. F. Giles, "19 - Polymer Structure," in *Extrusion (Second Edition)*, J. R. Wagner, E. M. Mount, and H. F. Giles, Eds., Oxford: William Andrew Publishing, 2014, pp. 225–232. doi: https://doi.org/10.1016/B978-1-4377-3481-2.00019-3.

[38] S. H. Tabatabaei, L. Parent, P. Cigana, A. Ajji, and P. J. Carreau, "Effect of machine direction orientation conditions on properties of HDPE films," *Journal of Plastic Film and Sheeting*, vol. 25, no. 3–4, pp. 235–249, 2009, doi: 10.1177/8756087910369423.

[39] A. Shrivastava, "1 - Introduction to Plastics Engineering," in *Introduction to Plastics Engineering*, A. Shrivastava, Ed., William Andrew Publishing, 2018, pp. 1–16. doi: https://doi.org/10.1016/B978-0-323-39500-7.00001-0.

[40] T. I. Butler, "PE processes," in *Multilayer Flexible Packaging: Technology and Applications for the Food, Personal Care, and Over-the-Counter Pharmaceutical Industries*, Elsevier, 2009, pp. 15–30. doi: 10.1016/B978-0-8155-2021-4.10002-4.

[41] M. Rubinstein and R. H. Colby, *Polymer Physics*. Oxford University Press, 2003. doi: 10.1093/oso/9780198520597.001.0001.

[42] I. V Gofman, V. E. Yudin, O. Orell, J. Vuorinen, A. Ya. Grigoriev, and V. M. Svetlichnyi, "Influence of the Degree of Crystallinity on the Mechanical and Tribological Properties of High-Performance Thermoplastics Over a Wide Range of Temperatures: From Room Temperature up to 250°C," *Journal of Macromolecular Science, Part B*, vol. 52, no. 12, pp. 1848–1860, Dec. 2013, doi: 10.1080/00222348.2013.808932.

[43] D. Vaes and P. Van Puyvelde, "Semi-crystalline feedstock for filament-based 3D printing of polymers," *Prog Polym Sci*, vol. 118, p. 101411, 2021, doi: https://doi.org/10.1016/j.progpolymsci.2021.101411.

[44] G. Brunner, “Chapter 9 - Reactions of Synthetic Polymers with Water,” in *Supercritical Fluid Science and Technology*, vol. 5, G. Brunner, Ed., Elsevier, 2014, pp. 511–523. doi: https://doi.org/10.1016/B978-0-444-59413-6.00009-1.

[45] S. M. Kurtz, “Chapter 1 - A Primer on UHMWPE,” in *UHMWPE Biomaterials Handbook (Second Edition)*, S. M. Kurtz, Ed., Boston: Academic Press, 2009, pp. 1–6. doi: https://doi.org/10.1016/B978-0-12-374721-1.00001-8.

[46] S. Ronca, “Chapter 10 - Polyethylene,” in *Brydson’s Plastics Materials (Eighth Edition)*, M. Gilbert, Ed., Butterworth-Heinemann, 2017, pp. 247–278. doi: https://doi.org/10.1016/B978-0-323-35824-8.00010-4.

[47] Y. V Kissin, “Educational Minimum: Synthesis, Structure, and Properties of Polyethylene Resins,” in *Polyethylene*, Carl Hanser Verlag GmbH & Co. KG, 2020, pp. 1–41. doi: doi:10.3139/9781569908327.001.

[48] “Qenos | Polyethylene | Technical Guides.” Accessed: Jan. 20, 2025. [Online]. Available: https://www.qenos.com/internet/home.nsf/web/PolyethyleneTechGuides

[49] M. Kroon *et al.*, “Anisotropic Elastic-Viscoplastic Properties at Finite Strains of Injection-Moulded Low-Density Polyethylene,” *Exp Mech*, vol. 58, no. 1, pp. 75–86, 2018, doi: 10.1007/s11340-017-0322-y.

[50] A. Toda, “Spherulitic Growth in Crystalline Polymers,” in *Encyclopedia of Polymers and Composites*, S. Palsule, Ed., Berlin, Heidelberg: Springer Berlin Heidelberg, 2021, pp. 1–12. doi: 10.1007/978-3-642-37179-0_24-1.

[51] S. S. Katti and M. Schultz, “The microstructure of injection-molded semicrystalline polymers: A review,” *Polym Eng Sci*, vol. 22, pp. 1001–1017, 1982, [Online]. Available: https://api.semanticscholar.org/CorpusID:136569456

[52] F. Yan *et al.*, “Effects of combined melt stretching and fast cooling fields on crystallization of high-density polyethylene,” *Polymer (Guildf)*, vol. 275, p. 125930, 2023, doi: https://doi.org/10.1016/j.polymer.2023.125930.

[53] A. W. Phillips, A. Bhatia, P. Zhu, and G. Edward, “Shish Formation and Relaxation in Sheared Isotactic Polypropylene Containing Nucleating Particles,” *Macromolecules*, vol. 44, no. 9, pp. 3517–3528, May 2011, doi: 10.1021/ma200040s.

[54] P. C. Roozemond, Z. Ma, K. Cui, L. Li, and G. W. M. Peters, “Multimorphological Crystallization of Shish-Kebab Structures in Isotactic Polypropylene: Quantitative Modeling of Parent–Daughter Crystallization Kinetics,” *Macromolecules*, vol. 47, no. 15, pp. 5152–5162, Aug. 2014, doi: 10.1021/ma501108c.

[55] T. Kanaya *et al.*, "Hierarchic Structure of Shish-Kebab by Neutron Scattering in a Wide Q Range," *Macromolecules*, vol. 40, no. 10, pp. 3650–3654, May 2007, doi: 10.1021/ma062606z.

[56] B. S. Hsiao, L. Yang, R. H. Somani, C. A. Avila-Orta, and L. Zhu, "Unexpected Shish-Kebab Structure in a Sheared Polyethylene Melt," *Phys Rev Lett*, vol. 94, no. 11, p. 117802, Mar. 2005, doi: 10.1103/PhysRevLett.94.117802.

[57] D. Zhou, S.-G. Yang, J. Lei, B. S. Hsiao, and Z.-M. Li, "Role of Stably Entangled Chain Network Density in Shish-Kebab Formation in Polyethylene under an Intense Flow Field," *Macromolecules*, vol. 48, no. 18, pp. 6652–6661, Sep. 2015, doi: 10.1021/acs.macromol.5b01402.

[58] M. Wen *et al.*, "High-speed melt stretching produces polyethylene nanocomposite film with ultrahigh mechanical strength," *Compos Sci Technol*, vol. 218, p. 109134, 2022, doi: https://doi.org/10.1016/j.compscitech.2021.109134.

[59] F. C. Campbell, "Chapter 11 - Commercial Composite Processes: These Commercial Processes Produce Far More Parts than the High-performance Processes," in *Manufacturing Processes for Advanced Composites*, F. C. Campbell, Ed., Amsterdam: Elsevier Science, 2004, pp. 399–438. doi: https://doi.org/10.1016/B978-185617415-2/50012-5.

[60] L. W. McKeen, "3 - Production of Films, Containers, and Membranes," in *Permeability Properties of Plastics and Elastomers (Fourth Edition)*, L. W. McKeen, Ed., William Andrew Publishing, 2017, pp. 41–60. doi: https://doi.org/10.1016/B978-0-323-50859-9.00003-8.

[61] "Plastic Extrusion Explained | Fictiv." Accessed: Jan. 22, 2025. [Online]. Available: https://www.fictiv.com/articles/plastic-extrusion-explained

[62] J. R. Wagner, "10 - Blown Film, Cast Film, and Lamination Processes," in *Multilayer Flexible Packaging (Second Edition)*, J. R. Wagner, Ed., William Andrew Publishing, 2016, pp. 137–145. doi: https://doi.org/10.1016/B978-0-323-37100-1.00010-7.

[63] "Blown film extrusion,Blown film extrusion process,Blown film extruders,manufacturers,suppliers,exporters." Accessed: Jan. 22, 2025. [Online]. Available: http://www.industrialextrusionmachinery.com/plastic_extrusion_blown_film_extrusion.html

[64] "Understanding the Basics of Blown Film Manufacturing." Accessed: Jan. 22, 2025. [Online]. Available: https://www.swallowmachinery.com/knowledge-base/understanding-the-basics-of-blown-film-manufacturing

[65] K. Cantor, “Blown Film Extrusion,” in *Blown Film Extrusion 3e (Third Edition)*, K. Cantor, Ed., Hanser, 2019, pp. I–XIV. doi: https://doi.org/10.3139/9781569906972.fm.

[66] D. A. Plemmons, “Processing-Structure-Function Relationships in the Production of High-Performance Oriented Polyethylene by Dayne A Plemmons,” 2022.

[67] L. Lin and A. S. Argon, “Structure and plastic deformation of polyethylene,” *J Mater Sci*, vol. 29, no. 2, pp. 294–323, 1994, doi: 10.1007/BF01162485.

[68] P. B. Bowden and R. J. Young, “Deformation mechanisms in crystalline polymers,” *J Mater Sci*, vol. 9, no. 12, pp. 2034–2051, 1974, doi: 10.1007/BF00540553.

[69] M. F. Butler, A. M. Donald, and A. J. Ryan, “Time resolved simultaneous small- and wide-angle X-ray scattering during polyethylene deformation: 1. Cold drawing of ethylene-α-olefin copolymers,” *Polymer (Guildf)*, vol. 38, no. 22, pp. 5521–5538, 1997, doi: https://doi.org/10.1016/S0032-3861(97)00111-0.

[70] V. Gaucher-Miri and R. Séguéla, “Tensile Yield of Polyethylene and Related Copolymers: Mechanical and Structural Evidences of Two Thermally Activated Processes,” *Macromolecules*, vol. 30, no. 4, pp. 1158–1167, Feb. 1997, doi: 10.1021/ma9601878.

[71] D. Guleria, S. Ge, L. Cardon, S. Vervoort, and J. den Doelder, “Impact of resin density and short-chain branching distribution on structural evolution and enhancement of tensile modulus of MDO-PE films,” *Polym Test*, p. 108560, 2024, doi: https://doi.org/10.1016/j.polymertesting.2024.108560.

[72] D. Guleria, M. Edeleva, S. Vervoort, S. Ge, J. den Doelder, and L. Cardon, “Impact of molecular architecture and draw ratio on enhancement of targeted mechanical properties of machine direction oriented polyethylene films produced after blown film extrusion,” *Journal of Plastic Film & Sheeting*, p. 87560879241293390, Oct. 2024, doi: 10.1177/87560879241293392.

[73] P. J. Lemstra, C. W. M. Bastiaansen, and H. E. H. Meijer, “Chain-extended flexible polymers,” *Die Angewandte Makromolekulare Chemie*, vol. 145, no. 1, pp. 343–358, Nov. 1986, doi: 10.1002/APMC.1986.051450117.

[74] P. J. Lemstra, N. A. J. M. van Aerle, and C. W. M. Bastiaansen, “Chain-Extended Polyethylene,” *Polymer Journal 1987 19:1*, vol. 19, no. 1, pp. 85–98, 1987, doi: 10.1295/polymj.19.85.

[75] P. Smith, P. J. Lemstra, and J. P. L. Pijpers, “Tensile strength of highly oriented polyethylene. II. Effect of molecular weight distribution,” *Journal of Polymer Science: Polymer Physics Edition*, vol. 20, no. 12, pp. 2229–2241, Dec. 1982, doi: 10.1002/POL.1982.180201206.

[76] J. M. Andrews and I. M. Ward, "The cold-drawing of high density polyethylene," *J Mater Sci*, vol. 5, no. 5, pp. 411–417, May 1970, doi: 10.1007/BF00550003/METRICS.

[77] G. Capaccio and I. M. Ward, "Preparation of ultra-high modulus linear polyethylenes; effect of molecular weight and molecular weight distribution on drawing behaviour and mechanical properties," *Polymer (Guildf)*, vol. 15, no. 4, pp. 233–238, Apr. 1974, doi: 10.1016/0032-3861(74)90038-X.

[78] S. H. Tabatabaei, L. Parent, P. Cigana, A. Ajji, and P. J. Carreau, "Effect of machine direction orientation conditions on properties of HDPE films," *Journal of Plastic Film and Sheeting*, vol. 25, no. 3–4, pp. 235–249, 2009, doi: 10.1177/8756087910369423.

[79] Q. Chen, Z. Wang, S. Zhang, Y. Cao, and J. Chen, "Structure Evolution and Deformation Behavior of Polyethylene Film during Biaxial Stretching," *ACS Omega*, vol. 5, no. 1, pp. 655–666, Jan. 2020, doi: 10.1021/acsomega.9b03250.

[80] L. Jarecki and D. J. Meier, "Ultra-high modulus polyethylene. 1 Effect of drawing temperature," *Polymer (Guildf)*, vol. 20, no. 9, pp. 1078–1082, Sep. 1979, doi: 10.1016/0032-3861(79)90297-0.

[81] L. Jarecki and D. J. Meier, "Ultrahigh modulus polyethylene. II. Effect of drawing temperature on void formation and modulus," *Journal of Polymer Science: Polymer Physics Edition*, vol. 17, no. 9, pp. 1611–1621, Sep. 1979, doi: 10.1002/POL.1979.180170913.

[82] J. M. Andrews and I. M. Ward, "The cold-drawing of high density polyethylene," *J Mater Sci*, vol. 5, no. 5, pp. 411–417, 1970, doi: 10.1007/BF00550003.

[83] R. Séguéla, "On the natural draw ratio of semi-crystalline polymers: Review of the mechanical, physical and molecular aspects," Mar. 12, 2007. doi: 10.1002/mame.200600389.

[84] E. S. Sherman, R. S. Porter, and E. L. Thomas, "Microstructure of high modulus solid state extruded polyethylene: 1. Electron microscopy studies of 12, 24 and 36 × EDR," *Polymer (Guildf)*, vol. 23, no. 7, pp. 1069–1076, 1982, doi: https://doi.org/10.1016/0032-3861(82)90410-4.

[85] T. Radusin *et al.*, "Use of recycled materials as mid layer in three layered structures-new possibility in design for recycling," *J Clean Prod*, vol. 259, Jun. 2020, doi: 10.1016/j.jclepro.2020.120876.

[86] R. Esmaeilzade, S. Hosseini, R. Rashedi, S. Houshmandmoayed, K. Afzali, and A. Sepahi, "Study on the Rheological, Thermal, Mechanical, and Optical Properties of LDPE/LLDPE Blown Films Containing Recycled LDPE/LLDPE Pellets For Circular Economy," 2022, doi: 10.21203/rs.3.rs-2185814/v1.

[87] T. Andersson, B. Stålbom, and B. Wesslén, “Degradation of polyethylene during extrusion. II. Degradation of low-density polyethylene, linear low-density polyethylene, and high-density polyethylene in film extrusion,” *J Appl Polym Sci*, vol. 91, no. 3, pp. 1525–1537, Feb. 2004, doi: 10.1002/APP.13024.

[88] M. K. Loultcheva, M. Proietto, N. Jilov, and F. P. L. Mantia, “Recycling of high density polyethylene containers,” *Polym Degrad Stab*, vol. 57, no. 1, pp. 77–81, Jul. 1997, doi: 10.1016/S0141-3910(96)00230-3.

[89] C. Sadrmohaghegh and G. Scott, “The effects of reprocessing on polymers—I: Low density polyethylene,” *Eur Polym J*, vol. 16, no. 11, pp. 1037–1042, Jan. 1980, doi: 10.1016/0014-3057(80)90220-7.

[90] V. S. Cecon, P. F. Da Silva, K. L. Vorst, and G. W. Curtzwiler, “The effect of post-consumer recycled polyethylene (PCRPE) on the properties of polyethylene blends of different densities,” *Polym Degrad Stab*, vol. 190, Aug. 2021, doi: 10.1016/j.polymdegradstab.2021.109627.

[91] H. Jin, J. Gonzalez-Gutierrez, P. Oblak, B. Zupančič, and I. Emri, “The effect of extensive mechanical recycling on the properties of low density polyethylene,” *Polym Degrad Stab*, vol. 97, no. 11, pp. 2262–2272, 2012, doi: https://doi.org/10.1016/j.polymdegradstab.2012.07.039.

[92] A. Choudhury, M. Mukherjee, and B. Adhikari, “Mixtures of Recycled Milk Pouches with a Virgin LDPE-LLDPE Blend,” *Progress in Rubber, Plastics and Recycling Technology*, vol. 21, no. 3, pp. 219–230, Aug. 2005, doi: 10.1177/147776060502100304.

[93] P. Miller, I. Sbarski, E. Kosior, S. Masood, and P. Iovenitti, “Correlation of rheological and mechanical properties for blends of recycled HDPE and virgin polyolefins,” *J Appl Polym Sci*, vol. 82, no. 14, pp. 3505–3512, Dec. 2001, doi: 10.1002/APP.2212.

[94] M. Nofar, B. S. Yenigul, B. Ozdemir, C. Y. Kovanci, A. Ghanbari, and A. Jalali, “Mechanical and viscoelastic properties of polyethylene-based microfibrillated composites from 100% recycled resources,” *J Appl Polym Sci*, vol. 138, no. 32, p. 50793, Aug. 2021, doi: 10.1002/APP.50793.

[95] D. Czarnecka-Komorowska, K. Wiszumirska, and T. Garbacz, “FILMS LDPE/LLDPE MADE FROM POST - CONSUMER PLASTICS: PROCESSING, STRUCTURE, MECHANICAL PROPERTIES,” *Advances in Science and Technology. Research Journal*, vol. 12, no. 3, pp. 134–142, Sep. 2018, doi: 10.12913/22998624/92205.

[96] Z. O. G. Schyns and M. P. Shaver, “Mechanical Recycling of Packaging Plastics: A Review,” *Macromol Rapid Commun*, vol. 42, no. 3, p. 2000415, Feb. 2021, doi: https://doi.org/10.1002/marc.202000415.

[97] S. J. Hebert, C. Tzoganakis, and J. Perdikoulias, “Blown Film Extrusion of Post-Consumer Recycled Lldpe Film,” *Journal of Plastic Film & Sheeting*, vol. 9, no. 4, pp. 282–292, Oct. 1993, doi: 10.1177/875608799300900402.

[98] V. L. Lazić, J. Budinski-Simendić, J. J. Gvozdenović, and B. Simendić, “Barrier Properties of Coated and Laminated Polyolefin Films for Food Packaging,” 2010.

[99] C. F. Ayuso, A. A. Agüero, J. A. P. Hernández, A. B. Santoyo, and E. G. Gómez, “High Oxygen Barrier Polyethylene Films,” *Polymers and Polymer Composites*, vol. 25, no. 8, pp. 571–582, Oct. 2017, doi: 10.1177/096739111702500802.

[100] J. P. Paulos and E. L. Thomas, “Effect of postdrawing on the permeability of gases in blown polyethylene film,” *J Appl Polym Sci*, vol. 25, no. 1, pp. 15–23, Jan. 1980, doi: https://doi.org/10.1002/app.1980.070250102.

[101] J. L. Williams and A. Peterlin, “Transport properties of methylene chloride in drawn polyethylene as a function of the draw ratio,” *Journal of Polymer Science Part A-2: Polymer Physics*, vol. 9, no. 8, pp. 1483–1494, Aug. 1971, doi: https://doi.org/10.1002/pol.1971.160090808.

[102] H. Sha and I. R. Harrison, “CO2 permeability and amorphous fractional free-volume in uniaxially drawn HDPE,” *J Polym Sci B Polym Phys*, vol. 30, no. 8, pp. 915–922, Jul. 1992, doi: https://doi.org/10.1002/polb.1992.090300814.

[103] D. Breese, G. B.-T. E. P. Conference, and undefined 2005, “Effects of machine direction orientation (MDO) on the moisture and oxygen barrier properties of HMW-PE films,” *CiteseerDR Breese, G BeaucageTAPPI European PLACE Conference, 2005•Citeseer*, Accessed: Aug. 13, 2024. [Online]. Available: https://citeseerx.ist.psu.edu/document?repid=rep1&type=pdf&doi=98756ceb8d83a156b6e0307dea67c0b15236cf3d

[104] “Optical Properties of Polymers.” Accessed: Aug. 13, 2024. [Online]. Available: https://www.intertek.com/polymers-plastics/optical-properties/

[105] S. K. Paul, “Edible Films and Coatings for Fruits and Vegetables,” in *Encyclopedia of Renewable and Sustainable Materials*, S. Hashmi and I. A. Choudhury, Eds., Oxford: Elsevier, 2020, pp. 363–376. doi: https://doi.org/10.1016/B978-0-12-803581-8.11509-7.

[106] “High Clarity Linear Low Density Polyethylene for Packaging Applications - Paper, Film & Foil Converter.” Accessed: Aug. 13, 2024. [Online]. Available: https://www.pffc-online.com/magazine/1006-paper-high-clarity-linear

[107] A. Eldesouky, A. F. Pulido, and F. J. Mesias, “The Role of Packaging and Presentation Format in Consumers’ Preferences for Food: An Application of Projective

Techniques," *J Sens Stud*, vol. 30, no. 5, pp. 360–369, Oct. 2015, doi: https://doi.org/10.1111/joss.12162.

[108] H.-L. Nguyen *et al.*, "Biorenewable, transparent, and oxygen/moisture barrier nanocellulose/nanochitin-based coating on polypropylene for food packaging applications," *Carbohydr Polym*, vol. 271, p. 118421, 2021, doi: https://doi.org/10.1016/j.carbpol.2021.118421.

[109] R. Breese, "Flexible Packaging Substrates Benefits of machine direction-oriented (MDO) films in flexible-packaging applications." Accessed: Jul. 22, 2024. [Online]. Available: http://ccl-eclipse.com/News_Releases/Benefits%20of%20MDO%20in%20Flexible%20Packaging.pdf

Chapter – 2

Impact of resin density and short-chain branching distribution on structural evolution and enhancement of tensile modulus of MDO-PE films

Abstract

This Chapter explores the potential of PE-based mono-material flexible packaging as a sustainable alternative to traditional designs, emphasizing its efficient mechanical recyclability. Typically, non-PE materials are used in the outer layers of multilayer flexible packaging to ensure adequate stiffness and barrier properties. The stiffness of PE films can be significantly improved through the machine direction orientation (MDO) process. The study in this Chapter investigates the influence of key polyethylene (PE) resin parameters, specifically, resin density and short-chain branching (SCB) distribution, with indications of molecular weight on lab-scale MDO film stretching and its subsequent effects on mechanical properties. 5 distinct PE resins and blends were processed in a lab-scale setup to produce compression molded base sheets and further MDO-PE films, which were characterized using shear rheology, GPC, DSC, and iCCD analyses. Tensile testing provided insights into the mechanical characteristics, while X-ray scattering (SAXS and WAXS) and AFM studies analysed structural evolution and morphology. Uniaxial stretching notably enhanced the tensile modulus of MDO-PE films along the machine direction, particularly in higher density blends, comparable to conventionally used polymers. Challenges related to extremely high-density base sheets led to localized stretching and breakage. Certain resin compositions exhibited unique molecular architecture, facilitating enhanced tensile modulus and axial stiffness. This Chapter offers insights into the microstructural changes and surface morphology of MDO-PE films, underscoring the potential use of stiffness-enhanced MDO-PE films as outer layers in PE-based flexible packaging designs.

This Chapter is based on: Guleria D, Ge S, Cardon L, Vervoort S, den Doelder J. Impact of resin density and short-chain branching distribution on structural evolution and enhancement of tensile modulus of MDO-PE films. *J. Polym Test* 2024; 139: 108560

2.1 Introduction

Nearly 44% of the overall plastics produced in the world are used in the packaging industry [1]. Flexible packaging accounts for about 45% of the overall plastic packaging in the EU [2]. In 2023, the food and beverages segment was the most prominent sector for flexible packaging, commanding a substantial market share of about 55% globally [3]. Food packaging requires polymer films with specific properties, essential for preserving the quality and safety of food products. Typical application requirements are good barrier against permeation of oxygen and moisture for prolonging the food product shelf-life and good optical properties such as high clarity and low haze, for example, in the case of see-through packaging. In addition, the right balance of mechanical properties like modulus, stiffness, and tensile strength is also very critical to ensure integrity of the package and to allow easy handling. To combine all these properties, many flexible packages nowadays are composed of different layers made of different polymers [4].

Multilayer flexible packaging lacks efficient recycling methods currently as diverse materials like polyethylene (PE), polypropylene (PP), polyethylene terephthalate (PET), polyamides (PA) including coatings of polyvinylidene dichloride (PVDC), silicon oxides (SiOx), aluminium oxides (AlOx), metallized films and non-polymeric layers, such as aluminum foil are used to manufacture it [5]. Due to this challenge, they typically end up in landfills or are incinerated for energy recovery after their end of life, which affects our environment. When they do end up in a recycled stream, the multi-material nature poses challenges to the applicability of the recycled material. To improve recycling rates, mono-material multi-layered flexible packaging systems are emerging as a new alternative. Still multiple variations are typically needed to achieve initial use-phase functionality, but as these materials are from one chemical composition, when mixed during recycling process steps, the resulting recycled product has good potential to perform well. Polyethylene (PE) is one of the most used polymers in flexible packaging applications as it can provide various useful structural and functional properties because of its distinct available grades like low-density polyethylene (LDPE), linear low-density polyethylene (LLDPE), and high-density polyethylene (HDPE). There is promise in achieving both package functionality and recyclability when combining different grades of PE into a single package.

Conventional multilayer flexible packages typically use some non-PE material to impart stiffness and gas barrier properties against gases like oxygen. PE can reach a certain modulus by increasing resin density, but this is typically not sufficient. Sufficient polymer film stiffness is required for various packaging operations such as printing and lamination, and for the efficient running of packaging machine lines. Low-stiffness films might sag while running on packaging lines. The appropriate overall stiffness of the multilayer packaging structure is also required for special consumer-appealing package designs such as a stand-up pouch [6]. Conventionally, these outer film layers are made of relatively higher-modulus polymeric materials than PE such as polyethylene terephthalate (PET) and polyamide (PA).

The machine direction orientation (MDO) process is a novel commercial process in the flexible packaging industry in which the polymer film is stretched and oriented in the machine direction at a certain polymer-dependent orientation temperature, resulting in the

enhancement of desired properties [7]. In the semi-solid state, alignment achieved through processes such as tenter frame, double bubble, and machine direction orientation enhances both barrier and mechanical properties, presenting a pathway to the development of lighter packaging structures [8]. The MDO operation has the potential to significantly increase Young's modulus of the PE film, leading to enhanced stiffness of these PE films. Stiffness of a material is a function of its Young's modulus and therefore, enhancement in Young's modulus of PE film enhances stiffness. However, there are open questions relating to obtainable stiffness. More precisely, there is a desire to better understand the interaction between principal base resin parameters like density and processing-related parameters like orientation.

Various previous researchers have studied semi-solid state stretching of PE to produce ultra-drawn high modulus fibres and films [9], [10], [11], [12], [13]. Existing research recognizes the critical role played by MDO process parameters such as orientation temperature, draw ratio, stretch rate, and annealing time on final mechanical properties attained by MDO films. Tabatabaei *et al*. [14] studied the effect of machine direction orientation process conditions on the mechanical properties of HDPE films and found that Young's modulus decreased around the relatively low draw ratio of 6.5 and then started to increase beyond that. The Young's modulus of the films also increased with rising annealing temperature and decreased slightly with increase in stretching orientation temperature near the melting point. Chen *et al*. [15] also reported about 2 times increment in tensile modulus and about 4.5 times in tensile strength in sequential biaxial orientation (first machine direction and then transverse direction) of polyethylene films with an increase in draw ratio. Tabatabaei *et al.* [16] in another study, studied the structure and mechanical properties of MDO stretched polypropylene (PP) film and reported that tear resistance along the MD decreased significantly with an increase in draw ratio whereas puncture resistance increased drastically. Hatfield *et al.* [17] investigated the properties of medium molecular weight HDPE films with PA additive and reported significant enhancement of properties such as stiffness, gloss, haze, and water vapor transmission rate (WVTR) with increase in draw ratio.

However, only a few studies have systematically investigated the role of resin parameters such as density, branching, branching distribution (BD), molecular weight, and molecular weight distribution (MWD) on final mechanical properties attained by the MDO films. Ratta *et al.* [4] have briefly mentioned in their work that drawability and uniformity of drawing of the PE base sheet going through MDO operation increase with a decrease in overall crystallinity (density) of the base sheet. Thus, rapid quenching is often preferred in industry to prevent the formation of large spherulites which can increase the crystallinity, and thus the density, of the base PE film before MDO operation.

Krishnaswamy *et al.*[18] studied the effect of short chain branching distribution on crystallization kinetics and mechanical properties of HDPE and reported that placement of branches on the longer molecules results in slower crystallization kinetics, which further decreases spherulitic size. Li *et al.* [19] investigated the effect of comonomer content on the structure-property relationship of propylene-1-octene copolymer during uniaxial stretching. They reported that copolymers with lower octene content presented higher crystallinity and larger crystal sizes, which undergo lamellar fragmentation during stretching. Initially,

this led to a decrease in crystallinity, but at high strains, there was a subsequent increase due to strain-induced crystallization, resulting in overall high lamellar orientation.

This Chapter, focusing on the outer structural layers of novel designs, addresses the impact of principal structural resin parameters on the structural evolution and morphology attained in MDO-PE films and maps its enhancement of tensile modulus and stiffness.

In this Chapter, the role of key resin parameters of PE, i.e., resin density and short-chain branching (SCB) distribution coupled with molecular weight, in lab-scale MDO film stretching at the same fixed process parameters of orientation temperature, stretch rate, annealing time, and process draw ratio was investigated. From an extensive literature review on the MDO process, it was hypothesized that with the increase in resin density, the microstructural crystalline phase present for fibrillation during MDO operation will be higher, and thus higher fibrillation of the microstructure will be observed after the MDO operation at the fixed orientation temperature. Highly fibrillated and oriented microstructure in the stretch or MD direction is expected to result in a significant increase in modulus, and thus stiffness, of the MDO stretched films. This work also addresses the structural evolutions and changes in surface morphology of the PE base sheets after going through MDO operation and how they relate to the final overall tensile properties of the MDO films.

5 different PE resins were selected for the study and processed in a lab-scale setup to produce MDO-PE films. Blends were prepared to provide samples at intermediate densities and thus crystallinities for the investigation. The resins and their blends were characterized in detail using shear rheology, GPC (gel permeation chromatography), DSC (differential scanning calorimetry) and iCCD (improved chemical composition distribution) analyses. Tensile tests were performed before and after MD stretching to measure the tensile modulus. X-Ray scattering (SAXS and WAXS) was performed for the analysis of the shape, size, and orientation of the crystals. The surface morphology was analysed by atomic force microscopy (AFM).

2.2 Materials and methods

2.2.1 Materials

In total 5 PE resins composed of ethylene with an α-olefin copolymer were provided by Dow. D1, D2, and D3 resins are based on similar catalyst chemistry whereas X1 and X2 resins are based on hybrid catalyst chemistry. The density and melt flow index (MFI) of all the 5 base resins given in the Table 2.1 was measured during characterization experiments. The MFI was measured following ASTM D1238 using a Göttfert MI-4 plastometer under the standard weight of 2.16 kg at 190 ˚C. The density was measured according to the ASTM D792 standard procedure with isopropyl alcohol (IPA) used as a submerging liquid. The reported value of density in Table 2.1 is average of 3 measurements. To explore a finer grid of structural variation, binary blends were produced using the Haake Rheomix OS machine from Thermo Scientific, involving a mixing duration of 30 minutes at 150 ˚C and a screw speed of 15 rpm. The binary blends always featured a low-density grade (X1 or D1) as one component and a higher-density grade (D2, D3, or X2) as the other component. The weight

percentages of the low-density grade in the blend were systematically varied at 25, 50, and 75%.

Table 2.1 Characteristics of all the 5 base PE resins used in the study.

Resin	MFI (dg/min)	Density* (g/cm^3)
D1	1.020	0.9194 ± 0.0003
D2	1.472	0.9500 ± 0.0001
D3	4.102	0.9540 ± 0.0003
X1	1.872	0.9256 ± 0.0002
X2	1.126	0.9667 ± 0.0001

*Error is standard deviation in density column.

2.2.2 Characterization of base materials

2.2.2.1 Differential scanning calorimetry (DSC)

A DSC Q2000 instrument from TA instruments was used for the thermal analysis. A nominal 5 to 10 mg of sample in pellet form inside a closed aluminium pan was used in a heat-cool-heat cycle from 0 to 200 ˚C at a rate of 10 ˚C/min under a nitrogen atmosphere. Three observations for each sample were recorded. The degree of crystallinity (X_{DSC}) was computed according to the Equation 2.1.

$$X_{DSC} = \frac{\Delta H_m}{\Delta H^\circ_m} * 100 \qquad \textit{Equation 2.1}$$

Where ΔH_m is the melting enthalpy, and ΔH°_m is the melting enthalpy of 100% crystalline PE, i.e., 293 J/g [20].

2.2.2.2 Gel permeation chromatography (GPC)

Molecular weight distribution and architecture was measured using triple-detector gel permeation chromatography (TD-GPC) according to the procedure described in Yau *et al.* (2013) and Pathaweeisariyakul *et al.* (2015) [21], [22]. A GPC instrument equipped with triple detector technology from Polymer Char was used to determine the molecular weight distribution. The triple detector GPC-IR system from Polymer Char was composed of a 1260 Infinity isocratic pump from Agilent, an autosampler from Polymer Char, a high temperature GPC chromatograph equipped with four 20 µm Agilent "Mixed A" GPC columns, an IR5-MCT detector and a four-capillary bridge viscometer from Polymer Char and a 2-angle light scattering detector from Agilent. For absolute molecular weight determination, the 15 ° light scattering channel was used as a direct measurement. The polymer resins were first

dissolved in 1,2,4 trichlorobenzene (TCB) at 160 ˚C and a concentration of about 1.6 mg/ml. They were processed through a column packed with gel particles which separate the molecules by their size. The volumetric flow rate was 1 ml/min. This measurement allows to determine microstructural resin parameters such as average molecular weight, molecular weight distribution, comonomer distribution, and branching fractions.

2.2.2.3 Chemical composition distribution

The chemical composition distribution (CCD), also named short chain branching distribution (SCBD) was determined by an improved CCD (iCCD) technique using CCD equipment from Polymer Char with columns packed with gold-coated nickel particles. To prepare the solutions, about 32 mg of sample was added to a vial with 8 ml of 1,2-dichlorobenzene at 150 ˚C and shaken gently for about 1 hour in the Polymer Char autosampler. After injection, the sample was allowed to stabilize for two-minutes and then cooled down under quiescent conditions from 105 °C to 30 °C at a rate of -3 °C/min (crystallization step). When reaching the 30 °C mark, a flow rate of 0.5 ml/min was applied. After two minutes, the temperature again increased to 140 °C at a rate of 3 °C/min. During this step, the polymer fractions dissolved and eluted at the temperature corresponding to their composition and were measured by means of an IR5 detector. Data processing was performed using Polymer Char "GPC One" software with custom verified processing methods.

2.2.2.4 Shear rheology

Small amplitude oscillatory shear flow measurements were carried out under a nitrogen atmosphere in an ARES-G2 rotational rheometer from TA Instruments, equipped with a forced convection oven and set up with parallel plates of 25 mm diameter with a 1.8 mm gap. Frequency sweeps were performed from 0.1 to 100 rad/s, with five logarithmically spaced steps per decade, and at a strain in the linear viscoelastic range. Measurements were taken at three different temperatures:150, 170 and 190 °C.

2.2.3 Preparation of base sheets, lab scale MDO films and cast films

Base sheets from all five base resins of approximately 550 microns thickness were prepared at 190 °C and 150 bar pressure using a Colin compression molding press, followed by quench cooling with circulating room temperature water through channels in the hot press plates. Rectangular specimens of 20 mm width and 100 mm in length were cut from the base sheet. Lab scale stretching of the base sheet specimen was performed using a Lloyd LR10K Plus tensile tester equipped with an environmental chamber to provide the orientation temperature (pictorial representation in the appendix figure A2.1). The 20 mm wide strips were stretched to a fixed process draw ratio of 7, i.e., from 25 mm to 175 mm of grip separation (150 mm extension). All sheets were stretched at a temperature of 110 °C and at a constant extension rate of 200 mm/min, corresponding to a nominal strain rate of approximately 0.067 s^{-1}. It should be noted that optimum stretching or orientation temperature is dependent on micro-structural aspects of the polymer, and it can be different for different applications to produce desired results. Typically, temperatures

above the glass transition temperature and below the peak melting point temperature are used. Usually with increasing orientation temperature, the stretch ratios which can be obtained without film breakage increase [23]. After stretching, the samples were annealed for 2 minutes at a fixed temperature of 120 ˚C. Annealing step freezes the orientation provided in the stretching step and stabilizes the film from further dimensional changes. The annealing temperature and time also influence properties of the final MDO film, and it can be different for different desired final properties [24]. Few academic and industrial studies on MDO and bi-axial orientation process technologies explicitly discuss the annealing temperature. Those that do comment on it either suggest same annealing temperature [17] as it is stretched or slightly higher [23], [25], [26]. After annealing, the films were cooled under ambient room temperature. The lab scale stretching of the samples with clamped ends, was expected to be less uniform than the actual MDO process with continuous running web on draw rollers.

Cast films of approximately 220 microns thickness from resins D1 and X1 were produced in an OCS monolayer extruder for comparison of properties at similar thickness with MDO films. The temperature profile for the extruder was ranging from 195 to 235 °C at the die outlet. The screw speed of 70 rpm was used. Chill roll temperature was set at 40 °C.

2.2.4 Characterization of base sheets, lab scale MDO films and cast films

2.2.4.1 Measurement of tensile properties

Tensile properties were measured using an EZ20 universal testing machine from Lloyd Instruments following ASTM D882 for sample preparation and measurement. The compression molded and lab-scale stretched samples were cut into rectangular specimens (100 mm x 10 mm). Uniform width test sections were cut from the middle section of lab scale MDO stretched samples to be used for tensile testing at room temperature (23 ˚C) and three specimens of each material were measured. 50 mm gauge length was used for testing. The constant extension rate used for mechanical performance analysis was 100 mm/min, corresponding to a nominal strain rate of approximately 0.033 s^{-1}. The 2% secant modulus is one of the several methods used to measure modulus of elasticity, which is a measure of material's stiffness. The 2% secant modulus was quantified using integrated Nexygen software by measuring the slope of the line drawn from the origin of the stress-strain curve to the point where it intersected the curve at 2% strain. Axial stiffness was determined by integrated Nexygen software using modulus and sample dimension data.

2.2.4.2 X-Ray diffraction

Microstructural analysis of the samples was performed using two X-ray diffraction (XRD) techniques: small angle X-ray scattering (SAXS) and wide angle X-ray scattering (WAXS). Data was collected at the Advanced Photon Source (APS), DND-CAT, 5-ID-D beamline of Argonne National Laboratory (Lemont, IL, USA). The standard APS Undulator A was used as the X-ray source with the X-ray energy set at 17 keV (λ= 0.7293 Å). Data was analysed using the Irena package and Jade software respectively for SAXS and WAXS.

During the melt crystallization process, stacks of lamellae tend to form due to space filling constraints. The stacking period is usually extremely regular, and this period is called the long period of the crystallites. The long period is so regular that diffraction occurs from regularly spaced lamellae at very small angles using an X-ray [27].

The long period (LP) of the lamellae was obtained from the peak position on the Lorentz-corrected SAXS intensity profile (Equation 2.2) using Bragg's law [15].

$$L_p = \frac{2\pi}{q_{max}} \qquad \textit{Equation 2.2}$$

Where q_{max} is the maximum scattering vector of the relevant intensity profile.

The measurement of crystal structure and orientation was carried out using a wide-angle X-ray diffractometer. The two-dimensional WAXS (2D-WAXS) patterns were generated by placing the sample perpendicular to the projection beams. One-dimensional WAXS (1D-WAXS) data could be obtained by integrating 2D-WAXS patterns as a function of 2θ. The apparent crystallinity was calculated from the area ratio from Equation 2.3.

$$X_{XRD} = \frac{A_{crystalline}}{A_{total}} * 100 \qquad \textit{Equation 2.3}$$

The full width of half maximum (β), of the crystalline peak was used to calculate the crystallite size from Debye-Scherrer's equation (Equation 2.4).

$$L_{hkl} = \frac{K\lambda}{\beta * cos\theta} \qquad \textit{Equation 2.4}$$

Where L_{hkl} is crystallite dimension (in Å) along the direction perpendicular to the crystallographic plane hkl, β is the full width of the diffraction line at half maximum of peak related to the crystallographic plane hkl in radians, θ is the diffraction angle (Bragg's angle) of the hkl reflection, λ is the wavelength of X-ray, and K is the Scherrer constant with value of 0.89.

In the case of uniaxial orientation, the orientation distribution functions of the chain segments are defined by using a sequence of a series of orthogonal spherical harmonic functions. The characterization of crystalline orientation involves calculating the average squared cosine values, which indicate the average orientation of the normal to the crystalline plane about each of the reference axes. Herman's orientation function, which is the second harmonic orientation function is given by the Equation 2.5 [28].

$$f = \frac{3\langle\cos^2\varphi_{hkl,z}\rangle - 1}{2} \qquad \textit{Equation 2.5}$$

Where $\varphi_{hkl,z}$ is the angle between the chain axis and a reference axis z, which is the draw direction (DD). $\langle\cos^2\varphi_{hkl,z}\rangle$ is calculated from the scattering intensity $I(\varphi)$ by integrating over the azimuthal angle ϕ as given in Equation 2.6.

$$\langle\cos^2\varphi_{hkl,z}\rangle = \frac{\int_0^{\pi/2} I(\varphi)sin\varphi cos^2\varphi d\varphi}{\int_0^{\pi/2} I(\varphi)sin\varphi d\varphi} \qquad \textit{Equation 2.6}$$

The value of f is 1 (φ =0˚) for the perfect draw direction orientation, -1/2 (φ =90˚) for chains aligned normally to the draw direction, and 0 for a perfect random orientation. Five measurements were taken for each sample for the calculation of long period, crystallite dimension and apparent crystallinity.

2.2.4.3 Atomic Force Microscopy

Surface roughness of all samples was determined by atomic force microscopy (AFM). The samples were mounted on a stage using double-sided carbon tape and then blow-cleaned with duster for AFM analysis. AFM images were captured at ambient temperature by using a Bruker Icon AFM system with a MikroMasch probe in tapping mode. The probe had a spring constant of 40 N/m and a resonance frequency in the vicinity of 170 kHz. An imaging frequency of 0.5-2 Hz was used with a set point ratio of ~0.8. Surface roughness was calculated utilizing SPIP software and expressed as root mean square (RMS) roughness S_q, the geometric mean deviation of all points on the surface from the mean value of the data. For any *M* x *N* rectangular image, S_q is defined in Equation 2.7.

$$S_q = \sqrt{\frac{1}{MN}\sum_{k=0}^{M-1}\sum_{i=0}^{N-1}[z(x_k, y_i)]^2} \qquad \textit{Equation 2.7}$$

2.3 Results and discussion

2.3.1 Base resins characterizations

2.3.1.1 Melting behaviour

Knowing the thermal properties of a polymer is essential for developing the best methods to process the material into useful products and predicting performance during the product's lifetime[29]. Melting behaviour of the 5 base PE resins used in this work is presented in Figure 2.1

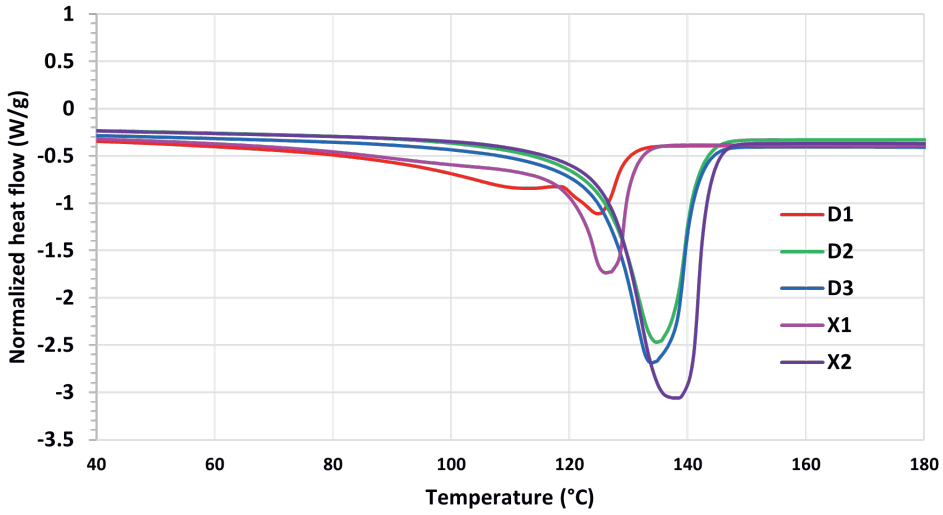

Figure 2.1 DSC melting curves obtained during 2nd heating cycle for all 5 base resins.

The enthalpy of melting increased with resin density, which implies an increase in base crystallinity of the resins as density increases. The D1 enthalpy line shows two peaks: one sharp like the peaks for the other materials, and one very broad at a lower temperature. The latter suggests the presence of PE molecules with higher branching content which was confirmed by GPC [30]. The picture provided by iCCD is the same (Figure 2.4): sharp narrow peaks at high temperatures for D2, D3 and X2, a broader peak at lower temperature for X1 and two peaks, one narrow, one broad, at low temperatures for D1.

The crystalline content was calculated from the normalized enthalpy via Eq. 2.1 and plotted against density. Figure 2.2 shows an almost perfect linear correlation between crystallinity and density for the 5 base resins used in the study. The lowest degree of crystallinity of 39% was observed for resin D1 and it rose to as much as 80% for resin X2.

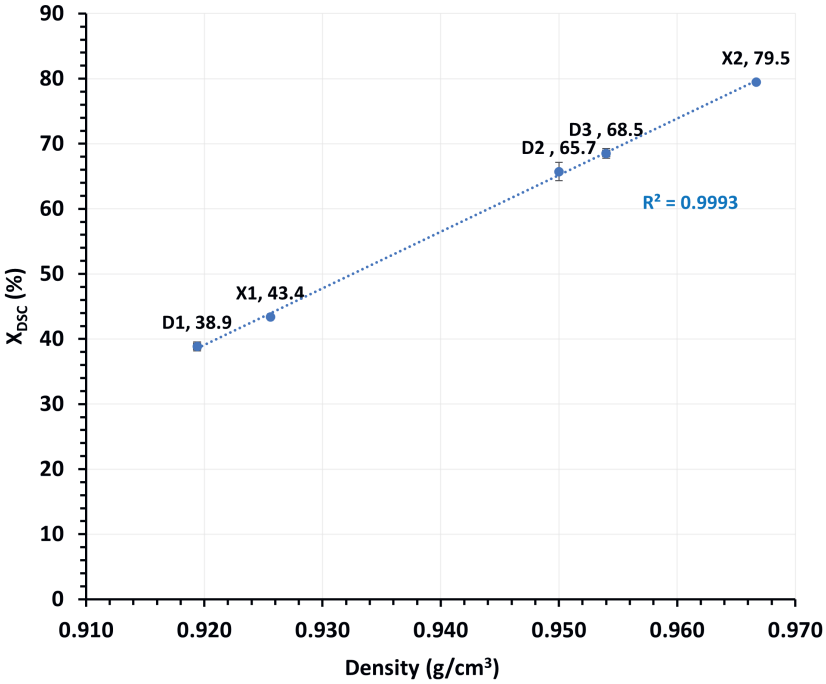

Figure 2.2 DSC percent crystallinity plotted against density for all 5 base resins (n=3).

2.3.1.2 GPC, iCCD and rheological characterization and analysis

A key aim of this work is to relate base resin microstructure to orientation-induced property enhancement. The compositional GPC (Figure 2.3) and iCCD (Figure 2.4) results provide detailed base resin macromolecular characterization. The results of the compositional GPC in Figure 2.3 show the molecular weight distribution (MWD) combined with an average comonomer content at each molecular weight(M). The MWD can be summarized by a series of moments, as given in Table 2.2. Figure 2.4 shows the iCCD, with SCB level (via Temperature, (T) at each T (SCB level)). CCD serves as a crucial structural parameter for characterizing product performance in various aspects, such as tie chain density, stiffness, seal window, seal strength, clarity, and other essential factors relevant to food packaging applications [31].

The weight average molecular weight (M_w) trends with MFI. The polydispersity ($Đ$) or MWD of most resins is similar, between 3.9 and 4.8, with as notable exception X2, which is much broader and shows a bimodal MWD. SCB is nearly absent for the higher density resins D2, D3, and X2. For lower density resins D1 and X2, there is clear SCB presence. The coupling between SCB and MWD is significantly different for those two. These structural variations will be connected to the base sheet and oriented film results in next sections of this Chapter. D2, D3, and X2 exhibit distinct features, showcasing very low comonomer content, creating an almost homopolymer structure. This compositional similarity is reflected in their high

densities. In contrast, D1 and X1 demonstrate a clear presence of comonomer, aligning with their lower densities. Further differentiation is observed between D1 and X1, as X1 concentrates comonomer in lower molecular weight molecules, while the highest molecular weight molecules have low comonomer content. This observation is also consistent in iCCD profile of X1, revealing two discernible fractions,one at high temperature and another at a lower temperature. Conversely, D1 exhibits a continuous decreasing SCB profile (from lower M to higher M) throughout its entire MWD, characterized by higher content of SCB at each molecular weight, in comparison to X1. Additionally, D2, D3, and X2 exhibit a single sharp peak in their iCCD profiles at higher temperature.

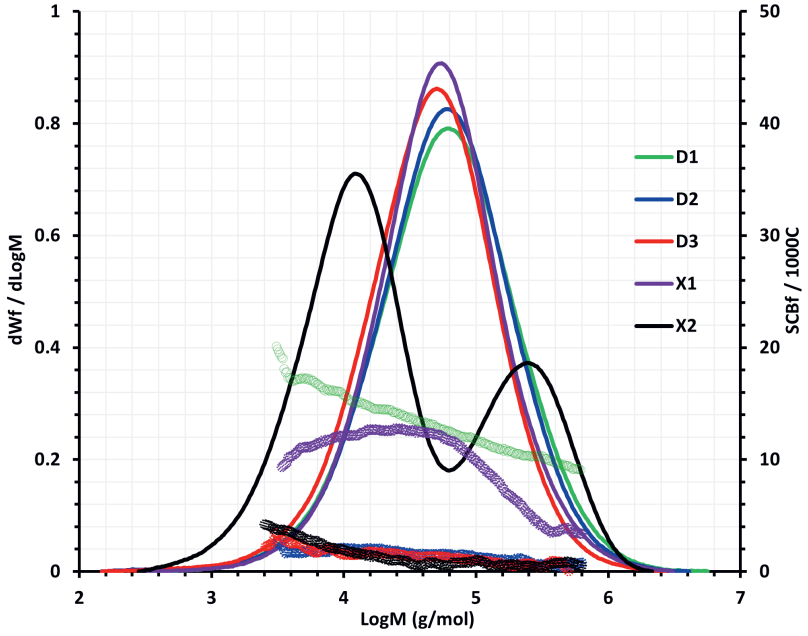

Figure 2.3 GPC curve for all 5 base resins. The left vertical axis represents the differential weight fractions (lines), and the right vertical axis represents the average SCB frequency per 1000 carbons at each molecular weight (open markers).

Table 2.2 Molecular weight moments and polydispersity index (MWD) of all 5 resins used in the study.

Resin	M_n (kg/mol)	M_w (kg/mol)	MWD $Đ$
D1	27.2	123.7	4.5
D2	23.2	110.5	4.8
D3	20.1	86.9	4.3
X1	26.6	102.8	3.9
X2	9.1	105.2	11.6

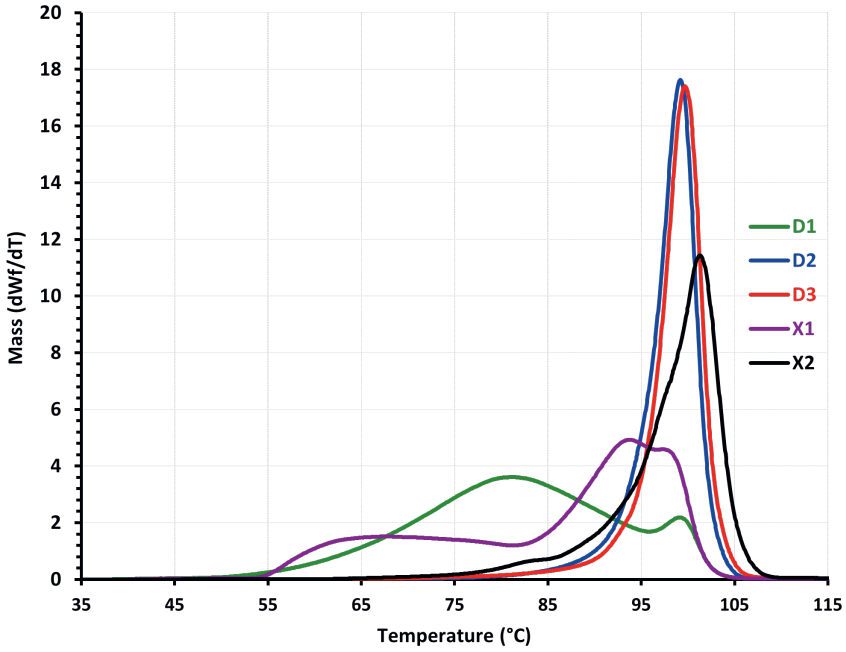

Figure 2.4 iCCD curve for all 5 base resins used. Differential mass fraction as a function of temperature.

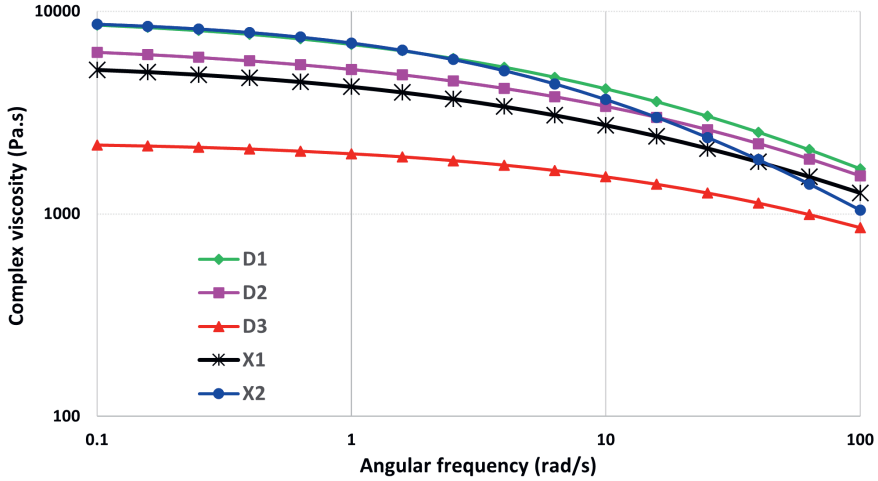

Figure 2.5 Flow curves of all 5 base resins at 190 ˚C.

The DMS linear viscoelasticity results of the base resins showed expected trends in view of the resin composition and in view of the measured MFI. As an illustration, the complex viscosity versus frequency at 190 °C is shown in Figure 2.5. The viscosity curves at low frequency are inversely proportional to the MFI and scale with average molecular weight according to known power-law relations [32], [33]. The shear thinning of the D-series (D1,D2,D3) and X1 is similar and in line with their similar dispersity. Resin X2 has higher dispersity and thus shows significantly more shear thinning and, despite its MFI of 1.7 dg/min, gets close to D3, with its higher MFI of 4.0 dg/min, at the higher frequencies. Similar flow curve behaviour for all the 5 resins was also observed at the temparature of 150 and 170 °C. The linear viscoelasticity results are fully explained by the MWD aspects of the molecular structure. Density and short-chain branching (SCB) variations play a negligible role in the melt rheology.

2.3.2 Compression molded base sheets, cast films and MDO films characterization

2.3.2.1 X-Ray characterization (SAXS and WAXS) and analysis

X-Ray diffraction experiments were performed on fabricated compression molded base sheets, cast films and MDO films to reveal the microstructural aspects such as crystallite dimension, long period, apparent crystallinity, and orientation of the crystallites of the PE films before and after MDO stretching. The raw data of the X-ray experiments is presented in the appendix Table A2.1 and A2.2.

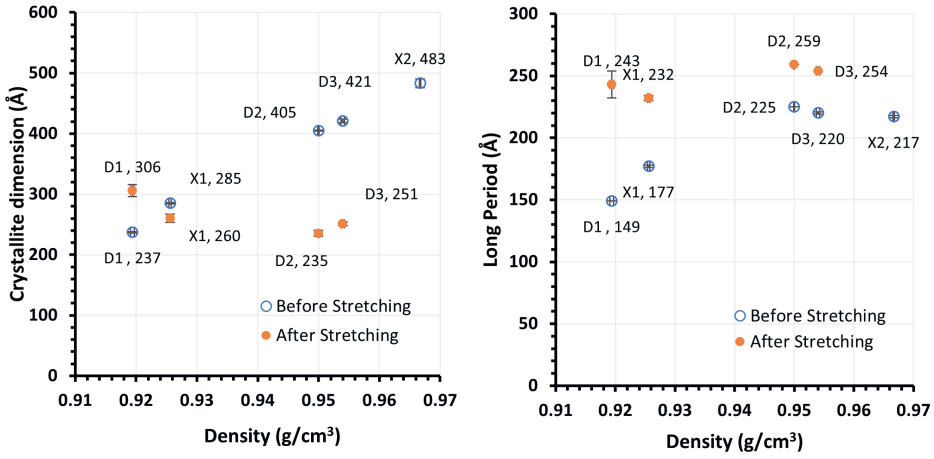

a) **b)**

Figure 2.6 a) Crystallite dimension, L (110) and **b)** long period for the compression molded base sheets (before stretching) and their counterpart MDO films (after stretching) of 5 base resins as a function of base sheet density (n=5). (Note: X2 could not be stretched to the process draw ratio of 7)

2.3.2.2 Morphological results from the SAXS and WAXS experiments

Figure 2.6a reveals that resin X1, due to its low comonomer concentration at higher molecular weight fractions (Figure 2.3) presented significantly larger crystallite dimension (285 Å) before stretching in its compression molded base sheets than D1 (237 Å), despite slight difference in density. Comparable findings were also revealed in the research conducted by Krishnaswamy *et al.* [18] where they studied the effect of short chain branching distribution on crystallization kinetics and mechanical properties of HDPE and reported that placement of branches on the longer molecules results in slower crystallization kinetics, which further decreased spherulitic size. The work of previous researchers teaches that the MDO operation disrupts the spherulitic superstructure of PE through mechanisms like lamellar shear, lamellar separation, and rotation [4], [34], [35], [36], [37], [38]. It was thus anticipated that the average crystallite dimension would decrease during the drawing process for films derived from high-density resins with larger crystallite sizes. This expectation was confirmed by the observed reduction in average crystallite dimension for D2 and D3 films after drawing, as evidenced from the Figure 2. 6a. Results for X2 were not obtained as X2 base sheet could not be stretched to the process draw ratio of 7.

Interestingly the same was not observed for the films made from low-density resins D1 and X1. The DSC (Figure 2.1) and iCCD (Figure 2.4) indicated that partial melting of crystalline phase was relatively higher for these resins as fixed orientation temperature of 110 ˚C was closer to the peak melting point of these resins as compared to higher density resins D2, D3, and X2. This possibly might have helped to retain similar (in case of X1) or even larger (in case of D1) crystallite size after the drawing process as its microstructure was relatively more mobile and thus less disintegrated and fibrillated under tensile load.

In Bonart and Hosemann's model of polyethylene [39] lamellar stacks consist of alternating crystalline and amorphous layers with varying thickness, collectively contributing to the long spacing or long period. It was also anticipated that the applied tensile force will lead to an increase in the regular spacing (long period) between crystalline lamellae after stretching. Upon analysis of the average crystallite dimensions depicted in Figure 2.6a, it becomes apparent that the crystalline microstructure of D1 and X1 exhibits lesser disintegration and fibrillation because of higher partially melted microstructure compared to D2 and D3 under stretching conditions. This phenomenon, accompanied by strain-induced amorphous section orientation and crystallization, contributes to a greater enhancement of their long period following stretching as depicted in Figure 2.6b.

2.3.2.3 Analysis of the orientations from WAXS

The 2D WAXS patterns gave insight on the orientation of the microstructure of base sheets, cast films and MDO films. The orientation was quantified using Herman’s orientation functions from WAXS data.

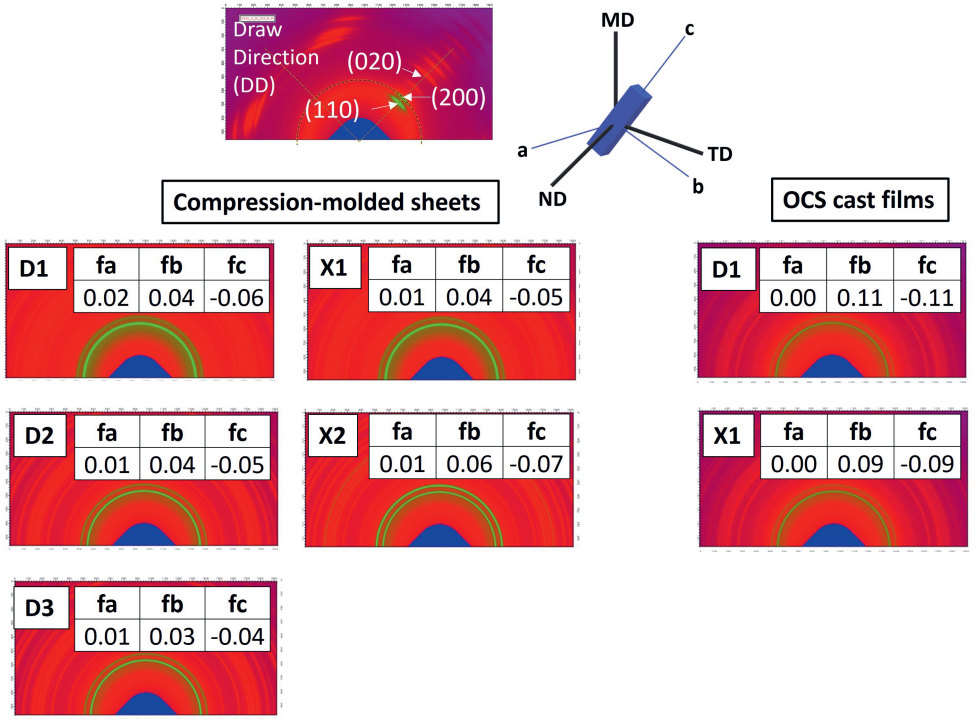

Figure 2.7 2D WAXS patterns for compression molded base sheets of all 5 base PE resins (D1,D2,D3,X1 and X2) and OCS cast films of D1 and X1 along with their Herman orientation factors.

PE films with orthorhombic crystal form typically scatter strongly from [110] and [200] reflecting planes (the latter corresponding to the a-axis) and relatively weaker [020] (corresponding to the b-axis)[40]. The [002] reflection plane (c-axis) is usually not visible. To evaluate the orientation of the crystalline phase, an intensity profile of a user-selected annulus vs azimuthal angle is obtained from [200] and [020] reflections. The intensity for a given azimuthal angle will depend on the amount of appropriately oriented crystallographic planes that will allow diffraction at that angle [28].

The intense uniform reflections from [110] and [200] planes of the orthorhombic unit cell are visible in the 2D WAXS patterns (Figure 2.7) of compression molded base sheets and cast film samples along with weaker reflections from other planes indicating a random orientation of their microstructure. No evidence of any strong orientation of microstructure was observed for all the samples as expected which was also confirmed with quantification by Herman orientation functions (shown with Figure 2.7). All three orientation factors fa, fb, and fc of the orthorhombic crystallographic axis a, b and c are close to 0 indicating the isotropic nature of the crystals. Although the cast film process was anticipated to introduce minor non-isotropic behavior in the resulting films, it had a limited impact on the orientation of the crystal structure.

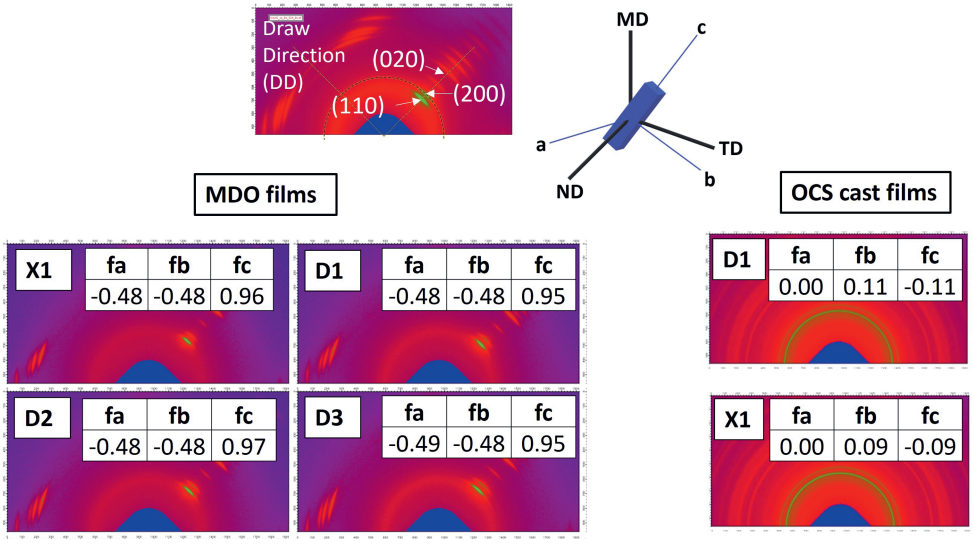

Figure 2.8 2D WAXS patterns for stretched MDO films (X1, D1, D2 and D3) and OCS cast films (D1, X1) along with their Herman orientation factors at similar thickness of 220 microns.

In contrast, the stretched MDO films (Figure 2.8) presented very strong crystalline orientation indicated by the strongly defined and intense equatorial diffraction arcs of the [110], [200] and [020] planes. The fc (orientation factor for the crystallographic c-axis) value being almost equal to 1 indicates that the c axis of the orthorhombic unit cell was almost perfectly aligned with the draw direction.

Quantifying amorphous section orientation is also feasible using 2D diffraction patters; yet it was challenging in this study due to the strong crystalline scattering peaks riding the amorphous halo. However, it was expected that applied tensile forces at the used orientation temperature during MDO process would also result in significant orientation of amorphous section towards the machine direction, especially in higher density base sheets because of the relatively lower proportion of amorphous section in their microstructure, which allows for easier disentanglement and orientation under the applied stretching load.

2.3.2.4 Apparent crystallinity analysis

From the XRD experiments, an apparent degree of crystallinity X_{XRD} of base sheets from all five base PE resins and their MDO-PE films was measured.

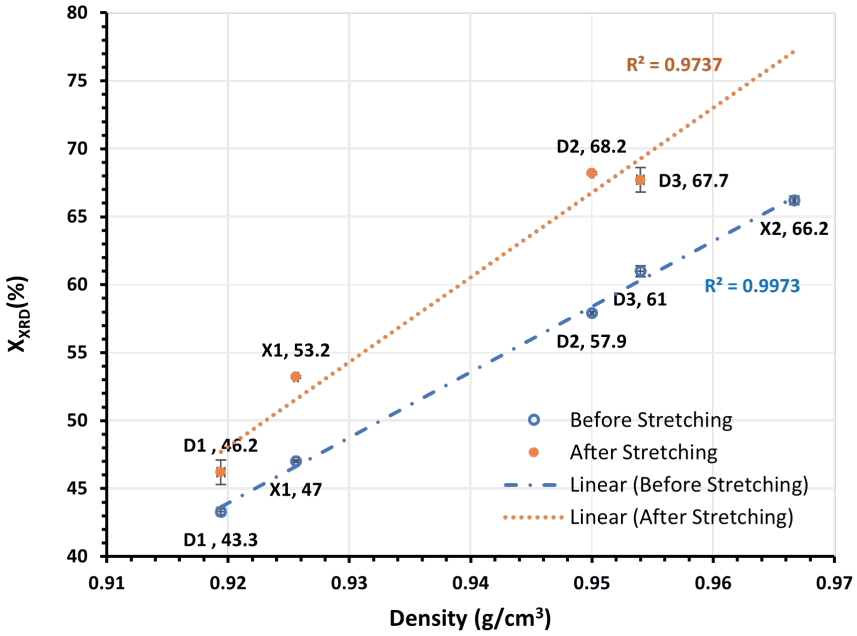

Figure 2.9 Apparent crystallinity (X_{XRD}) for the compression molded base sheets (before stretching) and their counterpart MDO films (after stretching) of 5 base resins as a function of base sheet density (n=5). (Note: X2 could not be stretched to the process draw ratio of 7)

Figure 2.9. compares the apparent crystallinity of the compression molded base sheet of all base resins D1, X1, D2, and D3 with the apparent crystallinity of MDO films obtained by the lab scale MDO process. Low-density resin D1 only shows about a 3% increase in apparent crystallinity whereas high-density resin D2 film showed as much as a 10% increase after stretching. This result is also an indication of higher fibrillation and strain induced re-crystallization in the initial crystalline structure of base sheets made from higher-density resin during stretching as was observed before. Interestingly among low density resins D1 and X1, X1 also showed a higher increment (about 6%) in apparent crystallinity as compared to D1(about 3%) because of the relatively larger crystallite dimension of X1 as compared to D1 before stretching due to its specific molecular architecture as shown in GPC and iCCD characterization.

To validate the apparent crystallinity results, the degree of crystallinity was also measured from enthalpy data using DSC 1st run curves for base sheets and MDO films of all five base resins used in the study. Figure 2.10 presents the comparison of the degree of crystallinity before and after stretching, as determined by DSC.

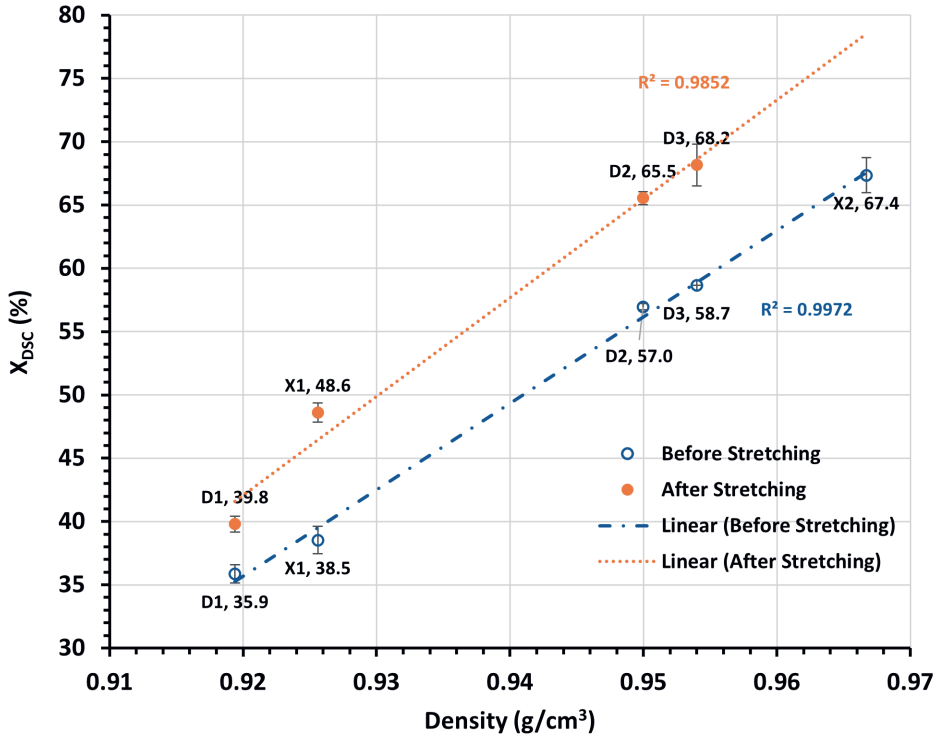

Figure 2.10 Degree of crystallinity (X_{DSC}) for the compression molded base sheets (before stretching) and their counterpart MDO films (after stretching) of 5 base resins as a function of base sheet density obtained from enthalpy data DSC 1st run (n=3). (Note: X2 could not be stretched to the process draw ratio of 7)

The figure indicates a slight difference in the degree of crystallinity measured by DSC compared to XRD. This difference was expected as DSC measures crystallinity based on heat flow associated with thermal transitions while X-Ray provides information about crystalline structure by analysing interaction of X-rays with atomic arrangement. Despite this slight variation, the overall trends in crystallinity measurements from DSC are similar to those obtained from XRD.

Stretch-induced crystallization is regarded as a promising method for modifying the properties of polymer films [41]. From X-Ray characterization along with DSC results, it is quite evident that MDO operation results in enhancement in overall crystallinity due to disintegration and fibrillation of the initial crystalline microstructure with strain induced crystallization in amorphous phase during stretching along with the oriented crystalline and amorphous microstructure towards the stretch direction.

2.3.2.5 AFM analysis

AFM analysis provided the surface morphology for compression molded base sheets (before stretching) and MDO films (after stretching). Under suitable drawing conditions, the morphology of the semicrystalline polymer transitions from isotropic to highly oriented [42]. The AFM topographical images in Figure 2.11. show a coarse isotropic morphology with no visible orientation for all the base sheets whereas it changed to larger fibrillar bundles with crystal fragments well oriented in the machine direction.

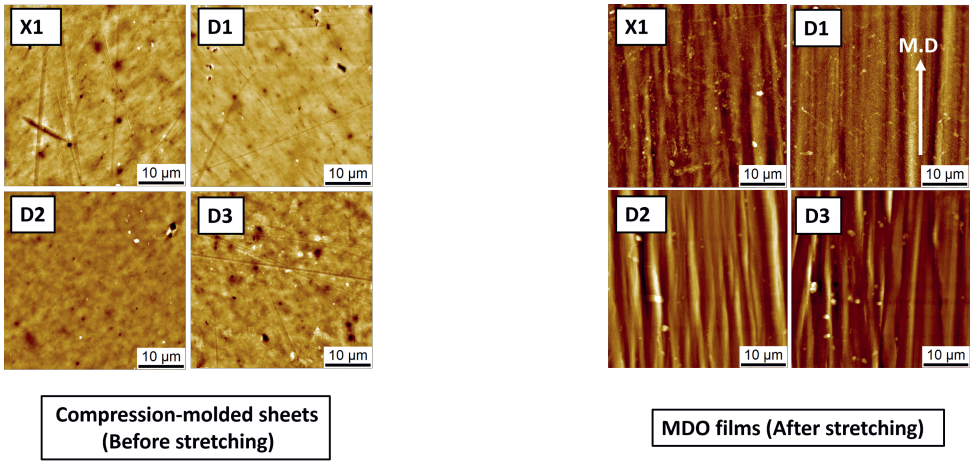

Figure 2.11 AFM Images of compression-molded base sheets and their counterpart MDO films for X1, D1, D2 and D3.

Higher disintegration and fibrillation of the initial crystalline phase was observed in high-density resin compression molded base sheets (D2 and D3) compared to low-density resins (D1 and X1) during the MDO process, as indicated by X-ray results. This was further validated by Atomic Force Microscopy (AFM), showing higher Root Mean Square (RMS) roughness at the surface in high-density resin MDO films (Figure 2.12), highlighting the influence of resin density on fibrillation and surface characteristics.

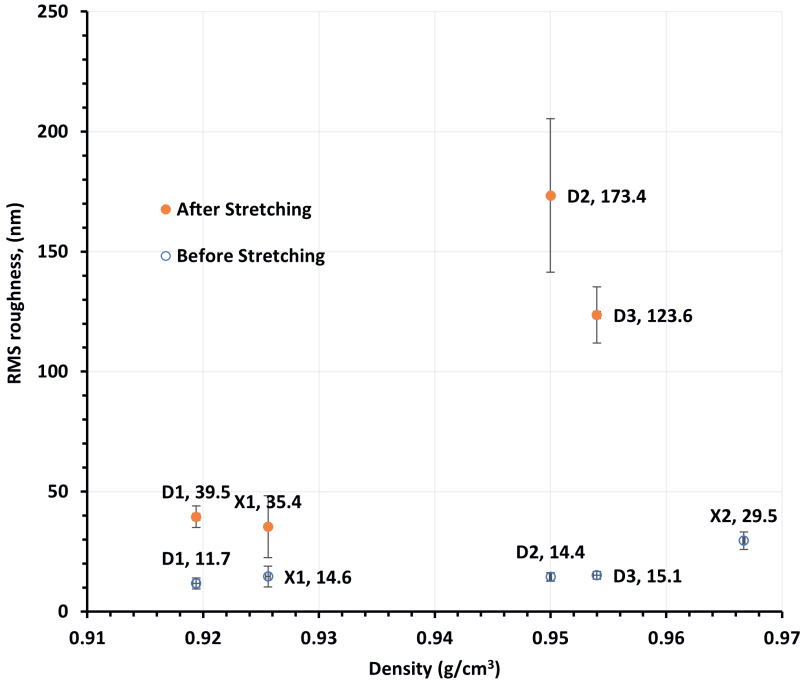

Figure 2.12 Root Mean Square (RMS) roughness at the surface for compression-molded base sheets and their counterpart MDO films for X1, D1, D2 and D3 as a function of base sheet density (n=5). (Note: X2 could not be stretched to the process draw ratio of 7).

The consistent influence of density on the disintegration and fibrillation of the initial crystalline phase, under fixed orientation or stretching temperature and draw ratio, was similarly observed after stretching the blended compression-molded base sheets comprising X1 and X2 into MDO films, as illustrated in Figure 2.13 and 2.14. Increase in density resulted in increased surface fibrillation, quantified by the RMS roughness.

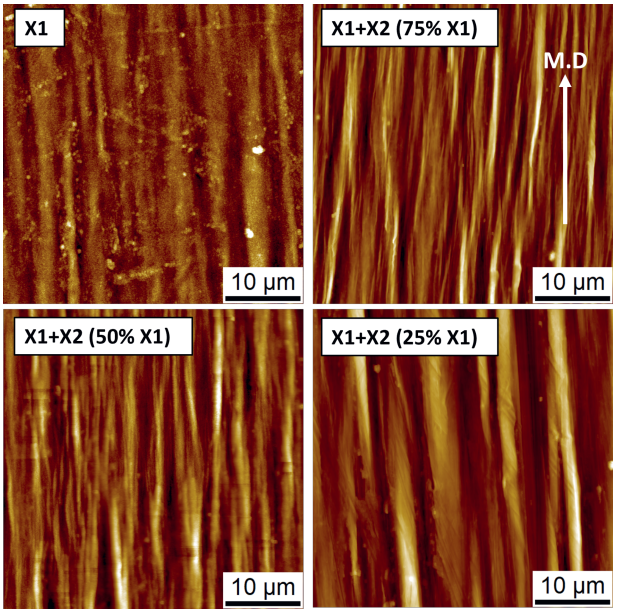

Figure 2.13 AFM Images for MDO-PE films of blends of X1-X2.

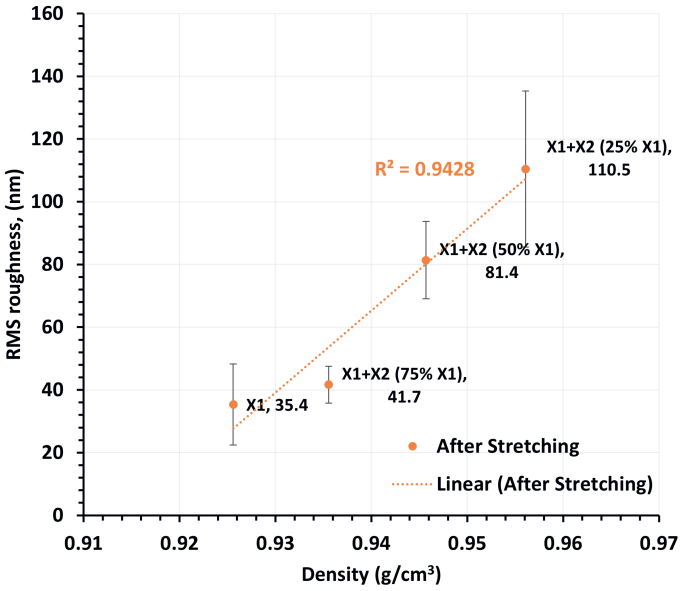

Figure 2.14 Root Mean Square (RMS) roughness at the surface for MDO-PE films of blends of X1-X2, plotted against density (n=5). (Note that X2 could not be stretched to the same length draw ratio of 7).

2.3.3 Investigation of tensile properties

All the base and blended resins were used for making compression molded base sheets and further their lab-scale stretched MDO films to investigate their tensile properties.

Nominal stress-strain curves at room temperature (23 °C) were plotted to analyse the mechanical performance of the compression-molded base sheets for all five resins used in the study, as depicted in Figure 2.15a and 2.15b.

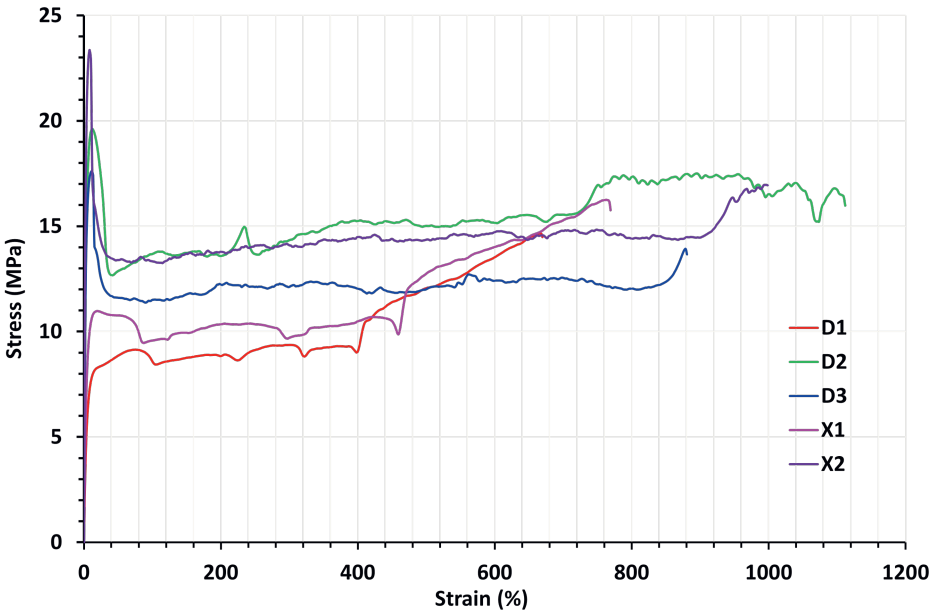

Figure 2.15a Nominal stress-strain curves at room temperature (23 °C) for base sheets (before MDO stretching) of all 5 base resins.

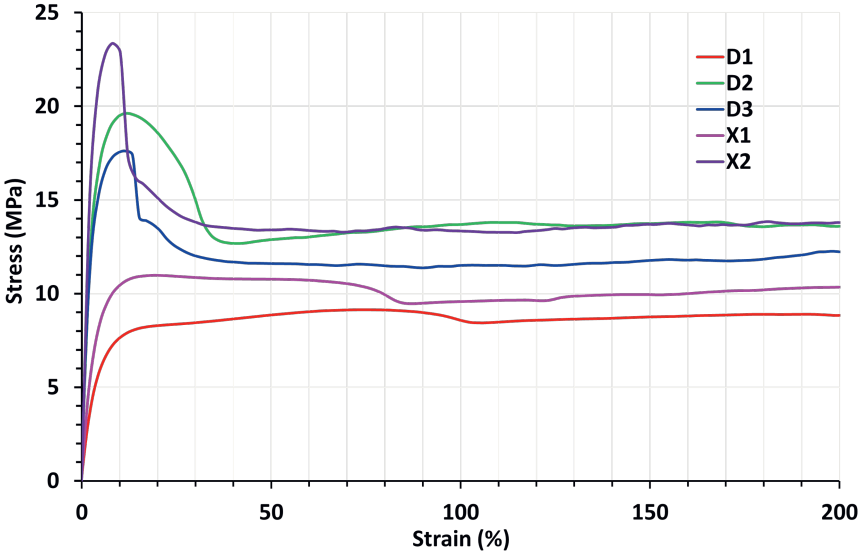

Figure 2.15b Nominal stress-strain curves at room temperature (23 °C) truncated at 200% strain on x-axis for base sheets (before MDO stretching) of all 5 base resins. (Note: The curves presented in Figure 2.15a are truncated at 200% strain on x-axis in this figure for better representation of yield properties)

From the stress-strain curves, it was observed that higher density generally led to higher modulus and yield stress, attributed to higher crystallinity. Specifically, the highest modulus and yield stress were recorded for the base sheet of the highest density resin, X2 (0.967 g/cm³), while the lowest values were observed for the base sheet of the lowest density resin, D1 (0.919 g/cm³). The lower density base sheets of D1 and X1 also exhibited onset of strain hardening behaviour at relatively lower percent strain values, attributed to the presence of substantial amorphous regions in their microstructure. In contrast, the higher density resin base sheets of D2, D3, and X2 demonstrated higher yield strength compared to those of D1 and X1. All five base sheets displayed ductile behaviour as expected.

The density of the blends was calculated theoretically using an inverse-additive mixing rule. It should be noted this may not be exact: if co-crystallization takes place, the true base sheet density of a blend can be higher than predicted by a simple mixing rule. The stretching process might have altered the densities of stretched films to a small amount, but in the analysis, all results of the stretched films are presented in terms of the densities of the base sheets. Equation 2.8 was used to calculate the percent change in modulus depicted in Figure 2.16.

$$\%\ Change\ in\ Modulus = \frac{Modulus\ of\ MDO\ films - Modulus\ of\ base\ sheets}{Modulus\ of\ base\ sheets} * 100 \qquad \textit{Equation 2.8}$$

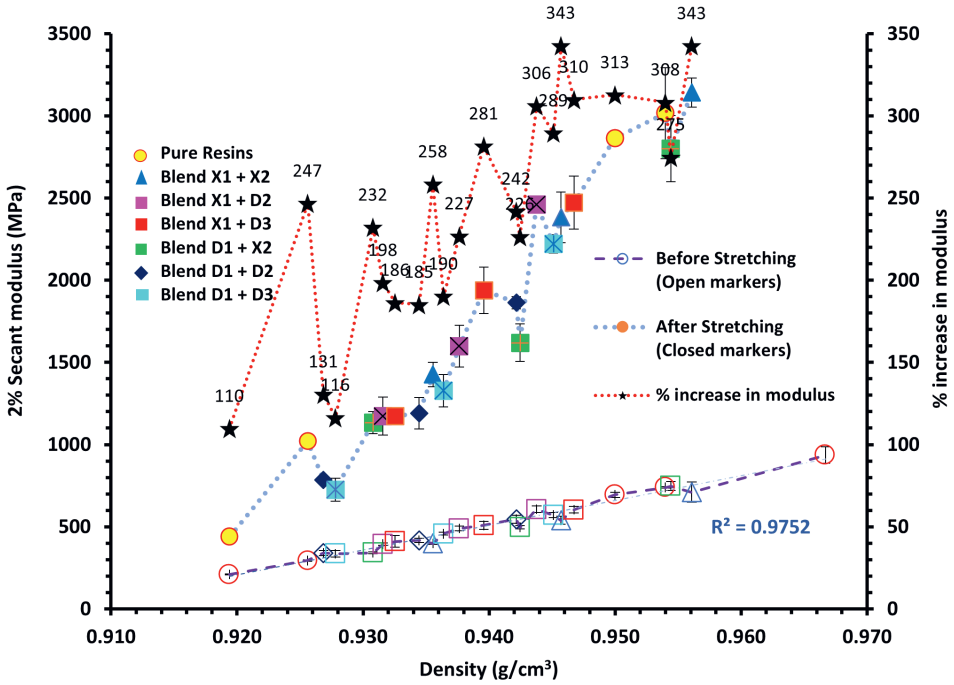

Figure 2.16 2% Secant modulus before (open symbols) and after (closed symbols) stretching for all base resins and their blends as a function of base-sheet density for base resins and theoretical base sheet density for blends (n=3). The red dotted line connecting star points represents the % increase in 2% secant modulus after stretching. (Note: X2 (density - 0.967 g/cm^3) could not be stretched to the process draw ratio of 7)

Figure 2.16. captures the combined base sheet and oriented MDO film modulus for all the materials. For the base sheets (unstretched), the relation between modulus and resin density was found to be dominantly linear. The varying nature of the resin microstructure beyond density is found to have a very minor effect on the modulus. The modulus ranges from about 200 MPa at the lower density of 0.919 g/cm^3 to about 900 MPa at the higher density of 0.967 g/cm^3. Next, it is observed that the lab-scale orientation under the present fixed conditions has a strong increasing effect on modulus, and in general the relative effect is higher at higher density, with about tremendous 350% increase for the 25%X1/75%X2 blend, reaching about 3100 MPa after stretching. This enhanced modulus is also comparable with the modulus of conventional polymers such as polyethylene terephthalate (PET) and polyamide (PA), that are used in the outer layer of multilayer flexible packaging systems: the typical modulus value for PET film is 2800 MPa, for PA film is 3000 MPa [43], [44]. The base sheet of resin X2 was not stretchable under the fixed orientation temperature of 110 ˚C due to its extremely high density and therefore crystallinity as compared to other resins and blends. Due to the high fraction of crystalline phase, its microstructure showed extreme fibrillation and necking during stretching at the used specific orientation temperature and thus ultimately broke off under tensile load. In case of HDPE, after necking,

deformation becomes highly concentrated in the neck region [45]. Work of Peterlin [46] teaches that the bundling of microfibrils into long, densely packed fibrils limit the possibility of deformation. Coates and Ward [47] investigating neck profiles in linear polyethylene also mentioned in their work that stabilization of neck is vital for continuous stretching. It is also reported in the literature that the "drawability" and "uniformity of drawing" of the base sheet to an MDO sheet is increased if the crystallinity can be decreased and if large spherulites are prevented from forming [4]. Thus, this extremely high crystallinity (about 80%) was the main reason for unstable neck formation because of development of densely packed fibrils during stretching and thus further unsuccessful stretching of the base sheet made from X2 which also has the highest density, 0.967 g/cm^3.

The generic enhancement in 2% secant modulus has been attributed in literature to the following phenomena that occur during MDO stretching of PE films [15] [14] [48].

- partial melting, fibrillation, and re-crystallization of the crystalline phase at the orientation temperature along with strain-induced crystallization in the amorphous phase enhancing overall crystallinity.
- highly oriented or aligned microstructure of films parallel to the stretch direction after the process.

The relatively stronger increase in modulus at higher density is attributed to the presence of an already significant fraction of crystalline phase in base sheets made from high-density resins and blends having relatively thicker crystallite dimensions than those made from low-density resins and blends. The presence of higher crystalline phase in relatively higher density resins is evident from the DSC and X-ray results mentioned before. Relatively thicker crystallite dimension and high crystallinity assist their microstructure to have less partial melting at the used fixed orientation temperature, which is relatively less mobile under tensile load during stretching. This relatively less partially melted microstructure shows comparatively more resistance to the tensile load and therefore high disintegration and fibrillation of the crystalline lamellae which further also helps in strain-induced crystallization of the amorphous phase alongside strong orientation of amorphous phase in stretch direction. This result was also verified during X-Ray and DSC characterizations.

The highest base sheet modulus (achieved at 0.967 g/cm^3 density) could already be surpassed by oriented MDO film at a density around 0.932 g/cm^3. In a type of example, a material substitution could require a modulus of about 3000 MPa. These results have shown this is achievable with these type of oriented PE as of a density of about 0.950 g/cm^3.

Nominal stress-strain curves at room temperature (23 °C) for a sample X1 base sheet and its MDO film were plotted to illustrate and compare the impact of MDO on mechanical performance, as shown in Figure 2.17.

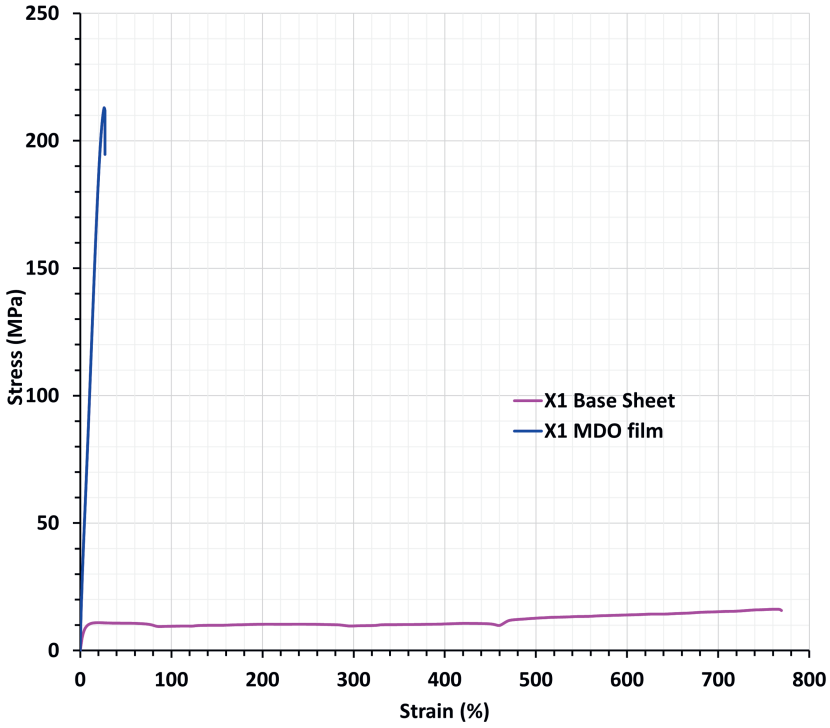

Figure 2.17 Nominal stress-strain curves at room temperature (23 °C) for base sheet (before stretching) and MDO film (after stretching) of X1.

The nominal stress-strain curves clearly demonstrate that the MDO film exhibited significantly greater stiffness (higher modulus), and tensile strength compared to the base sheets of the same material X1. Conversely, the base sheet exhibited higher toughness, as indicated by its greater elongation at break.

It should be noted that the stretching and orientation process during this lab-scale MDO could also impact other mechanical properties of the films like tear and impact strength, investigating these effects was outside the scope of this research. The enhancement in tensile modulus does translate into the enhancement of axial and bending stiffness which is prioritized in designing the outer layer of multilayer flexible packaging systems.

The relative shortcoming of MDO-PE films like low transverse direction (TD) strength compared to conventionally used PET films has also been noted in the work of Breese [49]. To address this issue, one potential solution is to optimize both the MD and TD strength of MDO films by fine-tuning key process parameters like MDO draw ratio, based on the end-use application. Employing relatively lower MDO draw ratios can enhance the MD strength of the film without significantly compromising TD strength, tailored to the specific requirements of the final application.

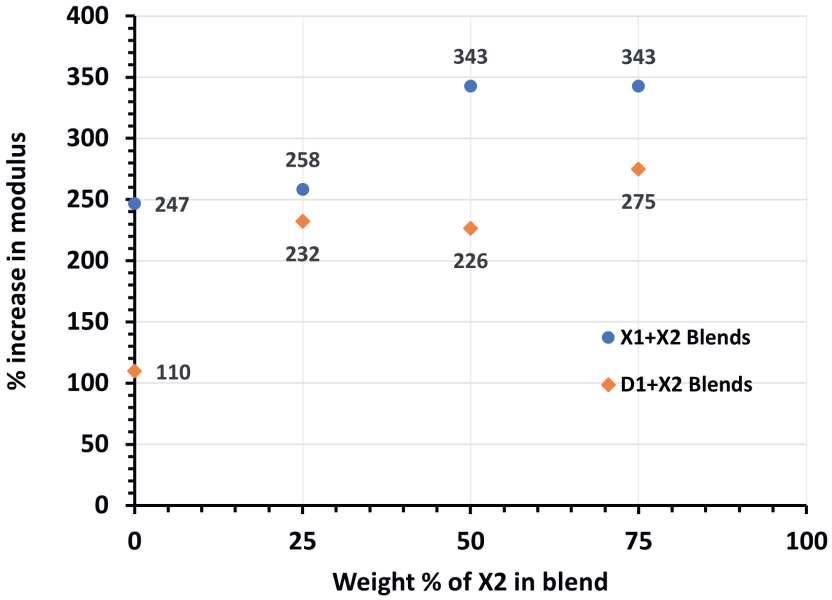

Figure 2.18 Percent (%) increase in secant modulus of films made of X1+X2 blends and D1+X2 blends after stretching at different weight composition of X2.

Having established the overall positive effect of orientation on modulus, and an overall more pronounced effect at higher densities, it is also observed that the modulus-density trend is less monotonic for the oriented samples than for the base samples, suggesting microstructural features beyond density affect the performance. This is important and deserves closer inspection. Thus, part of the data of Figure 2.16 is replotted in Figure 2.18 in terms of the binary blends involving X2. The X1+X2 series has larger modulus enhancement than the D1+X2 series, even though their densities were not significantly different.

As depicted in Figure 2.16, nearly all atypical upward fluctuations in the percentage increase in modulus were evident in blends incorporating X1, irrespective of increasing density. The origin of this phenomenon lies in microstructural variations and their impact on crystalline structure. GPC and X-ray characterization results reveals that X1, characterized by low comonomer concentration at higher molecular weight fractions, enables its base sheets to possess larger lamellae prior to fibrillation at the used orientation temperature. This attribute facilitates the orientation of microstructure and strain-induced crystallization of the amorphous phase during stretching, thereby augmenting overall crystallinity. Conversely, higher comonomer concentration at relatively lower molecular weight fractions contributes to uniform stretching.

2.3.3.1 Tensile properties of base sheets during stretching

Having analysed the pre-and post-stretching modulus, it is worth focusing on some specifics of the stretching process step itself. Specifically, the force required to perform the MDO stretching was measured as a relevant indicator for the ease of stretching for base sheets of different densities.

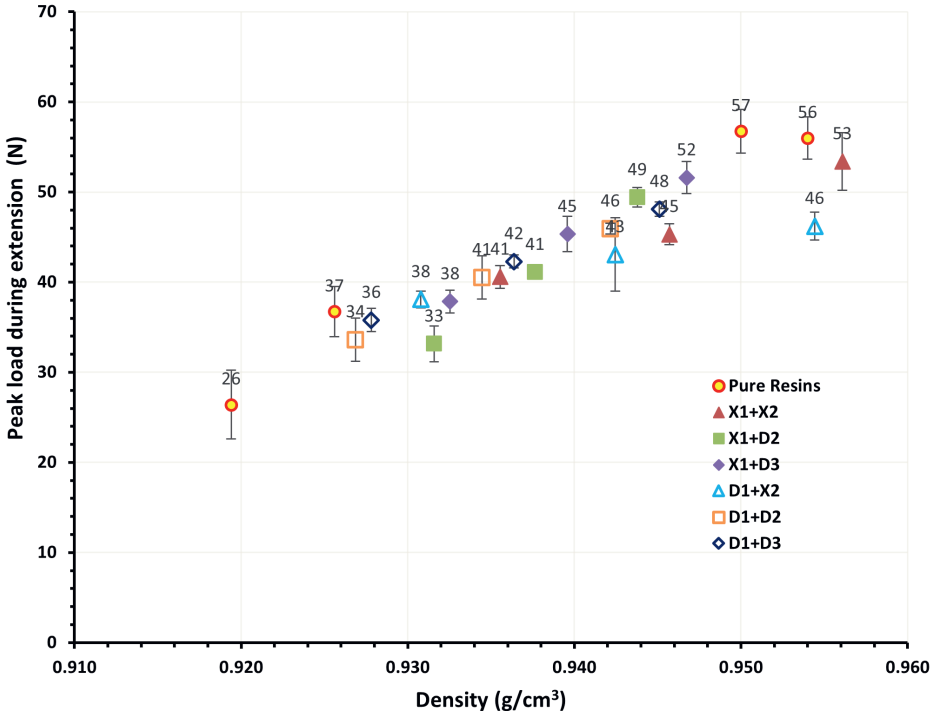

Figure 2.19 Peak load during extension (N) versus resin density for base sheets of initial thickness of 550 µm stretched to a process draw ratio of 7 (150 mm extension) (n=3). (Note: X2 (density - 0.967 g/cm^3) could not be stretched to the process draw ratio of 7.)

Peak load required to achieve constant maximum extension of 150 mm during stretching of base sheets inside lab-scale MDO setup to produce MDO films is plotted as a function of density in Figure 2.19. The peak load defined in this section, refers to the maximum load recorded by the load cell during the tensile stretching of the base sheet at the used orientation temperature. The samples were stretched to a constant maximum extension of 150 mm (600% strain), and both load at yield and load at maximum extension were recorded to determine the peak load to achieve 600% strain. Notably, none of the samples fractured during stretching, except for the base sheet of X2, which fractured due to its extremely high density of 0.967 g/cm^3. The load data at maximum extension and at yield point for all samples during stretching is provided in the Appendix Table A2.3. The peak load in general increased with an increase in resin density. For samples with densities up to 0.946 g/cm^3, the load recorded at maximum extension was higher than the load at yield. This is

primarily due to significant strain hardening of the amorphous regions during stretching in the limit of 600% strain at the used orientation temperature, as base sheets with relatively lower densities contained a significant amount of amorphous fractions in their microstructure. In contrast, for samples with densities greater than 0.946 g/cm^3, the load at yield was generally higher than the load at maximum extension. This is because higher density samples had lesser amorphous regions, resulting in less strain hardening in the maximum 600% strain limit used in the experiments

Hence, the optimization of PE density is crucial in accordance with the desired ease of stretching, and modulus enhancement during the MDO. Extremely high PE density may result in localized or non-uniform stretching and should therefore be carefully considered as observed from unsuccessful stretching of base sheet of base resin X2 (0.967 g/cm^3).

To better understand the tensile behaviour during stretching at the orientation temperature, stress-strain curves were plotted for two base sheets—one made of low-density resin (D1) and the other of high-density resin (D3)—undergoing uniaxial stretching, as shown in Figure 2.20.

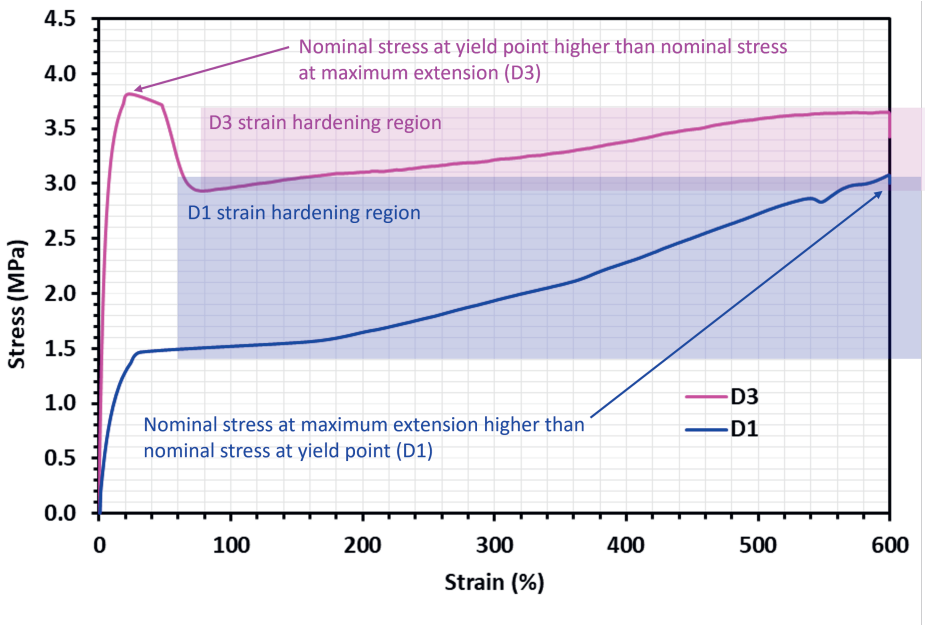

Figure 2.20 Nominal stress-strain curve for D1 and D3 base sheets during stretching at the used orientation temperature.

For the base sheet of lower-density resin D1, as expected, a significant amount of strain hardening was observed during stretching up to the maximum 600% strain limit used in the experiment as depicted in Figure 2.20. This is attributed to the presence of a substantial amount of amorphous sections in its microstructure, resulting in a higher nominal stress at maximum extension compared to the nominal stress at the yield point. Conversely, the base sheet of high-density resin D3 exhibited higher nominal stress at the yield point and

relatively less strain hardening behaviour, which can be attributed to its microstructure containing fewer amorphous sections.

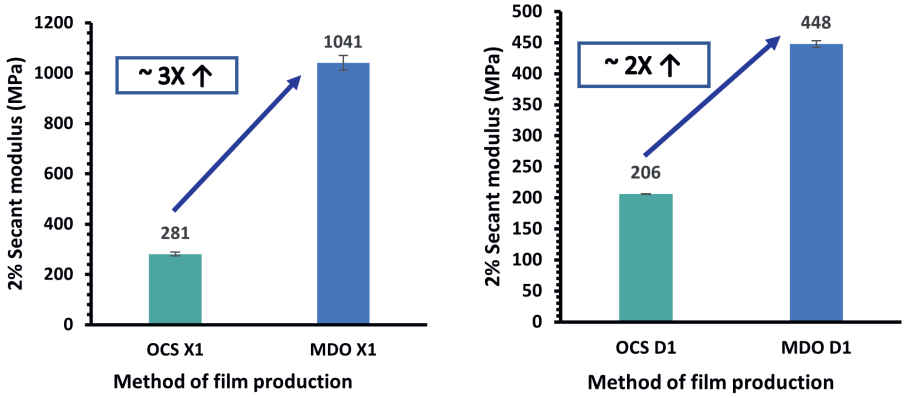

Figure 2.21 Comparison of 2% secant modulus of MDO stretched film with cast film at a similar thickness of about 220 µm (n=3).

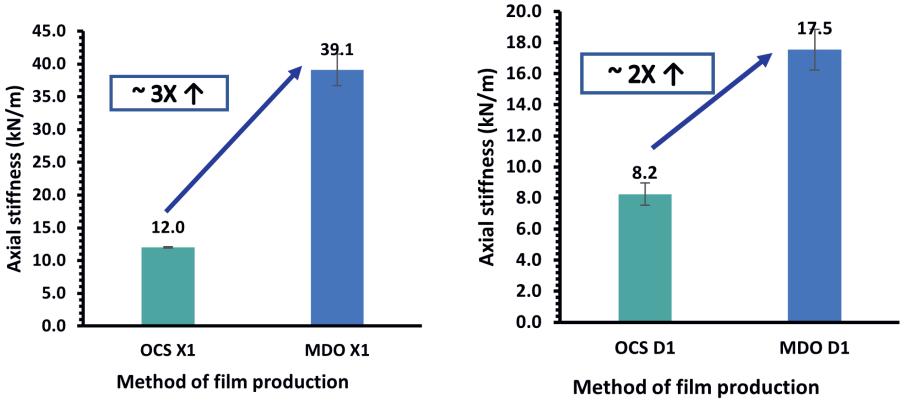

Figure 2.22 Comparison of axial stiffness of MDO stretched film with cast film at a similar thickness of about 220 µm (n=3).

Cast films from resins X1 and D1 were prepared on an OCS cast film line, matched in thickness to lab-scale MDO-PE films (about 220 µm), for a direct comparison of tensile properties while minimizing the impact of thickness variations. Figures 2.21 and 2.22 show that, at a similar 220 µm thickness, the 2% secant modulus and axial stiffness of MDO films were several times higher than of the casted films: 3 times higher in the case for films made from resin X1 and 2 times in the case of films made of D1. These results confirm that the MDO process significantly enhances modulus and axial stiffness, when compared at similar thickness level.

2.4 Concluding remarks

In conclusion, the uniaxial stretching of polyethylene (PE) films using the lab-scale machine direction orientation (MDO) process resulted in a significant enhancement of the tensile modulus and strength particularly along the machine direction. The key learnings from the Chapter are summarised as follows:

- The base sheets made of high-density resins and blends exhibited higher disintegration and fibrillation of the crystalline microstructure. This increased disintegration and fibrillation is attributed to a larger crystalline phase, which offers greater resistance to tensile load during stretching, resulting in a highly fibrillated microstructure.

- X-ray and DSC characterization demonstrated that MDO operation enhances overall crystallinity by disintegrating and fibrillating the initial crystalline microstructure, instigating strain induced crystallization in the amorphous phase, and aligning both crystalline and amorphous sections in the stretch direction.

- Extremely high PE density can lead to localized or non-uniform stretching, as evidenced by the unsuccessful stretching of the base sheet made from base resin X2 (0.967 g/cm^3). Thus, optimizing PE density (or crystallinity) is crucial for achieving the desired ease of stretching and modulus enhancement during the MDO process.

- Distinct molecular architecture of resin X1, characterized by low comonomer concentration at relatively higher molecular weight fractions, resulted in larger crystallite dimensions in its base sheets, facilitating higher enhancement in tensile modulus with relatively higher ease of stretching due to its low density.

- Low-density resin MDO films exhibited lower surface roughness in atomic force microscopy (AFM) analysis due to their more mobile microstructure resisting extreme disintegration and fibrillation during stretching at the used orientation temperature.

Prepared MDO films consistently demonstrated oriented microstructures aligned parallel to the stretch direction. These stiffness-enhanced MDO-PE films have potential applications as an outer layer in PE-based designs for flexible packaging, offering improved mechanical properties and performance.

2.5 Bibliography

[1] "Plastics-the Facts 2022 OCTOBER 2022, Plastics Europe." Accessed: Feb. 01, 2024. [Online]. Available: https://plasticseurope.org/knowledge-hub/plastics-the-facts-2022/

[2] "ETC/CE Report 4/2022 Flexible plastics in Europe's circular economy — Eionet Portal." Accessed: Apr. 08, 2024. [Online]. Available: https://www.eionet.europa.eu/etcs/etc-ce/products/etc-ce-products/etc-ce-report-4-2022-flexible-plastics-in-europe2019s-circular-economy

[3] "Flexible Packaging Market Size and Share Report, 2030." Accessed: Feb. 01, 2024. [Online]. Available: https://www.grandviewresearch.com/industry-analysis/global-flexible-packaging-market

[4] V. Ratta, G. L. Wilkes, and T. K. Su, "Structure–property-processing investigations of the tenter-frame process for making biaxially oriented HDPE film. I. Base sheet and draw along the MD," *Polymer (Guildf)*, vol. 42, no. 21, pp. 9059–9071, Oct. 2001, doi: 10.1016/S0032-3861(01)00387-1.

[5] "Pathways to Mono-Material Flexible Plastic Packaging - Working together for a Canada without plastic waste or pollution." Accessed: Apr. 08, 2024. [Online]. Available: https://plasticspact.ca/pathways-to-mono-material-flexible-plastic-packaging/

[6] B. A. Morris, "Commonly Used Resins and Substrates in Flexible Packaging," in *The Science and Technology of Flexible Packaging*, Elsevier, 2017, pp. 69–119. doi: 10.1016/b978-0-323-24273-8.00004-6.

[7] E. Hatfield, "Machine direction oriented film technology," in *Multilayer Flexible Packaging: Technology and Applications for the Food, Personal Care, and Over-the-Counter Pharmaceutical Industries*, Elsevier, 2009, pp. 113–118. doi: 10.1016/B978-0-8155-2021-4.10010-3.

[8] M. Paul, B. Morris, J. Weinhold, and K. Hausmann, "The effect of stretching and tie layer composition on adhesion strength of multi-layered films," *Journal of Plastic Film and Sheeting*, vol. 38, no. 3, pp. 351–368, Jul. 2022, doi: 10.1177/87560879211063475.

[9] P. J. Lemstra, C. W. M. Bastiaansen, and H. E. H. Meijer, "Chain-extended flexible polymers," *Die Angewandte Makromolekulare Chemie*, vol. 145, no. 1, pp. 343–358, Nov. 1986, doi: 10.1002/APMC.1986.051450117.

[10] P. J. Lemstra, N. A. J. M. van Aerle, and C. W. M. Bastiaansen, "Chain-Extended Polyethylene," *Polymer Journal 1987 19:1*, vol. 19, no. 1, pp. 85–98, 1987, doi: 10.1295/polymj.19.85.

[11] P. Smith, P. J. Lemstra, and J. P. L. Pijpers, "Tensile strength of highly oriented polyethylene. II. Effect of molecular weight distribution," *Journal of Polymer*

Science: Polymer Physics Edition, vol. 20, no. 12, pp. 2229–2241, Dec. 1982, doi: 10.1002/POL.1982.180201206.

[12] J. M. Andrews and I. M. Ward, "The cold-drawing of high density polyethylene," *J Mater Sci*, vol. 5, no. 5, pp. 411–417, May 1970, doi: 10.1007/BF00550003/METRICS.

[13] G. Capaccio and I. M. Ward, "Preparation of ultra-high modulus linear polyethylenes; effect of molecular weight and molecular weight distribution on drawing behaviour and mechanical properties," *Polymer (Guildf)*, vol. 15, no. 4, pp. 233–238, Apr. 1974, doi: 10.1016/0032-3861(74)90038-X.

[14] S. H. Tabatabaei, L. Parent, P. Cigana, A. Ajji, and P. J. Carreau, "Effect of machine direction orientation conditions on properties of HDPE films," *Journal of Plastic Film and Sheeting*, vol. 25, no. 3–4, pp. 235–249, 2009, doi: 10.1177/8756087910369423.

[15] Q. Chen, Z. Wang, S. Zhang, Y. Cao, and J. Chen, "Structure Evolution and Deformation Behavior of Polyethylene Film during Biaxial Stretching," *ACS Omega*, vol. 5, no. 1, pp. 655–666, Jan. 2020, doi: 10.1021/acsomega.9b03250.

[16] S. H. Tabatabaei, P. J. Carreau, and A. Ajji, "Structure and properties of MDO stretched polypropylene," *Polymer (Guildf)*, vol. 50, no. 16, pp. 3981–3989, Jul. 2009, doi: 10.1016/j.polymer.2009.06.059.

[17] E. Hatfield, R. Tate, K. Williams, and W. Todd, "NEW MDO MEDIUM MOLECULAR WEIGHT HIGH DENSITY POLYETHYLENE FILMS*," *JOURNAL OF PLASTIC FILM & SHEETING*, vol. 18, 2002, doi: 10.1177/875608702032871.

[18] R. K. Krishnaswamy, Q. Yang, L. Fernandez-Ballester, and J. A. Kornfield, "Effect of the distribution of short-chain branches on crystallization kinetics and mechanical properties of high-density polyethylene," *Macromolecules*, vol. 41, no. 5, pp. 1693–1704, Mar. 2008, doi: 10.1021/ma070454h.

[19] X. Li *et al.*, "The effect of comonomer content on structure and property relationship of propylene-1-octene copolymer during uniaxial stretching," *Polymer (Guildf)*, vol. 54, no. 17, pp. 4545–4554, Aug. 2013, doi: 10.1016/j.polymer.2013.06.017.

[20] R. L. Blaine, "Determination of Polymer Crystallinity by DSC. Therm. Anal. TA Instruments, 109 Lukens Drive, New Castle DE 19720, USA, 1-3." Accessed: Apr. 09, 2024. [Online]. Available: https://www.scirp.org/reference/referencespapers?referenceid=1920439

[21] W. Yau *et al.*, "A 'systematic approach' to TD-GPC data processing with band broadening correction," *Macromol Symp*, vol. 330, no. 1, pp. 53–62, Aug. 2013, doi: 10.1002/masy.201300029.

[22] T. Pathaweeisariyakul, K. Narkchamnan, B. Thitisuk, and W. Yau, "Methods of long chain branching detection in PE by triple-detector gel permeation chromatography," *J Appl Polym Sci*, vol. 132, no. 28, Jul. 2015, doi: 10.1002/app.42222.

[23] M. T. DeMeuse, "Equipment design and requirements of biaxially stretched films," in *Biaxial Stretching of Film*, Elsevier, 2011, pp. 14–26. doi: 10.1533/9780857092953.1.14.

[24] "MDO Films: Lots of Promise, Big Challenges | Plastics Technology." Accessed: Apr. 18, 2024. [Online]. Available: https://www.ptonline.com/articles/mdo-films-lots-of-promise-big-challenges

[25] "The Key Aspects of a Machine Direction Orienter - Part 1 Heating Methods." Accessed: Apr. 18, 2024. [Online]. Available: https://parkinsontechnologies.com/index.php/blog/the-key-aspects-of-a-machine-direction-orienter-part-1-heating-methods

[26] J. G. Drobny, "Processing Methods Applicable to Thermoplastic Elastomers, Pg. 141," in *Handbook of Thermoplastic Elastomers*, Elsevier, 2014, pp. 33–173. doi: 10.1016/b978-0-323-22136-8.00004-1.

[27] D. Campbell, R. A. Pethrick, and J. R. White, "Polymer Characterization: Physical techniques: Second Edition," *Polymer Characterization: Physical techniques: Second Edition*, pp. 1–481, Jan. 2017, doi: 10.1201/9781315274706/POLYMER-CHARACTERIZATION-DAN-CAMPBELL-RICHARD-PETHRICK-JIM-WHITE.

[28] A. Prasad, R. Shroff, S. Rane, and G. Beaucage, "Morphological study of HDPE blown films by SAXS, SEM and TEM: a relationship between the melt elasticity parameter and lamellae orientation," *Polymer (Guildf)*, vol. 42, no. 7, pp. 3103–3113, Mar. 2001, doi: 10.1016/S0032-3861(00)00612-1.

[29] "DSC Analysis of Polymers | Thermal | EAG Laboratories." Accessed: Feb. 01, 2024. [Online]. Available: https://www.eag.com/app-note/characterization-of-polymers-using-differential-scanning-calorimetry-dsc/

[30] X. Yao *et al.*, "CRYSTAF, DSC and SAXS Study of the Co-Crystallization, Phase Separation and Lamellar Packing of the Blends with Different Polyethylenes," *Polymers (Basel)*, vol. 15, no. 8, Apr. 2023, doi: 10.3390/polym15081940.

[31] R. Cong *et al.*, "Quantification of Chemical Composition Distribution of Polyolefin Materials for Improved Accuracy and Speed," *Macromolecules*, vol. 56, no. 4, pp. 1492–1502, Feb. 2023, doi: 10.1021/acs.macromol.3c00020.

[32] T. Bremner, A. Rudin, and D. G. Cook, "Melt flow index values and molecular weight distributions of commercial thermoplastics," *J Appl Polym Sci*, vol. 41, no. 7–8, pp. 1617–1627, 1990, doi: 10.1002/app.1990.070410721.

[33] S. M. Ghasemi and G. M. M. Sadeghi, “General and more precise relationships between molecular weight, blend ratio, and melt index of binary polyethylene blends,” *J Appl Polym Sci*, vol. 108, no. 5, pp. 2988–2993, Jun. 2008, doi: 10.1002/app.27788.

[34] A. Keller and D. P. Pope, “Identification of structural processes in deformation of oriented polyethylene,” *J Mater Sci*, vol. 6, no. 6, pp. 453–478, Jun. 1971, doi: 10.1007/BF00550302/METRICS.

[35] E. S. Clark and L. S. Scott, “Superdrawn crystalline polymers: A new class of high-strength fiber,” *Polym Eng Sci*, vol. 14, no. 10, pp. 682–686, Oct. 1974, doi: 10.1002/PEN.760141004.

[36] T. Tagawa and K. Ogura, “Piled-lamellae structure in polyethylene film and its deformation,” *Journal of Polymer Science: Polymer Physics Edition*, vol. 18, no. 5, pp. 971–979, May 1980, doi: 10.1002/POL.1980.180180505.

[37] A. Cowking, J. G. Rider, I. L. Hay, and A. Keller, “A study on the orientation effects in polyethylene in the light of crystalline texture,” *Journal of Materials Science 1968 3:6*, vol. 3, no. 6, pp. 646–654, Nov. 1968, doi: 10.1007/BF00757913.

[38] B. Cayrol and J. Petermann, “Elastic hard polyethylene fibers,” *Journal of Polymer Science: Polymer Physics Edition*, vol. 12, no. 10, pp. 2169–2172, Oct. 1974, doi: 10.1002/POL.1974.180121017.

[39] R. Bonart and R. Hosemann, “Fibrillarstrukturen in kaltverstrecktem linearen Polyäthylen,” *Kolloid-Zeitschrift und Zeitschrift für Polymere*, vol. 186, no. 1, pp. 16–29, Nov. 1962, doi: 10.1007/BF01797949/METRICS.

[40] L. E. (Leroy E. Alexander, “X-ray diffraction methods in polymer science,” p. 582, 1969, Accessed: Feb. 07, 2024. [Online]. Available: https://books.google.com/books/about/X_ray_Diffraction_Methods_in_Polymer_Sci.html?id=EgmFAAAAIAAJ

[41] L. Meng *et al.*, “Constrained and free uniaxial stretching induced crystallization of polyethylene film: A comparative study,” *Polym Test*, vol. 36, pp. 110–118, 2014, doi: 10.1016/j.polymertesting.2014.04.002.

[42] X. Liu *et al.*, “Strain dependent crystallization of isotactic polypropylene during solid-state stretching,” *Polym Test*, vol. 104, Dec. 2021, doi: 10.1016/j.polymertesting.2021.107404.

[43] B. A. Morris, “Chapter 9 - Strength, Stiffness, and Abuse Resistance,” in *The Science and Technology of Flexible Packaging*, Elsevier, 2017, pp. 309–350. doi: 10.1016/b978-0-323-24273-8.00009-5.

[44] R. Y. Wu, L. D. McCarthy, and Z. H. Stachurski, “Tearing resistance of multi-layer plastic films,” *International Journal of Fracture 1994 68:2*, vol. 68, no. 2, pp. 141–150, Jul. 1994, doi: 10.1007/BF00032464.

[45] S. Hao, X. Wu, and C. Lu, “Time courses of strains that induce necking and fracturing in high-density polyethylene,” *Polym Test*, vol. 120, Mar. 2023, doi: 10.1016/j.polymertesting.2023.107946.

[46] A. Peterlin, “Plastic deformation of polymers with fibrous structure,” *Colloid and Polymer Science Kolloid Zeitschrift & Zeitschrift für Polymere*, vol. 253, no. 10, pp. 809–823, Oct. 1975, doi: 10.1007/BF01452401/METRICS.

[47] P. D. Coates and I. M. Ward, “Neck profiles in drawn linear polyethylene,” *J Mater Sci*, vol. 15, no. 11, pp. 2897–2914, Nov. 1980, doi: 10.1007/BF00550561/METRICS.

[48] R. Breese, E. Chemicals, L. Company, O. Cincinnati, and J. J. Strebel, “Balancing tear strength and modulus of machine direction oriented films containing high molecular weight polyethylene,” 2006. [Online]. Available: https://www.researchgate.net/publication/289332735

[49] R. Breese, “Flexible Packaging Substrates Benefits of machine direction-oriented (MDO) films in flexible-packaging applications.” Accessed: Jul. 22, 2024. [Online]. Available: http://ccl-eclipse.com/News_Releases/Benefits%20of%20MDO%20in%20Flexible%20Packaging.pdf

2.6 Appendix 2

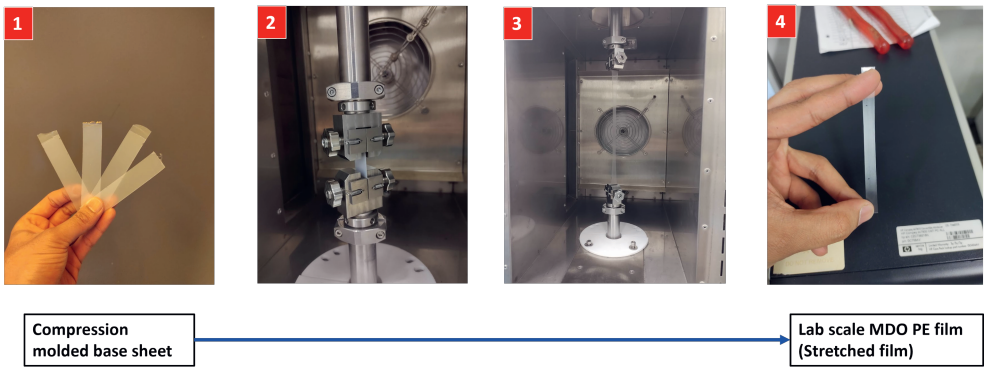

Figure A2.1 Lab-scale MDO stretching process.

X-Ray data

Table A2.1 Tabular data representing a summary of results from SAXS and WAXS experiments for selected base sheets and cast films sample (S38-S47) (n=5).

Sample	Resin/Blends	Long Period (Å)		Average crystal size (Å)		Apparent Crystallinity (%)	
		Mean	Std Dev	Mean	Std Dev	Mean	Std Dev
S38	**X1**	177	1	285	1	47	0.1
S39	**X2**	217	1	483	7	66.2	0.3
S40	**D1**	149	0	237	1	43.3	0.2
S41	**D2**	225	0	405	1	57.9	0.1
S42	**D3**	220	1	421	3	61	0.4
S43	**X1 Cast film**	170	5	267	8	45.5	0.4

S44	**D1 Cast film**	142	1	224	3	42	0.2
S45	**X1 + X2 (25% X1)**	219	0	470	3	64.2	0.1
S46	**X1 + X2 (50% X1)**	212	0	411	1	57.7	0
S47	**X1 + X2 (75% X1)**	199	1	346	1	52.8	0.2

Table A2.2 Tabular data representing a summary of results from SAXS and WAXS experiments for a sample of stretched films of X1, D1, D2, and D3 (S09-S12) (n=5).

Sample	**Resin**		**Long Period (Å)**		**Average Crystal size (Å)**		**Apparent Crystallinity (%)**	
		Density	**Mean**	**Std Dev**	**Mean**	**Std Dev**	**Mean**	**Std Dev**
S09	**X1**	0.9256	232	2	260	7	53.2	0.1
S10	**D1**	0.9194	243	11	306	10	46.2	0.9
S11	**D2**	0.9500	259	0	235	5	68.2	0.1
S12	**D3**	0.9540	254	0	251	3	67.7	0.9

Table A2.3 The load data at maximum extension and at yield for all samples during stretching. Note: The highlighted green cells in between the two table columns indicate the higher load between the load recorded at maximum extension and at the yield point during MDO stretching.

Resin	Density (g/cm^3)	Load at maximum extension (N)	Load at yield (N)
D1	0.919	26	18
X1	0.926	37	30
D1+D2(75% D1)	0.927	34	26
D1+D3 (75% D1)	0.928	36	29
D1+X2(75% D1)	0.931	38	30
X1+D2(75% X1)	0.932	33	28
X1+D3 (75% X1)	0.933	38	32
D1+D2(50% D1)	0.934	41	35
X1+X2(75% X1)	0.936	41	35
D1+D3 (50% D1)	0.936	42	36
X1+D2(50% X1)	0.938	41	37
X1+D3 (50% X1)	0.940	45	41
D1+D2(25% D1)	0.942	46	41
D1+X2(50% D1)	0.942	43	40
X1+D2(25% X1)	0.944	49	47
D1+D3 (25% D1)	0.945	48	46
X1+X2(50% X1)	0.946	45	43
X1+D3 (25% X1)	0.947	51	52
D2	0.950	57	54
D3	0.954	49	56
D1+X2(25% D1)	0.954	43	46
X1+X2(25% X1)	0.956	48	53

Chapter – 3

Impact of molecular architecture and draw ratio on enhancement of targeted mechanical properties of MDO-PE films produced after blown film extrusion

Abstract

Conventional multi-material multi-layer flexible packaging offers excellent properties. However, it has recycling challenges, necessitating a shift to mono-material multi-layer flexible packaging e.g. all-polyethylene (PE) packaging which can be tailored through various synthesis and processing methods for different layers. In this Chapter, the influence of the key molecular properties (number-average molecular weight (M_n), weight-average molecular weight (M_w), molecular weight distribution (MWD), comonomer content (short chain branching)) and the machine direction orientation (MDO) process draw ratio (DR) on the final morphology and mechanical properties of MDO-PE films, intended as the outer layer of mono-material all-polyethylene multi-layer flexible packaging is studied. Five PE grades and various blends were extruded and blown into films. Selected blown films were machine direction oriented to obtain the final MDO-PE films. Furthermore, one selected PE blown film was processed at different MDO process draw ratios while keeping other process parameters constant. From the molecular properties point of view, the higher molecular weight fractions provide a higher possibility for uniform stretching whereas lower molecular weight fractions provide a higher natural draw ratio and therefore higher modulus and stiffness enhancement. Further, the results show that increasing MDO process draw ratio leads to more fibrillation and increased crystallinity. Consequently, the tensile modulus and stiffness at the higher draw ratios increase as well and are comparable to conventionally used polymers in outer layers of multilayer flexible packaging.

This Chapter is based on: D. Guleria, M. Edeleva, S. Vervoort, S. Ge, J. den Doelder, and L. Cardon, "Impact of molecular architecture and draw ratio on enhancement of targeted mechanical properties of machine direction oriented polyethylene films produced after blown film extrusion," *Journal of Plastic Film & Sheeting*, p. 87560879241293390, Oct. 2024

3.1 Introduction

Multi-material multi-layer flexible packaging materials find many applications in food and pharmaceutical industries due to their exceptional tensile and barrier properties along with better user convenience because they are light weight and portable. However, it is challenging to recycle multi-material multi-layer packaging after its use, as the packages contain multiple materials, which need to be separated before mechanical recycling [1], [2], [3], [4]. Thus, from the sustainability point of view, there is a shift to mono-material multi-layer flexible packaging as it has the potential to combine functionality with efficient mechanical recycling. Polyethylene (PE) can be a material of choice for this application as its material properties can vary depending on the synthesis (low-density polyethylene (LDPE), linear low-density polyethylene (LLDPE), and high-density polyethylene (HDPE)), processing, and post-processing conditions, with the potential to satisfy combined application requirements. The PE recycling stream can utilize the store drop-off collection systems that were initially established for grocery shopping bags [5].

Polymers such as polyethylene, polypropylene (PP), polyethylene terephthalate (PET) and polystyrene (PS) are used to produce flexible packaging films [6]. Conventionally, the outer layer of multi-material multi-layer flexible packaging is made from non-PE materials such as PET and polyamide (PA) which provides adequate stiffness and barrier properties to the overall package. Orienting polymer films in the semi-solid state using processes like tenter frame, double bubble, and machine direction orientation enhances both barrier and mechanical properties, providing a pathway for developing lightweight packaging structures [7] and moving away from multi-material multilayer flexible packaging. The PE film stiffness can be enhanced significantly by the machine direction orientation (MDO) process (Figure 3.1).

During the machine direction orientation (MDO) process, the polymer film is stretched in the machine direction at a certain temperature which depends on the polymer's chemical nature. Consequently, numerous enhancements are observed in the film physical and barrier properties for food packaging applications, including stiffness, tensile strength, gloss, oxygen barrier and moisture barrier [8], [9], [10]. Although MDO technology has existed since the 1950s, its commercialization was delayed for many years due to process subtleties that were not immediately understood [11]. At present, large-scale oriented plastic film production is commonplace in the industry.

MD orientation can increase PE film Young's modulus increasing its stiffness which is an important property for printing, lamination and ability to run efficiently on packaging machine lines. Low-stiffness films might sag while running on packaging lines, compromising the packaging process. The appropriate multilayer packaging structure overall stiffness is also required for special consumer-appealing package designs such as a stand-up pouch [12]. Thus, the MDO process provides an opportunity to incorporate MDO-PE film as an outer layer when designing mono-material multi-layer all-polyethylene flexible packaging.

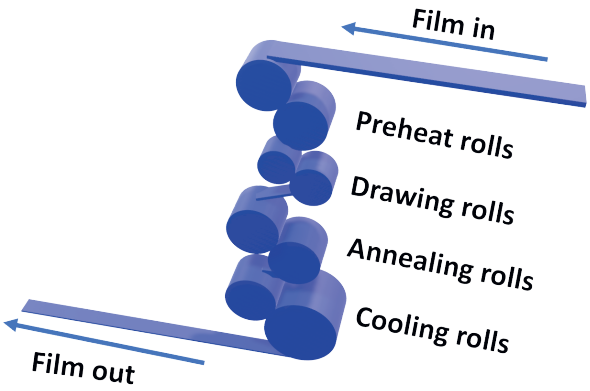

Figure 3.1 MDO process

Factors governing the ultimate modulus improvement during MDO operation include the PE molecular properties like molecular weight, molecular weight distribution, short-chain branching (SCB) and its distribution.

Many previous researchers have highlighted how comonomer content and SCB distribution influence the crystal morphology and further macro-physical properties of polyolefins. Krishnaswamy *et al.* [13] explored how SCB distribution influences HDPE crystal morphology and mechanical properties. They found that blends containing SCB primarily on the high-molecular-weight segments have better ultimate mechanical properties such as stress at break and therefore higher resistance against slow crack growth. This improved mechanical performance is linked to an increased tie chains resulting from the longer chains with SCB. Fall *et al.* [14] investigated the role of SCB in crystalline model PE's and reported that the crystalline morphology depends strongly on how many branches are on the linear backbone. In particular, the lamella thickness decreases with increasing SCB content.

Li *et al.*[15] investigated how comonomer content affects the propylene-1-octene copolymer structure-property relationship during uniaxial stretching at 60 °C. They reported that PP-Octene copolymers with lower octene content presented higher crystallinity and larger crystal sizes, which undergo lamellar fragmentation during stretching. Initially, this decreased crystallinity, but at high strains, the crystallinity increased due to strain-induced crystallization, resulting in higher lamellar orientation. Conversely, high octene copolymers demonstrated smaller initial crystal sizes and elastomeric behaviour.

Previous studies have demonstrated that for semi-crystalline polymers, comonomer content and SCB distribution significantly influence initial crystalline morphology before uniaxial stretching which further impacts the lamellar fragmentation process during uniaxial stretching, thereby playing a pivotal role in designing the resin architecture to attain specific modulus and stiffness characteristics.

Melt-processed ultra-high molecular weight polyethylene and polyethylene waxes (with molecular weight below 1 kg/mol) blends have been extruded and drawn in the solid-state,

representing an application of the bimodal molecular weight distribution strategy to achieve the necessary melt viscosity for high-molecular-weight resins [16], [17]. A PE with broad molecular weight distribution to target processability and strength properties can be accomplished using cascaded reactor systems, mixed catalyst systems and melt blending [18], [19], [20].

A polymer's molecular properties play a significant role in the MDO process and mostly determine the improved tensile properties after drawing. A few studies have discussed how the molecular weight and process draw ratio affects the oriented PE drawing behaviour and tensile properties. Jarecki *et al.* studied ultra-high modulus polyethylene and found that the high-molecular-weight fraction in ultra-high modulus polyethylene imparts the high modulus, while the low-molecular-weight fraction facilitates chain alignment and suppresses internal voiding during drawing at elevated temperatures [21], [22].

Most semi-crystalline polymer solids typically exhibit shear-yielding behaviour upon tensile load application implying that the specimen will neck after yield point. On micro-scale level it is accompanied by a significant change in the semi-crystalline structure from spherulitic to fibrillar [23]. Numerous prior investigators [23], [24], [25], [26], [27], [28] have examined semi-crystalline polymer necking behaviour during uniaxial tensile deformation, a phenomenon initially denoted as "cold drawing" by Carothers and Hill in 1932. Capaccio and Ward [29] studied how ultra-high modulus linear PE molecular weight characteristics influence cold drawing behaviour. They observed that a significant improvement in cold draw ratio can be achieved at a specific number-average molecular weight (M_n) by reducing the molecular weight distribution *i.e.*, by decreasing weight-average molecular weight (M_w). They also stated that for low-molecular-weight polyethylene (PE) the crystallization rate is significantly faster, leading to higher crystallinity. Conversely, high-molecular-weight PE possesses longer chains that spread across more lamellae, resulting in increased tie-chain concentration. Andrews and Ward [30] studied cold drawing HDPE and reported the natural draw ratio increased as molecular weight decreased. They defined natural draw ratio as the ratio of the cross-sectional areas before and after drawing. Séguéla [31] in his review also mentioned the draw ratio in the stable neck region of semi-crystalline polymers as natural draw ratio. High natural draw ratios result in higher microstructure fibrillation resulting in higher overall crystallinity and highly oriented microstructure towards the stretch direction which further increases the tensile modulus. Furthermore, Young's modulus increased monotonically with increasing natural draw ratio.

Capaccio *et al.* [29] and Andrews *et al.* [30] findings are in agreement with Plemmons' [32] review where he discussed oriented PE. He stated that for solid-state orientation of high-molecular-weight high-density polyethylene, the entanglement concentration rises to a level that hinders solid-state orientation due to the significant stress accumulation. On the other hand, low-molecular-weight PE lacks efficient stress transmission capability, making it unstable when subjected to drawing processes. This unstable drawing results in localized or non-uniform stretching across the specimen under load, inducing higher natural draw ratio. Hatfield *et al.*[9] also reported that medium molecular weight HDPE blown films with no long chain branching was not stretchable in the MDO process because of "stretch resonance" which is defined as non-uniform or uneven stretching.

Sherman *et al.* [33] studied the microstructure of high modulus solid state extruded polyethylene and reported that axial tensile modulus increased almost linearly with an increase in draw ratio. Smith *et al.* [34] studied the tensile properties of highly oriented PE and inferred that at elevated temperatures and extended loading durations, the tensile properties are anticipated to be more influenced by the remaining trapped entanglements in the oriented polymeric solid, making M_w a more dominant factor than M_n. Cappacio *et al.* [35], [36] studied the drawing behaviour of linear PE and reported that deformation showed significant localization for low M_w, resulting in a central draw ratio much larger than the overall strain imposed on the sample. In contrast, high M_w PE exhibited homogeneous drawing behaviour. They also suggested that the rate of local deformation in the neck was influenced by the initial crystallization conditions. Consequently, samples drawn from slow-cooled sheets might exhibit a higher draw ratio compared to those prepared by rapid quenching, for the same draw time.

The literature overview presented here well-describes how molecular weight averages and polydispersity (*Đ*) influence PE drawing, orientation and mechanical properties. However, in most studies, PE with isotropic structure before drawing in the form of compression molded sheets are used as the starting material, which is not always relevant for packaging materials. The recent MDO PE film substitution as an outer layer in mono-material PE multilayer flexible packaging has renewed interest in this field, prompting a desire to better comprehend how resin and process parameters influence achieving desired mechanical properties for flexible packaging applications. Yet, the influence of drawing on the blown film properties with pre-existing biaxial orientation remains unclear.

Blown film extrusion ranks among the foremost polymer processing methodologies, with an annual processing capacity of billions of pounds of polymer, predominantly polyethylene [37]. Hence, integrating the MDO process sequentially with film blowing can enhance the packaging materials characteristics and streamline the shift towards mono-material packaging, thereby positively impacting recyclability and polymer circularity. Consequently, selecting the polyethylene material for the MDO process is crucial.

This Chapter reports on how the molecular properties (average molecular weight, molecular weight distribution (MWD), comonomer content and SCB distribution) and MDO process parameter (stretch draw ratio) influence the final morphology and mechanical properties of MDO-PE films that are intended as the outer layer of multilayer flexible packaging systems. The films were produced via a film-blowing process meaning that a flow-induced orientation already existed in the films prior to drawing. Systematically altering the film molecular properties by blending different PE grades facilitated an examination of how molecular weight impacts the MDO-PE film's ultimate mechanical properties. It was expected that higher low-molecular-weight proportions in the PE film microstructure would lead to a greater natural draw ratio during stretching and an increased tensile modulus after stretching. Conversely, higher high-molecular-weight proportions were anticipated to promote uniform stretching with less pronounced necking. Additionally, higher process draw ratios were expected to induce more fibrillation and greater microstructure orientation in the machine direction, resulting in an increased natural draw ratio and further enhancing the MDO-PE film tensile modulus.

3.2 Materials and methods

Five different commercial linear PE resins, each with distinct molecular properties and densities, were provided by Dow (Table 3.1). The resins designated as D1, D2, and D3, are linear PE resins produced using a single catalyst system. The resins, designated as X1 and X2, are also linear PE resins but are synthesized using more complex catalyst chemistry and process designs. The melt flow index (MFI) was measured in accordance with ASTM D1238, using a Göttfert MI-4 plastometer with an average of 19 measuring points taken in a single measurement run for improved accuracy. The measurements were conducted under standard conditions for PE, (2.16 kg at 190°C). Density was measured following the ASTM D792 procedure, using isopropyl alcohol (IPA) as the submersion liquid. The density reported in Table 3.1 represent the average of three measurements and their standard deviation.

Table 3.1 The base PE resins used with their melt flow index (MFI) and density.

Resin	MFI (dg/min)	Density* (g/cm^3)
D1	1.020	0.9194 ± 0.0003
D2	1.472	0.9500 ± 0.0001
D3	4.102	0.9540 ± 0.0003
X1	1.872	0.9256 ± 0.0002
X2	1.126	0.9667 ± 0.0001

*+/- is standard deviation.

Table 3.2 shows blown film blend ratios, theoretical density for the blends and MDO film draw ratios used to understand how molecular weight and molecular weight distribution and their interaction affect the MDO process draw ratio for blown films that were prepared to be used in a pilot scale MDO setup. The dry blending technique was used to fabricate blown films with blown film production line. The initial blending trials used 25% X1 blended by weight with D2, D3, and X2. The theoretical blend density (Table 3.2) was calculated using an approximate inverse-additive mixing rule. This X1 low-density resin was required to promote stretching during the MDO operation as it lowers the overall density and crystallinity and thus facilitates uniform stretching throughout the film, following the teaching from Ratta *et al.* [38].

Then the density was kept constant at the X1/D2 (25/75) 0.9438 g/cm^3 density. The other blends were X1/D3 (35/65) and X1/X2 55/45), determined by inverse-additive mixing rule. This was done to make blown film blends with similar densities in order to compare mechanical properties before and after the MDO process.

To study the effect of the process draw ratio (DR) on tensile modulus, blown film made from base resin X1 was chosen as its lower density allows for relatively greater stretching at higher process draw ratios compared to other higher-density resins, due to its lower overall

crystallinity, as reported in the study by Ratta *et al.* [38]. The X1 blown film could be stretched up to 13.33X, the highest process draw ratio studied (Table 3.2).

Table 3.2 Blown films used with theoretically predicted density for the blends.

Blown film blend ratios	Theoretical Density (g/cm^3)	MDO film draw ratios
X1/D2 (25/75)	0.9438	2X 6X
X1/D3 (25/75)	0.9467	2X 6X
X1/X2 (25/75)	0.9561	2X 6X
X1/D3 (35/65)	0.9438	2X 3X
X1/X2 (55/45)	0.9438	2X 3X
X1	0.9256	2X 6X 13.33X

3.2.1 Preparation of blown films

The blown films were made in a LabTech blown film line (40 mm die diameter, 0.8 mm die gap) with approximately 110-micron thickness and approximately 145 mm lay-flat width. The blow-up ratio (BUR) was 2.31 and draw-down ratio (DDR) was 3.15. The mass flow rate was 90 g/min. The temperature profile for the extruder was:

Zone 1	Zone 2	Zone 3	Zone 4	Zone 5	Die 1	Die 2
160 °C	170 °C	180 °C	190 °C	190 °C	180 °C	160 °C

The nip roller speed was approximately 3 m/min, and it was adjusted to get the required BUR and DDR in each extrusion.

3.2.2 Preparation of MDO films

The heating chamber (oven) and rollers from a Konark extrusion line provided the required stretching temperature for the pilot-scale MDO setup to process lab-scale blown films (pictorial representation in Appendix). The heating chamber circulated the inside air to maintain a constant temperature during stretching. The MDO orientation temperature for each blown film was 15 °C below the peak melting temperature. The annealing step freezes the orientation established during the stretching process, thereby stabilizing the film and preventing further dimensional changes. The annealing temperature can vary depending on the desired final properties. While few academic and industrial studies explicitly discuss the MDO and biaxial orientation process technologies annealing temperature, it has been generally suggested that the annealing temperature should be either the same as, or slightly higher than, the stretching temperature [9], [39], [40], [41].

The heating chamber used to provide the necessary orientation temperature during the stretching was approximately 2.5 meters in length. The extended heating chamber length increased the residence time of the running web, allowing the films to undergo both

stretching and annealing simultaneously within the same step. No dimensional changes were observed in the films after stretching. Consequently, the annealing temperature was essentially the same as the film orientation temperature. After coming out from the heating chamber, the films were cooled under ambient room temperature.

It is important to note that the process draw ratio (Equation 3.1) differs from the previously mentioned natural draw ratio and is independent of the material properties.

$$Process\ draw\ ratio\ (speed) = \frac{Speed\ of\ the\ rollers\ after\ oven\ (m/min)}{Speed\ of\ the\ rollers\ before\ oven (m/min)} \quad \textit{Equation 3.1}$$

For each experimental set the roller speed before oven was specific to get desired process draw ratios (Table 3.2). Natural draw ratio was calculated using Equation 3.2

$$Natural\ draw\ ratio = \frac{cross\ sectional\ area\ of\ the\ film\ before\ stretching}{cross\ sectional\ area\ of\ the\ film\ after\ stretching} \quad \textit{Equation 3.2}$$

The first blown films used a constant 25 wt% X1 and were stretched to the maximum 6X achievable process draw ratio. The second set, which had a similar density, could only be drawn to a maximum 3X process draw ratio due to the X1/X2 (55/45) blend limitations, which could not withstand higher draw ratios. The film from this blend consistently broke inside the oven at higher draw ratios, likely due to the extreme partial melting of its microstructure at the orientation temperature, attributed to the higher comonomer content (Table 3.3) relative to other blends. The increased localized stress during stretching at higher draw ratios, in the regions where the film was partially melted, likely contributed to the observed breakage.

In the third experimental set, the X1 resin blown film was stretched at 2, 6 and 13.33 process draw ratios.

3.2.3 Tensile properties

Blown film and MDO film tensile testing was conducted using an INSTRON 5565 tensile testing machine in accordance with the ASTM D882 method. Samples, 10 mm wide with a gauge length of 50 mm, were mounted on the machine. A constant extension rate of 100 mm/min, corresponding to a nominal strain rate of approximately 0.033 s^{-1}, was used for the mechanical performance analysis. The 2% secant modulus, a measure of material stiffness was quantified using integrated Bluehill software, which measured the slope of the line drawn from the origin of the stress-strain curve to the point intersecting the curve at 2% strain. Five replicates were tested in both the machine and transverse directions.

3.2.4 Gel permeation chromatography (GPC)

Molecular weight distribution (MWD) and architecture were measured using triple-detector gel permeation chromatography (TD-GPC) according to the procedure described in Yau *et al.* (2013) [42] and Pathaweeisariyakul *et al.* (2015) [43]. The triple detector GPC-IR system from Polymer Char used had an Agilent 1260 Infinity isocratic pump, a Polymer Char autosampler, a high-temperature GPC chromatograph equipped with four 20 µm Agilent "Mixed A" GPC columns, an IR5-MCT detector, a four-capillary bridge viscometer from Polymer Char, and a 2-angle light scattering detector from Agilent. The 15° light scattering channel directly measured the absolute molecular weight. The polymer resins were dissolved in 1,2,4-trichlorobenzene (TCB) at 160 °C at approximately 1.6 mg/ml and processed through a column packed with gel particles, which separated the molecules by size. A 1 ml/min volumetric flow rate was used. This measurement determined the microstructural resin parameters, including average molecular weight, molecular weight distribution, comonomer distribution, and branching fractions.

3.2.5 Chemical composition distribution (CCD)

The chemical composition distribution (CCD), or the short chain branching distribution (SCBD), was determined using an improved CCD (iCCD) technique with CCD equipment from Polymer Char, featuring columns packed with gold-coated nickel particles. Approximately 32 mg was dissolved in 8 ml 1,2-dichlorobenzene at 150 °C, and the solution was gently shaken for about one hour in the Polymer Char autosampler. After injection, the sample was allowed to stabilize for two minutes before being cooled under quiescent conditions from 105 °C to 30 °C at -3 °C/min, during the crystallization step. Upon reaching 30 °C, a 0.5 ml/min flow rate was applied, and after two minutes, the temperature was increased to 140 °C at 3 °C/min. During this step, polymer fractions dissolved and eluted at the temperature corresponding to their composition, which was measured using an IR5 detector. Data processing was conducted using Polymer Char's "GPC One" software with custom-verified processing methods.

3.2.6 Shear rheology

Small amplitude oscillatory shear flow measurements, known as dynamic mechanical spectroscopy (DMS) were performed under a nitrogen atmosphere using an ARES-G2 rotational rheometer from TA Instruments, equipped with a forced convection oven. The setup involved parallel plates with a 25 mm diameter and a 1.8 mm gap. Frequency sweeps were conducted from 0.1 to 100 rad/s, with five logarithmically spaced steps per decade, at a strain within the linear viscoelastic range. Measurements were carried out at: 150 °C, 170 °C, and 190 °C.

3.2.7 Fourier transform infrared spectroscopy (FTIR)

The FTIR spectra were recorded on a Bruker Tensor 27 device, with OPUS 6.5 software at 4 cm^{-1} resolution and wave numbers from 4000 to 600 cm^{-1}.

3.2.8 Differential scanning calorimetry (DSC)

The Netzsch Polyma DSC was used to analyse the blown films and a DSC Q2000 from TA instruments was used to analyse the X1 blown film and its subsequent MDO films. A 5 to 10 mg film sample was used in a heat-cool-heat cycle from 0 to 200 °C at 10 °C/min under a nitrogen atmosphere. The degree of crystallinity (X_{DSC}) was computed according to Equation 3.3.

$$X_{DSC} = \frac{\Delta H_m}{\Delta H^{\circ}_m} * 100 \qquad \textit{Equation 3.3}$$

Where ΔH_m is the melting enthalpy, and ΔH°_m is the melting enthalpy of 100% crystalline PE, i.e., 293 J/g [44]. The enthalpy data was taken from the first melting curve of the heat-cool-heat cycle.

3.2.9 Scanning electron microscopy (SEM)

Imaging was with a scanning electron microscope (SEM) Quanta 3D FEG from Thermo Fisher Scientific. Before imaging, the samples were sputter-coated with gold (Au) using a Quorum Q150T S for 40s at 40 mA.

3.2.10 Atomic Force Microscopy (AFM)

The surface morphology was characterized using atomic force microscopy (AFM). Samples were mounted on a stage with double-sided carbon tape and blow-cleaned with a duster before AFM analysis. AFM images were acquired at ambient temperature using a Bruker Icon AFM system with a MikroMasch probe in tapping mode. The probe spring constant was 40 N/m and resonance frequency was around 170 kHz. Imaging was at 0.5-2 Hz with an approximate 0.8 set point ratio.

3.3 Results and discussion

3.3.1 Molecular properties

3.3.1.1 Fourier transform infrared spectroscopy (FTIR)

Figure 3.2a shows the FTIR blown films spectra from the five base resins indicating PE as the main component [45]. The clear crystalline splitting at 1472/1462 and 729/720 cm^{-1} indicates a crystalline phase (Figure 3.2b and 3.2c)**.** It is known that the polymer can degrade by unwanted chemical process like oxidation during processing as highlighted by many researchers [46], [47], [48], [49] . No oxidized groups were found, suggesting that the polymer architecture was not affected during the blown film extrusion step.

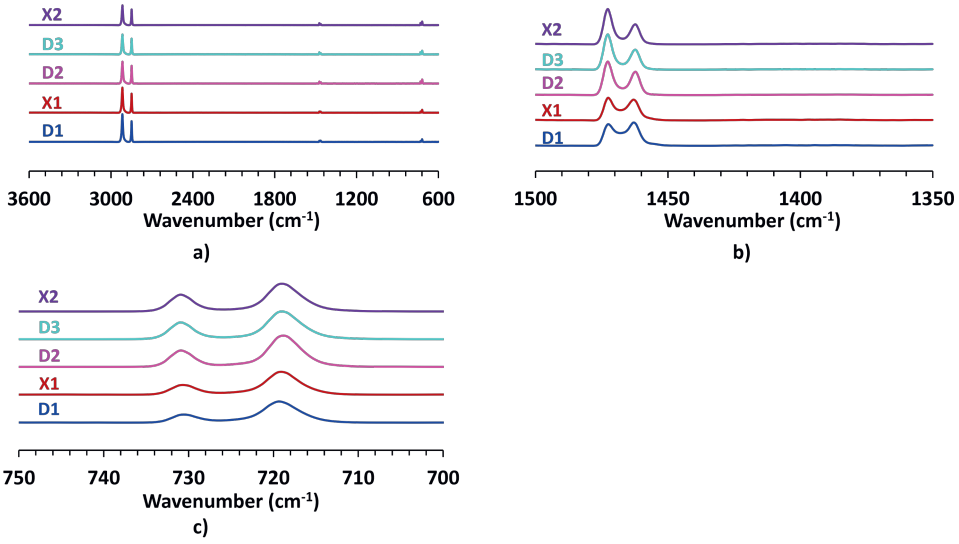

Figure 3.2 Base resin infrared spectrum : (a) 3600-600 cm^{-1} spectral range, (b) 1500-1350 cm^{-1} region, (c) 750-700 cm^{-1} region

3.3.1.2 Molecular weight, molecular weight distribution and chemical composition distribution analysis

To obtain the relation between the polymer microstructural properties, i.e. molecular weight averages and molecular weight distribution (MWD), and the orientation-induced tensile property enhancement, several different PE resin compositions used for making blown film of binary blends were used. Figure 3.3 presents the molecular weight distributions for the blown films made from the base resins as obtained from TD-GPC.

During PE's thermo-mechanical degradation induced by processing, two chemical processes can occur: chain scission resulting in shorter polymer chains and chain cross-linking resulting in longer polymer chains and increased branching [50]. Table 3.3 compares the TD-GPC data for the blown films made from the base resins with the TD-GPC data for the base resins prior to blown film extrusion (Table 2.2 and Figure 2.3 in Chapter 2), revealing similar values with

no indications of molecular degradation. Figure 3.3 also presents the SCB distribution for the blown films made from the base resins using the TD-GPC IR detector. Table 3.3 summarizes the molecular weight averages and octene comonomer content.

The average molecular weight trends with MFI (see Table 3.3 and Table 3.1). The polydispersity index for most base resin blown films falls between 3.9 and 4.7, with X2 being a notable exception, which exhibits a broader distribution and a bimodal MWD. SCB is nearly absent in the higher-density PE samples D2, D3, and X2. In contrast, lower-density PE's, D1 and X1, contain significant SCB. The coupling between SCB and MWD differs significantly between these two. D2, D3, and X2 show distinct characteristics, with very low comonomer content, resulting in an almost homopolymer-like structure. This compositional similarity is reflected in their high densities. On the other hand, D1 and X1 clearly has comonomer, consistent with their lower densities. Further differentiation between D1 and X1 is observed, as comonomer is concentrated in lower molecular weight molecules in resin X1, while the highest molecular weight molecules exhibit low comonomer content.

Among the relatively lower density resins, D1 and X1, X1 was selected for blending with the higher density resins D2, D3, and X2 for making blown film of blends. This choice was based on lower comonomer content and its distinct distribution in the molecular architecture of resin X1 which was anticipated to result in relatively larger crystal size in its blown films. The larger crystal size was expected to contribute more effectively to microstructural orientation and modulus enhancement during the MDO process.

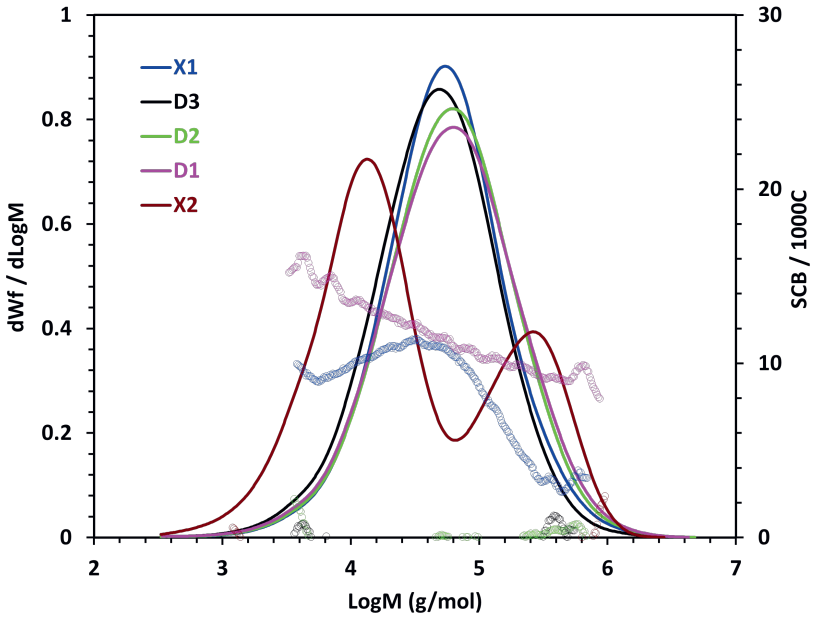

Figure 3.3 GPC curves for the blown films made from the five base resins. The left vertical axis represents the differential weight fractions (lines), and the right vertical axis represents the average SCB per 1000 C atoms at each molecular weight (open markers).

Figures 3.4a and 3.4b presents the MWD for the blown film from the blends and their SCB content. Table 3.3 summarizes the MWD data.

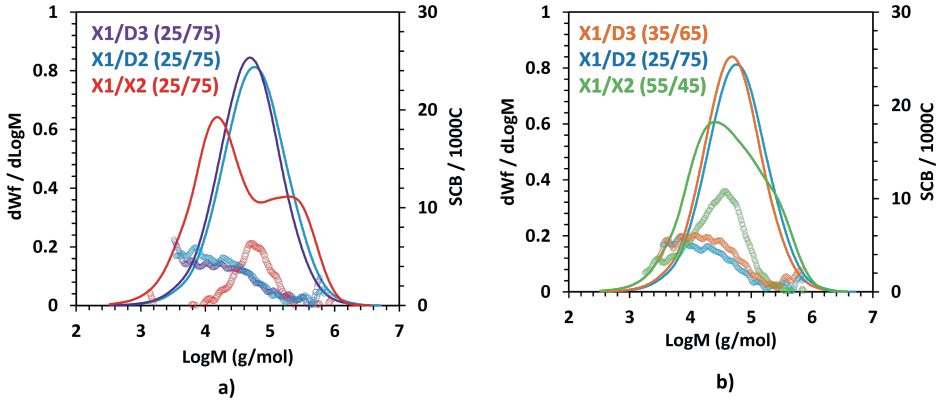

Figure 3.4 Molecular weight (lines) and SCB distribution (open markers) for the blown films made from 25 wt.% X1 with D2, D3 and X2 **(a)**, and with constant density blends (0.9438 g/cm^3) **(b)**.

Figure 3.4a and Table 3.3 highlight notable variations in the weight average molecular weight of blown films obtained from all blends with 25% weight percentage of X1 in the blend.

Table 3.3 Molecular weight averages (number-average molecular weight (M_n), weight-average molecular weight (M_w)), polydispersity ($Đ$) and octene comonomer content for the base PE blown films and blown films made from blends measured with TD-GPC.

No.	Blown film	M_n (kg/mol)	M_w (kg/mol)	$Đ$ (-)	Octene comonomer (wt %)
1	D1	26	124	4.7	9.59
2	D2	27	115	4.2	0.31
3	D3	22	88	3.9	0.31
4	X1	26	104	3.9	7.96
5	X2	9	106	10.9	0.95
6	X1/D2 (25/75)	26	112	4.3	2.67
7	X1/D3 (25/75)	23	93	4.1	2.75
8	X1/X2 (25/75)	11	106	9.1	2.57
9	X1/D3 (35/65)	23	97	4.2	3.68
10	X1/X2 (55/45)	15	108	7.2	5.55

The X1/D3 (25/75) blend exhibited the lowest, while X1/D2 (25/75) blend showed the highest weight-average molecular weight, consistent with the D3 and D2 molecular weights. Additionally, a slight polydispersity index reduction was observed in the X1/X2 (25/75) blend compared to X2, indicating an influence on molecular weight distribution due to blending with X1. Slight percentages (about 2.5%) of SCB were introduced into the microstructure of all three blown films of blends, in comparison to the blown films composed of base resins D2, D3, and X2, as a result of blending with low-density resin X1.

Table 3.4 Theoretically predicted and TD-GPC measured M_w data for blown films made from blends.

Blown films of blends	Theoretical M_w $(\sum W_i M_i)$, (kg/mol)	TD-GPC measured M_w(kg/mol)	% Difference in M_w
X1/D2 (25/75)	113	112	+ 0.5
X1/D3 (25/75)	92	93	- 0.4
X1/X2 (25/75)	106	106	0.0
X1/D3 (35/65)	94	97	- 3.2
X1/X2 (55/45)	105	108	- 2.4

Table 3.4 shows no significant differences between the theoretically predicted and TD-GPC measured M_w data which confirms the correct blend ratios. The molecular architecture after blown film processing was not measurably different.

Figure 3.4b shows the molecular variations, including molecular weight and molecular weight distribution, for the blown films that used X1/X2 (25/75), X1/D3 (35/65), and X1/D3 (55/45) blends with similar density.

Figure 3.4b and Table 3.3 indicate that, at similar density as well, the X1/D3 (35/65) blend has the lowest weight-average molecular weight (M_w), while the X1/D2 (25/75) blend has the highest. Moreover, the increased X1 weight % in the X1/X2 (55/45) blend resulted in a further decrease in the polydispersity index compared to X1/X2 (25/75) blend, along with higher short chain branching in its microstructure.

Additionally, Figure 3.5 overlays the MWD curves for the blown films of X1, X2, and their blends, demonstrating the expected molecular weight distribution corresponding to the blend ratios.

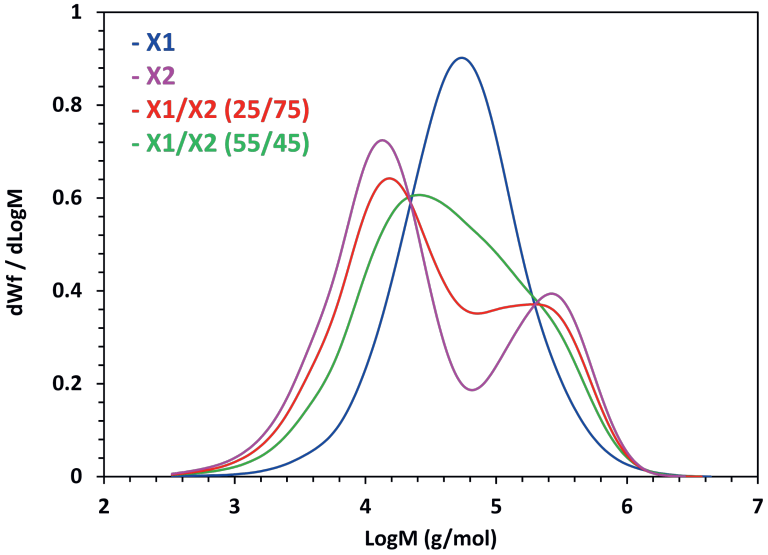

Figure 3.5 Overlay MWD curves of blown films of X1, X2 and their blends.

Figure 3.6 shows the iCCD curves for the blown films of base resins and Figures 3.7a, 3.7b presents it for blown films with blends with information regarding the crystallizable fractions in their microstructure at each specific temperature.

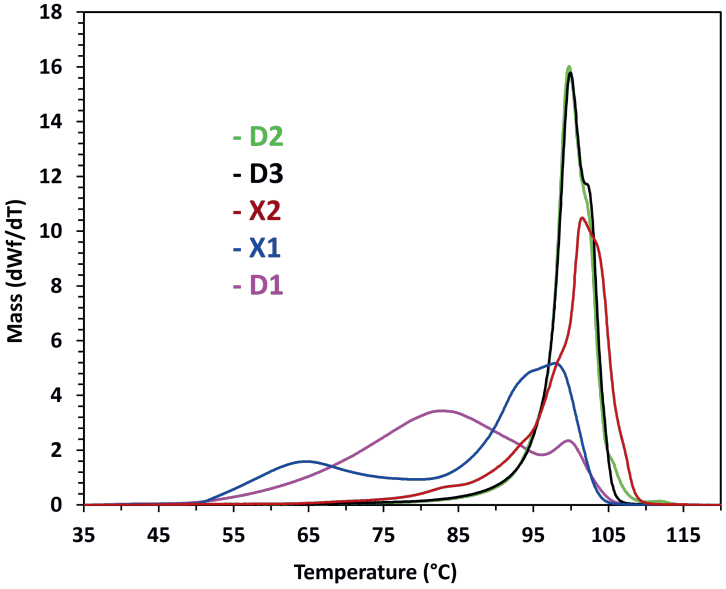

Figure 3.6 iCCD curves for the blown films from base resins used in the study.

Figure 3.7a illustrates distinct temperature profiles for the peak elution of crystallizable mass fractions among three different blown films from blends with same 25 wt% of X1.

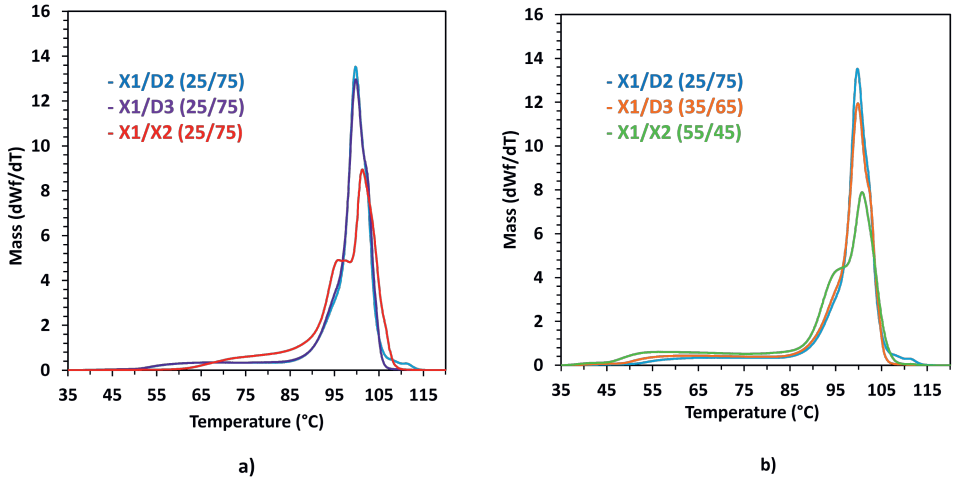

Figure 3.7 iCCD curves for the blown films from 25 wt% X1 blends with D2, D3 and X2 **(a)**, and with constant density **(b)**.

Notably, the X1/X2 (25/75) blended film exhibited the highest peak elution temperature, whereas the curves for the films X1/D2 (25/75) and X1/D3 (25/75) displayed comparable profiles. This observation aligns with expectations, given the higher X2 density, indicating a greater crystallizable fractions in its microstructure.

In contrast, Figure 3.7b shows a decrease in the peak height for the crystallizable mass fractions in the X1/D3 (35/65) and X1/X2 (55/45) blown film in comparison to curves in Figure 3.7a. This aligns with the overall density decrease with higher X1 concentration compared to Figure 3.7a. The curves are broader with increased X1 weight percentage in blends with D3 and X2, consistent with elevated comonomer content seen in GPC curves and data (Figure 3.4b and Table 3.3).

Figure 3.8 shows a similar trend in the iCCD curves for the X1, X2 blown films, and their blends. As the X1 weight percentage in the blends increased, the crystallizable mass fractions peak height and peak elution temperature decrease, along with peak broadening. This is consistent with the increased comonomer content with the increased X1 weight percentage in the X1/X2 blend microstructure.

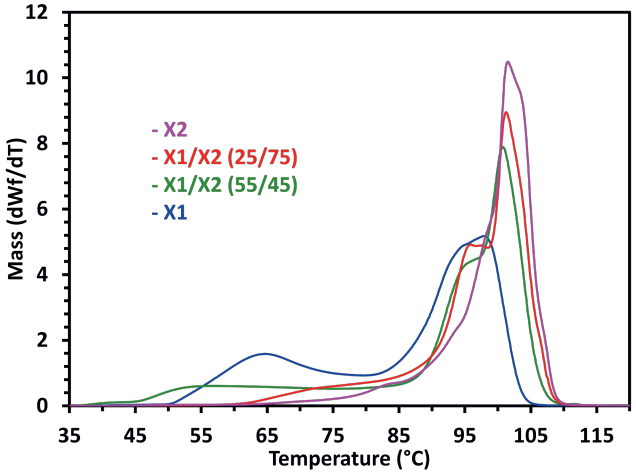

Figure 3.8 iCCD curves for the X1, X2 blown films and their blends.

3.3.1.3 Rheological characterization

The DMS linear viscoelastic property trends were consistent with the resin composition and measured MFI. Figure 3.9 presents the relationship between complex viscosity and frequency at 190 °C. At low frequencies, the viscosity curves are inversely related to the MFI and follow known power-law scaling behavior with respect to the average molecular weight [51], [52]. The shear thinning behaviour of the D-series (D1, D2, D3) and X1 is comparable, reflecting their similar polydispersity (between 3.9 and 4.7). In contrast, resin X2, with the highest polydispersity (10.9), exhibits markedly more pronounced shear thinning behaviour, approaching D3, which has the lowest weight-average molecular weight, at higher frequencies. The linear viscoelasticity results can be comprehensively explained by the molecular structure related to the molecular weight distribution.

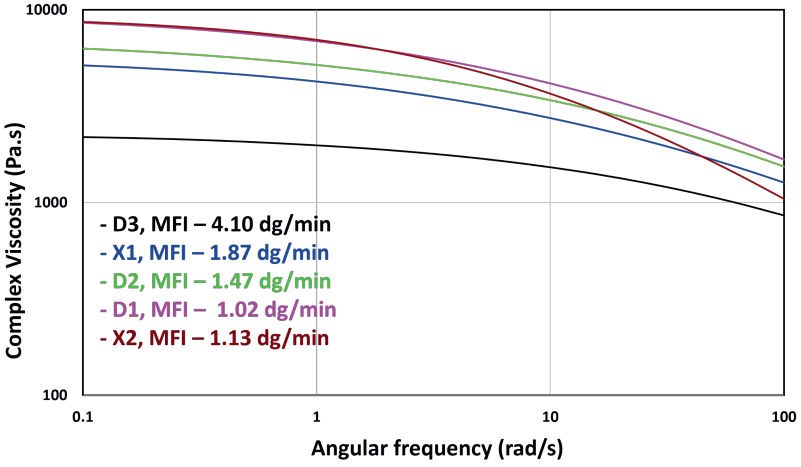

Figure 3.9 Base resin flow curves at 190 °C with their respective indicated MFI.

3.3.2 Thermal properties of the blown films from blends

DSC analysis provides additional insights into the blown film crystallinity. Figure 2.1 in Chapter 2 presented the DSC traces for base PE resins X1, X2, D1, D2, D3. Figure 3.10a shows the 1st heat DSC melting curves for the blown films made from 25 wt% X1 in the blends. The melting enthalpy and % crystallinity was highest for the X1/X2 (25/75) blend (211.3 J/g, 72 %), while the X1/D2 (25/75) and X1/D3 (25/75) showed similar values (178.3 J/g, 61 % and 184.9 J/g, 63 %). This aligns with predicted density trends: indeed, both density and melting enthalpy depends on the crystalline fraction. The peak melting temperature followed a similar pattern.

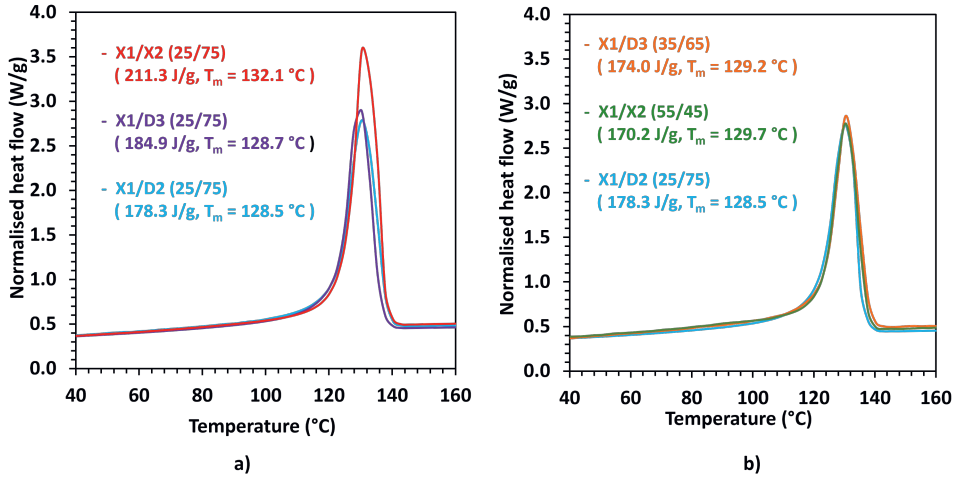

Figure 3.10 DSC melting curves for 1st heating cycle (Endo up) along with their enthalpy of melting and peak melting temperature for the blown films from X1 blends with D2, D3 and X2 **(a)** at constant 25% weight percentage X1, and **(b)** at constant density.

Figure 3.10 b shows that the enthalpy of melting and percent crystallinity are similar for all three blends, in alignment with the constant target density within this series. Only subtle differences were found with the lowest enthalpy and crystallinity observed for X1/X2 (55/45) (170.2 J/g, 58%). This outcome was in line with the higher comonomer content in the X1/X2 (55/45) microstructure compared to X1/D3 (35/65) and X1/D2 (25/75), due to the higher low-density X1 weight percent. The higher comonomer content in the microstructure hinders growing thicker lamella [14].

3.3.3 Material properties

3.3.3.1 Tensile properties of blown films of all five base resins

Figures 3.11 and 3.12 present the machine direction (MD) and transverse direction (TD) tensile properties for blown films for base resins.

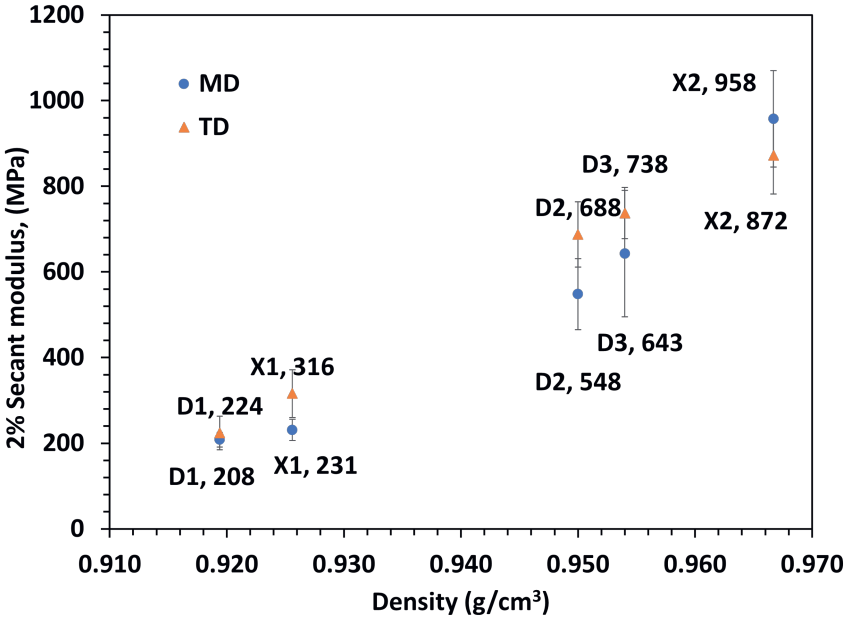

Figure 3.11 MD and TD modulus versus density for blown films from the base resins (n=5).

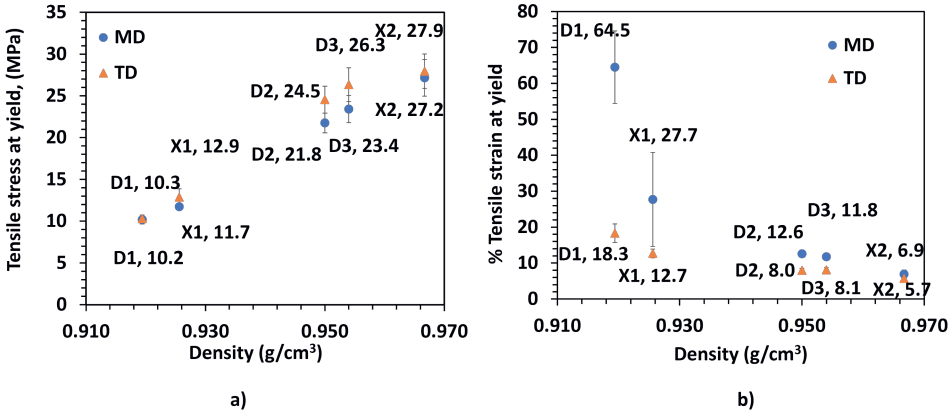

Figure 3.12 Tensile stress and Tensile strain at yield versus density for base resin blown films (n=5); **(a)** stress at yield, **(b)** strain at yield.

The tensile data shows that higher density blown films exhibited higher modulus and stress at yield in both MD and TD (Figure 3.11 and 12a). This is due to an increased crystallinity with increasing density. Specifically, the highest modulus and yield stress in both MD and TD were for the blown film with the highest density resin, X2 (0.967 g/cm³), while the lowest values were for the blown film with the lowest density resin, D1 (0.919 g/cm³). In contrast, the percent strain at yield (Figure 3.12b) decreased with increase in density in both MD and

TD as expected due to decreasing amorphous fractions in the microstructure with increasing density.

3.3.3.2 Molecular architecture effects on MDO-PE film tensile modulus

Subsequently, the modulus was examined as a function of draw ratio and resin architecture. Particular attention was placed on the effect of molecular weight and results were presented for blown films of blends in which large variations in density were minimized compared to the base resin blown films.

As mentioned earlier, to understand the effect of molecular weight and molecular weight distribution and their interaction with MDO process draw ratio, lower-density PE resin X1 was blended at 25 wt% with three relatively high-density PE resins of different molecular architectures: D2, D3, and X2. The measured octene comonomer content was very similar (2.67, 2.75 and 2.57%) for these three blends. Figure 3.13 shows that in all three cases, an exponential-like increase in machine direction (MD) modulus was observed with increasing MDO draw ratio. The highest increment at each draw ratio was achieved for the X1/X2 (25/75) blend, with about 4000 MPa at 6 DR. This high modulus increase can be attributed to two main factors. First, the X1/X2 (25/75) blown film had the highest density (0.9561 g/cm^3), leading to improved disintegration and fibrillation of relatively larger crystals with less partial melting at the orientation temperature, facilitating amorphous phase alignment and strain-induced crystallization. Second, the blend contained more low-molecular-weight material shown by its polydispersity value of 9.1, which was the highest among the blends examined (Table 3.3 and Figure 3.4a). This resulted in localized deformation, contributing to a higher natural draw ratio, as evidenced by the narrower lay-flat width after stretching shown in Figure 3.13.

For the almost equal density blends i.e., the 0.9438 g/cm^3 X1/D2 (25/75) and the 0.9467 g/cm^3 X1/D3 (25/75), it was observed that the X1/D3 blend modulus was higher at higher process draw ratios, than the X1/D2 blend. A marginally higher X1/D3 (25/75) MDO film modulus at highest process draw ratio of 6 versus the X1/D2 (25/75) MDO film was anticipated due to its slightly higher density. However, the significantly larger observed difference was unexpected and atypical (Figure 3.14b). A possible explanation is that the X1/D3 (25/75) blown film contained higher low-molecular-weight material (Table 3.3 and Figure 3.4a) in addition to its slightly higher density, therefore it showed a higher natural draw ratio and comparatively more localized deformation during MDO stretching compared to the X1/D2 (25/75) blown film. This resulted in higher X1/D3 (25/75) film microstructure alignment in the draw direction during MDO, leading to higher MD modulus at higher process draw ratios. Consequently, the X1/D3 (25/75) film exhibited a narrower lay-flat width at the highest process draw ratio (Figure 3.13), attributed to its higher natural 9.1 draw ratio, compared to 6.6 for the X1/D2 (25/75) blend (see Table 3.5).

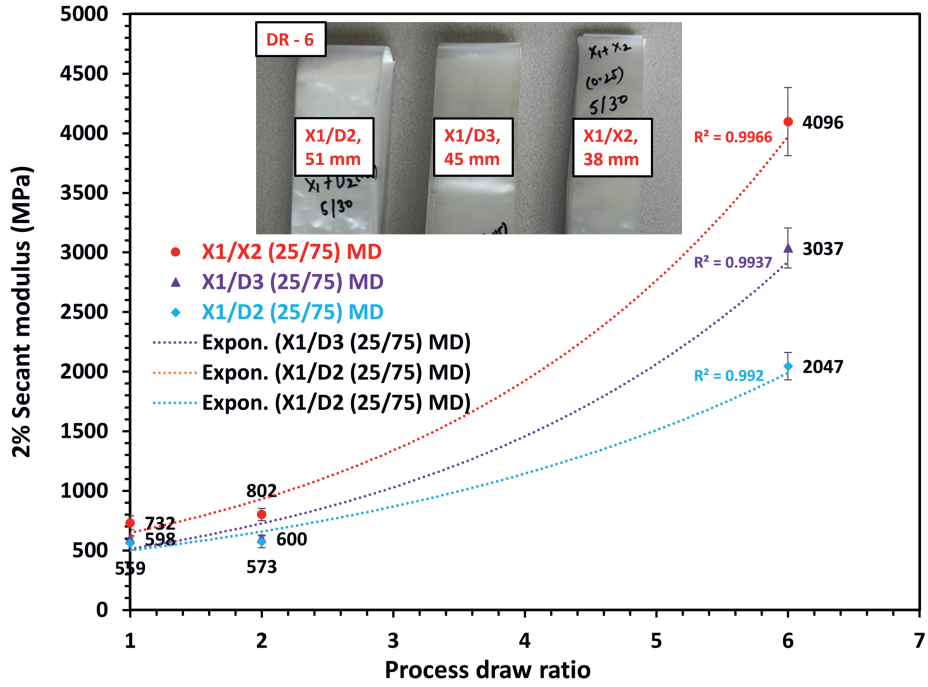

Figure 3.13 2% Secant Modulus (n=5) versus Process Draw Ratio (DR) for 25 wt% X1 blends and MDO film lay flat width (mm) at 6 DR. (roller speed before MDO oven: 1.6 m/min) Note: Process draw ratio 1 represents blown film before MDO operation.

Table 3.5 Calculated natural draw ratio for 25 wt% X1 blown films of blends at 6 DR.

Blown film type	Natural draw ratio
X1/D2 (25/75)	6.6
X1/D3 (25/75)	9.1
X1/X2 (25/75)	10.3

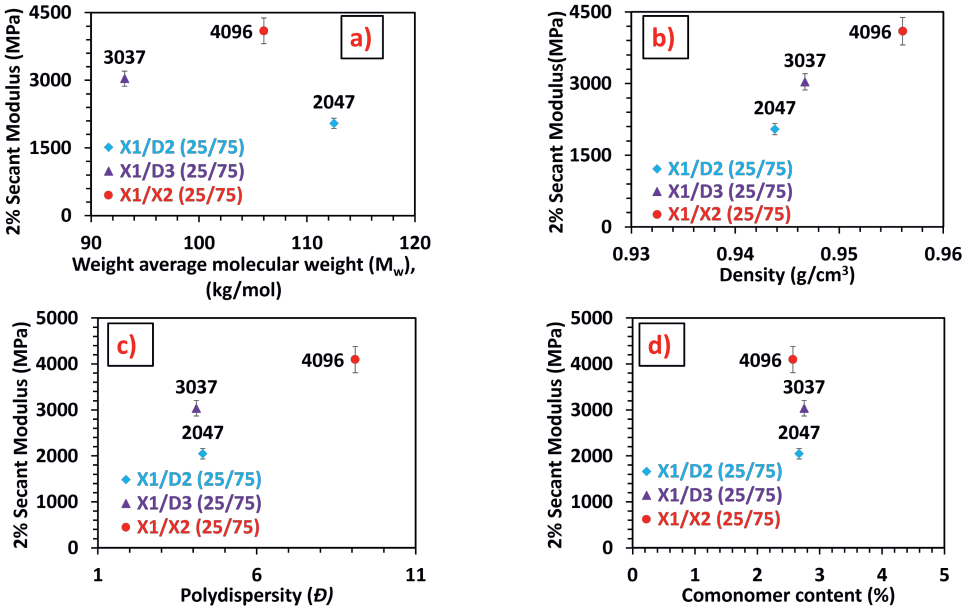

Figure 3.14 2% Secant modulus (n=5) for 25 wt% X1 blends versus **a)** weight average molecular weight (M_w), **b)** Density and **c)** Polydispersity ***(Đ)*** and **d)** % comonomer content at 6 DR .

Figure 3.15 shows 2% Secant Modulus versus Process Draw Ratio (DR) for the similar density blends, where the X1 weight percentage was altered to 35% and 55% in D3 and X2 blends to match the X1/D2 blend density (0.9438 g/cm^3). Notably, the modulus change versus DR differed from that in Figure 3.13 with all three blends having closer natural draw ratios (Table 3.6) at the maximum possible 3X process draw ratio. While the increased modulus is comparable for the X1/D2 (25/75) and X1/D3 (35/65) blown films, the X1/X2 (55/45) blown film shows the least increase at the maximum possible 3X process draw ratio among the three blown films of blends. From the GPC results (see Figure 3.4b and Table 3.3), it was learned that the 5.55% octene comonomer content was highest for the X1/X2 (55/45) blown film, followed by 3.68% for X1/D3 (35/65), and the lowest at 2.67% for X1/D2 (25/75) blend. Li *et al.*[15] teaches us that copolymers with lower octene content present higher crystallinity and larger crystals, which undergo lamellar fragmentation during stretching. Subsequently, crystallinity increases due to strain-induced crystallization, resulting in overall high lamellar orientation. Numerous previous researchers have also demonstrated that the increased comonomer content reduces the crystallization of the microstructure and its ability to form larger crystals [15], [53], [54], as also indicated in our study by the DSC curves in Figure 3.10b and iCCD curves in Figure 3.7b, which further leads to a decrease in strain induced crystallization during stretching and overall orientation of the microstructure. Therefore, an explanation for the contrasting results presented in Figure 3.15 is that the larger crystal sizes formed in the blown film prior to stretching because of relatively lower comonomer content facilitates strain-induced crystallization and amorphous region orientation during MDO, leading to higher modulus.

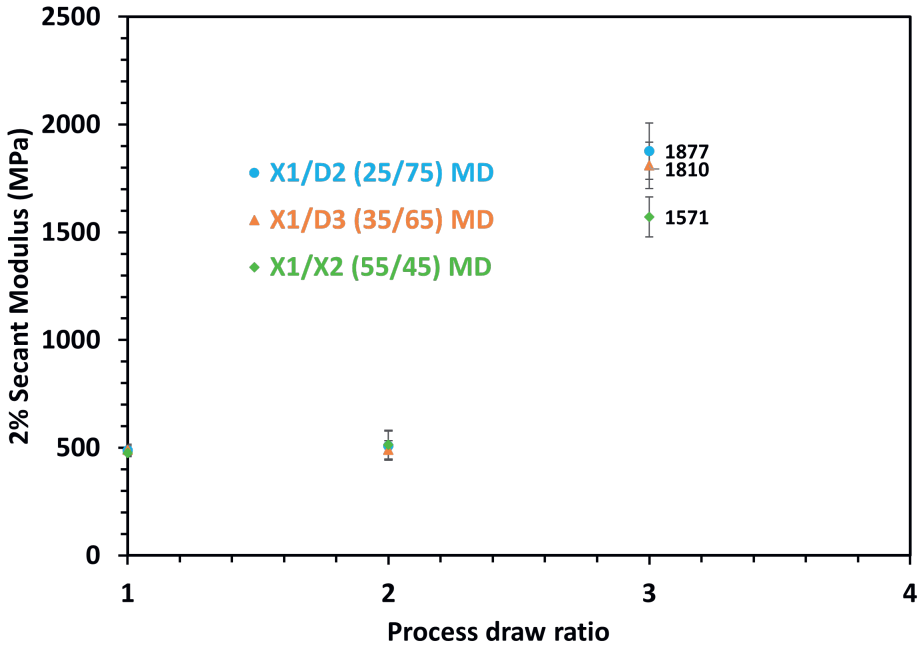

Figure 3.15 2% Secant Modulus (n=5) versus Process Draw Ratio for blown films from X1 with D2, D3, and X2 blends at constant density (0.9438 g/cm^3). (roller speed before MDO oven: 3.1 m/min) Note: Process draw ratio of 1 represents blown film before MDO operation.

Table 3.6 Calculated natural draw ratio for X1 blends with D2, D3, and X2 at constant density (0.9438 g/cm^3) at 3 DR.

Blown film type	Natural draw ratio
X1/D2 (25/75)	5.4
X1/D3 (35/65)	6.2
X1/X2 (55/45)	6.4

3.3.3.3 Process draw ratio effects on MDO-PE film tensile modulus

The X1 blown film was stretched at 2, 6 and 13.33 process draw ratios to further analyse how the process draw ratio affects tensile properties. Figure 3.16 shows an exponential-like increase in MD modulus with increased draw ratio.

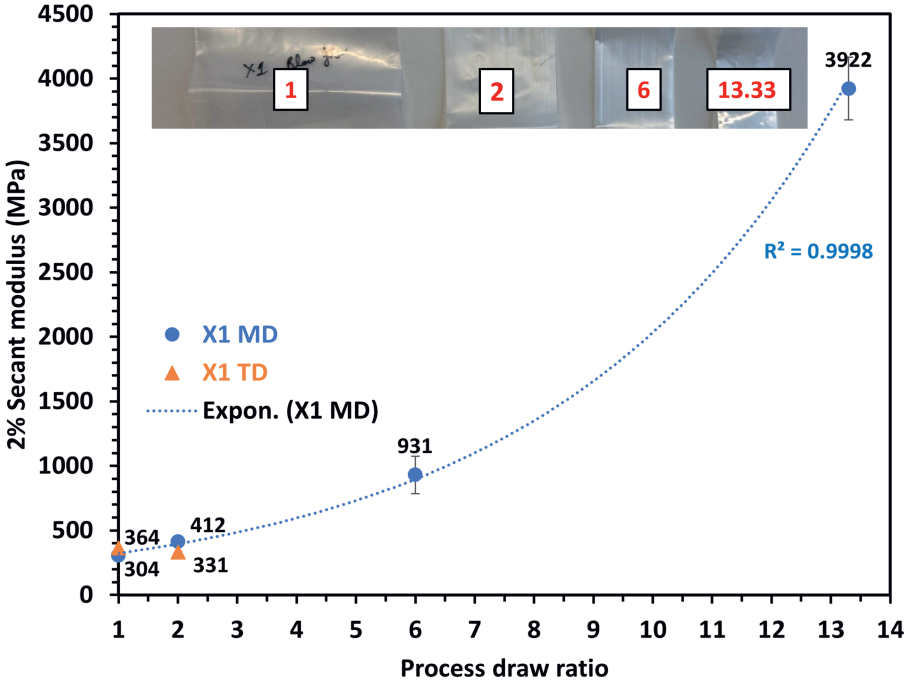

Figure 3.16 2% Secant Modulus (n=5) versus Process Draw Ratio (DR) for X1 resin along with pictorial representation at used process draw ratios. (roller speed before MDO oven: 0.9 m/min) Note: Process draw ratio 1 represents blown film before MDO operation.

The X1 MD modulus increased to around 4000 MPa at the maximum used process draw ratio (13.33). This is almost 13 times higher compared to the unstretched blown film MD modulus. This higher modulus is also comparable with the modulus of polymers such as polyethylene terephthalate (PET) and polyamide (PA), which are conventionally used in multilayer flexible packaging systems outer layer: the PET film typical modulus is 2800 MPa and for PA film it is 3000 MPa [55], [56] . This large increase in modulus at the highest used process draw ratio is attributed to high fibrillation of the initial crystalline structure accompanied by strain-induced crystallization and amorphous phase orientation with increasing draw ratio, resulting in the overall increased crystallinity and a highly oriented microstructure in the machine direction.

MDO films thermal analysis confirmed this. The DSC melting curves in Figure 3.17 show a notable rise in the enthalpy of melting and % crystallinity, progressing from 127.1 J/g (43.4% crystalline) for the X1 blown film to a maximum of 151.9 J/g (51.8% crystalline) for its MDO film at 13.33 DR. During stretching a fibrillar structure with higher crystallinity is formed [57], [58], [59], [60]. Steep melting curves at 13.33 DR with higher melting enthalpy clearly indicates a fibrillar morphology with higher overall crystallinity. The peak melting temperature decreased slightly for MDO films compared to blown films, indicating that the

crystals in the blown films were disintegrated, leading to forming more relatively smaller crystals after MDO stretching.

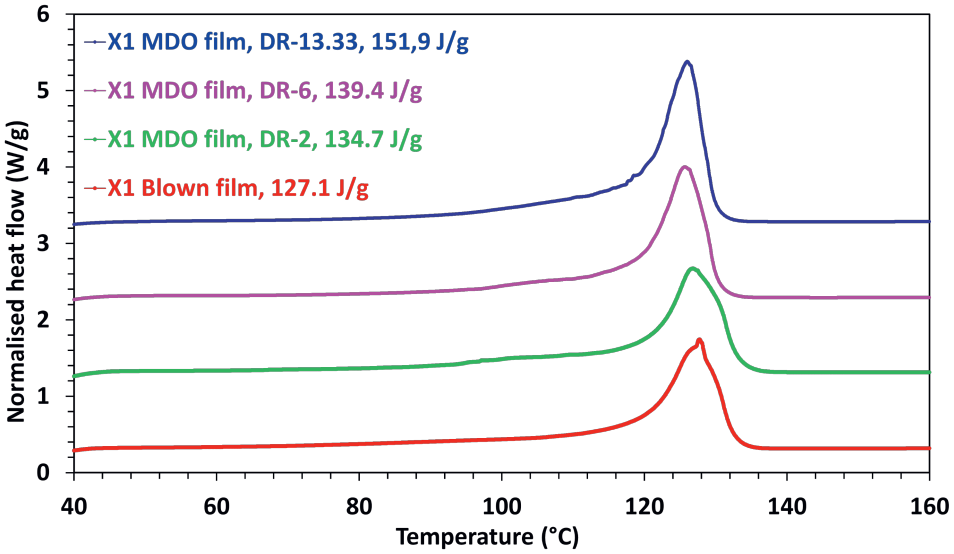

Figure 3.17 X1 DSC melting curves (1st heating cycle, Endo up) for process draw ratio along with enthalpy of melting. (Note: Curves at the process draw ratio of 2, 6 and 13.33 are presented with offset of 1,2 and 3 respectively on y-axis for better comprehension)

Figure 3.18 shows the nominal stress versus strain curves for X1 and its MDO films at 2, 6, and 13.33 DR.

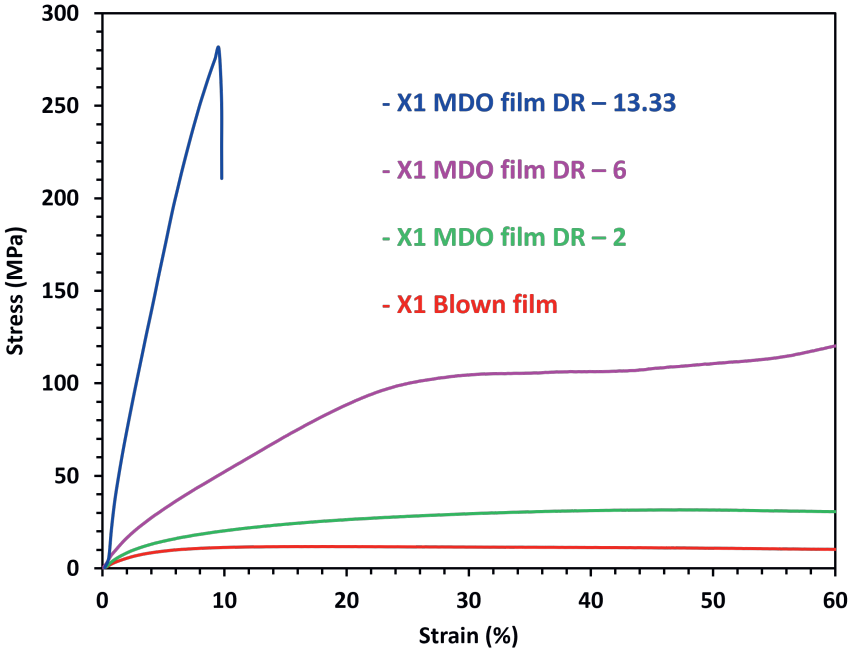

Figure 3.18 Nominal stress versus strain at room temperature (23 °C) for X1 blown film and its MDO films at 2, 6 and 13.33 DR. (Note: The curves are truncated at 60% strain on x-axis for better representation)

The nominal stress versus strain curves clearly shows that increasing draw ratios create stiffer and stronger behaviour. The yield stress increased while the yield strain decreased with the increasing draw ratios as expected. The 13.33X MDO film showed extremely high tensile strength (about 280 MPa). Conversely, its strain at break was lower at about 10%.

Examining the SEM and AFM images from Figure 3.19, the X1 blown film exhibited a coarse randomly oriented morphology. It was expected as blown film induces both machine direction (MD) and transverse direction (TD) orientations simultaneously. Both the 2.31 blow-up ratio (BUR) and the 3.15 draw-down ratio (DDR) were moderate and close to each other, giving the film balanced overall orientation and therefore randomly oriented morphology.

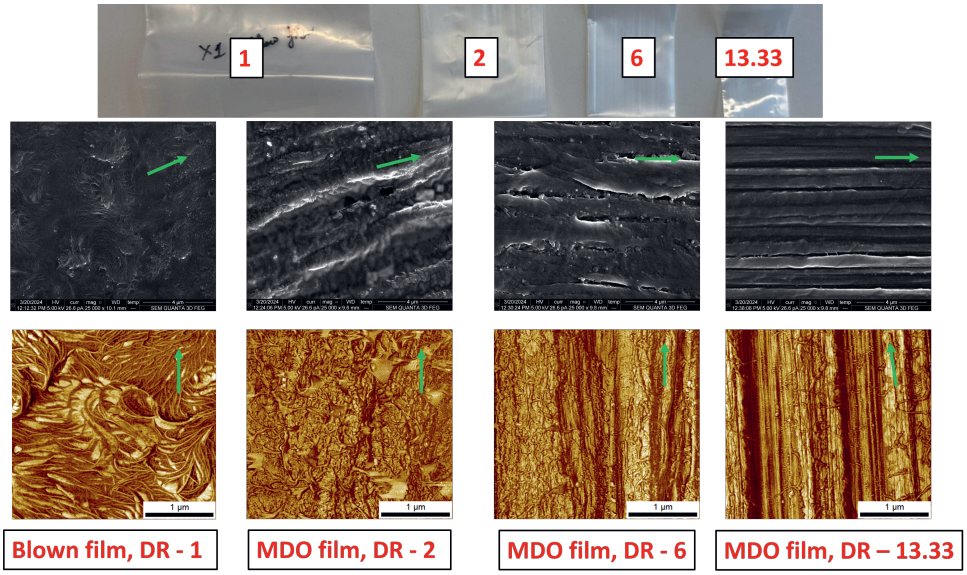

Figure 3.19 SEM (top) and AFM (bottom) images of the X1 blown film and its subsequent MDO films at 2, 6 and 13.33 DR. Green arrows represent machine direction and the picture above images are pictures of the four films.

The SEM and AFM images with process draw ratio increasing from 2 to 6 shows the destruction of randomly oriented microstructure to fibril development oriented in the MD. SEM and AFM images at 13.33 DR, present well-pronounced fibrils with a strong MD orientation with no evidence of the previously present randomly oriented morphology in its blown film.

3.4 Concluding remarks

In this Chapter the effects of molecular properties such as average molecular weight, molecular weight distribution, comonomer content, as well as critical MDO process parameters such as the process draw ratio, on the final morphology and the enhancement of targeted mechanical properties in MDO-PE films produced in series with the blown film operation were studied. For that, five commercial PE resins and their blends with different average molecular weight, density, comonomer content, polydispersity were studied and correlated it with final targeted mechanical properties of the PE film with MDO orientation for outer layer application in multi-layer mono-material PE based flexible packaging. The effect of the MDO process draw ratio on the targeted mechanical property of modulus was further investigated. Key conclusions of the Chapter are presented as follows:

- A higher fraction of low-molecular-weight chains results in a higher natural draw ratio, leading to the higher modulus in the MDO films.
- The blend with lower comonomer content exhibited greater modulus increase after stretching, likely due to the larger crystal sizes formed in its blown film prior

to stretching, which facilitates higher strain-induced crystallization and amorphous region orientation during MDO.

- The increased crystallinity and highly oriented microstructure in the MDO-PE films machine direction (MD) resulted in higher MD modulus compared to biaxially oriented blown films.
- SEM and AFM results indicated that a higher MDO process draw ratio transforms randomly oriented microstructure into fibrils which are strongly oriented towards MD.
- The tensile modulus increased exponentially with the process draw ratio, reaching values similar to high-modulus polymers like PET and PA used in the outer layer of multilayer flexible packaging.

3.5 Bibliography

[1] C. Y. Barlow and D. C. Morgan, “Polymer film packaging for food: An environmental assessment,” *Resour Conserv Recycl*, vol. 78, pp. 74–80, Sep. 2013, doi: 10.1016/J.RESCONREC.2013.07.003.

[2] K. Kaiser, M. Schmid, and M. Schlummer, “Recycling of Polymer-Based Multilayer Packaging: A Review,” *Recycling 2018, Vol. 3, Page 1*, vol. 3, no. 1, p. 1, Dec. 2017, doi: 10.3390/RECYCLING3010001.

[3] T. W. Walker *et al.*, “Recycling of multilayer plastic packaging materials by solvent-targeted recovery and precipitation,” *Sci Adv*, vol. 6, no. 47, p. eaba7599, Jun. 2024, doi: 10.1126/sciadv.aba7599.

[4] C. T. de M. Soares, M. Ek, E. Östmark, M. Gällstedt, and S. Karlsson, “Recycling of multi-material multilayer plastic packaging: Current trends and future scenarios,” *Resour Conserv Recycl*, vol. 176, p. 105905, 2022, doi: https://doi.org/10.1016/j.resconrec.2021.105905.

[5] B. A. Morris, “Flexible packaging past, present and future: Reflections on a century of technology advancement,” *Journal of Plastic Film & Sheeting*, vol. 40, no. 2, pp. 151–170, 2024, doi: 10.1177/87560879241234946.

[6] J. R. Wagner and S. B. Marks, “Chapter 1 - Introduction,” in *Multilayer Flexible Packaging*, J. R. Wagner, Ed., in Plastics Design Library. , Boston: William Andrew Publishing, 2010, pp. 3–11. doi: https://doi.org/10.1016/B978-0-8155-2021-4.10001-2.

[7] M. Paul, B. Morris, J. Weinhold, and K. Hausmann, “The effect of stretching and tie layer composition on adhesion strength of multi-layered films,” *Journal of Plastic Film and Sheeting*, vol. 38, no. 3, pp. 351–368, Jul. 2022, doi: 10.1177/87560879211063475/ASSET/IMAGES/LARGE/10.1177_875608792110634 75-FIG11.JPEG.

[8] T. Chatterjee *et al.*, “Machine direction orientation of high density polyethylene (HDPE): Barrier and optical properties,” *Polymer (Guildf)*, vol. 55, no. 16, pp. 4102–4115, Aug. 2014, doi: 10.1016/j.polymer.2014.06.029.

[9] E. Hatfield, R. Tate, K. Williams, and W. Todd, “New MDO Medium Molecular Weight High Density Polyethylene Films,” *Journal of Plastic Film & Sheeting*, vol. 18, no. 2, pp. 117–127, Apr. 2002, doi: 10.1177/8756087902018002006.

[10] D. Carullo *et al.*, “Testing a coated PE-based mono-material for food packaging applications: an in-depth performance comparison with conventional multi-layer configurations,” *Food Packag Shelf Life*, vol. 39, p. 101143, 2023, doi: https://doi.org/10.1016/j.fpsl.2023.101143.

[11] E. Hatfield, “Machine direction oriented film technology,” in *Multilayer Flexible Packaging: Technology and Applications for the Food, Personal Care, and Over-the-*

Counter Pharmaceutical Industries, Elsevier, 2009, pp. 113–118. doi: 10.1016/B978-0-8155-2021-4.10010-3.

[12] B. A. Morris, "Commonly Used Resins and Substrates in Flexible Packaging," in *The Science and Technology of Flexible Packaging*, Elsevier, 2017, pp. 69–119. doi: 10.1016/b978-0-323-24273-8.00004-6.

[13] R. K. Krishnaswamy, Q. Yang, L. Fernandez-Ballester, and J. A. Kornfield, "Effect of the distribution of short-chain branches on crystallization kinetics and mechanical properties of high-density polyethylene," *Macromolecules*, vol. 41, no. 5, pp. 1693–1704, Mar. 2008, doi: 10.1021/ma070454h.

[14] W. S. Fall, J. Baschnagel, O. Lhost, and H. Meyer, "Role of Short Chain Branching in Crystalline Model Polyethylenes," *Macromolecules*, vol. 55, no. 19, pp. 8438–8450, Oct. 2022, doi: 10.1021/acs.macromol.2c00938.

[15] X. Li *et al.*, "The effect of comonomer content on structure and property relationship of propylene-1-octene copolymer during uniaxial stretching," *Polymer (Guildf)*, vol. 54, no. 17, pp. 4545–4554, Aug. 2013, doi: 10.1016/j.polymer.2013.06.017.

[16] L. Shen, J. Severn, and C. W. M. Bastiaansen, "Drawing behavior and mechanical properties of ultra-high molecular weight polyethylene blends with a linear polyethylene wax," *Polymer (Guildf)*, vol. 153, pp. 354–361, Sep. 2018, doi: 10.1016/j.polymer.2018.01.083.

[17] S. J. A. Houben, R. C. P. Verpaalen, and T. A. P. Engels, "Processing and Properties of Melt Processable UHMW-PE Based Fibers Using Low Molecular Weight Linear Polyethylene's," *Macromol Mater Eng*, vol. 305, no. 10, p. 2000360, Oct. 2020, doi: https://doi.org/10.1002/mame.202000360.

[18] T. I. Butler, "PE processes," in *Multilayer Flexible Packaging: Technology and Applications for the Food, Personal Care, and Over-the-Counter Pharmaceutical Industries*, Elsevier, 2009, pp. 15–30. doi: 10.1016/B978-0-8155-2021-4.10002-4.

[19] M. Stürzel, S. Mihan, and R. Mülhaupt, "From Multisite Polymerization Catalysis to Sustainable Materials and All-Polyolefin Composites," Feb. 10, 2016, *American Chemical Society*. doi: 10.1021/acs.chemrev.5b00310.

[20] I. V Sedov, V. D. Makhaev, and P. E. Matkovskii, "Single-site catalysts in the industrial production of polyethylene," *Catal Ind*, vol. 4, no. 2, pp. 129–140, 2012, doi: 10.1134/S2070050412020109.

[21] L. Jarecki and D. J. Meier, "Ultra-high modulus polyethylene. 1 Effect of drawing temperature," *Polymer (Guildf)*, vol. 20, no. 9, pp. 1078–1082, Sep. 1979, doi: 10.1016/0032-3861(79)90297-0.

[22] L. Jarecki and D. J. Meier, "Ultrahigh modulus polyethylene. II. Effect of drawing temperature on void formation and modulus," *Journal of Polymer Science: Polymer*

Physics Edition, vol. 17, no. 9, pp. 1611–1621, Sep. 1979, doi: 10.1002/POL.1979.180170913.

[23] M. Kuriyagawa and K. H. Nitta, "Structural explanation on natural draw ratio of metallocene-catalyzed high density polyethylene," *Polymer (Guildf)*, vol. 52, no. 15, pp. 3469–3477, Jul. 2011, doi: 10.1016/j.polymer.2011.05.028.

[24] P. D. Coates and I. M. Ward, "Neck profiles in drawn linear polyethylene," *J Mater Sci*, vol. 15, no. 11, pp. 2897–2914, 1980, doi: 10.1007/BF00550561.

[25] N. W. Brooks, R. A. Duckett, and I. M. Ward, "Investigation into double yield points in polyethylene," *Polymer (Guildf)*, vol. 33, no. 9, pp. 1872–1880, 1992, doi: https://doi.org/10.1016/0032-3861(92)90486-G.

[26] M. P. C. Watts, A. E. Zachariades, and R. S. Porter, "Shrinkage as a measure of the deformation efficiency of ultra-oriented high density polyethylene," *J Mater Sci*, vol. 15, no. 2, pp. 426–430, 1980, doi: 10.1007/PL00020076.

[27] A. N. Gent and J. Jeong, "Plastic deformation of crystalline polymers," *Polym Eng Sci*, vol. 26, no. 4, pp. 285–289, Feb. 1986, doi: https://doi.org/10.1002/pen.760260404.

[28] C. J. G. Plummer and H.-H. Kausch, "Micronecking in thin films of isotactic polypropylene," *Macromol Chem Phys*, vol. 197, no. 6, pp. 2047–2063, Jun. 1996, doi: https://doi.org/10.1002/macp.1996.021970621.

[29] G. Capaccio and I. M. Ward, "Preparation of ultra-high modulus linear polyethylenes; effect of molecular weight and molecular weight distribution on drawing behaviour and mechanical properties," *Polymer (Guildf)*, vol. 15, no. 4, pp. 233–238, 1974, doi: https://doi.org/10.1016/0032-3861(74)90038-X.

[30] J. M. Andrews and I. M. Ward, "The cold-drawing of high density polyethylene," *J Mater Sci*, vol. 5, no. 5, pp. 411–417, 1970, doi: 10.1007/BF00550003.

[31] R. Séguéla, "On the natural draw ratio of semi-crystalline polymers: Review of the mechanical, physical and molecular aspects," Mar. 12, 2007. doi: 10.1002/mame.200600389.

[32] D. A. Plemmons, "Processing-Structure-Function Relationships in the Production of High-Performance Oriented Polyethylene by Dayne A Plemmons," 2022.

[33] E. S. Sherman, R. S. Porter, and E. L. Thomas, "Microstructure of high modulus solid state extruded polyethylene: 1. Electron microscopy studies of 12, 24 and 36 × EDR," *Polymer (Guildf)*, vol. 23, no. 7, pp. 1069–1076, 1982, doi: https://doi.org/10.1016/0032-3861(82)90410-4.

[34] P. Smith, P. J. Lemstra, and J. P. L. Pijpers, "Tensile strength of highly oriented polyethylene. II. Effect of molecular weight distribution," *Journal of Polymer Science: Polymer Physics Edition*, vol. 20, no. 12, pp. 2229–2241, Dec. 1982, doi: https://doi.org/10.1002/pol.1982.180201206.

[35] G. Capaccio, T. A. Crompton, and I. M. Ward, “The drawing behavior of linear polyethylene. I. Rate of drawing as a function of polymer molecular weight and initial thermal treatment,” *Journal of Polymer Science: Polymer Physics Edition*, vol. 14, no. 9, pp. 1641–1658, Sep. 1976, doi: https://doi.org/10.1002/pol.1976.180140910.

[36] G. Capaccio, T. A. Crompton, and I. M. Ward, “Drawing behavior of linear polyethylene. II. Effect of draw temperature and molecular weight on draw ratio and modulus,” *Journal of Polymer Science: Polymer Physics Edition*, vol. 18, no. 2, pp. 301–309, Feb. 1980, doi: https://doi.org/10.1002/pol.1980.180180213.

[37] K. Cantor, “Blown Film Extrusion,” in *Blown Film Extrusion 3e (Third Edition)*, K. Cantor, Ed., Hanser, 2019, pp. I–XIV. doi: https://doi.org/10.3139/9781569906972.fm.

[38] V. Ratta, G. L. Wilkes, and T. K. Su, “Structure–property-processing investigations of the tenter-frame process for making biaxially oriented HDPE film. I. Base sheet and draw along the MD,” *Polymer (Guildf)*, vol. 42, no. 21, pp. 9059–9071, 2001, doi: https://doi.org/10.1016/S0032-3861(01)00387-1.

[39] M. T. DeMeuse, “Equipment design and requirements of biaxially stretched films,” in *Biaxial Stretching of Film*, Elsevier, 2011, pp. 14–26. doi: 10.1533/9780857092953.1.14.

[40] “The Key Aspects of a Machine Direction Orienter - Part 1 Heating Methods.” Accessed: Apr. 18, 2024. [Online]. Available: https://parkinsontechnologies.com/index.php/blog/the-key-aspects-of-a-machine-direction-orienter-part-1-heating-methods

[41] J. G. Drobny, “Processing Methods Applicable to Thermoplastic Elastomers, Pg. 141,” in *Handbook of Thermoplastic Elastomers*, Elsevier, 2014, pp. 33–173. doi: 10.1016/b978-0-323-22136-8.00004-1.

[42] W. Yau *et al.*, “A ‘systematic approach’ to TD-GPC data processing with band broadening correction,” *Macromol Symp*, vol. 330, no. 1, pp. 53–62, Aug. 2013, doi: 10.1002/masy.201300029.

[43] T. Pathaweeisariyakul, K. Narkchamnan, B. Thitisuk, and W. Yau, “Methods of long chain branching detection in PE by triple-detector gel permeation chromatography,” *J Appl Polym Sci*, vol. 132, no. 28, Jul. 2015, doi: 10.1002/app.42222.

[44] R. L. Blaine, “Determination of Polymer Crystallinity by DSC. Therm. Anal. TA Instruments, 109 Lukens Drive, New Castle DE 19720, USA, 1-3.” Accessed: Apr. 09, 2024. [Online]. Available: https://www.scirp.org/reference/referencespapers?referenceid=1920439

[45] B. C. Smith, “The Infrared Spectra of Polymers, Part I: Introduction.” Accessed: Mar. 18, 2024. [Online]. Available: https://www.spectroscopyonline.com/view/the-infrared-spectra-of-polymers-part-i-introduction

[46] K. De Smit, M. Edeleva, A. D. Trigilio, Y. W. Marien, P. H. M. Van Steenberge, and D. R. D’hooge, “Kinetic Monte Carlo residence time distributions and kinetics in view of extrusion-based polymer modification and recycling,” *React Chem Eng*, vol. 8, no. 3, pp. 563–576, Nov. 2022, doi: 10.1039/d2re00387b.

[47] T. Andersson, B. Stålbom, and B. Wesslén, “Degradation of polyethylene during extrusion. II. Degradation of low-density polyethylene, linear low-density polyethylene, and high-density polyethylene in film extrusion,” *J Appl Polym Sci*, vol. 91, no. 3, pp. 1525–1537, Feb. 2004, doi: 10.1002/app.13024.

[48] A. A. Mendes, A. M. Cunha, and C. A. Bernardo, “Study of the degradation mechanisms of polyethylene during reprocessing,” *Polym Degrad Stab*, vol. 96, no. 6, pp. 1125–1133, Jun. 2011, doi: 10.1016/j.polymdegradstab.2011.02.015.

[49] D. V. A. Ceretti, M. Edeleva, L. Cardon, and D. R. D’hooge, “Molecular Pathways for Polymer Degradation during Conventional Processing, Additive Manufacturing, and Mechanical Recycling,” *Molecules*, vol. 28, no. 5, 2023, doi: 10.3390/molecules28052344.

[50] H. Jin, J. Gonzalez-Gutierrez, P. Oblak, B. Zupančič, and I. Emri, “The effect of extensive mechanical recycling on the properties of low density polyethylene,” *Polym Degrad Stab*, vol. 97, no. 11, pp. 2262–2272, 2012, doi: 10.1016/j.polymdegradstab.2012.07.039.

[51] T. Bremner, A. Rudin, and D. G. Cook, “Melt flow index values and molecular weight distributions of commercial thermoplastics,” *J Appl Polym Sci*, vol. 41, no. 7–8, pp. 1617–1627, 1990, doi: 10.1002/app.1990.070410721.

[52] S. M. Ghasemi and G. M. M. Sadeghi, “General and more precise relationships between molecular weight, blend ratio, and melt index of binary polyethylene blends,” *J Appl Polym Sci*, vol. 108, no. 5, pp. 2988–2993, Jun. 2008, doi: 10.1002/app.27788.

[53] W. Meng, H. Li, J. Li, and B. Chen, “The effect of comonomer type and content on the properties of ziegler-natta bimodal high-density polyethylene,” *Journal of the Korean Chemical Society*, vol. 55, no. 4, pp. 673–679, Aug. 2011, doi: 10.5012/jkcs.2011.55.4.673.

[54] Z.-X. Du, J.-T. Xu, Q. Dong, and Z.-Q. Fan, “Effects of comonomer content, comonomer distribution and crystallization condition on crystallinity and dimension of crystal lattice of ethylene-propylene copolymers.,” *e-Polymers 2010;10(1): 079. https://doi.org/10.1515/epoly.2010.10.1.866*, 2010.

[55] B. A. Morris, “Chapter 9 - Strength, Stiffness, and Abuse Resistance,” in *The Science and Technology of Flexible Packaging*, Elsevier, 2017, pp. 309–350. doi: 10.1016/b978-0-323-24273-8.00009-5.

[56] R.-Y. Wu, L. D. McCarthy, and Z. H. Stachurski, “Tearing resistance of multi-layer plastic films,” *Int J Fract*, vol. 68, no. 2, pp. 141–150, 1994, doi: 10.1007/BF00032464.

[57] D. Guleria, S. Ge, L. Cardon, S. Vervoort, and J. den Doelder, “Impact of resin density and short-chain branching distribution on structural evolution and enhancement of tensile modulus of MDO-PE films,” *Polym Test*, p. 108560, 2024, doi: https://doi.org/10.1016/j.polymertesting.2024.108560.

[58] S. H. Tabatabaei, P. J. Carreau, and A. Ajji, “Structure and properties of MDO stretched polypropylene,” *Polymer (Guildf)*, vol. 50, no. 16, pp. 3981–3989, Jul. 2009, doi: 10.1016/j.polymer.2009.06.059.

[59] S. H. Tabatabaei, L. Parent, P. Cigana, A. Ajji, and P. J. Carreau, “Effect of machine direction orientation conditions on properties of HDPE films,” *Journal of Plastic Film and Sheeting*, vol. 25, no. 3–4, pp. 235–249, 2009, doi: 10.1177/8756087910369423.

[60] M. B. Elias, R. Machado, and S. V Canevarolo, “Thermal and Dynamic-Mechanical Characterization of Uni- and Biaxially Oriented Polypropylene Films,” *J Therm Anal Calorim*, vol. 59, no. 1, pp. 143–155, 2000, doi: 10.1023/A:1010187913049.

3.6 Appendix 3

Pictorial representation of pilot-scale MDO process

Step-wise pilot scale MDO setup

Lab scale blown film setup

Lab scale MDO setup with oven

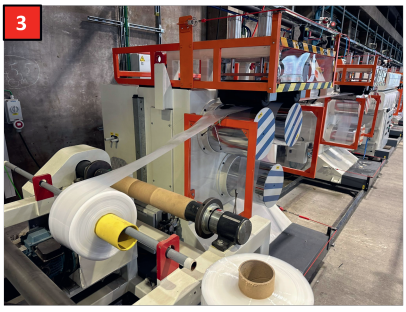

blown film mounted on the setup

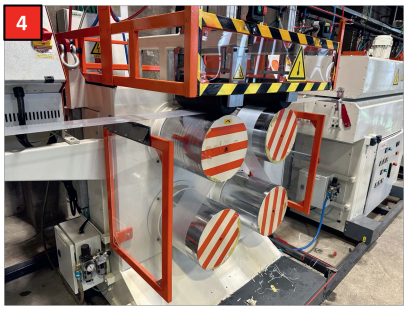

blown film through the rollers going inside the oven

MDO film coming out of the oven

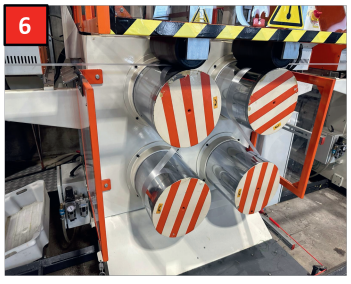

MDO film passing through the rollers after the oven

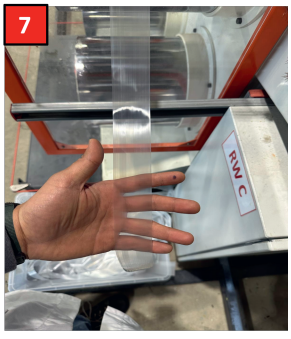

MDO film being collected

Chapter – 4

Assessing mechanical recyclability of blown films and integration of PCR for high modulus MDO-PE film application

Abstract

Multi-material multi-layer plastic packaging, widely used in packaging of fast-moving consumer goods (FMCG), presents significant challenges for mechanical recycling due to its complex composition. These packages often consist of multiple layers of various polymers and metals, making traditional recycling methods ineffective. To address this, a shift toward mono-material multi-layer packaging has gained attention, particularly in polyethylene (PE) based mono-material multi-layer flexible packaging. Traditionally, the outer layer of multi-material flexible packaging is made from non-PE materials like polyethylene terephthalate (PET) and polyamide (PA) for enhanced stiffness and barrier properties. However, orienting polymer films through processes like machine direction orientation (MDO) has the potential to improve both mechanical and barrier properties, facilitating the development of lightweight, mono-material packaging. This Chapter examines the mechanical recyclability of virgin polyethylene (PE) blown films and the incorporation of post-consumer recyclate (PCR) for subsequent machine direction orientation (MDO) operation, intended for use in the outer layer of mono-material flexible packaging. Two set of experiments were conducted. The first set assessed the recyclability of virgin PE blown films after two reprocessing cycles, revealing that slight molecular degradation affected the crystallinity and tensile modulus of reprocessed films. Despite these changes, the reprocessed films retained approximately 77% of the tensile modulus of virgin MDO films. The second set integrated mixed polyolefin PCR into virgin PE blends at 5% and 30% by weight. The 5% PCR blend demonstrated a tensile modulus comparable to virgin MDO films, highlighting its potential for high-end packaging applications like mono-material PE based flexible packaging. This study supports the feasibility of using recycled materials in MDO processes for stiffness enhanced outer layer of mono-material PE based flexible packaging.

4.1 Introduction

Plastic, an extensively used material in modern society, has witnessed a steady increase in production due to its cost-effectiveness, adaptability, and durability in various useful applications. However, the surge in plastic production has led to concerns regarding waste management and environmental sustainability. Should the current trajectory of plastics demand persist, projections indicate that global volumes of plastic waste could escalate to about 460 million tons annually by the year 2030 [1]. In 2020, within the EU27+3 countries, out of the 30 million tonnes of post-consumer plastic waste collected, merely 35% underwent recycling, while 42% was incinerated for energy recovery, and the remaining 23% was disposed of in landfills [2].

The majority of global plastic waste originates from five primary types of plastic: polyethylene terephthalate (PET), low-density polyethylene (LDPE), high-density polyethylene (HDPE), polypropylene (PP), and polystyrene (PS) [3], [4] with the primary application being packaging material. Thus, recycling of plastic packaging plays a pivotal role in polymer waste management. The limited lifespan of these articles prevents the materials from undergoing major thermo-oxidative degradation [5]. Polyolefins (PO), including polyethylene (PE) and polypropylene, are widely utilized as packaging materials and constitute over half of the plastic waste gathered annually in the EU [4], [6], [7]. Because of their abundance, brief product lifespan, rising cost of virgin resin, and legislative pressure, discarded polyolefin packaging materials are increasingly recognized as a valuable resource, thus becoming a focal point of plastic recycling initiatives [8], [9].

Two major approaches utilized for plastic waste recycling are mechanical and chemical recycling with the former being the predominant approach. This method generally involves the collection, sorting, washing, grinding, extrusion and quenching of the material for re-pelletization without significantly changing the chemical structure of the recyclate [9], [10], [11]. The main changes in the molecular properties arise from thermo-mechanical degradation during re-processing and from the presence of contaminants [12]. Mechanical recycling of polymers plays a pivotal role in reducing the utilization of non-renewable resources required for synthesizing the corresponding monomer units as it requires less energy than manufacturing new products from virgin materials [9]. Mechanical recycling hinges on several factors, including the effective segregation and categorization of diverse plastic waste types like PET, PP, LDPE, HDPE, PS, and others, alongside the minimization of impurities or contaminants such as residues from consumer products [13].

Flexible packaging serves to deliver a product from its manufacturer or distributor to the retailer or end consumer, while also safeguarding it throughout transportation, display, and storage. Multi-layer flexible packaging involves the integration of two or more layers into a composite web, offering functional, protective, and decorative attributes [14]. Multi-material multi-layer plastic packaging, commonly used in fast-moving consumer goods (FMCG), integrates functionalities from various materials. These structures improve resource-use efficiency and barrier performance, resulting in extended shelf life. They are extensively utilized in food packaging due to their exceptional performance, including mechanical strength, thermal characteristics, and effective barriers against moisture, gases,

and light. These configurations typically consist of multiple layers, sometimes as many as 11, providing optimal protection [15]. A major challenge in the mechanical recycling of flexible packaging plastic waste lies in its multi-material composition, potentially comprising various layers of thin plastic films such as PE, PP, PA, PET, PVC, as well as non-ferrous metals like aluminum and tin. Traditional plastic reprocessing methods like mechanical recycling are not viable for these multi-material multi-layered packages due to chemical incompatibilities among the layers [16], [17]. Due to embedded heterogeneity, they pose challenges to current recycling systems, as conventional waste management systems are not adapted to identify, sort and recycle multi-material multi-layers, thus undermining circular economy principles [18], [19], [20], [21], [22]. Some methods explored to recycle multi-material multi-layer packaging involve delamination to separate individual materials for recycling [23], dissolution of specific polymers [21] or usage of compatibilizing agents to process immiscible polymer phases [22], [24], [25]. These emerging methods are not yet fully technically or economically viable. Consequently, these packages are either disposed of in landfills or used for energy recovery [26], [27], [28].

One concept which can enhance the recyclability of multi-layers is designing for recycling, which entails maximizing the recyclable components within structures, avoiding hazardous materials or non-recyclables, and reducing complexity [29]. This concept proposes to use multi-layers in another form which involves the use of multiple layers composed of the same polymer type, which are physically or chemically modified to exhibit distinct functionalities, referred to as mono-material multi-layers [30]. The packaging industry has recognized the potential of high-performance mono-material plastic packaging as a significant step towards recyclability by designed products, supported by various scholarly works and industry reports [13], [27], [30], [31], [32], [33].

Polyolefin-based mono-material flexible films are receiving attention as promising candidates for meeting the circular economy's demands due to their facile mechanical recyclability, as documented by several studies [17], [27], [34], [35]. Conventionally, the outer layer of multi-layer flexible packaging is made from non-PE materials such as polyethylene terephthalate (PET) or polyamide (PA) which can provide adequate stiffness and barrier properties to the overall package. Orienting PE polymer films in the semi-solid state using processes like tenter frame, double bubble, and machine direction orientation enhances both mechanical and barrier properties, providing a pathway for developing lightweight packaging structures [36] and moving away from multi-material multi-layer applications.

The stiffness of PE films can be enhanced significantly by the machine direction orientation (MDO) process. During the MDO process, the polymer film is stretched in the machine direction at a certain temperature which depends on the polymer’s chemical nature and is typically close to the melting point of the polymer. Consequently, numerous enhancements are observed in the physical (modulus, stiffness and tensile strength) and barrier properties of the films, crucial for food packaging applications [15], [37], [38]. Blown film extrusion ranks among the foremost polymer processing methodologies, with an annual processing capacity of billions of pounds of polymer, predominantly polyethylene [39]. Hence, integrating the MDO process sequentially with film blowing can enhance the characteristics

of packaging materials and streamline the shift towards mono-material packaging, thereby positively impacting recyclability and polymer circularity.

Re-extrusion is a widely used method for recycling mono-material fractions. The process requires sorting, cleaning, and drying to remove residues, which are effectively managed by existing recycling infrastructure [13], [40], [41]. Polyolefins tend to undergo thermo-mechanical degradation during compounding and conversion into final products, leading to alterations of the molecular properties like molar mass, branching degree and molar mass distribution [42]. Thermo-mechanical and thermo-oxidative degradation processes during processing expose polymeric materials to chain scission, branching, and crosslinking reactions [43]. Linear PE grades such as linear low-density polyethylene (LLDPE) and high-density polyethylene (HDPE) mainly experience degradation through chain scission [44], [45], [46], [47], [48]. Blending recycled and virgin polyethylene stands as a recognized method for modifying the properties of recycled material [49]. While numerous studies have investigated the recycling and degradation of polyethylene during processing, particularly those used in packaging applications [49], [50], [51], [52], [53], research on blown films containing recycled polyethylene [54] remains limited [43].

In this Chapter, we studied both the mechanical recyclability of virgin polyethylene (PE) blown films and the incorporation of post-consumer recyclate (PCR) for in-line machine direction orientation (MDO) PE film applications, with a focus on desired mechanical properties of modulus and stiffness for the outer layer of mono-material PE-based flexible packaging design. Two virgin PE resins and one mixed polyolefin PCR resin were selected for the study. Blown films of dry blends were produced and subsequently used to make MDO films on a pilot-scale MDO line.

In the first set of experiments, blown films were produced using equal fractions of two virgin PE resins. These films were shredded, re-pelletized, and reprocessed to create new blown films. The process was repeated twice, resulting in three sets: virgin (V), reprocessed once (R1), and reprocessed twice (R2). MDO films were then made from each set, and their mechanical properties were assessed. Reprocessing was expected to cause slight material degradation, impacting the modulus and stiffness. In the second set of experiments, PCR material was blended with virgin materials at two different weight percentages to study its effect on the properties of blown and MDO films. It was expected that PCR integration could impact modulus and stiffness due to its composition and potential contamination or degradation from previous lifecycle. The goal was, for this specific PCR, to identify the PCR percentage that minimally affects the material properties of MDO films, supporting the circular economy of flexible packaging. It is acknowledged that the composition of PCR can vary due to factors such as origin, manufacturer, collection methods, and contamination. Consequently, the findings of this study are not intended to define specific limits for PCR incorporation with virgin materials but are presented to highlight broader opportunities for generic PCR incorporation in MDO applications.

4.2 Materials and methods

4.2.1 Materials

Two different types of virgin PE resin with different molecular properties and densities were provided by Dow (Table 4.1). One PCR MPO (mixed polyolefin, grade 7821) resin composed of recycled LDPE mainly from films and packaging material with the composition of LDPE+LLDPE ca. 95% and PP ca. 5% was provided by ECOO, Belgium. The material was selected based on circularity criterium: the PCR MPO consists of mainly packaging and the films produced in the current work are intended for packaging material. The melt flow index (MFI) was measured following ASTM D1238 using a Göttfert MI-4 plastometer under the weight of 2.16 kg at 190 ℃, which are standard conditions for PE. The density was measured according to the ASTM D792 standard procedure with isopropyl alcohol (IPA) used as a submerging liquid.

Table 4.1 The two virgin resins used for the study with their respective melt flow index (MFI) and density.

Resin type	MFI (dg/min)	Density* (g/cm^3)
X1	1.872	0.9256 ± 0.0002
X2	1.126	0.9667 ± 0.0001

*Error is standard deviation.

The composition and characteristic features of PCR, such as density and molecular weight and molecular weight distribution are discussed in detail in the molecular properties section 4.3.1 of this chapter.

The blended blown films used in this study were produced with the resin compositions detailed in Table 4.2.

Table 4.2 The five base blended blown films prepared for the study and their composition.

Material type	Material form	Composition (wt%)
V (Virgin Blend)	Blown film	X1/X2 (50/50)
R1 (Reprocessed once)	Blown film	X1/X2 (50/50)
R2 (Reprocessed twice)	Blown film	X1/X2 (50/50)
5% PCR	Blown film	PCR/X1/X2 (5/47.5/47.5)
30% PCR	Blown film	PCR/X1/X2 (30/35/35)

4.2.2 Preparation of blown films

The resins were processed to make blown films in a LabTech blown film line (40 mm die diameter, 0.8 mm die gap) with approximately 110-micron thickness and lay-flat width of approximately 145 mm. The blow-up ratio (BUR) and draw-down ratio (DDR) were approximately 2.31 and 3.15, respectively. The mass flow rate was approximately 90 g/min. The temperature profile for the extruder was ranging from 160 °C to 190 °C and the lower and upper temperature at the die outlet were 180 °C and 160 °C, respectively. The speed of the nip rollers was approximately 3 m/min, and it was varied slightly in accordance with the required BUR and DDR in each extrusion. After exiting the die, all blown films were cooled at similar rates at ambient room temperature under constant process parameters. Blown films of base resins X1 and X2 were prepared to analyse base blown films characteristics.

A dry blending process was used to prepare the blown films of blends. Blended films were produced using the blown film process, and these films were subsequently used to create machine direction orientation (MDO) films via a pilot-scale MDO line. In the 1st set of experiments, which aimed to validate the mechanical recyclability of the virgin materials, a blended blown film was produced with equal weight fractions (50%) of two virgin resins, X1 and X2, as shown in Figure 4.1. This blended film was then shredded into flakes using a mechanical shredder. The flakes were re-pelletized using a twin-screw extruder equipped with a water bath and pelletizer to further produce a re-processed blown film with the same composition. This process was repeated twice, resulting in three sets of blown films: from virgin materials (V), re-processed once (R1), and re-processed twice (R2). For each set of virgin and reprocessed blown films, MDO films were produced, and the mechanical properties of both the blown films and the MDO films were evaluated.

The density of the blends was calculated theoretically using an inverse-additive mixing rule. It should be noted that this method may not be exact: if co-crystallization occurs, the true base sheet density of a blend can be higher than that predicted by a simple mixing rule. The predicted density of the X1/X2 50/50 blend is 0.9437 g/cm^3.

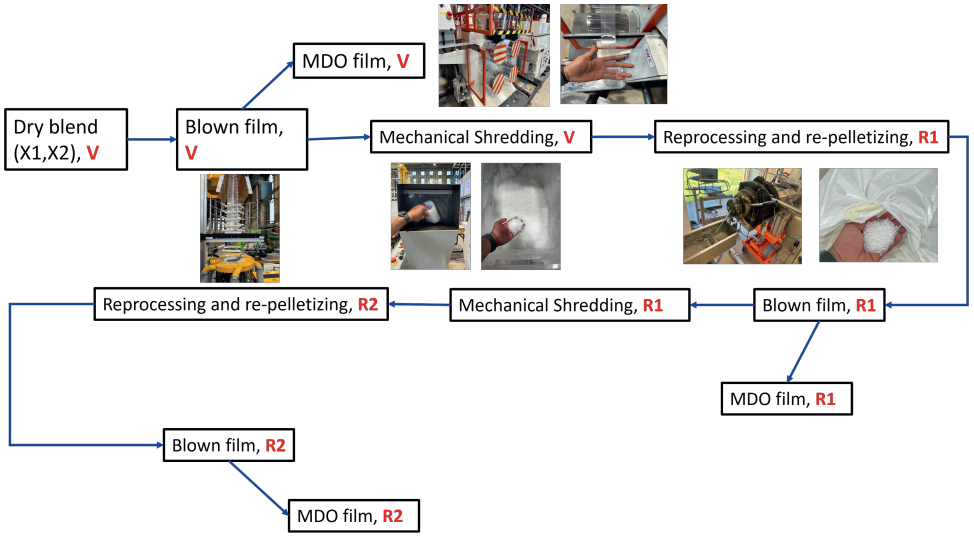

Figure 4.1 Process flow diagram of 1st set of experiments with pictorial representations of different processes.

In the 2nd set of experiments, PCR material was integrated with the virgin materials at two different PCR weight percentages of 5% and 30%, while the relative weight percentages of virgin resin X1 and X2 were kept constant, to evaluate the impact of PCR integration on the properties of blown and subsequently MDO films, as shown in Figure 4.2.

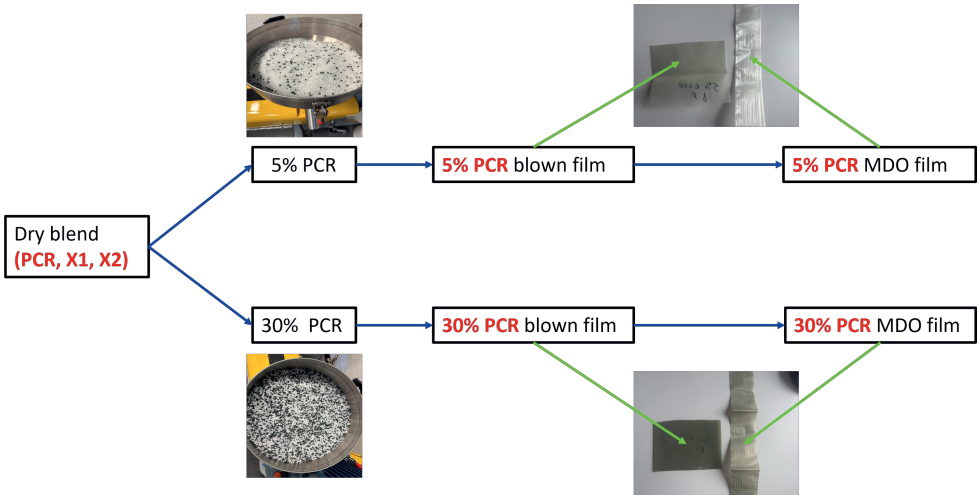

Figure 4.2 Process flow diagram of 2nd set of experiments with pictorial representations.

In total 5 blown films of blends were produced to be used further for making MDO films. The weight percentage composition of each resin in all 5 blown films of blends is shown in Table 4.2.

4.2.3 Preparation of MDO films

The heating chamber (oven) from a Konark extrusion line was utilized to provide the desired stretching temperature for the pilot-scale MDO setup to process lab-scale blown films. The heating chamber was supported with inside air circulation to maintain the constant temperature across it during stretching. The orientation temperature used for MDO operation for each blow film was 15 °C below the peak melting temperature. The heating chamber used to provide the necessary orientation temperature during the stretching was approximately 2.5 meters in length. The extended heating chamber length increased the residence time of the running web, allowing the films to undergo both stretching and annealing simultaneously within the same step. No dimensional changes were observed in the films after stretching. Consequently, the annealing temperature was essentially the same as the film orientation temperature. After coming out from the heating chamber, the films were cooled under ambient room temperature. Each blown film was subjected to a process draw ratio of 6 to produce final MDO film with a constant 1.6 m/min of rollers speed before the MDO oven. The process draw ratio is defined by Equation 4.1.

$$Process\ draw\ ratio\ (speed) = \frac{Speed\ of\ the\ rollers\ after\ oven\ (m/min)}{Speed\ of\ the\ rollers\ before\ oven (m/min)} \quad \textit{Equation 4.1}$$

4.2.4 Shredding

A MDS 340/150 shredder from Hellweg equipped with 3 rotor knives and 2 stator knives rotating at 280 rpm with screen diameter of 6 mm was used to shred the blown films into flakes. The flakes were collected in a clean bucket for further re-processing.

4.2.5 Reprocessing and repelletizing

A MAS 24 twin-screw extruder, rotating at 50 rpm, was used to process flakes obtained from mechanically shredded films. The flakes were first melted into a melt strand using the twin screw extruder, and the material was then pelletized by a cutter after the melt strand passed through a water bath. The temperature in the twin-screw extruder varied from 120, 150, 170, 190 °C in initial zones to 190°C in the final zone 5, where the melt strand emerged from the die outlet. The thickness of the melt strand was adjusted by passing it through the Vexta parallel shaft gearhead and adjusting its speed accordingly, which pulled the melt strand out of the die. The solidified melt strand inside the water bath was subsequently passed through a BM15-HD laboratory pelletizer from Accrapak Systems Ltd. The re-pelletized PE resins were collected in a clean bucket and dried with hot air to remove moisture before further use in the blown film line.

4.2.6 Fourier transform infrared spectroscopy (FTIR)

The ATR-FTIR spectra were recorded on a Bruker Tensor 27 device, with OPUS 6.5 software at a resolution of 4 cm^{-1} and wave number range from 4000 to 600 cm^{-1}.

4.2.7 Gel Permeation Chromatography (GPC)

Molar mass distribution and architecture were measured using triple-detector gel permeation chromatography (3D-GPC) according to the procedure described in Yau *et al.* (2013)[55] and Pathaweeisariyakul *et al.* (2015)[56]. The triple detector GPC-IR system from Polymer Char was composed of a 1260 Infinity isocratic pump from Agilent, an autosampler from Polymer Char, a high temperature GPC chromatograph equipped with four 20 µm Agilent "Mixed A" GPC columns, an IR5-MCT detector, a four-capillary bridge viscometer from Polymer Char and a 2-angle light scattering detector from Agilent. For absolute molar mass determination, the 15° light scattering channel was used as a direct measurement. The polymer resins were first dissolved in 1,2,4 trichlorobenzene (TCB) at 160 ˚C and a concentration of about 1.6 mg/ml. They were processed through a column packed with gel particles which separate the molecules by their size. The volumetric flow rate was 1 ml/min. The 3D-GPC measurement allows to determine microstructural resin parameters such as average molar mass, molar mass distribution, comonomer distribution, and branching fractions.

4.2.8 Differential scanning calorimetry (DSC)

The Netsch Polyma DSC was used for the thermal analysis of the blended blown films and a DSC Q2000 from TA instruments was used for the thermal analysis of X1 blown film and its subsequent MDO films. A nominal 5 to 10 mg of sample in film form was used in a heat-cool-heat cycle from 0 to 200˚C at a rate of 10˚C/min under a nitrogen atmosphere. The degree of crystallinity (X_{DSC}) was computed according to Equation 4.2.

$$X_{DSC} = \frac{\Delta H_m}{\Delta H^\circ_m} * 100 \qquad \textit{Equation 4.2}$$

Where ΔH_m is the melting enthalpy, and ΔH°_m is the melting enthalpy of 100 % crystalline PE, i.e., 293 J/g [57]. The enthalpy data was taken from the first melting curve of the heat-cool-heat cycle.

4.2.9 Scanning electron microscopy (SEM)

Imaging of the films was done with a scanning electron microscope (SEM) namely Quanta 3D FEG from Thermo Fisher Scientific. Before Imaging the samples were sputter coated using a Quorum Q150T S with Gold (Au) for 40s at 40 mA. Elemental analysis of the PCR resin and films was performed with energy dispersive X-Ray spectroscopy (EDX) by using Phenom ProX.

4.2.10 Atomic Force Microscopy (AFM)

Surface morphology of all samples was determined by atomic force microscopy (AFM). The samples were mounted on a stage using double-sided carbon tape and then blow-cleaned with duster for AFM analysis. AFM images were captured at ambient temperature by using a Bruker Icon AFM system with a MikroMasch probe in tapping mode. The probe had a

spring constant of 40 N/m and a resonance frequency in the vicinity of 170 kHz. An imaging frequency of 0.5-2 Hz was used with a set point ratio of ~0.8.

4.2.11 Haze analysis

Haze refers to the milky or cloudy appearance observed in plastic films and is a crucial quality parameter for manufacturers. It is caused by the scattering of light within the transparent material and is quantified as the percentage of light transmission that deviates by more than 2.5 degrees from the incident beam. A lower haze value indicates higher clarity of the material. Haze measurements were taken on a dual beam xenon flash HunterLab Ultrascan VIS Spectrophotometer with a wavelength range from 360 to 780 nanometers (nm).

4.2.12 Tensile properties

The blown and MDO films underwent tensile testing using the INSTRON 5565 tensile testing machine following ASTM D882 method. 10-mm wide samples with gauge length of 50 mm were mounted on the machine The constant extension rate used for mechanical performance analysis was 100 mm/min, corresponding to a nominal strain rate of approximately 0.033 s^{-1}. The 2% secant modulus is one of the several methods used to measure modulus of elasticity, which is a measure of material's stiffness. The 2% secant modulus was quantified by integrated Bluehill software by measuring the slope of the line drawn from the origin of the stress-strain curve to the point where it intersected the curve at 2% strain. Five samples were tested in both machine and transverse directions.

4.2.13 Tear properties

Trouser tear method for determining the tear resistance of blown films was used according to ISO 6383-1 guidelines using the INSTRON 5565 tensile testing machine. Rectangular test samples with dimensions 150 x 50 mm were prepared with 75 mm slit from the centre of the specimen. One of the slitted two parts of the samples were mounted on upper and one on the lower grips of the machine with initial grip separation of 75 mm. Extension rate of 200 mm/min between the grips was used for tear propagation and tear propagation load was recorded. Five samples were tested in both machine and transverse directions.

4.3 Results and discussion

4.3.1 Molecular properties

4.3.1.1 Fourier transform infrared spectroscopy (FTIR) analysis

Figure 4.3 shows the FTIR spectra of all the five blown films described in Table 4.2 and indicates PE as the main component [59]. The clear crystalline splitting at 1472/1462 and 729/720 cm^{-1} indicates the presence of a crystalline phase (Figures 4.3b and 4.3c) [40]**.** It is known that the polymer can degrade by unwanted chemical processes like oxidation during processing as highlighted by many researchers [12], [58], [59], [60]. No traces of oxidized groups were found in the FTIR spectra of films. However, EDX surface elemental analysis of

the PCR resin revealed an oxygen concentration of approximately 3-3.5% by weight (data provided in Appendix A4.1 and A4.2), indicating minor thermo-oxidative degradation of the PCR resin during processing in production or the presence of some other species. Similarly, the FTIR analysis revealed no presence of PP in the films with 5 and 30% of PCR as the concentration was below the detection limit. Indeed, if the presence of 5% PP in PCR is assumed, the maximal fraction of PP is calculated to be 1.5 wt.% in the film containing 30% PCR which is quite low.

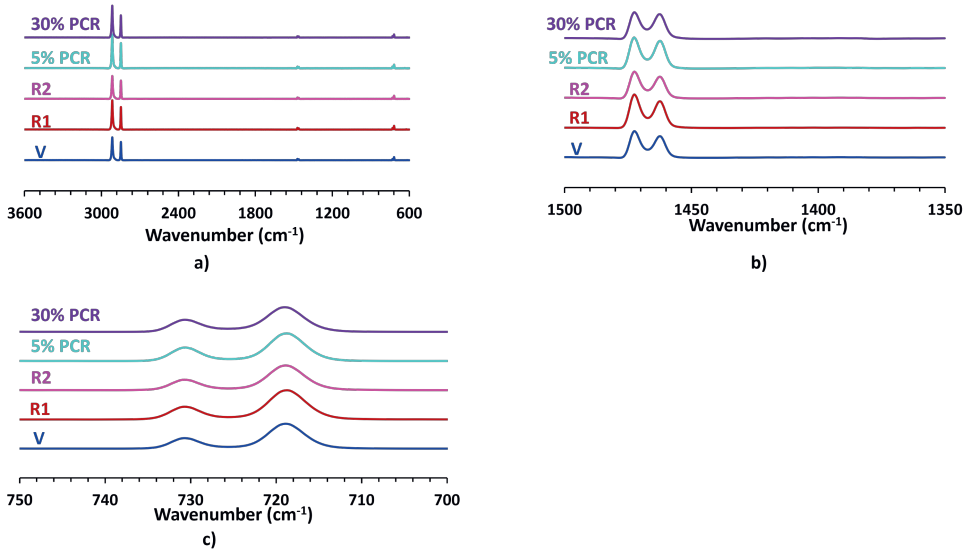

Figure 4.3 The infrared spectrum of all blown films used in the study: (a) 3600-600 cm^{-1} spectral range, (b) zoom in 1500-1350 cm^{-1} region, (c) zoom in 750-700 cm^{-1} region.

4.3.1.2 Effect of mechanical reprocessing and integration of PCR on the molecular architecture of films

Gel permeation chromatography was used to analyse the molecular architecture parameters like number-average molecular weight (M_n), weight-average molecular weight (M_w), comonomer content and polydispersity ($Đ$) of all the selected materials i.e. resins, blown films and MDO films. GPC curves obtained from the analysis of the blown films from selected materials that were used in both 1st and 2nd set of experiments are shown in Figure 4.4.

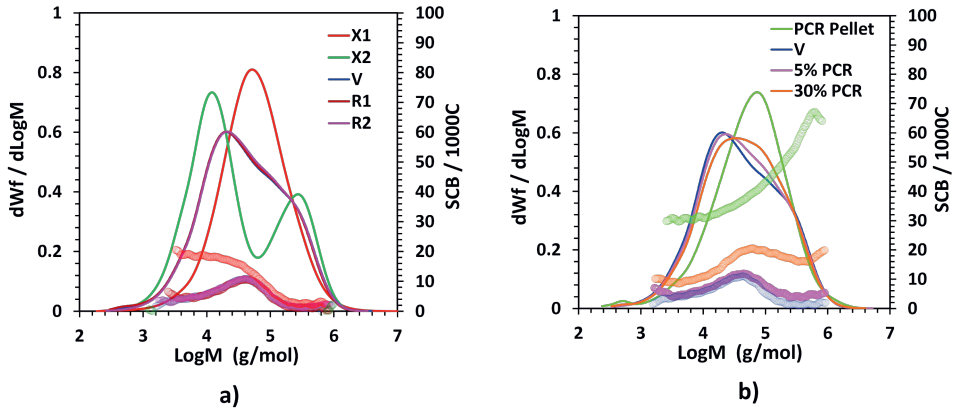

Figure 4.4 GPC curves for the blown films used in **a)** 1st set of experiments, and **b)** 2nd set of experiments. The left vertical axis represents the differential weight fractions (lines), and the right vertical axis represents the average number of SCB per 1000 C atoms at each molar mass (open markers). **Note:** Figure 4.4b also depicts GPC curve of PCR pellet alongside blown films.

Table 4.3 shows measured M_n, M_w, and comonomer content for different materials used for the study.

Table 4.3 GPC data representing M_n, M_w, polydispersity ($Đ$) and comonomer content for different materials used for the study.

Material type	Material form	Composition (wt%)	M_n (kg/mol)	M_w (kg/mol)	$Đ$ (-)	Comonomer Content (wt%)
X1	Blown film	X1	26.7	104.4	3.9	7.96
X2	Blown film	X2	9.8	106.5	10.9	0.95
V	Blown film	X1/X2 (50/50)	13.6	106.8	7.8	4.08
R1	Blown film	X1/X2 (50/50)	12.6	102.6	8.2	3.97
R2	Blown film	X1/X2 (50/50)	14.3	106.9	7.5	4.34
R2 MDO	MDO film	X1/X2 (50/50)	14.1	106.2	7.6	4.23
PCR Pellet	Pellet	PCR	15.4	183.3	11.9	31.98
5% PCR	Blown film	PCR/X1/X2 (5/47.5/47.5)	14.2	110	7.7	5.46
30% PCR	Blown film	PCR/X1/X2 (30/35/35)	14.6	126.9	8.7	12.20

The M_w measured on the virgin blown film V confirms its composition was accurate, with X1 and X2 each constituting 50% of the mixture. Additionally, the incorporation of short chain branching (SCB) in the V blown film of blend, as compared to pure X2 blown film, effectively reduces the overall density. This reduction facilitates uniform stretching and crystal fibrillation during the MDO process. Multiple extrusion cycles were used during the processing of blown films of blends in the 1st set of experiments, with V, R1, and R2 blown films representing 1, 3, and 5 extrusion cycles, respectively. M_n, M_w and polydispersity ($Đ$) data of blown films of this 1st set of experiments are plotted as a function of number of extrusion cycles in Figure 4.5.

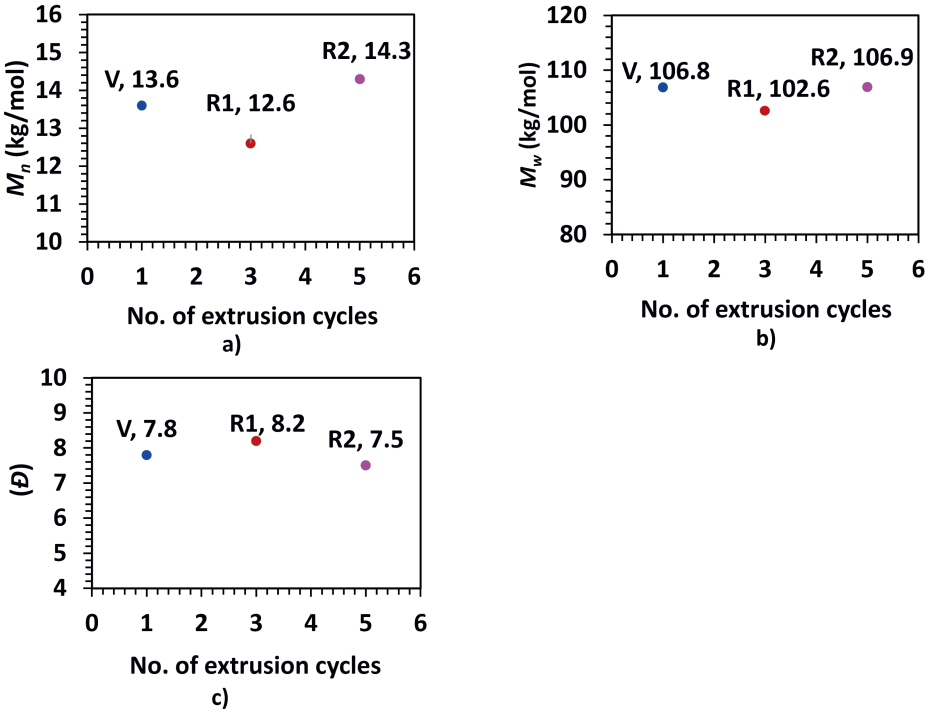

Figure 4.5 Molecular parameters **a)** M_n , **b)** M_w , **c)** polydispersity ($Đ$) of blown films of 1st set of experiments as a function of number of extrusions cycles.

As shown in Figure 4.5 and Table 4.3, no significant differences in M_n and M_w were observed after 5 extrusion cycles. Oblak et al. [61] studied the degradation behaviour of HDPE under one hundred consecutive extrusion cycles through a twin-screw extruder. They reported significant changes in the peak value of polydispersity index only after the 30th extrusion cycle.

This study aimed to investigate the degradation behaviour during only the initial reprocessing cycles in contrast to past studies with extensive extrusion cycles, as material from these cycles is typically suitable for high-end applications like MDO operations. The GPC analysis for the PE blown film of blends (V, R1 and R2) presented no severe degradation in the molecular architecture up to 5 extrusion cycles.

The MDO operation requires temperatures between the glass transition temperature and the melting temperature, which were not expected to induce significant degradation. This is confirmed by comparing the GPC data of the R2 blown film with its counterpart, R2 MDO film. As shown in Table 4.3, the M_n, M_w, and polydispersity values are nearly identical, indicating no measurable changes in the molecular architecture. Figure 4.6 compares the molecular architecture of the virgin blend V blown film to the R2 MDO film, with the curves showing good overlap, further indicating no significant changes in molecular architecture after multiple extrusion cycles and MDO operation.

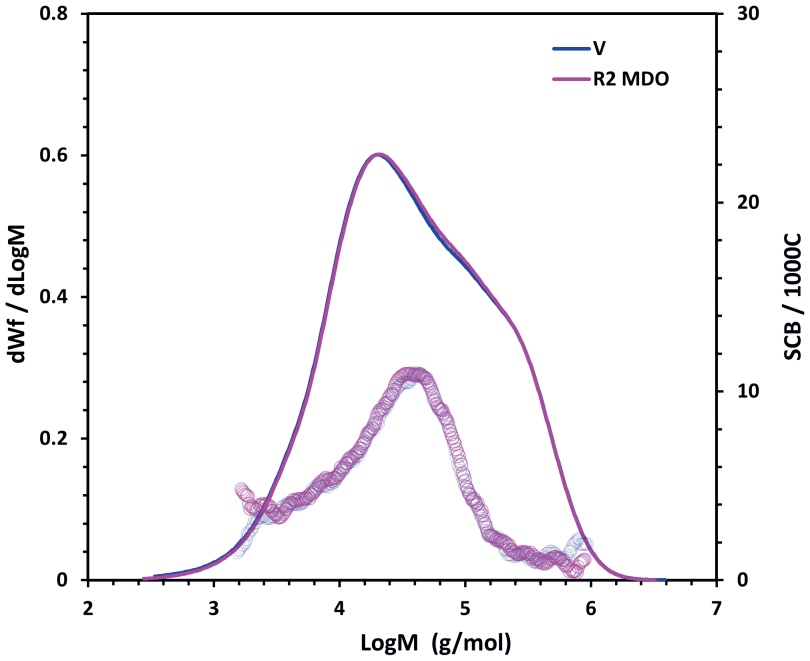

Figure 4.6 GPC curves for V blown film and R2 MDO film. The left vertical axis represents the differential weight fractions (lines), and the right vertical axis represents the average number of SCB per 1000 C atoms at each molar mass (open markers).

In the 2nd set of experiments, as illustrated in Figure 4.4b, the PCR pellet exhibits the highest molecular weight (M_w) and comonomer content by weight percentage due to its composition, which majorly include LDPE, LLDPE and PP, with a large proportion of high-comonomer content containing species. High comonomer content in PCR indicated a relatively low overall density relative to the virgin blend. The impact of blending the PCR pellet with the virgin blend is evident in the microstructure, as the M_w increases with the rising weight percentage of PCR in the blend. The comonomer content also increases with higher PCR weight percentages in the blown film of blends, corresponding to an increase in short chain branching (SCB) fractions across different molecular weight distributions. This augmentation results in a decrease in the overall density of the blend, which becomes more pronounced when increasing the PCR fraction from 5% to 30%.

4.3.1.3 Effect of mechanical reprocessing and integration of PCR on crystallinity of films.

The thermal properties of the blown and machine-direction-oriented (MDO) films for both the 1st and 2nd sets of experiments were analysed using differential scanning calorimetry (DSC).

In the 1st set of experiments, as depicted in Figure 4.7a and summarized in Table 4.4, no significant changes were observed in the percent crystallinity of the reprocessed blown films R1 compared to the virgin blown film V (Figure 4.7a).

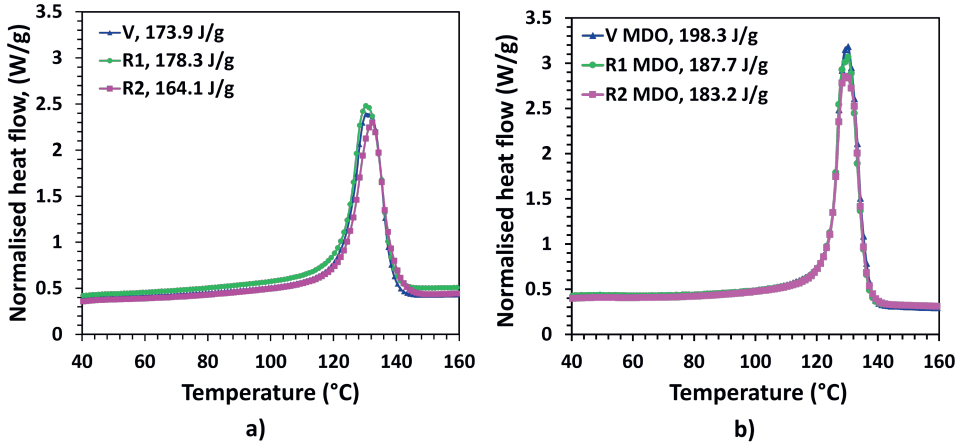

Figure 4.7 DSC melting curves obtained during 1st heating cycle (endo up) along with their enthalpy of melting for the films from 1st set of experiments **(a)** blown films and **(b)** MDO films.

Table 4.4 Percent crystallinity data for blown and MDO films used in 1st set of experiments. (Note: After exiting the die, all blown films were cooled at similar rates at ambient room temperature under constant process parameters. Similarly, all MDO films were cooled at ambient room temperature after exiting the heating chamber.)

Material type	% Crystallinity (Blown film)	% Crystallinity (MDO film)
V	59.4	67.7
R1	60.9	64.1
R2	56.0	62.5

Among the three blown films, R2 exhibited the lowest percent crystallinity, in line with the findings of Zeng et al [62] where they reported recycled HDPE films showed lower enthalpy of melting compared to virgin HDPE films. This reduction was attributed to the decreased molecular ability to pack and form crystals [63], a possible consequence of the onset of chain branching and cross-linking in the reprocessed material.

For the counterpart MDO films (Figure 4.7b), the highest percent crystallinity of 67.7% was observed in the virgin blend (V), while the R2 MDO film exhibited the lowest percent crystallinity at 62.5%. During the MDO operation, the crystals undergo disintegration, fibrillation and get aligned in the machine direction at the used orientation temperature (Figure 4.11). As the tensile forces on the films increase during MDO processing, these disintegrated and fibrillated crystals induce strain-induced crystallization in the amorphous

regions, enhancing overall crystallinity. The results suggest that the onset of slight degradation in the molecular architecture of R1 and R2 may have impacted the crystal size and overall crystallinity, with R2 being more affected than R1. Larger crystal sizes and higher overall crystallinity in the blown films before stretching lead to higher overall crystallinity in their MDO counterparts, as evidenced by the highest percent crystallinity observed in the V MDO film. These findings indicate that multiple reprocessing cycles likely affect the molecular ability to form larger crystals and influence overall crystallinity, which in turn impacts strain-induced crystallization and the orientation of amorphous regions during MDO operation.

In the 2nd set of experiments, post-consumer recycled (PCR) material was incorporated into the virgin X1 and X2 blends at concentrations of 5% and 30%. Given that this PCR is a mixture of recycled LDPE and PP [64] with a high weight percentage of comonomer in its molecular architecture, it was anticipated that introducing PCR would reduce the overall density of the films. Figure 4.8a revealed traces of PP in PCR, which were not observed in the FTIR results. Additionally, PCR's relatively lower melting enthalpy of 119.2 J/g indicated its lower density nature. Figure 4.8a further revealed that the addition of 5% PCR did not result in a significant change in percent crystallinity compared to the virgin V blend, as evidenced by an enthalpy of melting of 177.1 J/g, which is comparable to that of the virgin blend (173.9 J/g). However, at a 30% PCR level, the enthalpy of melting decreased to 153.9 J/g.

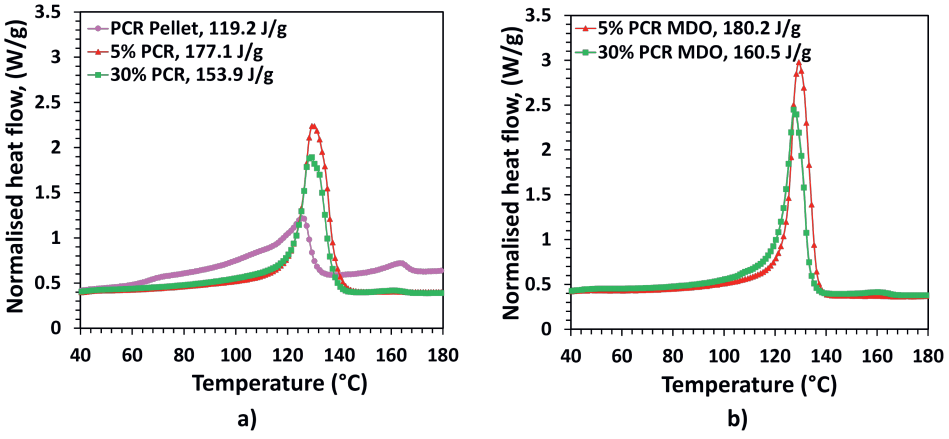

Figure 4.8 DSC melting curves obtained during 1st heating cycle (endo up) along with their enthalpy of melting for the material from the 2nd set of experiments **(a)** PCR pellet and blown films and **(b)** MDO films.

In the corresponding MDO films, the enthalpy of melting for the 5% PCR blend blown film increased to 180.2 J/g, which is comparable to the R1 and R2 MDO films. For the 30% PCR blend, the measured DSC melting enthalpy in the MDO film was 160.5 J/g, which was the lowest value observed among the MDO films across both experimental sets. This can be attributed to the lowest overall crystallinity and smaller crystals in the 30% PCR blown film, due to the composition of PCR (LDPE and PP), which reduced crystalline microstructure fibrillation and further strain-induced crystallization during the MDO process. In contrast,

the 5% PCR blown film, with higher crystallinity, was more capable of undergoing these processes. Additionally, impurities and gel particles present in PCR likely further inhibited the molecular ability to pack and form crystals, thereby decreasing overall crystallinity.

4.3.2 Analysis of mechanical properties

4.3.2.1 Blown films

Mechanical properties (tensile modulus and tear resistance) were analyzed for all five blown films produced from blends, as shown in Figure 4.9. Tensile modulus is a critical property for the outer layer of multi-layer flexible packaging systems. A high tensile modulus indicates greater stiffness, which is essential for the efficient operation of packaging webs on industrial packaging lines and for the structural integrity of specialized designs, such as stand-up pouches.

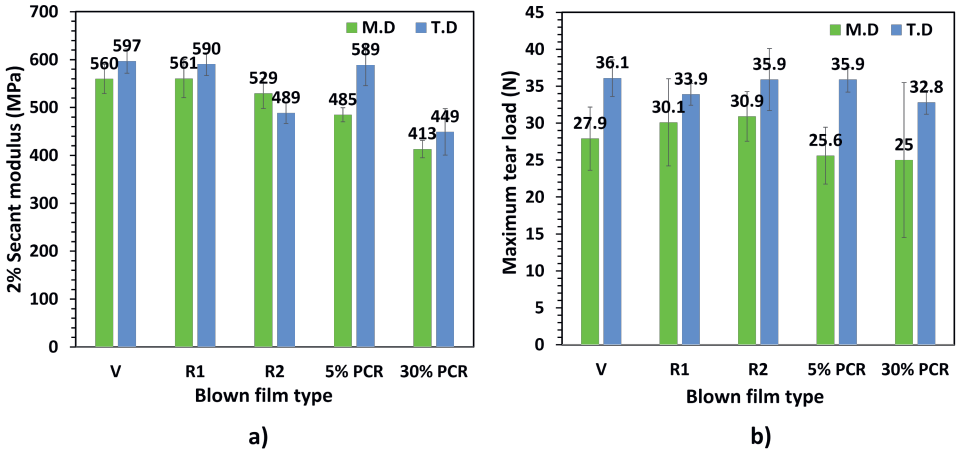

Figure 4.9 Mechanical properties of all prepared blown films of blends: **a)** Tensile modulus and **b)** Tear resistance. (n=5) Note: Error bars indicate standard deviations.

The modulus of polyethylene is a function of its crystallinity. In the 1st set of experiments, the virgin (V) and R1 films exhibited similar modulus properties consistent with their comparable DSC percent crystallinity results (Figure 4.7a). However, for the R2 blown film (after 5 extrusion cycles), reduction in modulus was observed in the transverse direction (TD) compared to V Blown film (Note: Statistical significance was assessed using ANOVA. p=.002, α=.05). Specifically, the TD modulus decreased from approximately 600 MPa to 490 MPa compared to the V blown film. This reduction can be attributed to the onset of slight degradation in the molecular architecture of R2 relative to V, which diminished the molecular ability to pack and form crystals, thus reducing overall crystallinity as indicated by the DSC results.

In the 2nd set of experiments, the introduction of PCR reduced the overall crystallinity in the 5% and 30% PCR-blended blown films, which was also reflected in the tensile modulus results (Figure 4.9a). At 5% PCR, small reduction in modulus was observed in the machine direction (MD) compared to V blown film (p=.012, α=.05). At 30% PCR, the tensile modulus

significantly decreased to approximately 410 MPa in the MD ($p<.001$, $\alpha=.05$) and 450 MPa in the TD ($p<.001$, $\alpha=.05$) compared to the virgin blown film. The substantial introduction of LDPE and PP fractions from PCR at this concentration reduced the overall crystallinity and, consequently, the modulus.

Usually, stiff polymers like PET and PA are unable to provide sufficient tear strength in the conventional multi-layer flexible packaging system. Most flexible packaging films include a ductile polyethylene or ethylene copolymer sealant layer, known for their high tear strength due to plastic yielding during tear propagation. The low yield strength of polyethylene creates a large plastic deformation zone ahead of a propagating crack, enhancing tear strength. HDPE film usually exhibits the low stress Keller-Machin structure without twisted lamella [65].

The trouser tear test was conducted to evaluate the tear strength of blown films. Upon comparing the maximum tearing loads required for tear propagation (Figure 4.9b), it was observed that the V, R1, and R2 blown films exhibited similar tear strength properties ($p=1$, $\alpha=.05$), with the transverse direction (TD) showing higher tear strength than the machine direction (MD). This finding is consistent with a study by Zhang et al. [66] on HDPE, which also noted higher tear strength in the TD compared to the MD. This phenomenon can be attributed to the short lamellae of HDPE oriented perpendicular to the main orientation of long nucleating chains in the MD, facilitating tear propagation along these lamellae interfaces. The incorporation of PCR, specifically in 30% PCR blown film presented relatively high standard deviations in the MD maximum tear load, likely due to the presence of a fraction of stiffer PP from the PCR, which is generally less extensible and requires lower force for tear propagation and fracture [67]. Additionally, the presence of inorganic contaminants and point gels may have contributed to sustaining tear propagation.

4.3.2.2 MDO films

Following the comparison of the tensile modulus of blown films, it was interesting to examine the tensile modulus of the machine direction oriented (MDO) films derived from two separate sets of experiments. Figure 4.10 illustrates the machine direction (MD) tensile modulus for all five MDO films produced (V, R1, R2, 5% PCR, and 30% PCR). This data is presented alongside the MD tensile modulus of their corresponding blown films, as well as the percentage increase in modulus resulting from the MDO process.

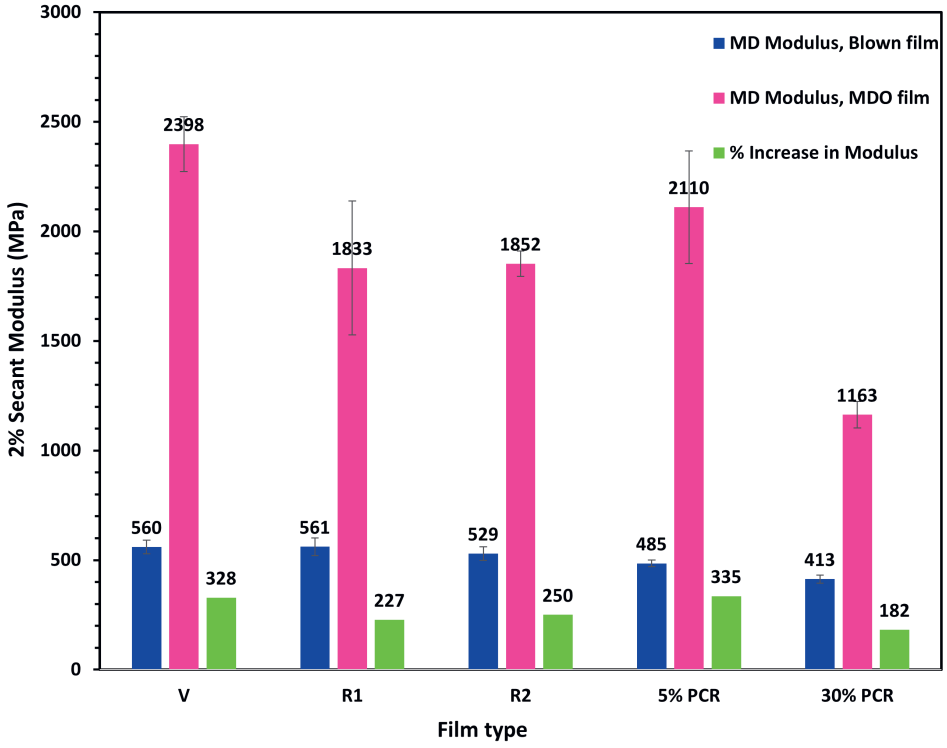

Figure 4.10 MD tensile modulus (n=5) comparison for blown and MDO films of all blended films used in the study.

In the first set of experiments, it is noteworthy that the V MDO film exhibited the greatest enhancement in modulus compared to its blown film MD modulus (approximately 330%) after MDO processing. R1 and R2 MDO films also showed improved modulus by about 250%, compared to their respective blown film MD moduli. The DSC results indicate that after 5 extrusion cycles, the R2 blown film exhibited the lowest percent crystallinity among the three blown films, possibly due to onset of slight degradation in its molecular architecture. This reduction in crystallinity also impacts the modulus results after MDO operation, with the V MDO film displaying the highest crystallinity at 67.7% among the three MDO films, followed by the R1 MDO film (64.1%) and the R2 MDO film (62.5%).

The initial crystallinity and crystal size of the base film are critical factors in selecting a film for MDO processing, as they significantly influence the resulting modulus enhancement. Films with higher initial crystallinity and larger crystal sizes are preferable when aiming for greater modulus enhancement after MDO processing [68]. This preference arises because films with higher crystallinity and larger crystals experience less partial melting at the specific orientation temperature used. This minimally melted crystalline microstructure withstands tensile deformation better, allowing for effective fibrillation and orientation in the machine direction during MDO processing. Moreover, less partially melted larger crystals facilitate strain-induced crystallization in the amorphous regions when subjected to

tensile forces during MDO operation. It is important to note that even after 5 extrusion cycles, the R2 MDO film achieved approximately 77% of the MD modulus of the V MDO film. This finding is significant for considerations in designing MDO films aimed at reprocessing older films with similar compositions to create new MDO films.

In the second set of experiments, incorporating 5% PCR into the blend also slightly reduced the MD modulus of the MDO film compared to the V MDO film (Figure 4.9). This could be attributed to the lower density of the PCR material as indicated by DSC and GPC results, compared to the V blend. In that sense, when looking for generic learnings from PCR incorporation, it would be interesting to compare these results to, e.g., the effect of higher density PCR at higher PCR loadings. The incorporation of 5% PCR slightly reduced the overall density and crystallinity, thereby limiting its ability to achieve similar modulus enhancement through fibrillation of the crystalline microstructure compared to V blown film. This reduction in MD modulus was more pronounced in the case of the 30% PCR MDO film, decreasing to 1163 MPa, approximately half of the V MDO film modulus ($p<.001$, $\alpha=.05$). When going from blown film to MDO film, the modulus of the 30 % PCR film still increased, yet this increase was roughly only half as important as for the virgin and the 5 % PCR cases. These findings suggest that incorporating a moderate amount of PCR can enhance the MD modulus of their MDO films to a considerable extent compared to the starting blown film, contributing positively to the circular plastics economy initiative.

4.3.3 Morphological analysis by SEM and AFM

The surface morphology of the films was analysed using scanning electron microscopy (SEM) and atomic force microscopy (AFM), with results presented in Figures 4.11 and 4.13. For the 1st set of experiments, the surface morphology of two extremes, the blown and MDO films of V and R2, is depicted in Figure 4.11. The blown films of both V and R2 exhibited a randomly oriented microstructure with spherulitic morphology, as observed in the SEM and AFM images. Additionally, the SEM images of the R2 blown film revealed pits and cracks, indicating a relatively rougher surface compared to the V blown films. This increased roughness in the R2 blown film is likely due to the film undergoing five extrusion cycles. Work of Zeng *et al.* [69] on HDPE teaches us that repeated exposure to high temperatures leads to cross-linking of the polymer chains, resulting in surface irregularities and increased roughness.

After MDO the spherulitic morphology was changed to fibrillar bundles oriented in the machine direction as can be seen from the SEM and AFM images of V and R2 MDO films. Like R2 blown film, R2 MDO film also showed higher surface roughness compared to V MDO film (Figure 4.12), possibly due to already present surface defects in its blown film which enhances further during crystals fibrillation during MDO operation.

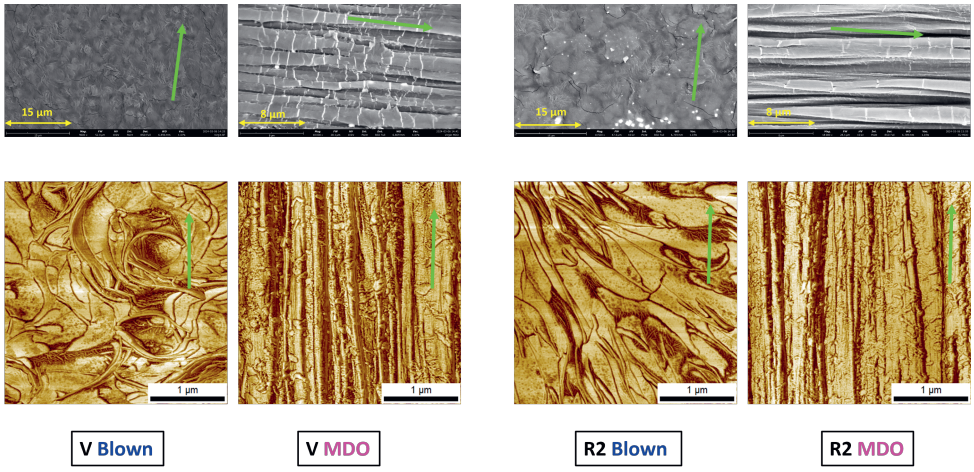

Figure 4.11 SEM (top) and AFM (bottom) images of the V and R2 blown and their subsequent MDO films. (Note: Green arrow in the images represents machine direction.)

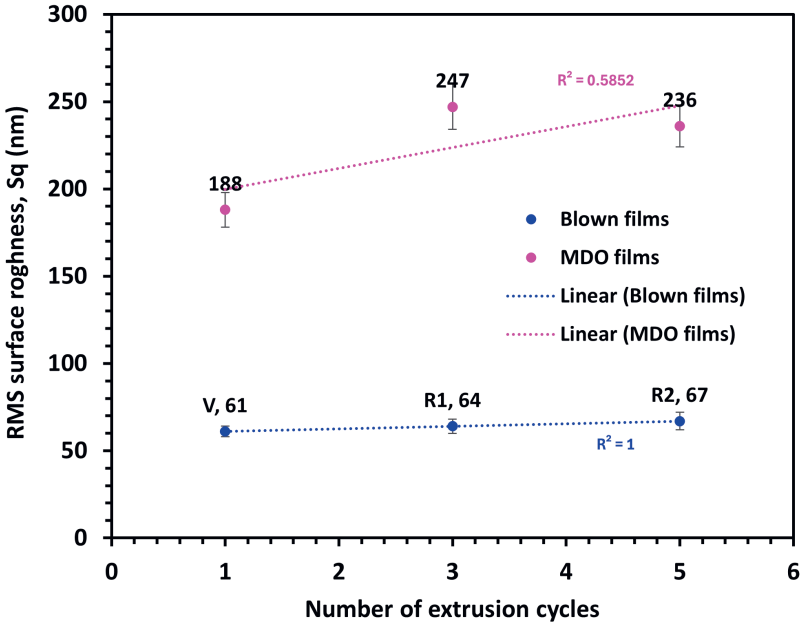

Figure 4.12 RMS (root mean square) surface roughness (n=5) for the films from 1st set of experiments as quantified by AFM.

For the PCR-integrated blown films, the 5% PCR films exhibited similar morphology to the V blown films in both SEM and AFM images (Figure 4.13), displaying a small amount of gel and fiber defects. These defects were more pronounced in the images of the 30% PCR blown and MDO films. The presence of these defects is attributed to possible contamination with

inorganic and organic foreign materials in the PCR resin during recycling. Despite these defects, the 30% PCR MDO film demonstrated a fibrillar morphology and oriented microstructure. Such contamination and defects can impact the tear and impact properties of the MDO films. Therefore, the quality of PCR material is crucial when designing MDO films with PCR to achieve the desired final properties.

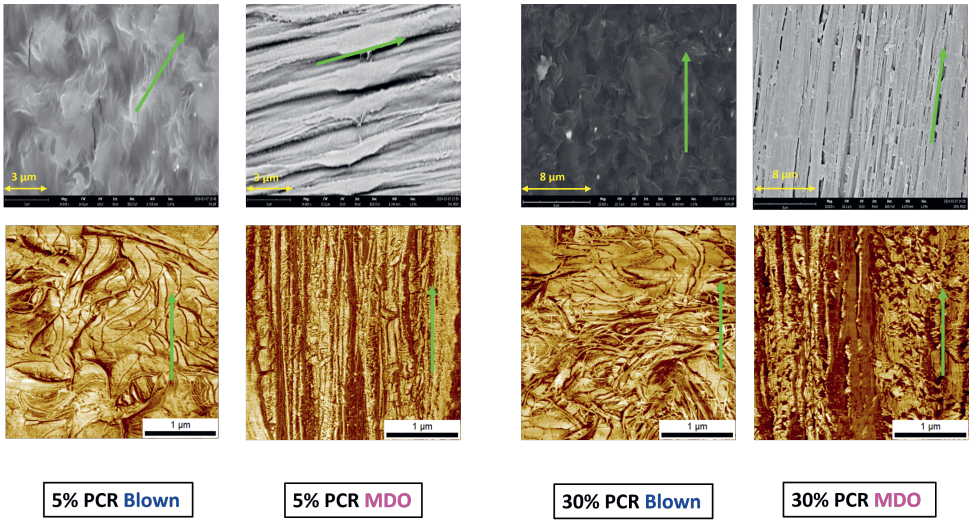

Figure 4.13 SEM (top) and AFM (bottom) images of the blown films and its subsequent MDO with integrated PCR. (Note: Green arrow in the images represents machine direction.)

4.3.3.1 Haze analysis

Optical properties such as haze and clarity in blown films are primarily influenced by three factors: surface irregularities induced by melt flow phenomena, crystallization behaviour, and melt and solid inhomogeneities. These irregularities become fixed in the film as it solidifies in the freeze line or frost line region. High-density polyethylene (HDPE) films tend to exhibit significant opacity due to their high degree of crystallinity [70]. Thus, haze was quantified to gain insights on optical properties of blown and MDO films (Figure 4.14).

The study by Zeng et al.[62] demonstrates that recycled HDPE (rHDPE) pellets display rough and uneven surface defects, and rHDPE bottles with higher recycled content exhibit rougher surface morphologies and thinner, more porous cross-sections compared to virgin HDPE (vHDPE) bottles. These characteristics result from alterations in the polymer molecular chain and cross-linking of polymer chains following repeated exposure to high temperatures, which lead to increased surface irregularity and roughness. Similar observations were made in the 1st set of experiments. As shown in Figure 4.14a, the V blown film exhibited the lowest haze percentage at 59.3%. With an increase in extrusion cycles, the haze rose to 80.1% for R1 and 84.1% for R2 blown films. This increase in haze is attributed to changes in bulk microstructural crystal sizes after re-extrusion alongside rise in surface irregularities and roughness, as quantified by AFM. Notably, all MDO films exhibited higher haze levels compared to their blown films. This was observed primarily due to the disintegration and

fibrillation of the bulk microstructure at the fixed specific draw ratio employed during the MDO process, which significantly contributed to increased surface roughness (as confirmed by AFM analysis) alongside increase in overall crystallinity.

In the second set of experiments (Figure 4.14b), haze increased with the amount of PCR material for two primary reasons. Firstly, the dark grey colour of the PCR blocked light transmission, reducing overall light transmission. Secondly, the presence of inorganic contaminants and point gel defects in the PCR, which did not melt during film blowing, further scattered light transmission by more than 2.5 degrees, thereby increasing haze in both blown and MDO films.

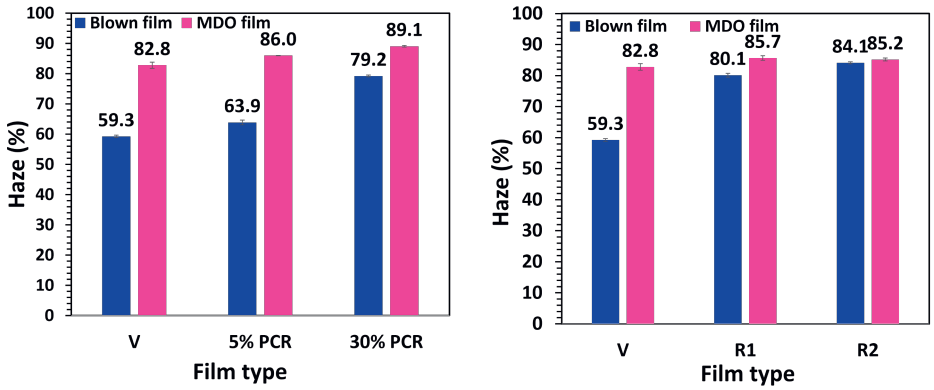

Figure 4.14 Percent haze data (n=3) for the blown films used in **a)** 1st set of experiments: simulated recycling with virgin resin, and **b)** 2nd set of experiments, using real recycled content.

4.4 Concluding remarks

In this Chapter, mechanical recyclability of virgin PE blown films and the integration of PCR for sequential machine direction orientation (MDO) PE film applications aimed at high tensile modulus in the outer layer for mono-material PE-based flexible packaging designs were examined.

Two distinct studies were conducted: the 1st aimed to validate the mechanical recyclability of virgin PE blown films through two cycles of mechanical reprocessing for the MDO-PE film application. Results indicated that reprocessing created onset of slight degradation in the molecular structure of reprocessed blown films, which impacted the tensile modulus of both blown and MDO films in the machine direction. Differential scanning calorimetry (DSC) results demonstrated that multiple extrusion cycles reduced the molecular ability to pack and form crystals, thereby decreasing the overall crystallinity of reprocessed blown and MDO films. SEM and AFM analyses revealed rougher surface morphologies in the reprocessed films compared to virgin films. MDO films exhibited a fibrillated morphology with well-oriented structures in the machine direction. Haze increased with additional

extrusion cycles, attributed to the changes in microstructural crystal sizes alongside rise in surface irregularities. Despite slight degradation, the R2 blown film achieved approximately 77% of the MD modulus of the virgin MDO film. This finding is significant for designing MDO films that incorporate reprocessed film resins with similar compositions, supporting the creation of new MDO films from recycled materials.

In the 2nd study, mixed polyolefin PCR (LDPE, LLDPE and PP) resin was incorporated into virgin blown film blend at 5% and 30% by weight for the MDO film application. The density of the blend decreased with increasing PCR content, attributed to the presence of relatively lower-density polymers PP and LDPE in the PCR composition. PCR resin presented high comonomer concentration in its molecular architecture, as quantified by 3D-GPC. Additionally, both melting enthalpy and crystallinity decreased with increasing PCR content, impacting the tensile modulus of both blown and MDO films. AFM and SEM images of PCR blown and MDO films showed point gels and fibre defects, likely due to contamination with inorganic and organic foreign materials during PCR production. Notably, at the 5% PCR level, the MDO film achieved a tensile modulus nearly equivalent to that of the virgin MDO film. This demonstrates that it is feasible to integrate PCR material in low concentrations for high-end applications such as MDO operations, where a high tensile modulus is desired in the outer layer of PE-based mono-material flexible packaging. It is important to acknowledge that the composition of PCR materials can vary due to factors such as origin, manufacturer, collection methods, and contamination. Therefore, the findings of this Chapter are not intended to establish specific limits for incorporating PCR with virgin materials. Instead, they aim to underscore the broader potential for generic PCR integration in MDO films with desired final application. This Chapter focused on mono-layer films; however, in industrial applications multilayer films are typically oriented together. It remains to be seen whether similar outcomes can be achieved following the orientation of a multilayer structure. This presents an opportunity for further investigation in future research.

4.5 Bibliography

[1] "Recycling and the future of the plastics industry | McKinsey." Accessed: Sep. 23, 2024. [Online]. Available: https://www.mckinsey.com/industries/chemicals/our-insights/how-plastics-waste-recycling-could-transform-the-chemical-industry

[2] "Plastics - the Facts 2022 • Plastics Europe." Accessed: Sep. 23, 2024. [Online]. Available: https://plasticseurope.org/knowledge-hub/plastics-the-facts-2022/

[3] R. Meys, F. Frick, S. Westhues, A. Sternberg, J. Klankermayer, and A. Bardow, "Towards a circular economy for plastic packaging wastes – the environmental potential of chemical recycling," *Resour Conserv Recycl*, vol. 162, Nov. 2020, doi: 10.1016/j.resconrec.2020.105010.

[4] R. Geyer, J. R. Jambeck, and K. L. Law, "Production, use, and fate of all plastics ever made," *Sci Adv*, vol. 3, no. 7, p. e1700782, Sep. 2024, doi: 10.1126/sciadv.1700782.

[5] N. T. Dintcheva, N. Jilov, and F. P. La Mantia, "Recycling of plastics from packaging," *Polym Degrad Stab*, vol. 57, no. 2, pp. 191–203, 1997, doi: https://doi.org/10.1016/S0141-3910(96)00232-7.

[6] M. Gall, P. J. Freudenthaler, J. Fischer, and R. W. Lang, "Characterization of composition and structure–property relationships of commercial post-consumer polyethylene and polypropylene recyclates," *Polymers (Basel)*, vol. 13, no. 10, May 2021, doi: 10.3390/polym13101574.

[7] E. Karaagac, M. P. Jones, T. Koch, and V. M. Archodoulaki, "Polypropylene contamination in post-consumer polyolefin waste: Characterisation, consequences and compatibilisation," *Polymers (Basel)*, vol. 13, no. 16, Aug. 2021, doi: 10.3390/polym13162618.

[8] B. Hu, S. Serranti, N. Fraunholcz, F. Di Maio, and G. Bonifazi, "Recycling-oriented characterization of polyolefin packaging waste," *Waste Management*, vol. 33, no. 3, pp. 574–584, 2013, doi: https://doi.org/10.1016/j.wasman.2012.11.018.

[9] D. Jubinville, E. Esmizadeh, S. Saikrishnan, C. Tzoganakis, and T. H. Mekonnen, "A comprehensive review of global production and recycling methods of polyolefin (PO) based products and their post-recycling applications," *Sustainable Materials and Technologies*, vol. 25, 2020, [Online]. Available: https://api.semanticscholar.org/CorpusID:225221815

[10] S. M. Al-Salem, P. Lettieri, and J. Baeyens, "Recycling and recovery routes of plastic solid waste (PSW): A review," *Waste Management*, vol. 29, no. 10, pp. 2625–2643, 2009, doi: https://doi.org/10.1016/j.wasman.2009.06.004.

[11] K. Ragaert, L. Delva, and K. Van Geem, "Mechanical and chemical recycling of solid plastic waste," *Waste Management*, vol. 69, pp. 24–58, 2017, doi: https://doi.org/10.1016/j.wasman.2017.07.044.

[12] D. V. A. Ceretti, M. Edeleva, L. Cardon, and D. R. D'hooge, "Molecular Pathways for Polymer Degradation during Conventional Processing, Additive Manufacturing, and Mechanical Recycling," *Molecules*, vol. 28, no. 5, 2023, doi: 10.3390/molecules28052344.

[13] A. Ahamed, A. Veksha, A. Giannis, and G. Lisak, "Flexible packaging plastic waste – environmental implications, management solutions, and the way forward," *Curr Opin Chem Eng*, vol. 32, p. 100684, 2021, doi: https://doi.org/10.1016/j.coche.2021.100684.

[14] T. I. Butler and B. A. Morris, "PE-Based Multilayer Film Structures," in *Multilayer Flexible Packaging: Second Edition*, Elsevier Inc., 2016, pp. 281–310. doi: 10.1016/B978-0-323-37100-1.00017-X.

[15] D. Carullo *et al.*, "Testing a coated PE-based mono-material for food packaging applications: an in-depth performance comparison with conventional multi-layer configurations," *Food Packag Shelf Life*, vol. 39, Nov. 2023, doi: 10.1016/j.fpsl.2023.101143.

[16] Y. Ma, "Changing Tetra Pak: From Waste to Resource," *Sci Prog*, vol. 101, no. 2, pp. 161–170, Jun. 2018, doi: 10.3184/003685018X15215434299329.

[17] C. Y. Barlow and D. C. Morgan, "Polymer film packaging for food: An environmental assessment," *Resour Conserv Recycl*, vol. 78, pp. 74–80, 2013, doi: https://doi.org/10.1016/j.resconrec.2013.07.003.

[18] C. T. de M. Soares, M. Ek, E. Östmark, M. Gällstedt, and S. Karlsson, "Recycling of multi-material multilayer plastic packaging: Current trends and future scenarios," *Resour Conserv Recycl*, vol. 176, Jan. 2022, doi: 10.1016/j.resconrec.2021.105905.

[19] L. S. Dilkes-Hoffman, J. L. Lane, T. Grant, S. Pratt, P. A. Lant, and B. Laycock, "Environmental impact of biodegradable food packaging when considering food waste," *J Clean Prod*, vol. 180, pp. 325–334, Apr. 2018, doi: 10.1016/j.jclepro.2018.01.169.

[20] G. Faraca and T. Astrup, "Plastic waste from recycling centres: Characterisation and evaluation of plastic recyclability," *Waste Management*, vol. 95, pp. 388–398, Jul. 2019, doi: 10.1016/j.wasman.2019.06.038.

[21] T. W. Walker *et al.*, "Recycling of multilayer plastic packaging materials by solvent-targeted recovery and precipitation," *Sci Adv*, vol. 6, no. 47, p. eaba7599, Sep. 2024, doi: 10.1126/sciadv.aba7599.

[22] K. Kaiser, M. Schmid, and M. Schlummer, "Recycling of Polymer-Based Multilayer Packaging: A Review," *Recycling*, vol. 3, no. 1, 2018, doi: 10.3390/recycling3010001.

[23] T. Anukiruthika, P. Sethupathy, A. Wilson, K. Kashampur, J. A. Moses, and C. Anandharamakrishnan, "Multilayer packaging: Advances in preparation techniques

and emerging food applications," *Compr Rev Food Sci Food Saf*, vol. 19, no. 3, pp. 1156–1186, May 2020, doi: 10.1111/1541-4337.12556.

[24] M. Avella, R. Avolio, I. Bonadies, C. Carfagna, M. E. Errico, and G. Gentile, "Recycled multilayer cartons as cellulose source in HDPE-based composites: Compatibilization and structure-properties relationships," *J Appl Polym Sci*, vol. 114, no. 5, pp. 2978–2985, Dec. 2009, doi: 10.1002/app.30913.

[25] S. Yang, S. Bai, W. Duan, and Q. Wang, "Production of Value-Added Composites from Aluminum-Plastic Package Waste via Solid-State Shear Milling Process," *ACS Sustain Chem Eng*, vol. 6, no. 3, pp. 4282–4293, Mar. 2018, doi: 10.1021/acssuschemeng.7b04733.

[26] A. L. Mourad, E. E. C. Garcia, G. B. Vilela, and F. Von Zuben, "Influence of recycling rate increase of aseptic carton for long-life milk on GWP reduction," *Resour Conserv Recycl*, vol. 52, no. 4, pp. 678–689, Feb. 2008, doi: 10.1016/j.resconrec.2007.09.001.

[27] M. Guerritore *et al.*, "Recyclable-by-design mono-material flexible packaging with high barrier properties realized through graphene hybrid coatings," *Resour Conserv Recycl*, vol. 179, Apr. 2022, doi: 10.1016/j.resconrec.2021.106126.

[28] O. Horodytska, F. J. Valdés, and A. Fullana, "Plastic flexible films waste management – A state of art review," *Waste Management*, vol. 77, pp. 413–425, 2018, doi: https://doi.org/10.1016/j.wasman.2018.04.023.

[29] J. Maris, S. Bourdon, J.-M. Brossard, L. Cauret, L. Fontaine, and V. Montembault, "Mechanical recycling: Compatibilization of mixed thermoplastic wastes," *Polym Degrad Stab*, vol. 147, pp. 245–266, 2018, doi: https://doi.org/10.1016/j.polymdegradstab.2017.11.001.

[30] M. K. Pettersen, M. S. Grøvlen, N. Evje, and T. Radusin, "Recyclable mono materials for packaging of fresh chicken fillets: New design for recycling in circular economy," *Packaging Technology and Science*, vol. 33, no. 11, pp. 485–498, Nov. 2020, doi: 10.1002/pts.2527.

[31] R. Grace, "New Mono-Material Flexible Pouch Follows Cradle to Cradle Principles: Werner & Mertz partners with Mondi, three others to close the loop on package design," *Plastics Engineering*, vol. 75, no. 1, pp. 14–19, Jan. 2019, doi: 10.1002/peng.20053.

[32] "DESIGNING FOR A CIRCULAR ECONOMY An introduction," 2020. Accessed: Sep. 02, 2024. [Online]. Available: https://guidelines.ceflex.eu/assets/public_docs/D4ACE_guidelines_An_Introduction.pdf

[33] M. K. Eriksen, J. D. Christiansen, A. E. Daugaard, and T. F. Astrup, "Closing the loop for PET, PE and PP waste from households: Influence of material properties and

product design for plastic recycling," *Waste Management*, vol. 96, pp. 75–85, Aug. 2019, doi: 10.1016/j.wasman.2019.07.005.

[34] K. Ragaert *et al.*, "Design from recycling: A complex mixed plastic waste case study," *Resour Conserv Recycl*, vol. 155, Apr. 2020, doi: 10.1016/j.resconrec.2019.104646.

[35] V. Srebrenkoska, G. B. Gaceva, M. Avella, M. E. Ericco, and G. Gentile, "Utilization of recycled polypropylene for production of Eco-composites," *Polymer - Plastics Technology and Engineering*, vol. 48, no. 11, pp. 1113–1120, 2009, doi: 10.1080/03602550903147247.

[36] M. Paul, B. Morris, J. Weinhold, and K. Hausmann, "The effect of stretching and tie layer composition on adhesion strength of multi-layered films," *Journal of Plastic Film and Sheeting*, vol. 38, no. 3, pp. 351–368, Jul. 2022, doi: 10.1177/87560879211063475.

[37] T. Chatterjee *et al.*, "Machine direction orientation of high density polyethylene (HDPE): Barrier and optical properties," *Polymer (Guildf)*, vol. 55, no. 16, pp. 4102–4115, Aug. 2014, doi: 10.1016/j.polymer.2014.06.029.

[38] E. Hatfield, R. Tate, K. Williams, and W. Todd, "New MDO Medium Molecular Weight High Density Polyethylene Films," *Journal of Plastic Film & Sheeting*, vol. 18, no. 2, pp. 117–127, Apr. 2002, doi: 10.1177/8756087902018002006.

[39] K. Cantor, "Blown Film Extrusion," in *Blown Film Extrusion 3e (Third Edition)*, K. Cantor, Ed., Hanser, 2019, pp. I–XIV. doi: https://doi.org/10.3139/9781569906972.fm.

[40] L. Pietrelli, G. Poeta, C. Battisti, and M. Sighicelli, "Characterization of plastic beach debris finalized to its removal: a proposal for a recycling scheme," *Environmental Science and Pollution Research*, vol. 24, no. 19, pp. 16536–16542, Jul. 2017, doi: 10.1007/s11356-017-9440-4.

[41] C. Picuno, A. Alassali, Z. K. Chong, and K. Kuchta, "Flows of post-consumer plastic packaging in Germany: An MFA-aided case study," *Resour Conserv Recycl*, vol. 169, Jun. 2021, doi: 10.1016/j.resconrec.2021.105515.

[42] T. Radusin *et al.*, "Use of recycled materials as mid layer in three layered structures-new possibility in design for recycling," *J Clean Prod*, vol. 259, Jun. 2020, doi: 10.1016/j.jclepro.2020.120876.

[43] R. Esmaeilzade, S. Hosseini, R. Rashedi, S. Houshmandmoayed, K. Afzali, and A. Sepahi, "Study on the Rheological, Thermal, Mechanical, and Optical Properties of LDPE/LLDPE Blown Films Containing Recycled LDPE/LLDPE Pellets For Circular Economy," 2022, doi: 10.21203/rs.3.rs-2185814/v1.

[44] T. Andersson, B. Stålbom, and B. Wesslén, "Degradation of polyethylene during extrusion. II. Degradation of low-density polyethylene, linear low-density

polyethylene, and high-density polyethylene in film extrusion," *J Appl Polym Sci*, vol. 91, no. 3, pp. 1525–1537, Feb. 2004, doi: 10.1002/APP.13024.

[45] M. K. Loultcheva, M. Proietto, N. Jilov, and F. P. L. Mantia, "Recycling of high density polyethylene containers," *Polym Degrad Stab*, vol. 57, no. 1, pp. 77–81, Jul. 1997, doi: 10.1016/S0141-3910(96)00230-3.

[46] C. Sadrmohaghegh and G. Scott, "The effects of reprocessing on polymers—I: Low density polyethylene," *Eur Polym J*, vol. 16, no. 11, pp. 1037–1042, Jan. 1980, doi: 10.1016/0014-3057(80)90220-7.

[47] V. S. Cecon, P. F. Da Silva, K. L. Vorst, and G. W. Curtzwiler, "The effect of post-consumer recycled polyethylene (PCRPE) on the properties of polyethylene blends of different densities," *Polym Degrad Stab*, vol. 190, Aug. 2021, doi: 10.1016/j.polymdegradstab.2021.109627.

[48] H. Jin, J. Gonzalez-Gutierrez, P. Oblak, B. Zupančič, and I. Emri, "The effect of extensive mechanical recycling on the properties of low density polyethylene," *Polym Degrad Stab*, vol. 97, no. 11, pp. 2262–2272, 2012, doi: https://doi.org/10.1016/j.polymdegradstab.2012.07.039.

[49] A. Choudhury, M. Mukherjee, and B. Adhikari, "Mixtures of Recycled Milk Pouches with a Virgin LDPE-LLDPE Blend," *Progress in Rubber, Plastics and Recycling Technology*, vol. 21, no. 3, pp. 219–230, Aug. 2005, doi: 10.1177/147776060502100304.

[50] P. Miller, I. Sbarski, E. Kosior, S. Masood, and P. Iovenitti, "Correlation of rheological and mechanical properties for blends of recycled HDPE and virgin polyolefins," *J Appl Polym Sci*, vol. 82, no. 14, pp. 3505–3512, Dec. 2001, doi: 10.1002/APP.2212.

[51] M. Nofar, B. S. Yenigul, B. Ozdemir, C. Y. Kovanci, A. Ghanbari, and A. Jalali, "Mechanical and viscoelastic properties of polyethylene-based microfibrillated composites from 100% recycled resources," *J Appl Polym Sci*, vol. 138, no. 32, p. 50793, Aug. 2021, doi: 10.1002/APP.50793.

[52] D. Czarnecka-Komorowska, K. Wiszumirska, and T. Garbacz, "FILMS LDPE/LLDPE MADE FROM POST - CONSUMER PLASTICS: PROCESSING, STRUCTURE, MECHANICAL PROPERTIES," *Advances in Science and Technology. Research Journal*, vol. 12, no. 3, pp. 134–142, Sep. 2018, doi: 10.12913/22998624/92205.

[53] Z. O. G. Schyns and M. P. Shaver, "Mechanical Recycling of Packaging Plastics: A Review," *Macromol Rapid Commun*, vol. 42, no. 3, p. 2000415, Feb. 2021, doi: https://doi.org/10.1002/marc.202000415.

[54] S. J. Hebert, C. Tzoganakis, and J. Perdikoulias, "Blown Film Extrusion of Post-Consumer Recycled Lldpe Film," *Journal of Plastic Film & Sheeting*, vol. 9, no. 4, pp. 282–292, Oct. 1993, doi: 10.1177/875608799300900402.

[55] W. Yau *et al.*, "A 'systematic approach' to TD-GPC data processing with band broadening correction," *Macromol Symp*, vol. 330, no. 1, pp. 53–62, Aug. 2013, doi: 10.1002/masy.201300029.

[56] T. Pathaweeisariyakul, K. Narkchamnan, B. Thitisuk, and W. Yau, "Methods of long chain branching detection in PE by triple-detector gel permeation chromatography," *J Appl Polym Sci*, vol. 132, no. 28, Jul. 2015, doi: 10.1002/app.42222.

[57] R. L. Blaine, "Determination of Polymer Crystallinity by DSC. Therm. Anal. TA Instruments, 109 Lukens Drive, New Castle DE 19720, USA, 1-3." Accessed: Apr. 09, 2024. [Online]. Available: https://www.scirp.org/reference/referencespapers?referenceid=1920439

[58] K. De Smit, M. Edeleva, A. D. Trigilio, Y. W. Marien, P. H. M. Van Steenberge, and D. R. D'hooge, "Kinetic Monte Carlo residence time distributions and kinetics in view of extrusion-based polymer modification and recycling," *React Chem Eng*, vol. 8, no. 3, pp. 563–576, Nov. 2022, doi: 10.1039/d2re00387b.

[59] T. Andersson, B. Stålbom, and B. Wesslén, "Degradation of polyethylene during extrusion. II. Degradation of low-density polyethylene, linear low-density polyethylene, and high-density polyethylene in film extrusion," *J Appl Polym Sci*, vol. 91, no. 3, pp. 1525–1537, Feb. 2004, doi: 10.1002/app.13024.

[60] A. A. Mendes, A. M. Cunha, and C. A. Bernardo, "Study of the degradation mechanisms of polyethylene during reprocessing," *Polym Degrad Stab*, vol. 96, no. 6, pp. 1125–1133, Jun. 2011, doi: 10.1016/j.polymdegradstab.2011.02.015.

[61] P. Oblak, J. Gonzalez-Gutierrez, B. Zupančič, A. Aulova, and I. Emri, "Processability and mechanical properties of extensively recycled high density polyethylene," *Polym Degrad Stab*, vol. 114, pp. 133–145, 2015, doi: 10.1016/j.polymdegradstab.2015.01.012.

[62] S. F. Zeng, H. R. Zhang, Z. K. Li, C. Y. Hu, and Z. W. Wang, "Effect of mechanical recycling on crystallization, mechanical, and rheological properties of recycled high-density polyethylene and reinforcement based on virgin high-density polyethylene," *J Appl Polym Sci*, vol. 141, no. 11, Mar. 2024, doi: 10.1002/app.55097.

[63] T. Kealy, "Rheological analysis of the degradation of HDPE during consecutive processing steps and for different processing conditions," *J Appl Polym Sci*, vol. 112, no. 2, pp. 639–648, Apr. 2009, doi: 10.1002/app.29418.

[64] "Ecoo Regranulate - Sustainable Raw Materials." Accessed: Sep. 18, 2024. [Online]. Available: https://www.ecoo.eu/nl/grondstoffen/ecoo-regranulaat

[65] B. A. Morris, "Chapter 9 - Strength, Stiffness, and Abuse Resistance," in *The Science and Technology of Flexible Packaging*, Elsevier, 2017, pp. 309–350. doi: 10.1016/b978-0-323-24273-8.00009-5.

[66] X. M. Zhang, S. Elkoun, A. Ajji, and M. A. Huneault, “Oriented structure and anisotropy properties of polymer blown films: HDPE, LLDPE and LDPE,” *Polymer (Guildf)*, vol. 45, no. 1, pp. 217–229, Jan. 2004, doi: 10.1016/j.polymer.2003.10.057.

[67] E. Andreasson, N. Mehmood, and S. Kao-Walter, “Trouser tear tests of two thin polymer films,” in *13th International Conference on Fracture, June 16–21, Beijing, China*, 2013. Accessed: Sep. 24, 2024. [Online]. Available: https://www.academia.edu/103015420/Trouser_tear_tests_of_two_thin_polymer_films

[68] D. Guleria, S. Ge, L. Cardon, S. Vervoort, and J. den Doelder, “Impact of resin density and short-chain branching distribution on structural evolution and enhancement of tensile modulus of MDO-PE films,” *Polym Test*, p. 108560, 2024, doi: https://doi.org/10.1016/j.polymertesting.2024.108560.

[69] S. F. Zeng, P. Guo, C. Y. Hu, and Z. W. Wang, “Effects of mechanical recycling on optical properties and microstructure of recycled high-density polyethylene pellets and bottles,” *J Appl Polym Sci*, vol. 140, no. 6, Feb. 2023, doi: 10.1002/app.53446.

[70] S. Mirams, “THE EFFECTS OF PROCESSING CONDITIONS ON THE OPTICAL PROPERTIES OF POLYETHYLENE FILMS,” 2018. Accessed: Jun. 27, 2024. [Online]. Available: https://www.qenos.com/internet/home.nsf/web/technicalwhitepapers

4.6 Appendix 4

EDX elemental analysis of PCR resin

A4.1

1st analysis

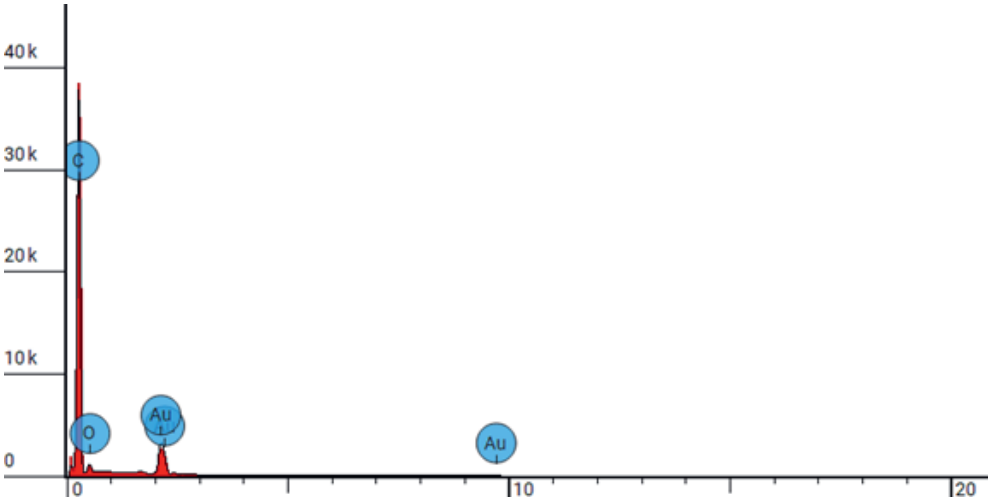

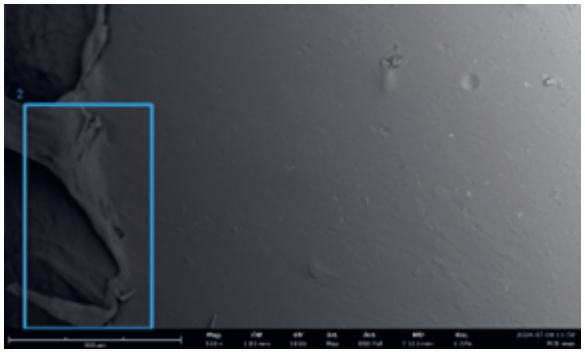

	Element Number	Element Symbol	Element Name	Atomic Conc.	Weight Conc.
	6	C	Carbon	94.432	70.971
	8	O	Oxygen	3.499	3.504
	79	Au	Gold	2.068	25.526

A4.2

2nd analysis

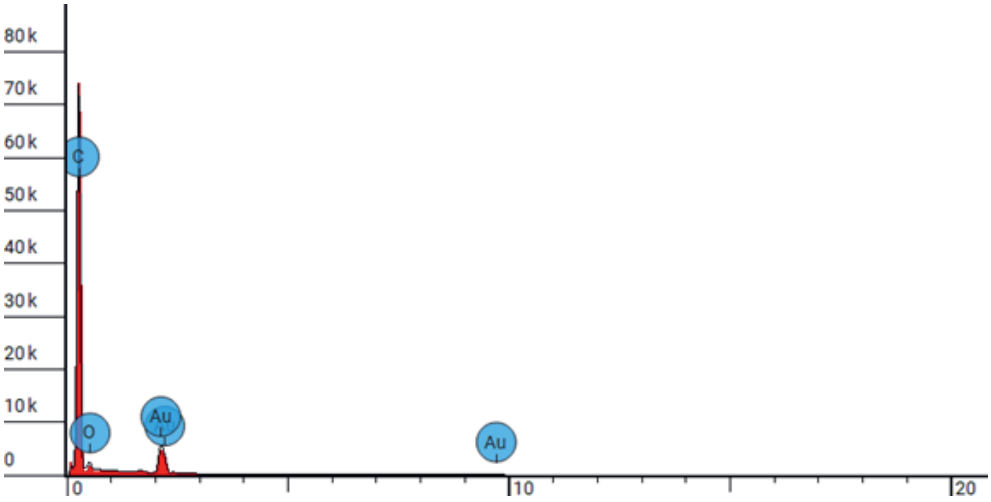

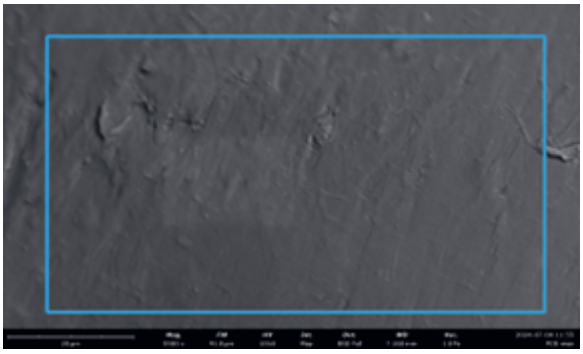

	Element Number	Element Symbol	Element Name	Atomic Conc.	Weight Conc.
	6	C	Carbon	95.111	72.673
	8	O	Oxygen	2.950	3.003
	79	Au	Gold	1.939	24.324

Chapter – 5

Influence of uniaxial orientation on gas barrier, functional barrier, and optical properties of polyethylene films

Abstract

The transition from traditional materials like glass and metal to plastic films in food packaging has been driven by the latter's flexibility, versatility, and lightweight nature. However, challenges related to the recycling of multi-layered, multi-material flexible packaging have emerged, prompting interest in mono-material solutions for improved recycling and sustainability. Polyethylene (PE), a widely used polymer in flexible packaging, offers various structural and functional properties but faces issues with high oxygen permeability. This Chapter investigates the potential of uniaxial orientation or machine direction orientation (MDO) to enhance the oxygen barrier, functional barrier, and optical properties of PE films. In the first set of experiments, oxygen barrier properties was evaluated for MDO films of varying resin densities, with the results correlating structural changes during stretching with improved barrier performance. The second set of experiments assessed the functional barrier of oriented PE films against harmful substances from recycled paperboard, including mineral oil saturated hydrocarbons (MOSH) and mineral oil aromatic hydrocarbons (MOAH). In the third set, the impact of MDO on optical properties such as gloss and haze were examined to assess the films suitability for flexible packaging applications requiring both high barrier and visual appeal. The findings demonstrated that uniaxial orientation improved the oxygen and functional barriers of PE films, depending on resin type and processing conditions, primarily through enhanced crystallinity and microstructural orientation. Additionally, uniaxial orientation impacted the optical properties of the films, increasing optical haze after MDO operation due to changes in crystalline and surface morphology, while instrumental gloss first increased and then gradually decreased at higher draw ratios.

5.1 Introduction

Historically, the predominant materials utilized for food packaging have included glass, metals (such as aluminium foil, tin-free steel), and various types of chemically composed paper [1], [2]. Metal packaging ensures a long shelf life by blocking microbes, light, and oxygen, while glass offers inert, nontoxic protection with excellent barrier properties; however, both are increasingly being replaced by plastics due to their flexibility, versatility, thermal stability, and lightweight nature [3].

Polymers are extensively utilized in contemporary food and beverage packaging industries [4]. Plastic packaging materials play a crucial role in the economy by preserving food, pharmaceuticals, and biomedical products [5], [6], [7].

The primary purpose of food packaging is to preserve food quality from production to consumer use [8]. Effective barrier properties are essential for plastic films in food packaging to preserve nutritional and organoleptic qualities as well as safety of the product [9]. Multi-layer configurations are widely used in food packaging for their superior performance, combining up to 11 layers to offer excellent mechanical resistance, thermal properties, sealing, and barriers against vapours, gases, and light [10]. However, multi-layer configurations pose significant recycling challenges due to difficulties in separating different plastic polymer types and the inability to recycle mixed polymers with diverse properties [10], [11], [12].

A significant challenge in the mechanical recycling of flexible packaging plastic waste stems from its multi-layered structure, which often consists of diverse thin plastic film layers, such as polyethylene (PE), polypropylene (PP), polyamide (PA), polyethylene terephthalate (PET), and polyvinyl chloride (PVC), along with non-ferrous metals like aluminium and tin. Conventional plastic reprocessing techniques like mechanical recycling are ineffective for such multi-material, multi-layered configurations due to inherent chemical incompatibilities between the constituent layers [13], [14]. Thus, embedded heterogeneity of these flexible packaging systems poses significant challenges to current recycling systems, as conventional waste management infrastructure lacks the capability to effectively identify, sort, and recycle these complex materials, thereby undermining the principles of a circular economy [15], [16], [17], [18], [19].

To improve recycling rates, mono-material multi-layered flexible packaging systems are emerging as a new alternative. Still multiple variations are typically needed to achieve initial use-phase functionality, but as these materials are from one chemical composition, when mixed during recycling process steps, the resulting recycled product has good potential to perform well. Polyolefin-based mono-material flexible films have emerged as promising candidates for fulfilling the demands of a circular economy, owing to their ease of mechanical recyclability, as evidenced by numerous studies [14], [20], [21]. Polyethylene (PE) is one of the most used polymers in flexible packaging applications as it can provide various useful structural and functional properties because of its distinct available grades and types like low-density polyethylene (LDPE), linear low-density polyethylene (LLDPE), and high-density polyethylene (HDPE). There is promise in achieving both package functionality and recyclability when combining different grades of PE into a single package.

A major issue with polyethylene is its high oxygen permeability [9]. The permeability of gases or moisture in polymers is influenced by the solubility and diffusion of the permeants, which is governed by factors such as crystallinity, polarity, and molecular weight [7]. Oxygen being apolar dissolve more into apolar polymers such as PE, PP and most polyolefins as compared to polar polymers such as PET and Nylon [22]. The molecular structure of PET is composed of rigid aromatic benzene rings and polar ester group, creating polarity, which helps in tight intermolecular interactions whereas, the molecular structure of PE consists of long, apolar hydrocarbon chains with repeating (CH2) units, which are relatively more flexible and are packed relatively less tightly. Polar groups cause polymer chains to be mutually attracted, which ultimately increase glass transition temperature and reduces free volume [23]. Therefore, due to relatively lesser free volume, PET has higher barrier for the diffusion of oxygen in comparison to PE. However, it has been demonstrated in previous studies that oxygen as well as moisture barrier of PE films can be enhanced by MDO operation.

Traditionally, the outer layer of multilayer flexible packaging is composed of non-PE materials, such as PET or PA, which provide the overall package with sufficient stiffness and barrier properties. Orientation of PE film in the semi-solid state through techniques such as tenter frame, double bubble, and machine direction orientation significantly enhances its mechanical and barrier properties. This further facilitates the development of lightweight packaging structures [24],offering a viable alternative to move away from multi-material multilayer structures.

During the MDO process, the precursor polymer film made from cast or blown film process is stretched further in the machine direction to a certain extent and at a certain rate and temperature which depends on the polymer's chemical nature. Consequently, numerous enhancements are observed in the physical and barrier properties of the films for food packaging applications, including stiffness, tensile strength, gloss, oxygen resistance, and moisture barrier [4], [25], [26]. During stretching a fibrillar structure with higher crystallinity is formed [27], [28], [29], [30], [31].

Multiple factors have been suggested to account for the enhanced barrier properties observed in oriented polymers. These include reduced free volume in amorphous regions, increased diffusion path tortuosity due to crystal alignment, and higher overall crystallinity, along with denser packing and microfibrillar crystal formation [4], [32], [33], [34], [35].

Chatterjee *et al.* [4] investigated water vapor barrier of HDPE MDO films and reported that initially the oriented films demonstrated an increase in the water vapor transport rate with increasing draw ratio and beyond a critical draw ratio it gradually decreased. Breese *et al.* [35] investigated effect of MDO on the moisture and oxygen barrier properties of HMW-PE films and reported that a significant decrease in both moisture and oxygen transmission rates is observed with the machine direction orientation of homopolymer HMW-PE films. They further reported that intermediate and lower density films do not show such a significant decrease, and actually present a maximum at moderate draw ratios where the transmission rate is greater after orientation than that of the undrawn sample.

Most of the studies in literature to investigate the barrier properties are based on MDO process parameters like draw ratio but only few studies focus on the role of structural parameters of the resins like resin density and correlate it with changes in structural morphology during stretching. Therefore, in the 1st set of experiments of this Chapter, oxygen barrier of the MDO films was evaluated and further correlated with resin density and film morphology while keeping the other MDO process parameters constant like draw ratio, orientation temperature and stretch rate.

Recycling serves as a crucial end-of-life strategy for paper and board materials. However, it has been shown that recycled paper and board can contain various toxicologically relevant substances that are sufficiently volatile to migrate, predominantly through the gas phase, into packaged foods during long-term storage at room temperature [36], [37], [38], [39], [40], [41]. These substances may originate from printing inks, adhesives, manufacturing processes, or residues from previous applications [41], [42], [43]. The most extensively studied substances in this regard are mineral oils, specifically mineral oil saturated hydrocarbons (MOSH) and mineral oil aromatic hydrocarbons (MOAH), due to increased concerns regarding their potential carcinogenicity. Plastic packaging can be employed to prevent direct contact between food and recycled paper packaging, provided that it offers an adequate functional barrier against the migration of these harmful substances for packaging designs such as bag in box.

According to European Commission Regulation (EU) 10/2011, a functional barrier is considered effective when it limits migration to below a conventional detection threshold of 0.01 mg/kg of food [44], [45]. Hence in the 2nd set of experiments of this work, in addition to oxygen barrier, functional barrier of the oriented PE films against these harmful substances was evaluated. The idea was to evaluate the effect of orientation on functional barrier of the PE films for potential applications like plastic bag containing food inside a recycled paperboard box as no such studies in literature has been reported in this aspect before to the best of our knowledge.

The optical properties of polymers, including gloss, transparency, clarity, haze, color, surface appearance, and refractive index, are closely associated with the quality and visual performance of plastic products [46]. The internal and surface microstructure of the film collectively plays a crucial role in determining its overall optical properties [47]. Consumers frequently base their purchasing decisions primarily on the visual appearance of a product. Packaging with high gloss enhances the appeal of the package and increases the likelihood of consumer purchase [48]. Optical transparency enables consumers to assess food freshness and appearance through visual inspection before purchase [2], [49]. Additionally, transparency is crucial for integrating optical sensing systems into the development of intelligent food packaging materials [2], [50].

Hatfield *et al.* studied properties of medium molecular weight MDO HDPE films and reported gloss increased by over 70 percent at a draw ratio of 6:1 [26], [51]. Chatterjee *et al.* studied barrier and optical properties of MDO HDPE films and reported that MD orientation significantly reduced the total haze of the stretched films compared to blown films at similar thickness [4]. Hence in the 3rd set of experiments, impact of orientation was

evaluated on optical properties like clarity, haze and gloss to assess optical performance of MDO-PE films.

5.2 Materials and Methods

5.2.1 Materials

Five PE resins composed of ethylene copolymerized with an α-olefin, were provided by Dow for this study. Resins D1, D2, and D3 are synthesized using similar catalyst chemistry, whereas X1 and X2 are based on hybrid catalyst chemistry. The measured density and melt flow index (MFI) of all five resins are presented in Table 5.1. The MFI was measured in accordance with ASTM D1238, using a Göttfert MI-4 plastometer with an average of 19 measuring points taken in a single measurement run for improved accuracy. The measurements were conducted under standard conditions for PE, (2.16 kg at 190°C). Density measurements were conducted following the ASTM D792 protocol, using isopropyl alcohol (IPA) as the immersion liquid. The density values reported in Table 5.1 represent the average of three measurements.

Table 5.1 Characteristics of all the 5 base PE resins used in the study.

Resin	MFI (dg/min)	Density* (g/cm^3)
D1	1.020	0.9194 ± 0.0003
D2	1.472	0.9500 ± 0.0001
D3	4.102	0.9540 ± 0.0003
X1	1.872	0.9256 ± 0.0002
X2	1.126	0.9667 ± 0.0001

*Error is standard deviation in density column.

5.2.2 Base sheets and lab scale MDO stretching

Base sheets from all five base resins of approximately 550 microns thickness were prepared at 190 °C and 150 bar pressure using a Colin compression molding press, followed by quench cooling with circulating room temperature water through channels in the hot press plates. Rectangular specimens of 20 mm width and 100 mm in length were cut from the base sheet. The specimens were stretched under laboratory conditions using a Lloyd LR10K Plus tensile tester equipped with an environmental chamber to regulate the orientation temperature (Figure 5.1). The 20 mm-wide strips were stretched to a fixed length draw ratio of 7, corresponding to an extension from 25 mm to 175 mm of grip separation. Stretching was conducted at a temperature of 110°C with a constant rate of 200 mm/min. It is important to note that the optimal stretching or orientation temperature depends on the polymer's microstructural properties and may vary for different applications to achieve the desired results. Typically, orientation is performed at temperatures above the glass transition temperature and below the peak melting temperature, as higher orientation temperatures generally enable greater stretch ratios without film breakage [52]. Following the stretching process, the samples were annealed for 2 minutes at a fixed temperature of 120°C. The

annealing step freezes the orientation provided in the stretching step and stabilizes the film from further dimensional changes. After annealing, the films were cooled under ambient room temperature. In addition to five base resins, base sheets and lab-scale MDO films were produced from binary blends of low-density grade X1 and higher-density grade X2, with X1 proportions of 25%, 50%, and 75% by weight, denoted as X1/X2 (25/75), X1/X2 (50/50), and X1/X2 (75/25). The densities of the blends were theoretically estimated using an approximate inverse-additive mixing rule.

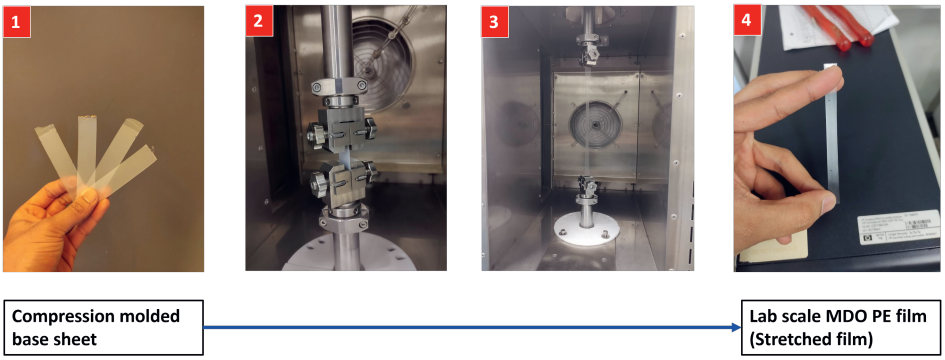

Figure 5.1 Pictorial representation of step-wise lab-scale MDO stretching process.

5.2.3 Preparation of blown and pilot-scale MDO films

Blown films were produced using a LabTech blown film line (40 mm die diameter, 0.8 mm die gap) with a thickness of approximately 110 µm and a lay-flat width of ~145 mm. The blow-up ratio (BUR) and draw-down ratio (DDR) were approximately 2.31 and 3.15, respectively, with a mass flow rate of approximately 90 g/min. The extruder temperature profile ranged from 160 °C to 190 °C, while the die outlet temperatures were 180 °C (lower) and 160 °C (upper). The nip roller speed was around 3 m/min, with slight adjustments to achieve the target BUR and DDR for each extrusion. After exiting the die, all blown films were cooled at similar rates at ambient room temperature under constant process parameters. The blown films were produced for all five base resins. The dry blending technique was employed to fabricate blown films of blends using resin X1 and X2 on the blown film production line, with X1 proportions of 25%, 50%, and 75% by weight, denoted as X1/X2 (25/75), X1/X2 (50/50), and X1/X2 (75/25). Incorporating the low-density resin X1 into the blown films was essential for facilitating stretching during the MDO process. This is because X1 reduces the overall density and crystallinity of the films, thereby promoting more uniform stretching, following the learnings from Ratta *et al.* [53]

The pilot scale-MDO films were produced after blown film extrusion (Figure 5.2). The heating chamber (oven) and rollers from a Konark extrusion line were used to provide the required stretching temperature for the pilot-scale MDO setup to process lab-scale blown films. The heating chamber was equipped with internal air circulation to maintain a uniform temperature throughout its volume during the stretching process. The orientation temperature for the MDO operation was set 15 °C below the peak melting temperature of each blown film. This orientation temperature used to produce pilot scale MDO films was

tailored to each specific blown film density and was slightly higher compared to the constant orientation temperature of 110 °C used to make lab-scale MDO films as with increasing orientation temperature, possibility of obtaining higher draw ratios in MDO film without film breakage increases [52]. The blown films and blown films were produced at specific process draw ratio (DR) depending on the material. The process draw ratio was calculated using Equation 5.1.

$$Process\ draw\ ratio\ (speed) = \frac{Speed\ of\ the\ rollers\ after\ oven\ (m/min)}{Speed\ of\ the\ rollers\ before\ oven (m/min)} \quad \textit{Equation 5.1}$$

X1/X2 (25/75), X1/X2 (50/50), and X1/X2 (75/25) pilot scale MDO films were produced using a constant process draw ratio of 6. The pilot-scale MDO films of pure material X1 were produced at the process draw ratio of 2, 6 and 13.33.

Lab scale blown film setup

Lab scale MDO setup with oven

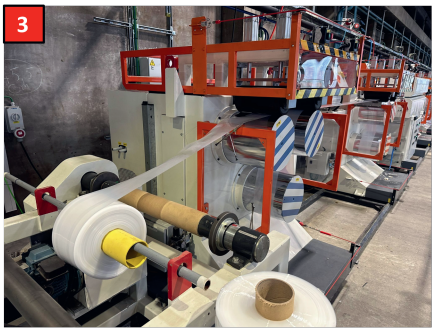

blown film mounted on the setup

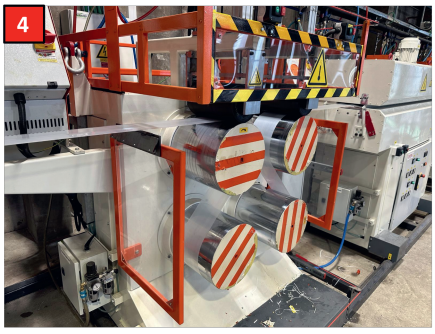

blown film through the rollers going inside the oven

MDO film coming out of the oven

MDO film passing through the rollers after the oven

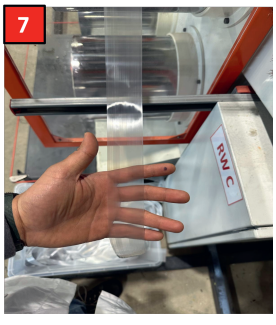

MDO film being collected

Figure 5.2 Stepwise (1-7) pictorial representation of pilot-scale MDO process.

In the subsequent sections of this study, the term "lab-scale MDO film" refers to films produced by stretching compression-molded base sheets, whereas the term "pilot-scale MDO film" refers to films produced by stretching blown films.

5.2.4 Materials and methods used for oxygen barrier analysis

In the 1st set of experiments, the objective was to quantify whether the microstructural orientation of uniaxially stretched lab-scale MDO films, prepared by stretching compression-molded base sheets, would lead to an enhancement in the oxygen barrier properties compared to randomly oriented blown PE films of same material. Multiple characterization techniques and permeability experiments were conducted to investigate the oxygen permeability behaviour of blown and lab-scale oriented PE films. The PE films utilized for the oxygen barrier analysis are further presented in Table 5.2.

Table 5.2 The PE films utilized for the oxygen barrier analysis along with their respective densities.

Material	Material type	Density (g/cm^3)
D1	Lab-scale MDO film, Blown film	0.9194
X1	lab-scale MDO film, Blown film	0.9256
D2	lab-scale MDO film, Blown film	0.9500
D3	lab-scale MDO film, Blown film	0.9540
X2	blown film	0.9667
X1/X2 (75/25)	lab-scale MDO film	0.9438
X1/X2 (50/50)	lab-scale MDO film, Blown film	0.9467
X1/X2 (25/75)	lab-scale MDO film	0.9541

For quantifying the oxygen permeability coefficient of randomly oriented or non-uniaxially oriented materials, blown films were selected instead of compression-molded base sheets (used to produce lab-scale MDO films. This choice was due to the high thickness of the compression-molded base sheets (approximately 550 microns), which made them challenging to use with the apparatus. In contrast, blown films, with a comparatively lower thickness of about 50 microns (exact value of thickness with standard deviation presented in Table A5.1 in Appendix), were more suitable for the experimental setup. Thickness data with standard deviation for lab-scale MDO films used in oxygen barrier analysis is presented in Table A5.2 in Appendix.

The various characterization techniques used for the analysis are detailed as follows:

5.2.4.1 Differential scanning calorimetry (DSC)

Thermal analysis was conducted using a DSC Q2000 instrument from TA Instruments. Samples weighing approximately 5 to 10 mg, were placed in a closed aluminium pan and subjected to a heat-cool-heat cycle from 0 to 200 ℃ at a rate of 10 ℃/min under a nitrogen atmosphere. Three measurements were taken for each sample. The degree of crystallinity X_{DSC} was calculated using Equation 5.2

$$X_{DSC} = \frac{\Delta H_m}{\Delta H^{\circ}{}_m} * 100$$ *Equation 5.2*

Where ΔH_m is the melting enthalpy, and $\Delta H^{\circ}{}_m$ is the melting enthalpy of 100% crystalline PE, i.e., 293 J/g [54].

5.2.4.2 X-Ray diffraction

Microstructural analysis of the samples was conducted using X-ray diffraction (XRD) technique: wide-angle X-ray scattering (WAXS). Data were collected at the Advanced Photon Source (APS), DND-CAT, 5-ID-D beamline at Argonne National Laboratory (Lemont, IL, USA), using the APS Undulator A as the X-ray source with an X-ray energy of 17 keV (λ = 0.7293 Å). Data analysis was performed using the Jade software. The crystallite size was calculated from the full width at half maximum (β) of the crystalline peak using Debye-Scherrer's Equation 5 (Equation 5 3).

$$L_{hkl} = \frac{K\lambda}{\beta * cos\theta}$$ *Equation 5.3*

Where L_{hkl} is crystallite dimension (in Å) along the direction perpendicular to the crystallographic plane hkl, β is the full width of the diffraction line at half maximum of peak related to the crystallographic plane hkl in radians, θ is the diffraction angle (Bragg's angle) of the hkl reflection, λ is the wavelength of X-ray, and K is the Scherrer constant with value of 0.89.

In uniaxial orientation, the distribution functions of the chain segment orientations are defined using a series of orthogonal spherical harmonic functions. Crystalline orientation is characterized by calculating the average squared cosine values, which represent the average orientation of the normal to the crystalline plane relative to each reference axis. Herman's orientation function, the second harmonic orientation function, is expressed using Equation 5.4 [55].

$$f = \frac{3\langle \cos^2 \varphi_{hkl,z} \rangle - 1}{2}$$ *Equation 5.4*

Where $\varphi_{hkl,z}$ is the angle between the chain axis and a reference axis z, which is the draw direction (DD). $\langle \cos^2 \varphi_{hkl,z} \rangle$ is calculated from the scattering intensity $I(\varphi)$ by integrating over the azimuthal angle ϕ as given in Equation 5.5.

$$\langle \cos^2 \varphi_{hkl,z} \rangle = \frac{\int_0^{\pi/2} I(\varphi) sin\varphi cos^2 \varphi d\varphi}{\int_0^{\pi/2} I(\varphi) sin\varphi d\varphi} \qquad \textit{Equation 5.5}$$

The value of f is 1 (φ =0̊ for the perfect draw direction orientation, -1/2 (φ =90̊ for chains aligned normally to the draw direction, and 0 for a perfect random orientation. Five measurements were taken for each sample for the calculation of crystallite dimension and apparent crystallinity.

5.2.4.3 Permeability

Oxygen permeability of the films was measured by an Mocon Ox-tran 702 instrument using the equal pressure method at 23°C, 1 atm pressure and 0% relative humidity (RH) on both sides of the material (Figure 5.3). Samples were masked with aluminium covers exposing only about 3 cm^2 area for blown films and about 1 cm^2 area for lab scale MDO-PE films for the passage for permeant. Air containing approximately 20.9% of oxygen was passed on one side of the film inside the unit cell as test gas and the formier gas (95% nitrogen + 5% hydrogen) as a carrier gas on the other side of the film inside the unit cell. All test measurements were recalculated to 100% oxygen as test gas. Measurement was taken at a duration of about 30 hours with each measurement being repeated and measured again after about 30 hours for accuracy. The uniaxially lab stretched MDO films had average thickness ranging from about 75 to 200 microns. The blown films had mean thickness of 48±4.5 microns, where error is standard deviation.

The Permeability coefficient (P) is normalised to a constant thickness at given temperature and pressure [56]. Hence P was quantified to negate the effect of thickness on transmission of oxygen. The permeability coefficient is given by the following Equation 5.6.

$$P = \frac{(quantity\ of\ permeant)(film\ thickness)}{(area)(time)(pressure\ drop\ across\ film)} \qquad \textit{Equation 5.6}$$

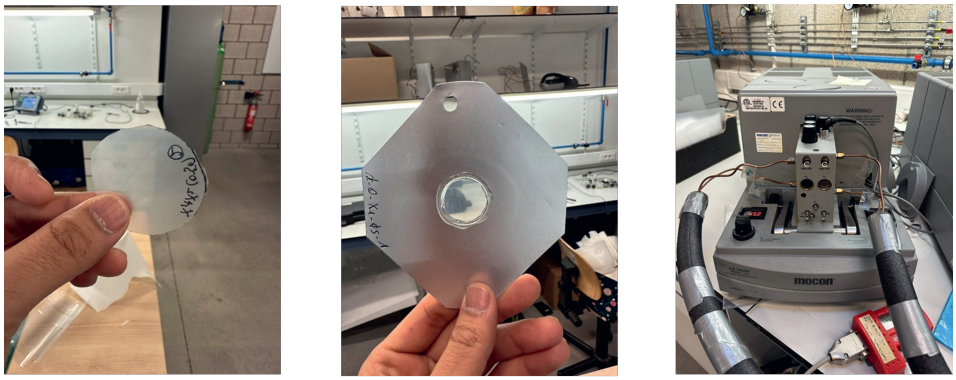

a) b) c)

Figure 5.3 Pictorial demonstration of **a)** cutting the sample **b)** sample preparation with masking area not to be utilized in the analysis **c)** the unit cell.

5.2.5 Materials and methods used for functional barrier analysis

The method proposed by Biedermann-Brem and Grob [57], and subsequently utilized in the study by Baele *et al.* [58], was employed to evaluate the functional barrier properties of the polymer films. The PE films utilized for the functional barrier analysis are presented in Table 5.3. For the analysis of functional barrier properties, the study was limited to two distinct pilot-scale MDO films, as other films did not meet the minimum surface area requirements for testing. Nonetheless, these two materials allowed for an initial assessment of the influence of orientation on functional barrier properties. It is recognized that a more comprehensive understanding of orientation on functional barriers would benefit from future research involving a broader range of oriented materials.

Table 5.3 The PE films utilized for the functional barrier analysis with their respective densities.

Material	Material type	Density (g/cm^3)
X1	Blown film, Pilot-scale MDO film (DR-6)	0.9256
X1/X2 (75/25)	Blown film, Pilot-scale MDO film (DR-6)	0.9438

The method included use of donor board (containing volatile migratable compounds), barrier film (blown and MDO-PE film) and receptor (silicon coated paper) making it donor-barrier-receptor system. Migration of volatiles surrogate chemicals representing MOAH, MOSH and plasticizers through barrier films was analysed to evaluate the impact of oriented film in comparison to biaxially oriented blown film.

5.2.5.1 Chemicals

Recycled paperboard (500 g/m²) was sourced from a local stationery retailer. Aluminum foil by Reynolds (Vileda Freshmate Professional) was utilized, and silicone-coated paper was acquired from BGB Analytik (Böckten, Switzerland). Methyl-t-butylether (99% purity, MTBE) and methanol (MeOH) were purchased from Fischer Scientific (Merelbeke, Belgium), while hexane and ethanol (EtOH) were supplied by Chemlab Analytical (Zedelgem, Belgium). n-Hexadecane (C16) and n-eicosane (C20) were obtained from Acros Organics (Geel, Belgium). Additional chemicals, including n-heptadecane (C17), n-octadecane (C18), 1,3,5-tri-t-butylbenzene (TTBB), 2,6-diisopropylnaphthalene (DIPN), t-butylanthracene (TBA), di-n-propylphthalate (DIPN), bicyclohexyl (Cycy), and Sudan Red II, were sourced from Sigma-Aldrich (Overijse, Belgium).

5.2.5.2 Preparation of donor board

Spiked donor boards were prepared following the procedure described by Biedermann-Brem *et al*. [57]. Recycled paperboard sheets, acting as the donor boards, were immersed for 2 minutes at room temperature in an MTBE solution containing 500 mg/L of each surrogate compound (TTBB, DIPN, TBA, C16, C17, C18, C20, DPP) and 300 mg/L of Sudan Red II (Figure 5.4a). The surrogate compounds were selected to simulate potentially migrating MOAH, MOSH, and plasticizer components, covering a range of volatilities, polarities, aromatic ring numbers, and aliphatic chain lengths. The surrogate compounds simulating MOAH, MOSH and plasticizers are listed in Table 5.4.

Following immersion in the MTBE solution, the sheets were left to dry for up to 2 minutes above the solution until all the solvent had evaporated. Multiple sheets were then prepared, securely wrapped in aluminum foil, and conditioned at 40 °C for 2 weeks prior to use.

The donor boards were then trimmed to a standard size of approximately 15x11 cm for blown films and 12x4 cm for pilot-scale MDO films.

Table 5.4 The surrogate compounds used in the study simulating MOAH, MOSH and plasticizers.

Compound	Simulates
1,3,5-Tri-t-butylbenzene (TTBB)	Mineral oil aromatic hydrocarbons (MOAH)
2,6-diisopropyl naphthalene (DIPN)	
t-butyl anthracene (TBA)	
n-hexadecane (C16)	Mineral oil saturated hydrocarbons (MOSH)
n-heptadecane (C17)	
n-octadecane (C18)	
n-eicosane (C20)	
Di-n-propyl phthalate (DPP)	Plasticizers

The donors were positioned on a sheet of aluminum foil slightly larger than the donor itself (Figure 5.4b). The edges of the foil were then folded over to form a packet, with one side of the donor fully covered by the aluminium foil. On the exposed side, a 15x11 cm window was left open for the blown films, and a 12x4 cm window was exposed for the MDO films.

The donor packet was positioned on the PE film under evaluation for its functional barrier properties, ensuring the exposed side of the donor was oriented toward the PE film. To secure the donor packet, office tape was applied tightly around its entire circumference, ensuring that migration occurred exclusively through the barrier and not via the gas phase adjacent to it (Figure 5.4c). Any excess tape or barrier material at the edges was trimmed to produce a clean, sealed assembly consisting of aluminum foil, the donor, and the barrier.

A piece of silicone paper, cut to match the dimensions of the donor boards, was affixed to the PE side of the packet using tape along one edge. Care was taken to align the silicone paper precisely with the exposed portion of the donor located beneath the PE film (Figure 5.4d).

Figure 5.4 The pictorial representation of migration setup of donor-barrier-receiver system with PE films acting as barrier layer. **a)** Immersion of recycled paperboard in simulant chemical solution, **b)** paperboard being securely wrapped in aluminium foil for 2 weeks at 40 °C, **c)** donor packet being tightly wrapped around with the barrier film with exposed side facing the barrier PE film, **d)** silicone coated paper being taped to other side of barrier film to act as receiver, **e)** whole system being wrapped in aluminium foil for further incubation in the oven.

The donor-barrier-receptor packet was secured to a sheet of aluminum foil using tape (Figure 5.4e). Multiple packets were stacked for storage, with additional weight placed on top to minimize headspace within each packet and to ensure close contact between the components of each assembly.

Packets were stored at an elevated temperature of 40°C. Based on the Arrhenius equation, storage at this temperature is expected to accelerate migration processes by a factor of 4.7 compared to storage at 25°C. Samples were retrieved at predefined intervals of 4 hours, 1 day, 7 days and 28 days by removing packets from the elevated-temperature storage. Prior to opening, the packets were equilibrated to room temperature to prevent evaporation during handling.

For sampling, strips of approximately 2x2 cm from the donor board and of about 9x2 cm from the receptor paper were cut out for extraction. A strip of approximately 5 mm was

discarded from the sides of the receptor, as well as the side where the previous sample was taken.

5.2.5.3 Extraction

All samples prepared for extraction were handled using metal tweezers that had been pre-cleaned with acetone and baked at 105°C overnight to ensure cleanliness. Donor board and silicone paper receptor samples were cut into small pieces (2×2 mm) and weighed into 20 mL vials. Approximately 1 g of donor board and 200 mg of silicone paper were used for extraction. The quantity of silicone paper was carefully limited to minimize the accumulation of co-extracted polysiloxanes in the chromatographic system. Extraction solvents were hexane:EtOH (1:1) for the donor board and MTBE:MeOH (95:5) for silicone paper.

To the vial containing the sample for extraction, 5 mL of solvent and 100 µL of internal standard solution (1 mg/mL Cycy in MTBE) were added, followed by thorough shaking. The vials were incubated at 40°C for 2 hours. After this period, the solvent was transferred to a clean vial, and an additional 5 mL of ethanol:hexane was added to the sample cuts. The vials were incubated again at 40°C for 2 hours. This process was repeated once more, resulting in a final extract volume of 15 mL. The combined extract was filtered through a Pasteur pipette fitted with a filter (Normax, Marinha Grande, Portugal) and collected into a GC vial for analysis.

5.2.5.4 Detection

Extracts were analyzed using an Agilent 7020A gas chromatograph equipped with a flame-ionization detector (GC-FID) (Agilent Technologies, Diegem, Belgium). A 5 µL aliquot of the sample was injected via a split/splitless inlet set to 250°C with a split ratio of 1:40. Chromatographic separation was performed on a VF-1MS column (30 m length, 0.25 mm internal diameter, 0.25 µm film thickness) coupled with a 2 m deactivated fused silica pre-column. The oven temperature program was as follows: an initial temperature of 150°C was held for 1 minute, followed by a ramp to 200°C at 10°C/min, with a hold at 200°C for 1 minute. The temperature was then increased to 320°C at 10°C/min and held for 14 minutes. The flame-ionization detector was maintained at 340°C. The detector flow rates were 400 mL/min for air, 30 mL/min for hydrogen fuel, and 25 mL/min for helium makeup gas, while the column flow rate was 0.713 mL/min using helium as the carrier gas.

A representative chromatogram is presented in Figure 5.5.

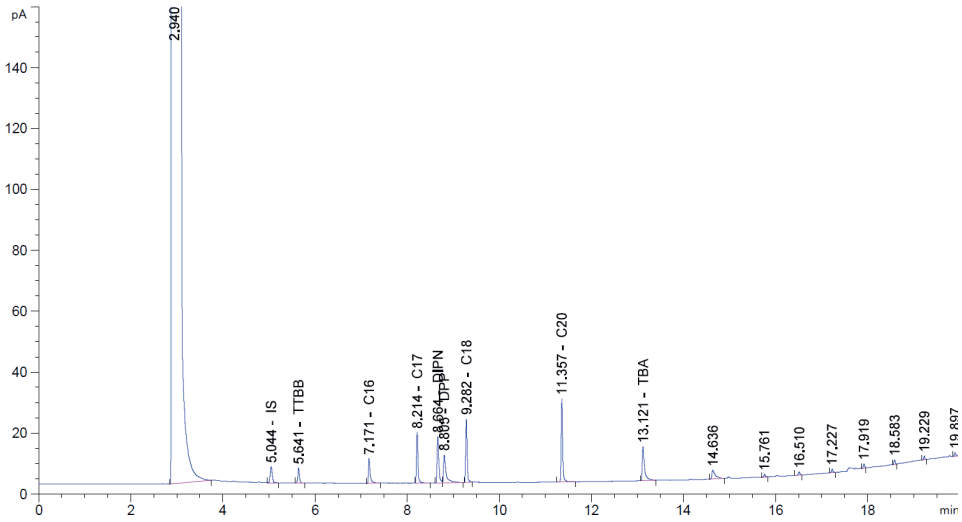

Figure 5.5 A Representative GC-FID chromatogram of recycled paperboard immersed with simulants.

To mitigate potential interference from paperboard extraction, solvent blanks and blank paperboard extracts were analyzed alongside each sample run. Calibration curves were prepared using hexane:ethanol (1:1) solutions containing 10 µg/mL of the internal standard (Cycy) and surrogate compounds at concentrations ranging from 2.5 µg/mL to 150 µg/mL.

5.2.6 Materials and methods used for optical properties analysis

The PE films utilized for the optical properties analysis are presented in Table 5.5.

Table 5.5 PE films utilized for the optical properties analysis along with their respective densities.

Material	Material type	Density (g/cm^3)
D1	Blown film	0.9194
X1	Blown film, Pilot-scale MDO film (DR-2,6,13.33)	0.9256
D2	Blown film	0.9500
D3	Blown film	0.9540
X2	Blown film	0.9667
X1/X2 (25/75)	Blown film, Pilot-scale MDO film (DR-6)	0.9438
X1/X2 (50/50)	Blown film, Pilot-scale MDO film (DR-6)	0.9467
X1/X2 (75/25)	Blown film, Pilot-scale MDO film (DR-6)	0.9561

The various characterization techniques used for the analysis are detailed as:

5.2.6.1 Haze analysis

Haze, a critical quality parameter for manufacturers, refers to the milky or cloudy appearance seen in plastic films. It results from the scattering of light within the transparent material and is quantified as the percentage of light transmission deviating by more than 2.5 degrees from the incident beam. A lower haze value indicates greater material clarity. Haze measurements were performed using a dual-beam xenon flash HunterLab Ultrascan VIS Spectrophotometer, which operates within a wavelength range of 360 to 780 nm.

5.2.6.2 Gloss analysis

Gloss is a key factor in the visual perception of objects, influencing the appearance of a product's finish, texture, and the conditions under which it is illuminated and observed. Surfaces with high reflectance are perceived as glossy, shiny, or lustrous, while surfaces with lower reflectance are seen as semi-gloss or matte [59]. Surface gloss analysis of films was performed with triple angle Elcometer 480 glossmeter at an angle of 60°.

5.2.6.3 Atomic force microscopy (AFM)

Surface roughness of all samples was analysed using atomic force microscopy (AFM). The samples were mounted on a stage with double-sided carbon tape and then blow-cleaned with duster to remove any debris before AFM analysis. AFM images were acquired at ambient temperature using a Bruker Icon AFM system equipped with a MikroMasch probe in tapping mode. The probe had a spring constant of 40 N/m and a resonance frequency of approximately 170 kHz. Imaging was performed at a frequency of 0.5–2 Hz, with a set point ratio of approximately 0.8. Surface roughness was calculated using SPIP software and expressed as root mean square (RMS) roughness S_q, which represents the geometric mean deviation of all surface points from the mean value. For any M × N rectangular image, S_q is defined by Equation 5.7.

$$S_q = \sqrt{\frac{1}{MN}\sum_{k=0}^{M-1}\sum_{i=0}^{N-1}[z(x_k, y_i)]^2} \qquad \textit{Equation 5.7}$$

5.2.6.4 Scanning electron microscopy (SEM)

Imaging of the films was done with a scanning electron microscope (SEM) namely Quanta 3D FEG from Thermo Fisher Scientific. Before Imaging the samples were sputter coated using a Quorum Q150T S with Gold (Au) for 40s at 40 mA.

5.3 Results and Discussions

5.3.1 Oxygen barrier analysis

In the 1st set of experiments, the objective was to quantify whether the microstructural orientation of uniaxially stretched lab-scale MDO films, prepared by stretching compression-molded base sheets, would lead to an enhancement in the oxygen barrier properties compared to randomly oriented blown PE films of same material.

The overall crystallinity data obtained from DSC analysis was evaluated for the compression-molded base sheets, their corresponding lab-scale MDO films. The crystallinity was also evaluated for blown films of the five base resins. Crystallinity is a key factor influencing barrier properties, as polymer crystals act as impermeable barriers to the passage of permeant molecules, with diffusion occurring primarily through the amorphous regions [4], [32], [34], [35].

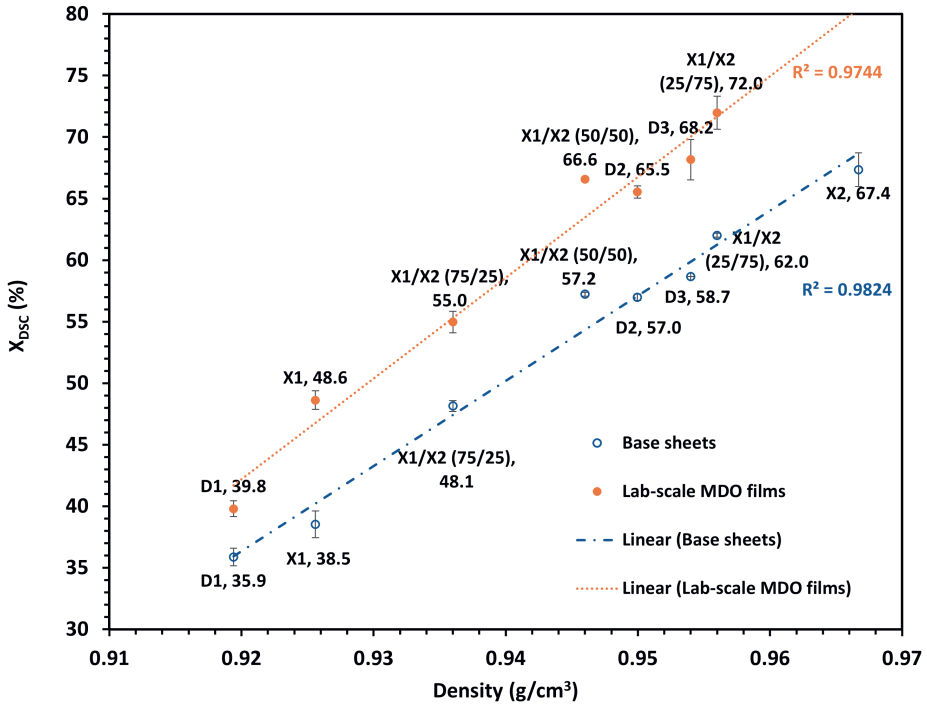

Figure 5.6 Degree of crystallinity (X_{DSC}) (DSC, 1st run) of all five base sheets and MDO films as a function of base resin density (n=3). (Note 1: X2 could not be stretched to the process draw ratio of 7) (Note 2: The linear curves are plotted by fitting the points into a linear equation)

Figure 5.6 compares overall crystallinity of the compression molded base sheet of all five base resins D1, X1, D2, and D3 and three blends of X1/X2 with crystallinity of MDO films obtained by the lab-scale MDO process as a function of base-resin density. The density of

the blends was calculated theoretically using an inverse-additive mixing rule. The stretching process might have altered the densities of stretched films to a small amount, but for the comparative analysis, results of the stretched films are presented in terms of the densities of the base sheets. Lowest density resin D1 only shows about a 4% increase in crystallinity whereas higher-density resins D3 and X1/X2 (25/75) film showed as much as about 10% increase after stretching. This result is also an indication of higher disintegration and fibrillation in the initial crystalline structure and strain-induced orientation and crystallization of the amorphous regions of base sheets made from higher-density resin during stretching at the used orientation temperature.

Figure 5.7 presents a comparison of the overall crystallinity between lab-scale MDO films and blown films produced from five base resins. The data demonstrates enhanced overall crystallinity of the lab-scale MDO-PE films of all five base resins compared to the blown films from same materials. Additionally, the crystallinity of the compression-molded base sheets of the five base resins was found to be quite similar to that of the blown films of base resins.

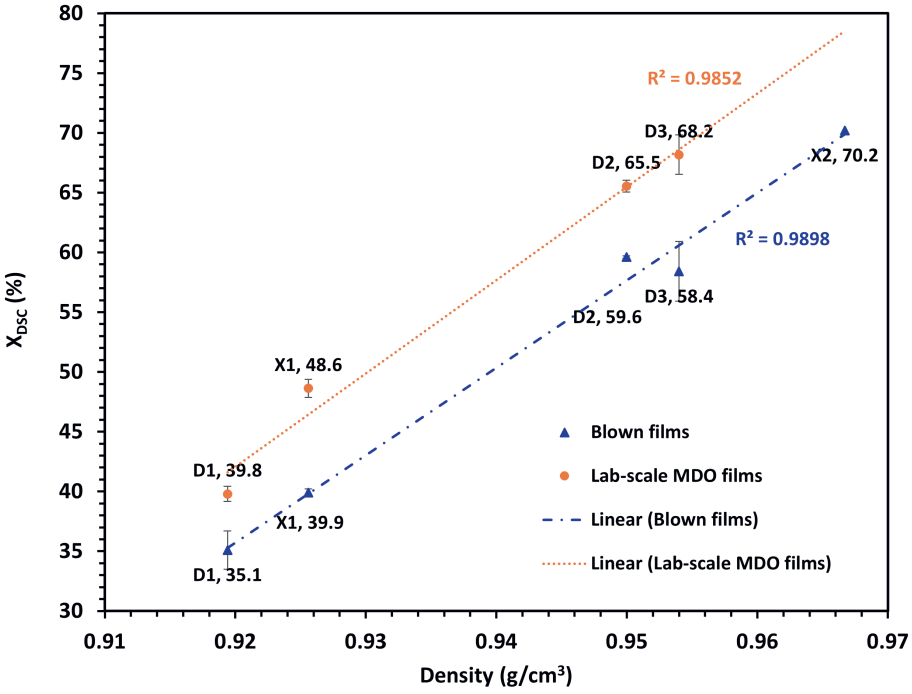

Figure 5.7 Degree of crystallinity (X_{DSC}) of all five blown films and lab-scale MDO films as a function of base resin density (n=3). (Calculated from enthalpy data from DSC, 1st run). (Note: X2 could not be stretched to the length draw ratio of 7)

5.3.1.1 WAXS analysis of microstructural evolution during lab-scale MDO stretching

The WAXS results offered a more comprehensive understanding of the structural evolution during lab-scale MDO operations by enabling the analysis of microstructural data such as crystallite dimensions, before and after the stretching process. Results for X2 were not obtained as X2 base sheet could not be stretched to the length draw ratio of 7 due to its extremely high density and crystallinity as compared to other resins and blends. Due to the high fraction of crystalline phase, its microstructure showed extreme fibrillation and necking during stretching at the used specific orientation temperature and thus ultimately broke off under tensile load.

It was anticipated that the average crystallite dimension would decrease during the drawing process for films derived from high-density resins with larger crystallite sizes. This expectation was confirmed by the observed reduction in average crystallite dimension for D2 and D3 films after drawing, as evidenced from the Figure 5. 8.

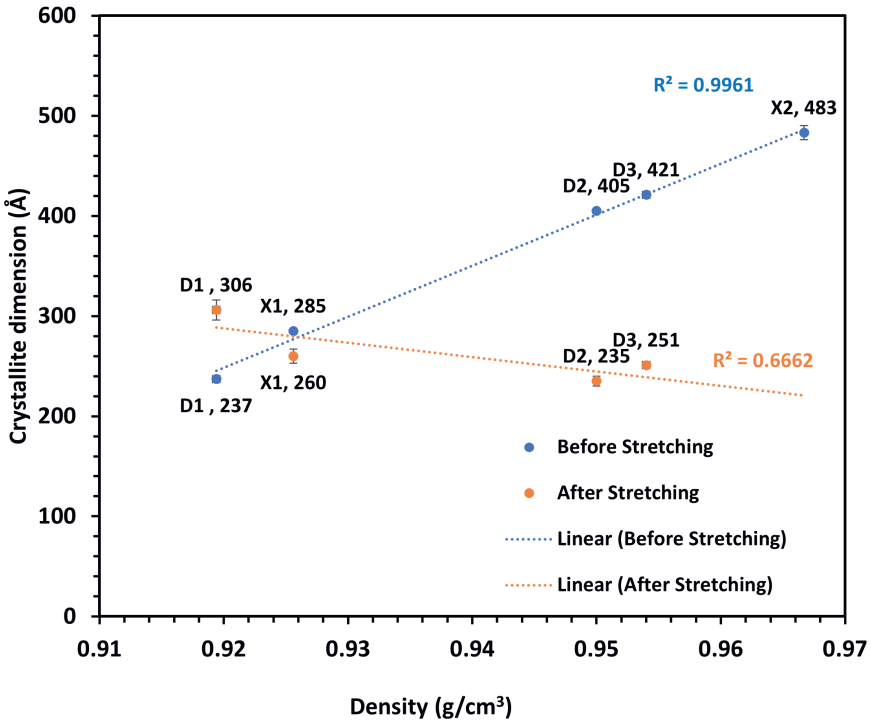

Figure 5.8 Crystallite dimension, L (110) for the compression molded base sheets (before stretching) and their counterpart lab-scale MDO films (after stretching) of 5 base resins as a function of base resin density (n=5). (Note: X2 could not be stretched to the process draw ratio of 7)

Interestingly the same was not observed for the films made from low-density resins D1 and X1. The DSC (Figure 5.9) indicated that partial melting of crystalline phase was relatively higher for these resins as fixed orientation temperature of 110 ℃ was closer to the peak melting point of these resins as compared to higher density resins D2, D3, and X2. This possibly might have helped to retain similar (in case of X1) or even larger (in case of D1) crystallite size after the drawing process at the fixed length draw ratio of 7, as its microstructure was relatively more mobile and thus less disintegrated and fibrillated under tensile load.

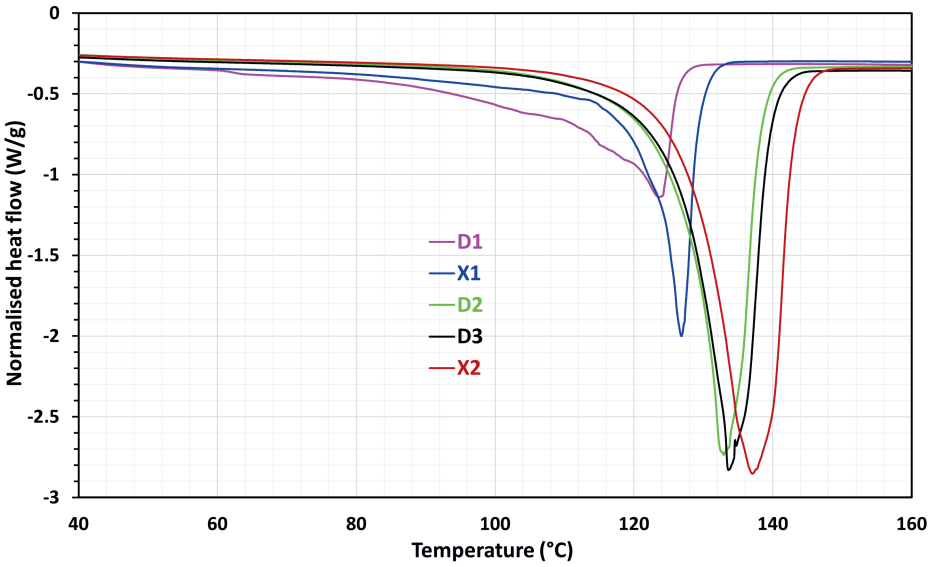

Figure 5.9 DSC melting curves obtained during 1st heat cycle for compression molded base sheets from all 5 base resins.

5.3.1.2 Analysis of the crystal orientations from WAXS

The 2D WAXS patterns gave insight on the orientation of the microstructure of base sheets, cast films and MDO films. The orientation was quantified using Herman's orientation functions from WAXS data.

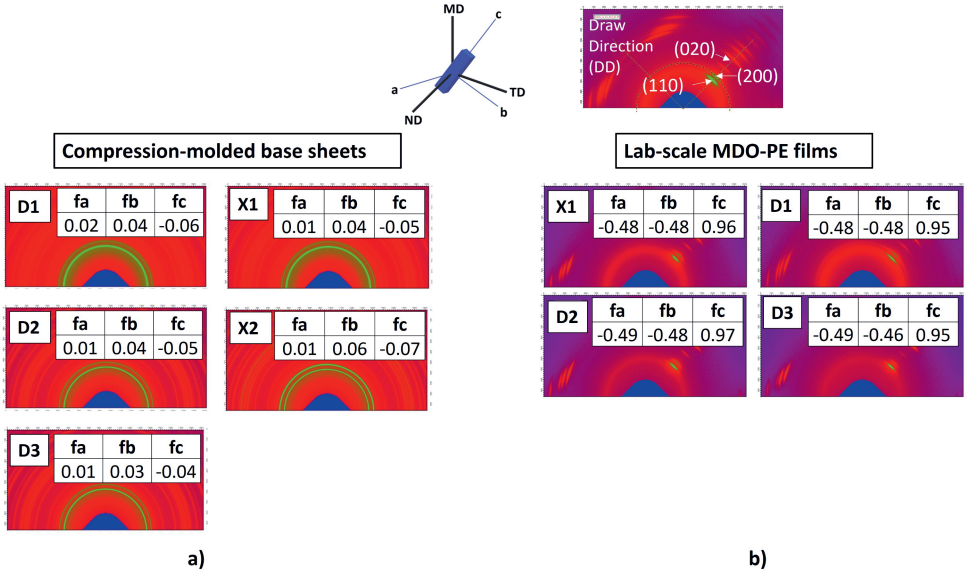

Figure 5.10 2D WAXS patterns for **a)** compression molded base sheets of all 5 base PE resins (D1, D2, D3, X1 and X2) and **b)** for lab-scale MDO films (X1, D1, D2 and D3) along with their Herman orientation factors.

Polyethylene (PE) films with an orthorhombic crystal structure typically exhibit strong scattering from the [110] and [200] reflection planes (with the latter corresponding to the a-axis) and relatively weaker scattering from the [020] plane (corresponding to the b-axis). The [002] reflection plane (c-axis) is generally not observed. To assess the orientation of the crystalline phase, an intensity profile is obtained by plotting the intensity versus azimuthal angle for a user-defined annular region, focusing on the [200] and [020] reflections. The intensity at a given azimuthal angle is dependent on the quantity of crystallographic planes oriented appropriately to permit diffraction at that angle.

In the 2D wide-angle X-ray scattering (WAXS) patterns (Figure 5.10a) of compression-molded base sheets, intense and uniform reflections from the [110] and [200] planes of the orthorhombic unit cell are observed, along with weaker reflections from other planes. This pattern suggests a random orientation of the microstructure. As expected, no strong microstructural orientation was detected across all samples, a finding further supported by the quantification using Herman's orientation functions (illustrated in Figure 5.10a). The orientation factors fa, fb, and fc for the orthorhombic crystallographic axes a, b, and c, respectively, are all close to 0, indicating an isotropic crystalline structure.

In contrast, the lab-scale machine-direction oriented (MDO) films (Figure 5.10b) exhibited a pronounced crystalline orientation, as evidenced by the strongly defined and intense equatorial diffraction arcs corresponding to the [110], [200], and [020] planes. The orientation factor fc for the crystallographic c-axis was nearly 1, indicating an almost perfect alignment of the c-axis with the draw direction.

Quantifying the orientation of the amorphous regions using 2D diffraction patterns is also possible; however, this was challenging in this study due to the strong crystalline scattering peaks superimposed on the amorphous halo. Nonetheless, it is expected that the tensile forces applied during the MDO process, particularly at the chosen orientation temperature, would also induce significant orientation in the amorphous regions toward the machine direction. This effect is likely more pronounced in higher-density base sheets due to the relatively lower proportion of amorphous regions, which facilitates easier disentanglement and orientation under the applied stretching load.

As mentioned before, for quantifying the oxygen permeability coefficient of randomly oriented or non-uniaxially oriented materials, blown films were selected instead of compression-molded base sheets (used to produce lab-scale MDO films). This choice was due to the high thickness of the compression-molded base sheets (approximately 550 microns), which made them challenging to use with the apparatus. In contrast, blown films, with a comparatively lower thickness of about 50 microns (exact value of thickness with standard deviation presented in Table A5.1 in Appendix), were more suitable for the experimental setup.

Figure 5.11 presents the analysis of permeability coefficient data to compare the oxygen permeability between lab-scale MDO films and blown films made from base resins and selected blends. This comparison is based on the general assumption that permeability coefficients are independent of film thickness.

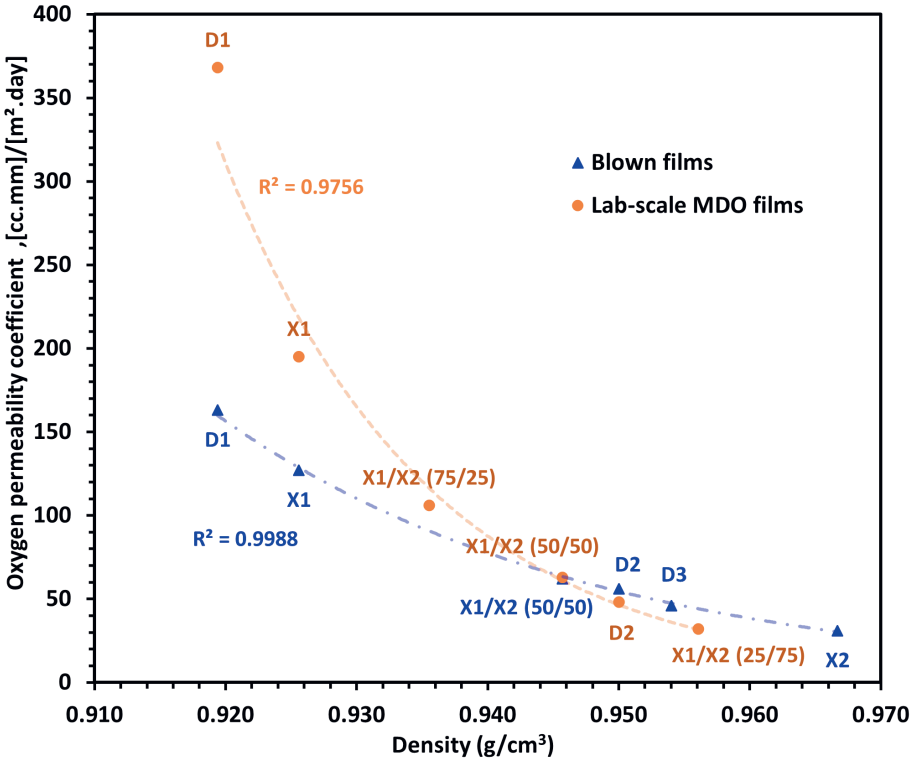

Figure 5.11 Oxygen permeability coefficients (n=2) for lab-scale MDO films and blown films made from base resins and selected blends as a function of base resin density with data points fitted for an exponential fit indicated by dashed trendlines. (Note: In case of blown films of blends, oxygen permeability coefficient of only one blend i.e. X1/X2 (50/50) was measured. Further lab-scale MDO film sample of D3 failed during measurement giving an outlier value of oxygen permeability coefficient greater than 3000)

In semi-crystalline polymers, polymer crystals serve as impermeable barriers, with small molecules diffusing primarily through the amorphous regions. Consequently, an increase in overall crystallinity or film density is expected to result in reduced permeability. This relationship is corroborated by the data presented in Figure 5.11, where decrease in permeability is observed as density increases for both blown and lab-scale MDO films. This decrease in oxygen permeability with increasing PE density is in line with the previous work from Alter [60].

It is important to note that permeability in the MDO process is also influenced by the draw ratio and orientation temperature, with permeability likely to be expected to decrease as the draw ratio increases and orientation temperature decreases [32], [35]. In this study, the lab-scale MDO operation was conducted using a fixed draw ratio and orientation temperature. Therefore, it is highly likely that varying the draw ratio and orientation

temperature in the lab-scale MDO process could yield different permeability results for the same material.

Interestingly from Figure 5.11, it was observed that MDO orientation did not always improved oxygen barrier in lab-scale MDO films compared to blown films. Specifically, in lower-density films, such as D1 and X1, oxygen permeability was higher in lab-scale MDO films. However, the trendline indicates that after surpassing a certain density (0.947 g/cm³ for X1/X2 (50/50)), the oxygen permeability in lab-scale MDO films at the fixed MDO length draw ratio of 7 and orientation temperature of 110 °C decreased relative to the blown films. It is further acknowledged that incorporating additional data points could refine the trendline and provide a more comprehensive understanding of the impact of orientation on permeability coefficients, which presents an opportunity for future investigation.

Figure 5.7 also presented that lab-scale MDO films exhibit higher overall crystallinity compared to blown films of similar resins. However, despite this increased crystallinity, the D1 and X1 lab-scale MDO films displayed higher oxygen permeability than their blown film counterparts. These findings indicate that merely increasing overall crystallinity after MDO does not necessarily enhance the gas permeability barrier of an oriented polymer film. The orientation and geometric configuration of both crystalline and amorphous regions after MDO operation also plays a crucial role in determining barrier properties of the oriented polymer film [32], [35].

The first DSC melting curves of base sheets produced from the five base resins, as shown in Figure 5.9, indicate that partial melting of the crystalline phase was more pronounced in the lower-density base sheets, D1 and X1, at the fixed orientation temperature of 110°C. This temperature is closer to the peak melting point of D1 and X1 resins, compared to the higher-density resins D2, D3, and X2. This partial melting likely contributed to the retention of similar (in the case of X1) or even larger (in the case of D1) crystallite sizes after the drawing process, as the microstructure of these lower-density sheets remained more mobile and therefore experienced less disintegration and fibrillation under tensile load.

For D1 and X1 base sheets, due to this higher partial melting of crystalline phase, there was minimal disintegration and fibrillation of crystalline phase as evidenced from the WAXS results that its crystallite dimension increases or remains same after MDO operation. The relatively less partially melted crystalline phase strongly aids the orientation and strain induced crystallization of amorphous phase as evidenced for higher density resin D2 and D3.

Paulos and Thomas [32], in their investigation of the effect of post drawing on gas permeability in blown polyethylene films, reported that a higher degree of sample orientation is preserved at lower orientation temperatures (or less partially melted microstructure) during post drawing. They attributed the significant reduction in the films transport properties primarily to the increased orientation of the amorphous phase. Similarly, Nakayama and Katsuna [61] demonstrated a similar relationship between the orientation of the amorphous phase and the orientation temperature.

As shown in the DSC results presented in Figure 5.6, the increase in overall crystallinity is minimal for the lowest-density resin, D1, compared to the other resins. This suggests that the extensive partial melting of the crystalline phase at the used orientation temperature

did not significantly produce strong amorphous orientation during MDO stretching. Consequently, this is reflected in the oxygen permeability properties of D1, which increased after stretching and orientation compared to its blown film. As resin density increases, the disintegration and fibrillation of the crystalline phase become more pronounced due to the relatively lower extent of partial melting at the used fixed orientation temperature. This, in turn facilitates stronger orientation and crystallization of the amorphous regions. The resulting decrease in oxygen permeability in lab-scale MDO films compared to blown films with increasing density is indicative of these relatively stronger amorphous orientations in higher density lab-scale MDO films.

Another factor contributing to the reduced oxygen barrier properties observed after orientation, particularly in low-density lab-scale MDO films D1 and X1, may be related to the geometric configuration of the lamellae. This phenomenon is supported by the findings of Breese et al. [35], who investigated the impact of MDO on the moisture and oxygen barrier properties of HMW (high molecular weight)-PE films. Their study revealed that MDO films produced from lower density materials exhibited increased moisture and oxygen transmission rates. They attributed this to the lamellae's (thin plate-like crystalline structural component in semi-crystalline polymers that forms during crystallization process by back-and-forth orderly folding of polymer chains) arrangement at low to moderate draw ratios, where the lamellae are aligned nearly parallel to each other, thereby exposing inter- and intra-lamellar stack voids that facilitate the permeation of moisture and oxygen through the films. However, no conclusive evidence was found to support this argumentation in the experiments.

The oxygen permeability of conventionally used outer polymer films for multilayer flexible packaging, such as PET and PA, typically ranges from 1 to 5 cc mm/m²/day for PET and 0.1 to 1 cc mm/m²/day for PA at 0% RH and 23°C, as reported in the literature [62]. These values are significantly lower than the lowest permeability observed in this study's measurements for lab-scale MDO-PE films, which was approximately 30 to 40 cc mm/m²/day.

Hence, it is suggested that while MDO-PE films can enhance oxygen barrier properties under certain conditions, they may still require an additional oxygen barrier layer for high-end packaging applications. This additional barrier, potentially in the form of ultra-thin coatings or high-performance barrier films, should also be compatible with mechanical recycling processes for mono-material PE-based multi-layer flexible packaging designed for high oxygen barrier requirements. Few companies and consortia, such as The Circular Economy for Flexible Packaging (CEFLEX) [63], which develop guidelines for the recycling of flexible packaging, accept the inclusion of strong barrier layers like ethylene vinyl alcohol (EVOH) and thin coatings like silicon oxide (SiOx) and aluminum oxide (AlOx), provided these materials do not exceed 5% by weight of the total packaging structure. This threshold ensures that the final quality of the recyclate is not compromised and that the packaging structure remains classified as mono-material flexible packaging.

5.3.2 Functional barrier analysis

In the 2nd set of experiments, the functional barrier properties of PE blown films and pilot-scale MDO films were evaluated to assess their effectiveness in preventing the migration of

MOAH, MOSH, and plasticizers from recycled paperboard. This investigation aimed to determine the influence of MDO orientation on the barrier performance of PE films and their potential to act as enhanced functional barriers against the migration of these harmful compounds.

Blown films and pilot-scale MDO films of X1, as well as X1/X2 (75/25) blends, with comparable thicknesses of approximately 50 microns (exact value of thickness with standard deviation presented in **Table A5.1** in Appendix), were analysed.

Different surrogates representing MOAH and MOSH compounds showed different migration behaviour. Apolar components, being less tightly bound to paperboard, exhibit greater migratory potential compared to polar compounds. These apolar compounds can readily traverse barriers of similar polarity but encounter greater resistance when attempting to migrate through polar barriers. Although exposure to polar contaminants cannot be entirely ruled out, it appears advantageous for functional barriers to possess a certain degree of polarity.

Polar surrogates such as DPP showed weakest migration tendency. Apolar volatile surrogates such as TTBB (simulating MOAH compounds) and C16 (simulating MOSH compounds) showed faster and higher migration. To analyze the impact of MD orientation, only TTBB and C16 were selected for functional barrier analysis. Their relatively higher migration values, compared to other surrogates, allowed for accurate quantification and clear comparison with randomly oriented blown film samples. Surrogate concentration of TTBB and C16 was measured inside recycled paperboard as presented in Table 5.6.

Table 5.6 Measured surrogate concentration of TTBB and C16 in spiked recycled paperboards (n = 4).

Surrogates	TTBB	C16
Concentration (mg/kg)	264 ± 20	228 ± 23

The migration of TTBB from the donor to the receptor, with blown films and pilot-scale MDO-PE films serving as barriers, is presented as a percentage of migration in Figure 5.12.

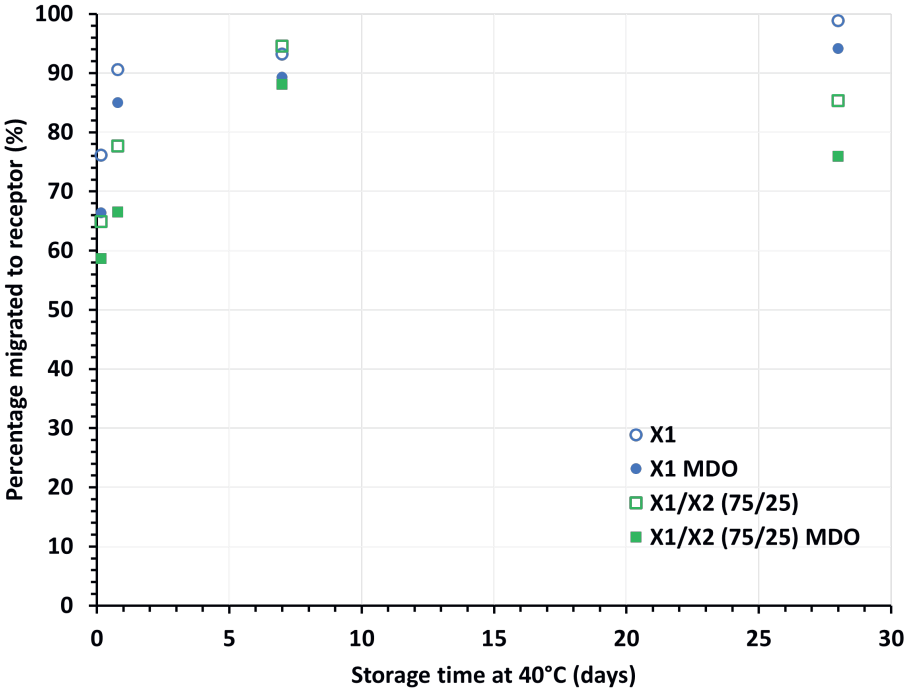

Figure 5.12 The percentage migration of the surrogate compound TTBB from the donor to the receptor with blown films and pilot-scale MDO films composed of X1 and X1/X2 (75/25) blends acting as barriers. (Note: Open markers represent blown PE films and closed markers represent pilot scale MDO-PE films)

From Figure 5.12, it can be concluded that both blown and MDO PE films presents weak barrier against apolar compounds such as TTBB as the threshold limit of migration of 0.01 mg/kg (less than 0.004%) was easily crossed within first measurement taken at 4 hours at 40 °C. Interestingly, in the case of TTBB, both X1 and X1/X2 (75/25) MDO films demonstrated slightly improved barrier performance against migration compared to their blown films. This trend was consistent across measurements taken at 4 hours, 1 day, 7 days, and 28 days under storage conditions at 40 °C. Another important observation from the results was that the higher-density X1/X2 (75/25) film exhibiting improved barrier performance against migration compared to the relatively lower-density X1 film.

For X1/X2 (75/25), the concentration of TTBB in the receptor, measured at 28 days, showed a decrease after initially reaching a maximum. This decline is attributed to the volatile nature of TTBB, suggesting that its high volatility likely resulted in losses from the receptor during the extended storage period of 28 days at 40 °C.

For C16 as presented in Figure 5.13, similar trends were observed, with higher-density films showing lower migration compared to lower-density films. Additionally, MDO films generally exhibited better barrier performance compared to blown films.

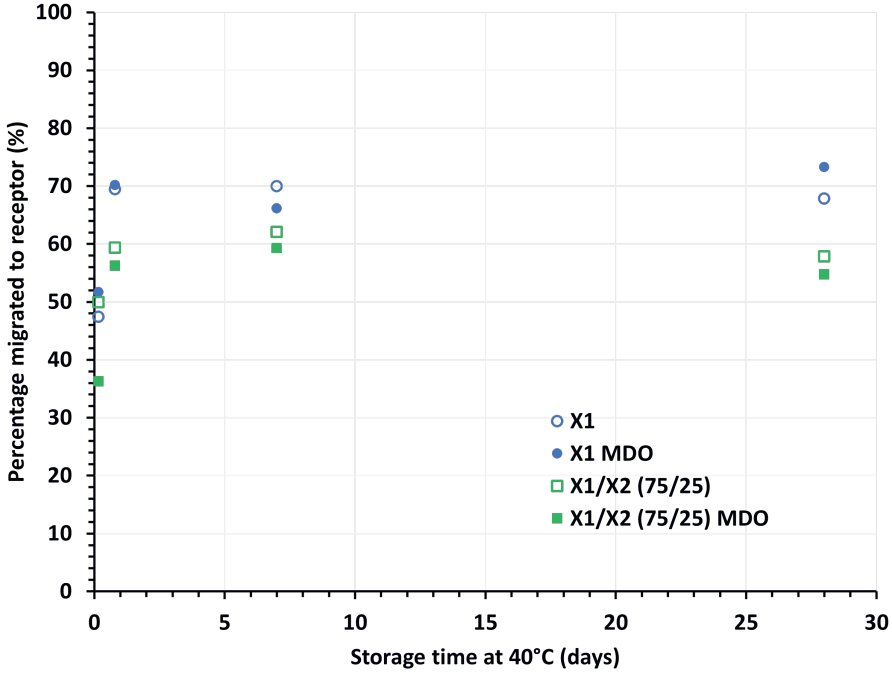

Figure 5.13 The percentage migration of the surrogate compound C16 from the donor to the receptor with blown films and pilot-scale MDO films composed of X1 and X1/X2 (75/25) blends acting as barriers. (Note: Open markers represent blown PE films and closed markers represent pilot scale MDO-PE films)

The results (Figure 5.12 and 5.13) clearly indicate that both the density and orientation of PE films influence the migration of surrogate compounds representing MOAH and MOSH. As the density increases, the crystalline microstructure of the films also increases, with the higher density of crystals reducing migration. MDO films, at similar thicknesses, exhibited better barrier performance compared to blown films, likely due to the increased overall crystallinity and better alignment of the microstructure, which creates a more tortuous path for migration.

These results contrast with those obtained in the previously mentioned oxygen permeability experiments for the low-density resin X1 and the X1/X2 (75/25) blend, in which the value of oxygen permeability coefficient was higher after orientation. In the functional barrier analysis, MDO films were produced using a pilot-scale setup, whereas the earlier lab-scale MDO films were limited by apparatus constraints, which restricted the maximum achievable draw ratio and orientation. Consequently, the pilot-scale setup allowed for higher draw ratios which likely resulted in higher disintegration and fibrillation of crystalline microstructure alongside strain induced crystallization to enhance overall crystallinity with strong microstructural orientation towards MD. This further contributed to the enhanced barrier performance against the migration of surrogate compounds.

5.3.3 Optical properties analysis

In the 3rd set of experiments, the effect of machine direction orientation (MDO) on key optical properties essential for flexible packaging applications such as optical clarity, haze, and gloss was evaluated. To assess the influence of resin density on haze, the total percentage haze was measured for blown films made from all five base resins. As shown in Figure 5.14a, an overall increase in haze was observed with increasing resin density. The haze of a polymer film is influenced by multiple factors, including surface irregularities, crystallization behavior, and inhomogeneities in the melt and solid phases.

The total haze of a film arises from contributions by both bulk and surface haze. It is widely acknowledged that, in thin polyethylene films, surface haze predominantly governs the total haze characteristics [4], [64], [65]. Study of Andreassen and Larsen [66] summarizes surface roughness due to flow defects/or crystalline structures as the major source of haze in blown films.

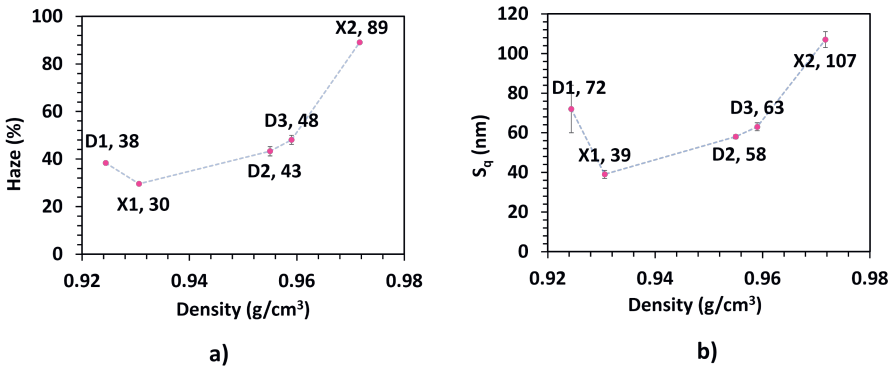

Figure 5.14 a) Percent total haze (n=3) and, **b)** RMS surface roughness (n=5) plotted as a function of density of blown films of all five base resins.

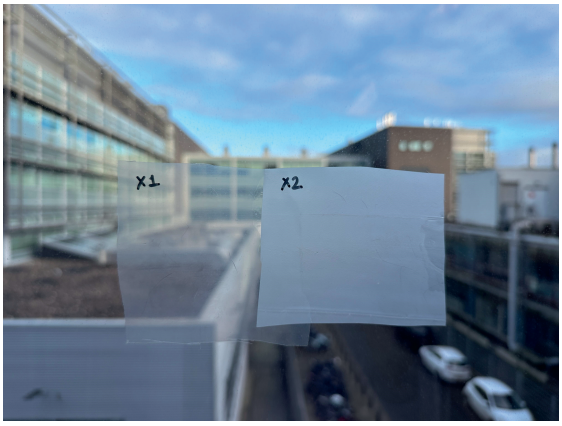

Figure 5.15 Visual representation of percent haze from pieces of blown film of X1 (with lowest percent haze) and X2 (with highest percent haze) among blown films of 5 base resins.

Figure 5.14b illustrates that in this study, surface roughness was the primary contributor to total haze, with additional contributions from bulk crystallinity (Figure 5.7). Notably, despite having higher RMS surface roughness than D2 and D3, D1 exhibited lower total haze, likely due to its significantly lower crystallinity compared to D2 and D3. Among the films, the X1 blown film demonstrated the lowest haze, while the X2 blown film exhibited the highest haze, consistent with the contributions of their respective RMS surface roughness and bulk crystallinity (Figure 5.15).

The impact of MDO or uniaxial orientation on total haze was investigated by analysing blown films of X1 and its three blends with X2 at 25, 50, and 75 wt% compositions as illustrated in Figure 5.16a. The haze values before and after the MDO process were compared. All MDO films exhibited higher haze than their blown counterparts, attributed to an increase in overall crystallinity and microstructural disintegration and fibrillation during the MDO process, which contributed to enhanced surface roughness, as quantified by atomic force microscopy (AFM). As shown in Figure 5.16b, surface roughness remained the primary contributor to total haze in MDO films, with additional contributions from bulk crystallinity.

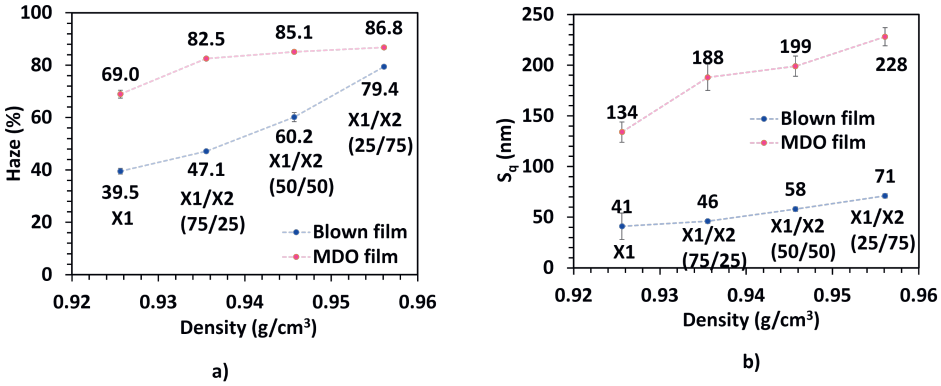

Figure 5.16 a) Percent total haze (n=3) and, **b)** RMS surface roughness (n=5) plotted as a function of density of blown films and their respective MDO films of base resin X1 and its blends with resin X2, i.e. X1/X2 (75/25), X1/X2 (50/50), X1/X2 (25/75).

MDO operations conducted near the vicinity of melting temperature may result in reduced bulk microstructural and surface disintegration due to increased partial melting of the microstructure, potentially leading to smoother films with improved optical clarity and reduced total haze. However, in the experiments conducted in this study, an increase in total haze was consistently observed after the MDO process, irrespective of the base film density, when a constant process draw ratio was maintained.

Gloss is another critical property influencing the visual perception of flexible packaging. Highly reflective surfaces are perceived as glossy, shiny, or lustrous, whereas surfaces with lower reflectance are perceived as semi-gloss or matte [67]. The literature indicates that gloss is influenced by the surface profile and the intrinsic refractive index of a polymer film. Surface roughness is linked to the crystalline morphology and deformation-induced defects

formed during the melt flow process [68]. Studies have reported that an increase in surface roughness leads to a decrease in instrumental surface gloss [69].

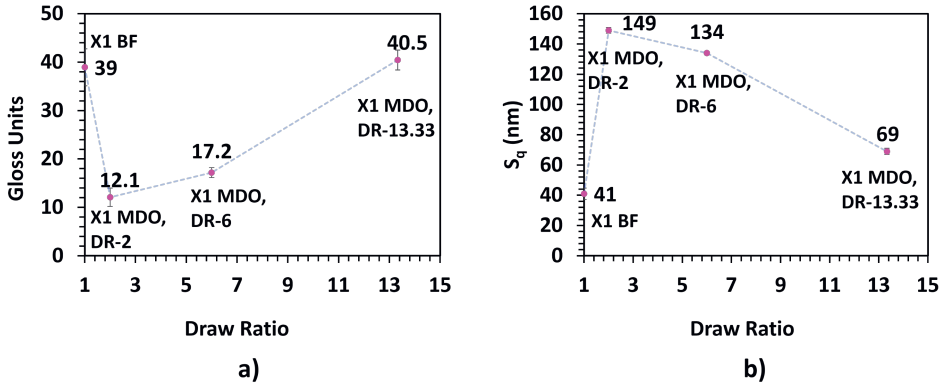

Figure 5.17a) Gloss (n=5) and **b)** RMS surface roughness (n=5) plotted as a function of draw ratio of blown film of base resin X1 and its MDO films at the draw ratio of 2,6 and 13.33.

Figure 5.17b demonstrate that for MDO films of X1, a decrease in average surface roughness with increase in draw ratio (from 2 to 13.33) is observed, as quantified by AFM, which further corresponded to an increase in gloss of the films (Figure 5.17a). The base blown film of X1 exhibited a relatively smoother surface compared to its MDO counterparts, likely due to uniform melt solidification facilitated by internal circulating air during the film blowing process.

As the draw ratio increased, the onset of bulk microstructural disintegration and fibrillation at lower draw ratios resulted in higher surface roughness, as presented in Figure 5. 17b for draw ratio of 2. SEM and AFM images (Figure 5.18) reveal that as the process draw ratio increased from 2 to 6, the initially random microstructure was progressively replaced by fibril development oriented along the machine direction. At a draw ratio of 13.33 MDX, SEM and AFM images show well-defined fibrils with a strong MD orientation, with no trace of the previously random morphology observed in the blown film. This fibrillation and the formation of a highly oriented microstructure reduced surface defects, leading to a gradual smoothing of the film surface. This reduction in surface roughness, as presented in Figure 5.17b, correlated with an increase in gloss values, as also evident in the visual appearance of the films depicted in Figure 3.19 in Chapter 3.

5.4 Concluding remarks

This Chapter investigated the effects of uniaxial orientation on the gas barrier, functional barrier, and optical properties of polyethylene films for mono-material PE based multi-layer flexible packaging designed to support mechanical recycling.

The first study evaluated the oxygen barrier properties of lab-scale MDO-PE films, demonstrating that higher-density films exhibited improved barrier performance due to increased crystallinity and structural orientation. In contrast, lower-density films showed

increased oxygen permeability after orientation, attributed to higher microstructural partial melting and possibly limited amorphous phase orientation during MDO. These results highlight the importance of optimizing resin density, orientation temperature, and draw ratio to achieve optimal oxygen barrier properties in MDO-PE films. While MDO improved barrier properties, the oxygen permeability of MDO-PE films remained higher than that of conventional barrier materials like PET and PA, underscoring the need for supplementary oxygen barrier layers for high-performance applications.

The second study focused on the functional barrier properties of MDO and blown films against surrogate compounds representing harmful MOAH and MOSH substances. Both film types exhibited weak barriers to apolar compounds, with migration exceeding acceptable limits. However, MDO films in general demonstrated better barrier performance due to increased crystallinity and microstructural orientation, which created more tortuous diffusion paths. Pilot-scale MDO films produced at higher draw ratios and orientations further enhanced barrier performance, emphasizing the importance of processing conditions in improving functionality.

The third study evaluated the impact of MDO on the optical properties of PE films, specifically haze and gloss. Haze increased with resin density and further after MDO processing, primarily due to surface roughness and bulk crystallinity. Gloss decreased at lower draw ratios due to fibrillation-induced surface roughness but improved at higher draw ratios as fibril alignment reduced surface defects. These findings highlight the interplay between processing parameters and microstructural changes in tailoring the optical properties of PE films for packaging applications.

5.5 Bibliography

[1] S. J. Risch, “Food Packaging History and Innovations,” *J Agric Food Chem*, vol. 57, no. 18, pp. 8089–8092, Sep. 2009, doi: 10.1021/jf900040r.

[2] S. Guzman-Puyol, J. J. Benítez, and J. A. Heredia-Guerrero, “Transparency of polymeric food packaging materials,” *Food Research International*, vol. 161, p. 111792, 2022, doi: https://doi.org/10.1016/j.foodres.2022.111792.

[3] “Why barrier properties are critical to food product quality.” Accessed: Aug. 12, 2024. [Online]. Available: https://terinexflexibles.com/wp-content/uploads/2023/10/TER012-White-Paper-Barrier-properties_v1.2_Pages-Web.pdf

[4] T. Chatterjee *et al.*, “Machine direction orientation of high density polyethylene (HDPE): Barrier and optical properties,” *Polymer (Guildf)*, vol. 55, no. 16, pp. 4102–4115, 2014, doi: https://doi.org/10.1016/j.polymer.2014.06.029.

[5] V. Jost, “Packaging related properties of commercially available biopolymers - An overview of the status quo,” *Express Polym Lett*, vol. 12, no. 5, pp. 429–435, May 2018, doi: 10.3144/expresspolymlett.2018.36.

[6] U. Qasim *et al.*, “Renewable cellulosic nanocomposites for food packaging to avoid fossil fuel plastic pollution: a review,” *Environ Chem Lett*, vol. 19, no. 1, pp. 613–641, 2021, doi: 10.1007/s10311-020-01090-x.

[7] B. M. Trinh, B. P. Chang, and T. H. Mekonnen, “The barrier properties of sustainable multiphase and multicomponent packaging materials: A review,” *Prog Mater Sci*, vol. 133, p. 101071, 2023, doi: https://doi.org/10.1016/j.pmatsci.2023.101071.

[8] V. L. Lazić, J. Budinski-Simendić, J. J. Gvozdenović, and B. Simendić, “Barrier Properties of Coated and Laminated Polyolefin Films for Food Packaging,” 2010.

[9] C. F. Ayuso, A. A. Agüero, J. A. P. Hernández, A. B. Santoyo, and E. G. Gómez, “High Oxygen Barrier Polyethylene Films,” *Polymers and Polymer Composites*, vol. 25, no. 8, pp. 571–582, Oct. 2017, doi: 10.1177/096739111702500802.

[10] D. Carullo *et al.*, “Testing a coated PE-based mono-material for food packaging applications: an in-depth performance comparison with conventional multi-layer configurations,” *Food Packag Shelf Life*, vol. 39, p. 101143, 2023, doi: https://doi.org/10.1016/j.fpsl.2023.101143.

[11] L. S. Dilkes-Hoffman, J. L. Lane, T. Grant, S. Pratt, P. A. Lant, and B. Laycock, “Environmental impact of biodegradable food packaging when considering food waste,” *J Clean Prod*, vol. 180, pp. 325–334, 2018, doi: https://doi.org/10.1016/j.jclepro.2018.01.169.

[12] G. Faraca and T. Astrup, “Plastic waste from recycling centres: Characterisation and evaluation of plastic recyclability,” *Waste Management*, vol. 95, pp. 388–398, 2019, doi: https://doi.org/10.1016/j.wasman.2019.06.038.

[13] Y. Ma, “Changing Tetra Pak: From waste to resource,” *Sci Prog*, vol. 101, no. 2, pp. 161–170, Jun. 2018, doi: 10.3184/003685018x15215434299329.

[14] C. Y. Barlow and D. C. Morgan, “Polymer film packaging for food: An environmental assessment,” 2013. doi: 10.1016/j.resconrec.2013.07.003.

[15] C. T. de M. Soares, M. Ek, E. Östmark, M. Gällstedt, and S. Karlsson, “Recycling of multi-material multilayer plastic packaging: Current trends and future scenarios,” *Resour Conserv Recycl*, vol. 176, Jan. 2022, doi: 10.1016/j.resconrec.2021.105905.

[16] T. W. Walker *et al.*, “Recycling of multilayer plastic packaging materials by solvent-targeted recovery and precipitation,” 2020. [Online]. Available: https://www.science.org

[17] K. Kaiser, M. Schmid, and M. Schlummer, “Recycling of polymer-based multilayer packaging: A review,” 2018, *MDPI AG*. doi: 10.3390/recycling3010001.

[18] L. S. Dilkes-Hoffman, J. L. Lane, T. Grant, S. Pratt, P. A. Lant, and B. Laycock, “Environmental impact of biodegradable food packaging when considering food waste,” *J Clean Prod*, vol. 180, pp. 325–334, Apr. 2018, doi: 10.1016/j.jclepro.2018.01.169.

[19] G. Faraca and T. Astrup, “Plastic waste from recycling centres: Characterisation and evaluation of plastic recyclability,” *Waste Management*, vol. 95, pp. 388–398, Jul. 2019, doi: 10.1016/j.wasman.2019.06.038.

[20] V. Srebrenkoska, G. B. Gaceva, M. Avella, M. E. Ericco, and G. Gentile, “Utilization of recycled polypropylene for production of Eco-composites,” *Polymer - Plastics Technology and Engineering*, vol. 48, no. 11, pp. 1113–1120, 2009, doi: 10.1080/03602550903147247.

[21] M. Guerritore *et al.*, “Recyclable-by-design mono-material flexible packaging with high barrier properties realized through graphene hybrid coatings,” *Resour Conserv Recycl*, vol. 179, Apr. 2022, doi: 10.1016/j.resconrec.2021.106126.

[22] “Why the permeability rate of a polymer material is dependent upon a variety of factors - Packaging South Asia.” Accessed: Aug. 13, 2024. [Online]. Available: https://packagingsouthasia.com/events/tokyo-pack/why-the-permeability-rate-of-a-polymer-material-is-dependent-upon-a-variety-of-factors/

[23] J. Comyn, “2 - What are adhesives and sealants and how do they work?,” in *Adhesive Bonding*, R. D. Adams, Ed., Woodhead Publishing, 2005, pp. 23–51. doi: https://doi.org/10.1533/9781845690755.1.23.

[24] M. Paul, B. Morris, J. Weinhold, and K. Hausmann, “The effect of stretching and tie layer composition on adhesion strength of multi-layered films,” *Journal of Plastic Film and Sheeting*, vol. 38, no. 3, pp. 351–368, Jul. 2022, doi: 10.1177/87560879211063475.

[25] D. Carullo *et al.*, “Testing a coated PE-based mono-material for food packaging applications: an in-depth performance comparison with conventional multi-layer configurations,” *Food Packag Shelf Life*, vol. 39, Nov. 2023, doi: 10.1016/j.fpsl.2023.101143.

[26] E. Hatfield, R. Tate, K. Williams, and W. Todd, “NEW MDO MEDIUM MOLECULAR WEIGHT HIGH DENSITY POLYETHYLENE FILMS*,” *JOURNAL OF PLASTIC FILM & SHEETING*, vol. 18, 2002, doi: 10.1177/875608702032871.

[27] D. Guleria, S. Ge, L. Cardon, S. Vervoort, and J. den Doelder, “Impact of resin density and short-chain branching distribution on structural evolution and enhancement of tensile modulus of MDO-PE films,” *Polym Test*, p. 108560, 2024, doi: https://doi.org/10.1016/j.polymertesting.2024.108560.

[28] S. H. Tabatabaei, P. J. Carreau, and A. Ajji, “Structure and properties of MDO stretched polypropylene,” *Polymer (Guildf)*, vol. 50, no. 16, pp. 3981–3989, Jul. 2009, doi: 10.1016/j.polymer.2009.06.059.

[29] S. H. Tabatabaei, L. Parent, P. Cigana, A. Ajji, and P. J. Carreau, “Effect of machine direction orientation conditions on properties of HDPE films,” *Journal of Plastic Film and Sheeting*, vol. 25, no. 3–4, pp. 235–249, 2009, doi: 10.1177/8756087910369423.

[30] M. B. Elias, R. Machado, and S. V Canevarolo, “Thermal and Dynamic-Mechanical Characterization of Uni- and Biaxially Oriented Polypropylene Films,” *J Therm Anal Calorim*, vol. 59, no. 1, pp. 143–155, 2000, doi: 10.1023/A:1010187913049.

[31] D. Guleria, M. Edeleva, S. Vervoort, S. Ge, J. den Doelder, and L. Cardon, “Impact of molecular architecture and draw ratio on enhancement of targeted mechanical properties of machine direction oriented polyethylene films produced after blown film extrusion,” *Journal of Plastic Film & Sheeting*, p. 87560879241293390, Oct. 2024, doi: 10.1177/87560879241293392.

[32] J. P. Paulos and E. L. Thomas, “Effect of postdrawing on the permeability of gases in blown polyethylene film,” *J Appl Polym Sci*, vol. 25, no. 1, pp. 15–23, Jan. 1980, doi: https://doi.org/10.1002/app.1980.070250102.

[33] J. L. Williams and A. Peterlin, “Transport properties of methylene chloride in drawn polyethylene as a function of the draw ratio,” *Journal of Polymer Science Part A-2: Polymer Physics*, vol. 9, no. 8, pp. 1483–1494, Aug. 1971, doi: https://doi.org/10.1002/pol.1971.160090808.

[34] H. Sha and I. R. Harrison, “CO2 permeability and amorphous fractional free-volume in uniaxially drawn HDPE,” *J Polym Sci B Polym Phys*, vol. 30, no. 8, pp. 915–922, Jul. 1992, doi: https://doi.org/10.1002/polb.1992.090300814.

[35] D. Breese, G. B.-T. E. P. Conference, and undefined 2005, “Effects of machine direction orientation (MDO) on the moisture and oxygen barrier properties of HMW-PE films,” *CiteseerDR Breese, G BeaucageTAPPI European PLACE Conference, 2005•Citeseer*, Accessed: Aug. 13, 2024. [Online]. Available: https://citeseerx.ist.psu.edu/document?repid=rep1&type=pdf&doi=98756ceb8d83a156b6e0307dea67c0b15236cf3d

[36] M. Biedermann and K. Grob, “Is comprehensive analysis of potentially relevant migrants from recycled paperboard into foods feasible?,” *J Chromatogr A*, vol. 1272, pp. 106–115, 2013, doi: https://doi.org/10.1016/j.chroma.2012.11.073.

[37] M. Biedermann and K. Grob, “Assurance of safety of recycled paperboard for food packaging through comprehensive analysis of potential migrants is unrealistic,” *J Chromatogr A*, vol. 1293, pp. 107–119, 2013, doi: https://doi.org/10.1016/j.chroma.2013.04.009.

[38] L. Bengtström *et al.*, “Non-targeted screening for contaminants in paper and board food-contact materials using effect-directed analysis and accurate mass spectrometry,” *Food Additives & Contaminants: Part A*, vol. 33, no. 6, pp. 1080–1093, Jun. 2016, doi: 10.1080/19440049.2016.1184941.

[39] M. Biedermann and K. Grob, “Is recycled newspaper suitable for food contact materials? Technical grade mineral oils from printing inks,” *European Food Research and Technology*, vol. 230, no. 5, pp. 785–796, 2010, doi: 10.1007/s00217-010-1223-9.

[40] M. L. Binderup, G. A. Pedersen, A. M. Vinggaard, E. S. Rasmussen, H. Rosenquist, and T. Cederberg, “Toxicity testing and chemical analyses of recycled fibre-based paper for food contact,” *Food Addit Contam*, vol. 19, no. sup1, pp. 13–28, Apr. 2002, doi: 10.1080/02652030110089878.

[41] M. Baele, A. Vermeulen, M. Claes, P. Ragaert, and B. De Meulenaer, “Migration of surrogate contaminants from paperboard to foods: Effect of food and surrogate properties,” *Food Additives & Contaminants: Part A*, vol. 37, no. 12, pp. 2165–2183, Dec. 2020, doi: 10.1080/19440049.2020.1778184.

[42] B. Aurela, “Migration of substances from paper and board food packaging materials,” 2001. Accessed: Aug. 14, 2024. [Online]. Available: http://hdl.handle.net/10138/21083

[43] M. Biedermann, R. Schum, and K. Grob, “Activated carbon added to recycled paperboard to prevent migration into food: approach for determining efficacy, and

first results," *Food Additives & Contaminants: Part A*, vol. 35, no. 9, pp. 1832–1844, Sep. 2018, doi: 10.1080/19440049.2018.1506162.

[44] "EUR-Lex - 02011R0010-20230831 - EN - EUR-Lex." Accessed: Aug. 14, 2024. [Online]. Available: https://eur-lex.europa.eu/legal-content/EN/TXT/?uri=CELEX:02011R0010-20230831

[45] R. Rodríguez-Ramos, A. Santana-Mayor, A. V Herrera-Herrera, B. Socas-Rodríguez, and M. A. Rodríguez-Delgado, "Recent advances in the analysis of plastic migrants in food," *TrAC Trends in Analytical Chemistry*, vol. 178, p. 117847, 2024, doi: https://doi.org/10.1016/j.trac.2024.117847.

[46] "Optical Properties of Polymers." Accessed: Aug. 13, 2024. [Online]. Available: https://www.intertek.com/polymers-plastics/optical-properties/

[47] S. K. Paul, "Edible Films and Coatings for Fruits and Vegetables," in *Encyclopedia of Renewable and Sustainable Materials*, S. Hashmi and I. A. Choudhury, Eds., Oxford: Elsevier, 2020, pp. 363–376. doi: https://doi.org/10.1016/B978-0-12-803581-8.11509-7.

[48] "High Clarity Linear Low Density Polyethylene for Packaging Applications - Paper, Film & Foil Converter." Accessed: Aug. 13, 2024. [Online]. Available: https://www.pffc-online.com/magazine/1006-paper-high-clarity-linear

[49] A. Eldesouky, A. F. Pulido, and F. J. Mesias, "The Role of Packaging and Presentation Format in Consumers' Preferences for Food: An Application of Projective Techniques," *J Sens Stud*, vol. 30, no. 5, pp. 360–369, Oct. 2015, doi: https://doi.org/10.1111/joss.12162.

[50] H.-L. Nguyen *et al.*, "Biorenewable, transparent, and oxygen/moisture barrier nanocellulose/nanochitin-based coating on polypropylene for food packaging applications," *Carbohydr Polym*, vol. 271, p. 118421, 2021, doi: https://doi.org/10.1016/j.carbpol.2021.118421.

[51] R. Breese, "Flexible Packaging Substrates Benefits of machine direction-oriented (MDO) films in flexible-packaging applications." Accessed: Jul. 22, 2024. [Online]. Available: http://ccl-eclipse.com/News_Releases/Benefits%20of%20MDO%20in%20Flexible%20Packaging.pdf

[52] M. T. DeMeuse, "Equipment design and requirements of biaxially stretched films," in *Biaxial Stretching of Film*, Elsevier, 2011, pp. 14–26. doi: 10.1533/9780857092953.1.14.

[53] V. Ratta, G. L. Wilkes, and T. K. Su, "Structure–property-processing investigations of the tenter-frame process for making biaxially oriented HDPE film. I. Base sheet and

draw along the MD," *Polymer (Guildf)*, vol. 42, no. 21, pp. 9059–9071, 2001, doi: https://doi.org/10.1016/S0032-3861(01)00387-1.

[54] R. L. Blaine, "Determination of Polymer Crystallinity by DSC. Therm. Anal. TA Instruments, 109 Lukens Drive, New Castle DE 19720, USA, 1-3." Accessed: Apr. 09, 2024. [Online]. Available: https://www.scirp.org/reference/referencespapers?referenceid=1920439

[55] A. Prasad, R. Shroff, S. Rane, and G. Beaucage, "Morphological study of HDPE blown films by SAXS, SEM and TEM: a relationship between the melt elasticity parameter and lamellae orientation," *Polymer (Guildf)*, vol. 42, no. 7, pp. 3103–3113, Mar. 2001, doi: 10.1016/S0032-3861(00)00612-1.

[56] B. A. Morris, "Barrier," in *The Science and Technology of Flexible Packaging*, Elsevier, 2017, pp. 259–308. doi: 10.1016/B978-0-323-24273-8.00008-3.

[57] S. Biedermann-Brem and K. Grob, "Barriers Against the Migration from Recycled Paperboard into Food: Measuring Efficiency by Surrogate Components," *Packaging Technology and Science*, vol. 27, no. 9, pp. 713–726, Sep. 2014, doi: https://doi.org/10.1002/pts.2062.

[58] M. Baele, A. Vermeulen, M. Claes, P. Ragaert, and B. De Meulenaer, "Migration of surrogate contaminants from paperboard to foods: Effect of food and surrogate properties," *Food Additives & Contaminants: Part A*, vol. 37, no. 12, pp. 2165–2183, Dec. 2020, doi: 10.1080/19440049.2020.1778184.

[59] "How to Measure Gloss using a Gloss Meter." Accessed: Nov. 27, 2024. [Online]. Available: https://www.elcometer.com/fr/how-to-measure-gloss-using-a-gloss-meter

[60] H. Alter, "A critical investigation of polyethylene gas permeability," *Journal of Polymer Science*, vol. 57, no. 165, pp. 925–935, Mar. 1962, doi: https://doi.org/10.1002/pol.1962.1205716572.

[61] K. Nakayama and H. Kanetsuna, "Hydrostatic extrusion of solid polymers," *J Mater Sci*, vol. 10, no. 7, pp. 1105–1118, 1975, doi: 10.1007/BF00541391.

[62] J. Lange and Y. Wyser, "Recent innovations in barrier technologies for plastic packaging—a review," *Packaging Technology and Science*, vol. 16, no. 4, pp. 149–158, Jul. 2003, doi: https://doi.org/10.1002/pts.621.

[63] "DESIGNING FOR A CIRCULAR ECONOMY An introduction," 2020. Accessed: Sep. 02, 2024. [Online]. Available: https://guidelines.ceflex.eu/assets/public_docs/D4ACE_guidelines_An_Introduction.pdf

[64] M. B. Johnson, G. L. Wilkes, A. M. Sukhadia, and D. C. Rohlfing, “Optical properties of blown and cast polyethylene films: Surface versus bulk structural considerations,” *J Appl Polym Sci*, vol. 77, no. 13, pp. 2845–2864, Sep. 2000, doi: https://doi.org/10.1002/1097-4628(20000923)77:13<2845::AID-APP6>3.0.CO;2-7.

[65] M. Kojima, J. H. Magill, J. S. Lin, and S. N. Magonov, “Structure and Morphology of Biaxially Oriented Films of Polyethylenes,” *Chemistry of Materials*, vol. 9, no. 5, pp. 1145–1153, May 1997, doi: 10.1021/cm960505h.

[66] E. Andreassen, Å. Larsen, K. Nord-Varhaug, M. Skar, and H. Øysæd, “Haze of polyethylene films—effects of material parameters and clarifying agents,” *Polym Eng Sci*, vol. 42, no. 5, pp. 1082–1097, May 2002, doi: https://doi.org/10.1002/pen.11014.

[67] “How to Measure Gloss Using a Gloss Meter.” Accessed: Nov. 30, 2024. [Online]. Available: https://www.elcometer.com/fr/how-to-measure-gloss-using-a-gloss-meter

[68] L. Wang, T. Huang, M. R. Kamal, A. D. Rey, and J. Teh, “Surface topography and gloss of polyolefin blown films,” *Polym Eng Sci*, vol. 40, no. 3, pp. 747–760, Mar. 2000, doi: https://doi.org/10.1002/pen.11204.

[69] S. Gorji Kandi, B. Panahi, and N. Zoghi, “Impact of surface texture from fine to coarse on perceptual and instrumental gloss,” *Prog Org Coat*, vol. 171, p. 107028, 2022, doi: https://doi.org/10.1016/j.porgcoat.2022.107028.

5.6 Appendix 5

Thickness measurements – oxygen permeability coefficient measurements samples

Table A5.1 Measured thickness (in microns) with standard deviation for blown films used in oxygen permeability coefficients analysis. (n=7)

Film type	Thickness (microns)
Blown film D1	42 ± 1.2
Blown film X1	49 ± 1.1
Blown film X1/X2 (50/50)	50 ± 0.9
Blown film D2	48 ± 1.1
Blown film D3	45 ± 1
Blown film X2	55 ± 1.8

Table A5.2 Measured thickness (in microns) with standard deviation for lab-scale MDO films used in oxygen permeability coefficients analysis. (n=7)

Film type	Thickness (microns)
Lab-scale MDO D1	193 ± 13.8
Lab-scale MDO X1	145 ± 8.8
Lab-scale MDO X1/X2 (75/25)	101 ± 2.8
Lab-scale MDO X1/X2 (50/50)	85 ± 3.1
Lab-scale MDO D2	116 ± 4.1
Lab-scale MDO D3	83 ± 4.7
Lab-scale MDO X1/X2 (25/75)	87 ± 4.4

Table A5.3 Measured thickness (in microns) with standard deviation for blown and pilot-scale MDO films of X1 and X1/X2 (75/25) used in functional barrier analysis. (n=7)

Film type	Thickness (microns)
X1 Blown film	49 ± 3.2
X1 pilot-scale MDO	50 ± 4.6
X1/X2 (75/25) Blown film	50 ± 3.3
X1/X2 (75/25) pilot-scale MDO film	52 ± 3

Chapter – 6

Epilogue

6.1 General conclusions

The experimental work presented in the Chapters 2,3,4 and 5 of this thesis explored the potential of MDO-PE films to provide performance comparable to polymers used in the outer layers of conventional multi-material flexible packaging, for PE based recyclable mono-material flexible packaging. Further, the experiments investigated and explored the mechanical recyclability of PE films and incorporation of PCR for subsequent MDO operations. The work also explored the interplay of key structural and process parameters in MDO operation to explore structure-property relationships of MDO-PE films and gain useful insights for better comprehension of the orientation process. The general conclusions from work performed in Chapter 2,3,4 and 5 is further summarised as follows:

High-density resins and blends of PE demonstrated greater disintegration and fibrillation of the crystalline microstructure, contributing to enhanced stiffness due to their larger crystalline phase from the investigations in Chapter 2. However, excessively high PE density led to localized stretching and breakage, underscoring the need for optimal density to achieve uniform orientation and improved mechanical properties. Strain-induced orientation and crystallization, driven by the MDO process, enhanced overall crystallinity and aligned both crystalline and amorphous phases, while variations in resin molecular architecture influenced stretching behaviour and modulus improvement. Additionally, surface morphology analyses revealed that low-density resins produced smoother surfaces, attributed to their resistance to extreme fibrillation because of their relatively more mobile microstructure during stretching.

By processing five PE types and their blends into blown films and subjecting them to pilot-scale MDO, the study in Chapter 3 demonstrated how average molecular weight, molecular weight distribution, comonomer content, and draw ratio influence the final properties of the films. Low-molecular-weight fractions were found to increase the natural draw ratio, enhancing the modulus of the MDO films. Additionally, blends with lower comonomer content exhibited greater modulus improvements due to the formation of larger crystals, which facilitated strain-induced crystallization and alignment during stretching. Higher MDO draw ratios transformed the microstructure into fibrils strongly oriented in the machine direction, significantly enhancing crystallinity and MD modulus to levels comparable to high-performance polymers such as PET and PA used in traditional flexible packaging.

The findings from Chapter 4 demonstrated that reprocessed PE films retained 77% of the tensile modulus of virgin MDO films, despite slight molecular degradation and reduced crystallinity due to multiple extrusion cycles. Surface morphology analyses revealed rougher textures and increased haze in reprocessed films, but fibrillated, well-oriented structures were still achieved in the MDO process. Additionally, incorporating 5% PCR into PE blends produced tensile properties comparable to virgin films, showcasing the feasibility of low-PCR-content blends for high-performance mono-material flexible packaging. However, higher PCR content (30%) led to reduced density, crystallinity, and modulus, along with visible defects due to contamination. These results highlight the potential for integrating PCR into MDO-PE films while emphasizing the variability of PCR composition and the need

for quality control. This study focused on a specific type of PCR; however, it is recognized that the composition of PCR materials can vary due to factors such as origin, manufacturer, collection methods, and contamination. Therefore, further research is needed to investigate the effects of other PCR materials with different chemical compositions for integrating with virgin materials to produce MDO films. While this study focused on mono-layer films, the extension of these findings to multilayer structures presents a promising avenue for future research, reinforcing the potential for sustainable, high-performance packaging solutions.

With regards to barrier properties, MDO processing generally enhanced oxygen and functional barrier properties by increasing crystallinity and microstructural orientation from the investigations in Chapter 5, though the degree of improvement depended on resin density and processing conditions. Higher-density PE films exhibited superior oxygen barrier performance after MDO, while lower-density films showed increased permeability due to higher partial melting of microstructure and limited amorphous phase orientation. However, even with improvements, MDO-PE films did not achieve oxygen barrier performance comparable to high-barrier polymers like PET and PA, highlighting the need for supplementary barrier layers compatible with mechanical recycling. Functional barrier studies revealed that MDO films provided better resistance to surrogate MOAH and MOSH compounds than blown films, owing to the tortuous diffusion paths created by increased crystallinity and orientation, particularly at higher draw ratios. MDO also impacted optical properties, with haze increasing due to surface roughness and crystallinity, while gloss decreased at lower draw ratios but improved at higher draw ratios due to better fibril alignment. These findings underscore the need for optimizing resin properties and processing parameters to tailor barrier and optical performance, enabling the design of sustainable, high-performance mono-material packaging solutions.

These findings underscore the importance of optimizing resin molecular properties and process parameters to produce MDO-PE films with superior mechanical, barrier and optical properties, enabling the design of sustainable, high-performance PE based mono-material packaging systems, and positioning them as a sustainable alternative for conventional multi-material multilayer flexible packaging.

6.2 Outlook for future research

The findings of this research present numerous possibilities of future investigation. While this entire research focused on monolayer systems, it is recognized that industrial-scale processes typically conduct the MDO operation on multilayer structures. These multilayer films may be produced through coextrusion via cast or blown film processes.

A critical area for future study involves examining the effects of MDO operation on the microstructure of individual layers when orienting multiple layers simultaneously. Additionally, understanding how such operation influences the overall performance of the multilayer system remains an important and unexplored aspect.

For mechanical performance, this research primarily focused on analysing the modulus and stiffness properties of the films. The observed enhancement in tensile modulus correlates with improvements in stiffness, which are critical considerations for mechanical

performance when designing the outer layers of multilayer flexible packaging systems. It is important to note that the orientation process during MDO operation may also affect other mechanical properties, such as tear resistance, puncture resistance and impact strength. However, investigating these properties was beyond the scope of this research. This presents an opportunity for future research to explore these aspects, especially as specific applications may demand tailored final properties and optimized overall packaging performance.

Regarding barrier properties, further research opportunities exist to investigate the influence of critical MDO process parameters, such as orientation temperature and draw ratio, when multiple layers are oriented simultaneously. Additionally, integrating compatible high-performance oxygen or functional barrier layers in these systems demands experimental validation to assess their compatibility with mechanical recycling processes.

The compatibility of key flexible packaging converting processes, such as printing, lamination, sealing, and pouching, with oriented films must be thoroughly analysed to ensure that these processes are compatible with oriented films. This is essential for the successful production of mono-material PE-based flexible packaging.

A key challenge in the converting process for mono-material PE-based flexible packaging is heat sealing. Since the oriented PE films for outer layers are less thermally stable compared to conventionally used polymers, there is a risk of damaging these outer layers during the heat-sealing process, which is mostly used in the production of flexible packaging. This issue must be thoroughly analysed and addressed to ensure the successful adaptation of mono-material PE based flexible packaging systems.

Further, the impact of inks, plasticizers, and other additives on mechanical recycling of mono-material PE-based packaging requires further investigation, as there is a limited body of research available on this topic. This analysis could provide valuable insights to refine the guidelines established by consortiums such as CEFLEX (A circular economy of flexible packaging), specifically regarding the safe incorporation of these materials for high compatibility with the mechanical recycling process to produce high quality recyclate materials for high performance applications.

Further, future work could explore the influence of MDO or uniaxial orientation on the properties of PE films developed from the PE resin and blend compositions which were not considered in scope of this thesis. This could involve a systematic study of PE resins and blends with a wide range of resin parameters, including resin density, average molecular weight, polydispersity, SCB, branching distribution, and comonomer content. One such limitations of the PE resins and blend compositions used for the investigations in this thesis was not having a wide range of polydispersity, as many resins and blends composition presented similar polydispersity. By examining these additional compositions, future researchers could further refine the findings and conclusions presented in this thesis. Moreover, such studies could provide deeper insights into the effects of PE resin compositions and their specific molecular characteristics, particularly those not considered within the scope of this research. This added understanding would contribute to optimizing the processing and performance of MDO-PE films.

6.3 Key challenges moving forward

Transitioning to mono-material flexible packaging is crucial for advancing the circular economy of flexible packaging systems. However, as with any new technological adaptation, it presents several challenges. To ensure widespread industrial and consumer adoption, these challenges must be effectively addressed in future developments.

A major challenge following the successful development of mono-materials is the effective sorting and collection of these materials for mechanical recycling from mixed waste streams. To address this, proper disposal channels and waste management systems must be established to ensure the efficient sorting and collection of these type of packaging, while also maintaining consumer convenience. Innovative technologies should be employed to enhance the efficiency of collection, sorting, and subsequent mechanical recycling of these materials. Additionally, clear guidelines and policies must be developed to facilitate the convenient recycling of these packaging systems.

Another key challenge is the cost of production. Although most production and converting processes for mono-material flexible packaging are compatible with existing packaging machinery, the integration of orienting machines to produce oriented films is still necessary. As this is an emerging technology in packaging, it is anticipated that not all industries will be able to easily adopt it due to the costs associated with acquiring new machinery and training operators. To address this, support is required for industries in integrating these novel technologies into their existing manufacturing processes. Additionally, policies such as Extended Producer Responsibility (EPR) should be implemented, holding producers and converters accountable for the recycling of their products and progressively increasing recycling targets.

Another challenge is the integration of PCR materials in applications like food and pharmaceutical packaging that meets regulatory compliance. Current regulations restrict the use of PCR in contact-sensitive applications within these industries. To address this, collaboration between manufacturers and recyclers is essential to ensure the high quality of the recycled materials, if it is permitted in future to use in such packaging.

Finally, given that the cost of mono-material production may exceed that of conventional flexible packaging in initial transition years, it is essential to implement policies that prevent these costs from being solely borne by industries and, ultimately by the consumers. Subsidies and policies should be introduced in the initial years to support industries in adapting the mono-material flexible packaging, ensuring its successful integration across both large and small-scale producers and converters.

6.4 Concluding thoughts

Amid growing concerns about the circularity of plastics, transitioning from multi-material flexible plastic packaging to mono-material flexible plastic structures offers significant potential to support the efficient mechanical recycling of flexible packaging. While some industries have already adopted mono-material flexible packaging for specific applications, further advancements in research and development are essential to ensure that mono-material flexible packaging can meet the stringent requirements needed for widespread adoption in key industries such as food and pharmaceuticals. MDO or uniaxially oriented polyethylene films play a crucial role in advancing mono-material PE-based flexible packaging. Their unique properties offer promising solutions to key design challenges in the shift from multi-material to mono-material PE-based packaging systems, thereby contributing to the achievement of a circular economy for flexible packaging.

Curriculum Vitae

Dixit Guleria was born on August 4, 1994, in Hamirpur, Himachal Pradesh, India. In 2012, he commenced his bachelor's degree in chemical engineering from University Institute of Chemical Engineering and Technology, Panjab University, Chandigarh, India. In 2016, he obtained his bachelor's degree with first division. Following his undergraduate education, Dixit pursued a Master of Technology degree in Packaging Technology from Indian Institute of Technology Roorkee, India. During his master's program, he was awarded DAAD scholarship, enabling him to undertake a 7-month master's thesis program at TU Dresden, Germany (2018–2019). During this period, he investigated on the topic "Bending stiffness improvement of multilayer paperboards using dry defibrated fibers" under the supervision of prof. dr. ir. André Wagenführ and prof. dr. Chhaya Sharma. He successfully completed his master's degree in 2019 with first division and distinction. After obtaining his master's degree he briefly worked in a multinational flexible packaging industry in Mumbai, India as a Quality Assurance Engineer.

In the year 2020, he started his PhD as a Marie Sklodowska-Curie (EU-H2020) PhD candidate, jointly at Eindhoven University of Technology (TU/e), The Netherlands, and Ghent University (UGent), Belgium under the supervision of prof. dr. ir. Jaap den Doelder (TU/e), prof. dr. Ludwig Cardon (UGent) & prof. dr. ir. Peter Ragaert (UGent). During his PhD research, he focused on machine direction orientation of polyethylene films and their structural-property relationships for the design of recyclable mono-material PE based flexible packaging systems.

List of Publications

Articles related to this thesis, in order of appearance

1. Impact of resin density and short-chain branching distribution on structural evolution and enhancement of tensile modulus of MDO-PE films. Dixit Guleria, Shouren Ge, Ludwig Cardon, Sylvie Vervoort, Jaap den Doelder. *Polymer Testing (Elsevier), September 2024*

2. Impact of molecular architecture and draw ratio on enhancement of targeted mechanical properties of machine direction oriented polyethylene films produced after blown film extrusion. Dixit Guleria, Mariya Edeleva, Sylvie Vervoort, Shouren Ge, Jaap den Doelder, Ludwig Cardon. *Journal of Plastic film & Sheeting (Sage), October 2024*

3. Assessing mechanical recyclability of blown films and integration of PCR for high modulus MDO-PE film application: A comparative study. Dixit Guleria, Simon Debrie, Shouren Ge, Sylvie Vervoort, Jaap den Doelder, Ludwig Cardon, Mariya Edeleva. *(Currently under review)*

4. Influence of uniaxial orientation on gas barrier, functional barrier, and optical properties of polyethylene films. Dixit Guleria, An Maes, Dimitri Adons, Jaap den Doelder, Ludwig Cardon, Roos Peeters, Bruno De Meulenaer, Peter Ragaert. *(to be submitted)*

Articles not related to this thesis

1. P. Main, D. Guleria, M. Moubarak, C. Kibuta, F. Lit, A. Fonseca, M. Lisiecki, T. Belé, A. Bashirgonbadi, E. Mahmoudi, B. Goshayeshi, R. Kol, N.G. Yalcin, M.K. Rabiu, N. Mhaddolkar, H. M. Logan, *Plastic Planet: A guide to recycling and caring for our environment, SuperTimeBooks-Copenhagen. 2023.*

Acknowledgements

This thesis would not have been possible without the enormous contributions of my promotors, colleagues, family, and friends.

Firstly, I would like to thank my first promotor Prof. Jaap den Doelder for your immense invaluable guidance and active involvement in this project throughout its duration. Even though you could not always be physically present in the locations where I worked during this project, it never felt like I was missing your guidance and supervision. You were always there, online or offline, whenever I needed you. I will sincerely miss our weekly or bi-weekly meetings where we could not only talk about science, but also about things like current football scenarios and weekend activities. I will always fondly remember our bike ride on my first day of industrial secondment at Dow Terneuzen from the office to home, when we got completely drenched in an unexpected torrential downpour :) I will always cherish our fun moments and memories with the C-PlaNeT (Circular Plastics Network for Training) group when we travelled for C-PlaNeT events in Copenhagen and Thessaloniki and organized one in Eindhoven!

Secondly, I would like to thank my co-promoter Prof. Ludwig Cardon for your extensive guidance and support during my stay at CPMT, Ghent University, and beyond. Thank you for accepting me under your supervision and being my co-promoter after the transition. You helped me access the essential machines I could use for the project and guided me on how to use them creatively. You also ensured I had proper training to use the machines and equipment safely. I will always miss our group's sandwich lunches and drink breaks in CPMT that helped us researchers become a bit more social! :)

I would like to thank my co-promoter Prof. Peter Ragaert for always being there from the start. You ensured I was welcomed and well-integrated into the group during my stay at the Ghent University Coupure campus. You made sure I had access to equipment, chemicals, and the training needed for the required experiments. You also organized our collaboration with Hasselt University, which brought important and interesting results for the project. I fondly remember our conversations where you patiently listened to my ideas and guided me on how to execute them. I also have great memories of our interactions during C-PlaNeT online and offline events :)

I would like to thank Prof. Remco Tuinier for chairing the defense ceremony at TU Eindhoven. Your love for science has always inspired me. It was a great pleasure to be part of the Polymer and Colloidal Science course team for three years. I fondly remember your science puns with the group which always made us laugh and our enjoyable SPC group trips together. The one in Ameland was truly special. Thank you so much for all these years.

I would like to thank the co-chairperson of my defense ceremony Prof. Joris Degroote for conducting the first meeting of my defense at Ghent University and for co-chairing the final defense ceremony at TU Eindhoven. I am grateful to all the other members of my defense committee - Prof. Frederik Desplentere, Prof. Imca Sampers, Prof. Mariya Edeleva, Prof. Alexey Lyulin and Prof. Albert Schenning for their critical reading of my thesis and for being part of my defense committee.

Then I would like to sincerely thank my initial co-promoter Prof. Kim Ragaert who provided me with a clear pathway during the initial years of this project. Your supervision at the project's start was crucial. You made sure I got the necessary online support and guidance when I could not travel to Europe during the first COVID lockdown. I also fondly remember how warmly you welcomed me into your new group when we met again at the PPS Switzerland conference. I will always cherish our moments together during C-PlaNeT events in Copenhagen and Eindhoven! :)

I would like to thank my Dow supervisor Dr. Sylvie Vervoort. The amount of support and guidance you provided me throughout this project is beyond words. You ensured I received daily support during my time at Dow Terneuzen and introduced me to team member like Thomas De Wilde, who helped me immensely. You also introduced me to Dow experts like Shouren Ge and helped me get support from Dow facilities across the ocean which were crucial in achieving key results. On top of that, your sporty attitude always motivated and inspired me. I fondly remember our group dinner in Ghent where you hesitantly ordered dessert and promised yourself to run it off over the weekend! :)

Next, I would like to thank my committee member Prof. Mariya Edeleva. First, thank you for being on my committee and evaluating this thesis. I am also grateful for your support and guidance throughout my journey from my stay at CPMT Ghent University and onwards. Your creative ideas always helped improve the execution of experiments. Thank you for being there, online and offline, to discuss the project's progress and for always motivating and inspiring me! :)

I would like to thank my colleagues Luuk Moone and Ryno van Niekerk for being my paranymphs. Luuk, you helped me so much especially during the final months of this journey with administrative stuff that I cannot thank you enough. You are a kind-hearted person, always willing to help others, and you inspire people to be kind and helpful too. Your door is always open, even for the smallest of questions. It's an honor to share our defenses in the same month. Ryno, you've been such a cool officemate. Your cheerful morning greetings always brightened my day. Your interesting conversations about science and sports were always engaging. Your love for Indian food is admirable and your love for South African wines is unmatched. Thank you so much for standing by me during my defense! :)

Ingeborg, thank you for always helping me so much with my experiments. Your role in the smooth functioning of the group is immense! Ton, thank you for arranging the storage of materials used in this project! Pleunie, thank you for managing everything so smoothly from the beginning! Max, thanks for being a cool officemate and inviting us to your home, introducing us to Frodo during the Christmas celebrations. I'll always fondly remember our chats, half-peeking at each other's faces between the computer screens! :) Gautam, thanks for the fun banter and talks about cricket and Indian politics and for treating us to delicious Indian food! Heiner, your innovative and creative suggestions during FAM presentations reflect your passion for science and are always helpful to the group! Catarina, your enthusiasm for science and positive energy is truly motivating and inspiring to the group! Mark, it was great to be part of the P&C course with you. Your science puns and anecdotes always livened up lunch sessions! Laura, thank you for welcoming me to Eindhoven and for your help when I first arrived from India during the COVID lockdown. It was a pleasure

teaming up with you for P&C guided self-study sessions. Your multitasking abilities always inspired us! Bert, thank you for sharing your wisdom and passion for science with the whole group! Rolf, thanks for the nice conversation while traveling for the group cooking activity! Tommasso, thanks for sharing your passion for science and football with the group! Lisette, thanks for sharing the passion for science at the IUPAC Chains conference and treating us to cakes so often. I'll fondly remember the ice cream session organized by you! Mallika, thank you for your light-hearted puns. They always made the group laugh, a truly invaluable skill! Dasol, thanks for introducing us to delicious South Korean food! Anne, thanks for the nice memories during group visits. Your photography skills are amazing! Pauline, thanks for the fun moments during group visits, I'll fondly remember our fantastic group cooking session! Volodymyr, thanks for the nice conversations whenever we met! Anne Floor, thanks for organizing and teaming up for the excellent Meerkamp! Eleonora, thanks for treating us with your baking skills and for chairing the PhD and postdoc meetings! Alba, Nitin, Ferid, Tijmen, Maarten, Francesco, even though we didn't get to interact much due to time constraints, it was a real pleasure meeting you all!

I would like to thank my ex-SPC colleagues Eva, Stijn, Joeri, Machi, Rick, Siyu, Stefan, Jeroen, Jiankang, Roman, Bernette and Mohammad. Without you all, this journey would have been far less enjoyable.

I would like to thank my Ghent University colleagues, especially Simon, Ellen, Mustafa, Tom, Tom W, Veerle, Laia, Gianni, Daniel, Elise, Erion, Hannelore, Chiara, Annabelle, Juan, Marah, An Maes, and An Dirckx. Thank you for making me feel welcomed and comfortable in the new group!

Thanks to Dr. Emine Gözde Dere, Thomas, Joana, Rudi, and Georg for making my stay at Dow Terneuzen pleasant and enjoyable!

Thanks to my students Federica and Jihye for your enthusiasm in this project and for producing such interesting results!

To my C-PlaNeT colleagues Laurens, Elisabeth, Fernando, Manon, Priyanka, Amir, Namrata, Tiago, Bahman, Ehsan, Christina, Mubarik, Nur, Heather, Maria, Alejandro, and Rita, thank you for sharing your diverse research interests in pursuit of circular plastics. You made all the C-PlaNeT events enjoyable and memorable. Special mention to Manon, without your efforts the wonderful children's book we created would not have been possible! :) Thank you so much Prof. Myriam Cloodt and Boukje for the successful co-organization of C-PlaNeT NTE (Network Training Event) in Eindhoven!

To my dear friends made along this journey, you always brought happiness, warmth, and support for me. Fernando, you being my friend and C-PlaNeT colleague at TU Eindhoven with a similar path made a lot of things easier for me. Thank you for your help, support, and fun group trips. Copenhagen, Edinburgh, London, Lyon, Greece, and Brittany were unforgettable. Your multilingual and multitasking skills are always inspiring! :)

Vincent, thank you for sharing this PhD journey all these years. Your driving skills and passion for food and travel took us to countless amazing places and gave us many fun memories. Your love for cooking and cast-iron pans is admirable. Thank you for sharing countless

cooking sessions and shoutout to the Ranveer Brar YouTube channel which always gave us ideas for delicious Indian meals! :)

Rocio, thank you for being such a cool friend all these years. Thanks for always treating us with delicious treats like lemon cheesecake, fajitas, empanadas, and cocktails. You always welcomed us warmly in your home Sisi, which now feels like our group home. Your management skills made every trip smooth and fun. Thank you for so many incredible memories! :)

Cesar, thank you for being my Lombokpad friend. Your fancy coffee setup always amazed me. Thank you for sharing your special brews and delicious meals. I'll always fondly remember our Thursday evening music sessions! ;)

Thank you so much Greta for sharing the nice food and drinks! Your chocolate brownie was very delicious! :) Salar, thanks for sharing the love for FC Barcelona! Visca Barca! :)

Thanks to Shikhar and Umesh for being there since I arrived in Eindhoven. You made me never miss India or Indian food. I fondly remember our Amsterdam and Giethoorn trips, Friday night gatherings, movies, and music! :) Vadi and Manjeeth, thank you for sharing food, fun banter, and holiday celebrations! Gaurav Bhaiya and Silky Di, thank you for inviting me to your home in Meerhoven for delicious meals and interesting conversations! :)

Special thanks to my beloved football team Pusphaira 7 and my teammates Stan, Joost, Bart, Erik, Atharva, Bruno, Mees, Ivan, Denis, Amer, Tim, Rijn, Max, Bas S, and Bas H. Without football, my time in Eindhoven wouldn't have been as special!

I would like to thank my longtime friends in India Shresht, Mohit, Tanzin, Kaushal, Kartik, and Naveen. You guys made my every trip to home memorable during all these years. Thank you for always being there for over 15 years now.

Finally, I would like to express my heartfelt gratitude to my family, who have always been my pillars of strength and unwavering support. I am deeply thankful to my grandparents and parents for their blessings and for always believing in my journey. To my parents, thank you for standing by me during difficult times, especially when the world was grappling with the challenges of COVID. Your support during that period and your encouragement to pursue my PhD abroad meant the world to me. Your lifelong sacrifices, love, and belief in me have been a constant source of my strength.

I would like to thank my elder brother Ankit Guleria and my sister-in-law for their continuous support and affection. Whether it was through countless video calls or during my visits to India, you were always there whenever I needed you, and I'm truly grateful for that.

If I've unintentionally missed mentioning anyone in these acknowledgements, please accept my sincere apologies. I truly hope to meet all of you in person sooner or later, whenever possible! :)

Dixit Guleria
Eindhoven, 2025